UNIVERSITY OF
KWAZULU-NATAL

INYUVESI
YAKWAZULU-NATALI

Separation of Binary Homogeneous Azeotropic Mixtures using Pervaporation

Ronel Mari

BSc.Eng. (Chemical Engineering)

In fulfilment of the degree of Master of Science in Engineering
in the School of Engineering, Discipline of Chemical Engineering
University of KwaZulu-Natal

July 2021

Supervisors: Dr. K. Moodley & Prof. P. Naidoo

ABSTRACT

The separation of mixtures containing homogeneous azeotropes is often complex and requires the use of enhanced distillation techniques. This leads to a significant increase in capital and operating costs. The use of membrane separation techniques to separate azeotropic mixtures is favoured over extractive distillation, azeotropic distillation and absorption as this is an effective low energy and low-cost alternative. Pervaporation is a membrane-based separation technique often used in industry to dehydrate alcohol-water azeotropes, to remove water from organic solvents or to remove organics from water. The process requires a liquid feed at a pressure high enough to maintain its phase while being depleted of components contained within the feed to form a liquid retentate. A membrane is typically selective for one component with finite permeability for the remaining components in the feed. A vapour phase must be maintained on the permeate side of the membrane by applying a vacuum downstream thereby creating a pressure gradient. A pervaporation unit generally consists of a series of membrane cells grouped together in modules, and interstage heat is applied to the feed of subsequent modules. This investigation focused on the dehydration of alcohols (ethanol, propan-1-ol and propan-2-ol) using a poly(vinyl alcohol) based membrane. An experimental study on ethanol-water under various operating conditions was performed. The effect of permeate pressure (2–5 kPa), feed temperature (338.15–348.15 K) and feed water concentration (1–5 wt.%) are reported in terms of flux and permeate quality. Results confirmed that pervaporation is a suitable method to break an azeotrope. Due to technical issues encountered with the equipment, the experimental determination of pervaporation performance was not pursued further. This prompted an extensive simulation study whereby semi-empirical models were developed for the alcohol-water systems using Aspen Custom Modeler® before exporting to Aspen Plus® for simulation and optimization. Dehydration of an industrial grade propan-2-ol aqueous solution (85 wt.% propan-2-ol) using pervaporation was then rigorously simulated as the final objective, as this is not explored in detail in the literature. Various interstage heat temperatures (363.15, 368.15, 373.15 K) and module arrangements (3, 5 and 8 cells per module) were considered to produce the required retentate stream of less than 2 wt.% water. A total of nine design cases were developed to meet the industry purification requirements (>98 wt.% propan-2-ol in retentate). An economic evaluation (inclusive of operating, investment, and maintenance cost) of the separation was performed. It was confirmed that a membrane setup of 3 modules with 3 cells per module including interstage heating to 373.15 K presented the lowest

total cost of 174.27 $/t. This arrangement provided the most feasible configuration for propan-2-ol dehydration using a PVA-based membrane and when compared to azeotropic distillation from literature, it was found that a saving of 34% could be achieved using pervaporation, assuming a pre-concentrator cost of 1/3 of the total process costs from the literature studies. The comparative economic analysis performed across various processes was based on the total cost per ton of propan-2-ol product, which served as a standardized cost. Two procedural assumptions were applied; an operational time of 300 days per year and 24 hours a day for an industrial plant, and a production rate of 257.69 $kg.h^{-1}$ propan-2-ol, as per the optimal design case.

DECLARATION

The work presented in this dissertation was carried out in the Thermodynamic Research Unit in the School of Engineering at the University of KwaZulu-Natal, Durban, under the supervision of Doctor K. Moodley and Professor P. Naidoo.

This dissertation is submitted as the full requirement for the degree M.Sc. (Eng.) in Chemical Engineering.

I, Ronel Mari, therefore declare that:

(i) The research reported in this dissertation, except where otherwise indicated, is my original work.

(ii) This dissertation has not been submitted for any degree or examination at any other university.

(iii) This dissertation does not contain other persons' data, pictures, graphs or other information, unless specifically acknowledged as being sourced from other persons.

(iv) This dissertation does not contain other persons' writing, unless specifically acknowledged as being sourced from other researchers. Where other written sources have been quoted, then:

a) Their words have been re-written but the general information attributed to them has been referenced;

b) Where their exact words have been used, their writing has been placed inside quotation marks, and referenced.

(v) This dissertation does not contain text, graphics or tables copied and pasted from the Internet, unless specifically acknowledged, and the source being detailed in the dissertation and in the References sections.

_____ 25/08/2021

Ronel Mari Date

As the candidate's supervisor, I, Dr. K. Moodley, approve this dissertation for submission.

_____ 25 August 2021_____

Doctor K. Moodley Date

As the candidate's co-supervisor, I, Prof. P. Naidoo, approve this dissertation for submission.

_____ _ 25 August 2021_____

Professor P. Naidoo Date

ACKNOWLEDGMENTS

Throughout this dissertation I have received a great deal of support and assistance.

I would like to express my sincere gratitude to my supervisors, Professor P. Naidoo and Doctor K. Moodley, whose expertise was invaluable in formulating the research questions and methodology. Your broad knowledge and insightful feedback motivated me and elevated my research.

I would like to acknowledge the National Research Foundation (NRF) for financial support for this project.

I would also like to express my appreciation to Mr. A. Khanyile, Ms. X. Hadebe, Mr. S. Deeraj, Mr. D. Padayachee, Mr. G. Addieah and Mr. P. Nayager for their continuous assistance both in and out of the laboratory. You provided me with the tools needed to successfully complete my dissertation.

In addition, I would like to express my deepest gratitude to my parents, Mr. and Mrs. Mari, sister and brother-in-law, Mrs. L. Mari-Naidoo and Mr. K. Naidoo, for their wise counsel, unconditional love and continuous support, patience, and motivation. Finally, I would like to thank my friends for their stimulating discussion, sympathetic ear and for providing happy distractions to rest my mind outside of research.

TABLE OF CONTENTS

LIST OF FIGURES

LIST OF TABLES

NOMENCLATURE

Latin Capital and Lowercase Letters

Symbol	Description
A	effective membrane area
A_i	peak area of component i
C	cost
c_i	molar concentration of component i
c_{il}	molar concentration of component i at the permeate
$c_{il(m)}$	molar concentration of component i at membrane/permeate interface
c_{io}	molar concentration of component i at the feed
$c_{io(m)}$	molar concentration of component i at the feed/membrane interface
c_{io}^{G}	molar concentration of component i of vapour equilibrium
c_{io}^{L}	molar concentration of component i of feed solution
D	diffusivity
D_i	diffusion coefficient for component i
D_o	diffusivity pre-exponential factor
E_D	diffusion energy
E_p	activation energy
E_{pi}	activation energy for component i
F_i	response factor
H	heat of adsorption or enthalpy of dissolution
H_i	Henry's constant
J	total flux
J_i	specie flux
j_i	molar flux of component i

K_i	liquid-phase sorption coefficient of component i
K_i^G	gas phase sorption coefficient of component i
l	liquid phase
L	thickness of membrane
L_i	coefficient of proportionality
m_i	mass of permeating specie i
M_i	molecular weight of component i
n_i	number of moles of component i
p	pressure
P	permeability
p_1	feed-side pressure
p_2	permeate-side pressure
$P_{i,ref}^G$	reference membrane permeability
$p_i°$	reference pressure
p_i^G	permeability coefficient
P_i^G	membrane permeability for component i
p_{il}	partial pressure
p_{io}	partial vapour pressure
p_{io}^G	partial vapour pressure
p_{isat}	saturation vapour pressure of component i
P_j^G	membrane permeability for component j
p_l	pressure of the permeate vapour
p_o	pressure of the liquid feed
P_o	permeability pre-exponential factor
P_X	price rate

R	Universal gas constant
S	solubility
S_o	solubility pre-exponential factor
T	temperature
t	time
T_d	thermal decomposition temperature
T_f	temperature of feed
T_g	glass transition temperature
T_m	melting point
T_p	temperature of permeate
T_{ref}	reference temperature
v	vapour phase
v_i	molar volume of component i
v_i^G	molar volume of gas i
x_i	weight fraction in liquid phase
X_{io}^L	mole fraction of component i in liquid feed
y_i	weight fraction in vapour phase
Y_i	mole fraction of component i
Y_{il}	mole fraction of component i in vapour permeate

Greek Letters

Symbol	Description
α_{ij}	separation factor
β_{ij}	selectivity
γ_i	activity coefficient of component i

γ_{il}	activity coefficient of component i at the permeate
$\gamma_{il(m)}$	activity coefficient at the membrane/permeate interface
γ_{io}	activity coefficient of component i at the feed
$\gamma_{io(m)}$	activity coefficient of at the feed/membrane interface
γ_{io}^{G}	activity coefficient of feed in equilibrium with vapour
γ_{io}^{L}	activity coefficient of feed in liquid phase
Δ	change in
μ_i	chemical potential of component i
$\mu_i°$	activity coefficient of component i
ρ	density

Subscripts

Symbol	**Description**
1	component 1
2	component 2
a	annual operation
bp	normal boiling point
COND	condenser
cw	cooling water
d	decomposition
dep	depreciation
elec	electricity
f	feed
g	glass transition
HE	interstage heaters

i	component i
I	investment
io	feed/membrane interface
ix	installation and auxiliary units
j	component j
m	melting
M	maintenance
mem	membrane
module	membrane modules
mpv	maintenance of pervaporation unit
o	pre-exponential factor
O	operating
PV	pervaporation unit
ref	reference
s	steam
T	total
VP	vacuum pump

Superscripts

Symbol	**Description**
°	reference
L	liquid-phase coefficients
G	gas-phase coefficients

Auxiliary Symbols

Symbol	Description
$\dot{m}$	mass flowrate
$\dot{V}$	volumetric flowrate

Abbreviations and Acronyms

Symbol	Description
C3	propanol isomers
CA/PAN	cellulose acetate/polyacrylonitrile
CAGR	compound annual growth rate
D/F	distillate-to-feed ratio
DEG	diethylene glycol
DEGME	diethylene glycol monoethyl ether
DES	deep eutectic solvent
DMC	dimethyl carbonate
DMF	N,N-dimethylformamide
DMSO	dimethyl sulfoxide
EGME	ethylene glycol monoethyl ether
EPDM	ethylene propylene diene monomer
EPDR	ethylene propylene diene rubber
HEC	(hydroxyethyl)cellulose
LDPE	low density polyethylene
mol	mole
NaAlg	sodium alginate

NaCl	sodium chloride
NBR	poly(butadiene-acrylonitrile)
NMP	N-methyl-2-pyrrolidone
no.	number
NRTL	non-random two-liquid
NS	number of stages
PA	polyamide
PAA	poly(acrylic acid)
PAN	polyacrylonitrile
PAN-co-AA	polyacrylonitrile-co-acrylic acid
PASAs	poly(amide-sulfonamide)s
PB	polybutadiene
PC	polycarbonate
PDMS	poly(dimethyl siloxane)
PEBA	polyetheramide-block-polymer
PFP	perfluoro polymer
PI	polyimide
PID	proportional-integral-derivative
PMA	poly(methyl acrylate)
PMAA	poly(methacrylic acid)
PMS	poly(methoxy siloxane)
POMS	poly(octylmethyl siloxane)
POUA	poly(oxiethylene urethane acrylate)
PP	polypropylene
PPO	poly(phenylene oxide)

PSI	pervaporation separation index
P'TMSP/PDMS	poly(trimethylsilylpropyne)/polydimethylsiloxane
PUR	polyurathane
PVA	poly(vinyl alcohol)
PVC	poly(vinyl chloride)
PVP	poly(vinylpyrrolidone)
PVP-PMAA	poly(vinylpyrrolidone)-poly(methacrylic acid)
R	reflux ratio
S/F	solvent-to-feed ratio
SBR	styrene butadiene rubber
TAC	total annual cost
TEG	triethylene glycol
UNIFAC	UNIQUAC functional group activity coefficient
wt.	weight

CHAPTER 1

Introduction

It is well known that the separation of azeotropic systems requires complex distillation column sequences or alternate techniques. For the enhanced distillation approach, this is often energy intensive and financially demanding. Over the years, pervaporation has grown to become an appealing method of separation due to the high efficiency and low energy consumption of the process as compared to conventional distillation.

In recent years, there has been a growing interest in the use of renewable energy resources such as bioalcohols as biofuels. The production of biofuels from bioalcohols requires the dehydration of alcohol-water mixtures. Pervaporation of ethanol-water systems have been studied extensively in the literature with a few articles referenced herein (An et al., 2014; Gil et al., 2008; Gomis et al., 2007; L Laroche et al., 1991; Li and Bai, 2012; Pham and Doherty, 1990; Rojas et al., 2016; Sander and Soukup, 1988; Wesslein et al., 1990; Win and Friedl, 2012). However, there is very little research concerning the use of PVA-based membranes to separate aqueous C3 alcohol mixtures, such as the propan-1-ol− and propan-2-ol−water systems. Such operations are necessary as these alcohols have many industrial applications and a significant market value.

Dehydrated alcohols such as propan-1-ol and propan-2-ol are used extensively as solvents in personal/home/health care, pharmaceutical and chemical industries. During the current COVID-19 pandemic, many of these industries increased production of these alcohols to meet the demand for their use as a disinfectant. According to an article published by The European Business Review on 28 May 2021, reports predict a compound annual growth rate (CAGR) of approximately 5% by 2024 for the market of global household cleaning products (containing C3 alcohols). Business Wire (2021) forecasted an 8.4% CAGR for the household care market of China for the period of 2021-2025. In addition, companies such as 3M, Unilever and Proctor & Gamble have already observed sales increases of 5 – 8% (Reuters, 2021), 4.5% (Unilever, 2021) and >30% (Amcor plc, 2021) respectively which also include alcohol based cleaners.

The heightened focus on personal hygiene may extend well past the pandemic period. If pervaporation can prove to be a cost-effective, environmentally friendly alternative to

conventional separation methods, the aforementioned industries can adopt the technique to secure feasible production in the future.

1.1 Aim and objectives

The aim of this study was to determine the separation efficiency of three binary homogeneous azeotropic systems, in particular ethanol–, propan-1-ol–, and propan-2-ol–water, across PVA-based membranes using the technique of pervaporation.

The objectives included:

1. Setting up a pervaporation unit and testing the apparatus on an ethanol + water system.
2. Preparing a semi-empirical model to predict membrane selectivity using a kinetic approach with Aspen Custom Modeler® V11 for simulating the ethanol + water pervaporation process.
3. Modelling and simulating an ethanol + water system using Aspen Plus® V11 using the experimental data to validate the model.
4. Comparing the model trend to experimental data in existing literature for varying permeate pressure, feed temperature and composition.
5. Modelling and simulating two additional alcohol systems (propan-1-ol + water, propan-2-ol + water), validating the models against experimental data and varying the operating conditions for an optimized design.
6. Designing and optimizing a membrane process for the dehydration of an industrial propan-2-ol stream with a comparison to commercial separation operations.
7. Performing an economic evaluation of the designed industrial process with a cost comparison to extractive distillation.

Although the concept of pervaporation has been applied for many years, most of the research studies have investigated the process solely on an experimental scale. There is little research available on how to model and simulate membrane separation such that the process can be adapted into large scale industries for commercial use, especially for aqueous C3 alcohol systems. The purpose of this study was to develop methodology and expertise in this area of membrane separation which was performed via experimental and simulation-based work.

1.2 Background

The focus of this study is the separation of azeotropic mixtures by pervaporation. Pervaporation is a simple yet effective technique in which the partially permeating specie is drawn through a membrane due to the driving force of vacuum pressure. Azeotropes form when systems deviate from Raoult's law and present themselves as minimum- or maximum-boiling points (Seader et al., 2011) at a specific composition. There are generally two types of azeotropes in terms of homogeneity; homogeneous and heterogeneous. Homogeneous azeotropes form in mixtures with one liquid phase whereas heterogeneous azeotropes appear when more than one liquid phase is present. The number of liquid phases correspond to the number of components in the system (Seader, et al., 2011). The vapour and liquid phases will be in equilibrium and will have the same composition at the mixture boiling point (Sinnott & Towler, 2009). The separation of azeotropic mixtures such as alcohol/water systems often require complex methods which include enhanced distillation techniques, membrane separation, absorption and adsorption.

Although enhanced distillation is capable of breaking an azeotrope, the additional expense of a solvent, supplementary distillation columns, corrosion and other mechanical failures render these options unfavourable. Absorption poses the problem of expensive packing/numerous trays and the requirement of an absorbent. Additionally, adsorption requires a suitable solvent and solvent recovery or additional heat for the desorption of the adsorbent (Abdel-rahman et al., 2014).

Unlike the abovementioned processes, pervaporation is based on relative affinity rather than relative volatility (Van Hoof et al., 2004). Various models can be used to predict mass transport in pervaporation with the nature of a model falling into three broad categories: theoretical, semi-empirical, and empirical. Theoretical models are more suited to membrane development applications due to its high mathematical complexity from the large number of molecular parameters used. In contrast, empirical models use low level mathematics and require a large number of experiments to create a database (Lipnizki and Trägårdh, 2001). This makes the model only suitable for preliminary process/module designs, and comparison of membranes. Semi-empirical models, however, can minimise the number of experiments required whilst boosting good extrapolation of results (Lipnizki and Trägårdh, 2001). Therefore, this approach is often implemented in process and module design and is the preferred model of choice in this work.

The process of pervaporation depends on component-component as well as component-membrane interactions (Lipnizki and Trägårdh, 2001). Since each system exhibits a completely unique behaviour, the model development must be customised using literature pertaining to the specific system being studied.

The simple separation method of pervaporation also has a reduced energy consumption as well as operating and capital cost (Aminabhavi et al., 2006). This is due to membrane stages being dependent on the amount of permeant in the feed (Seader et al., 2011). Generally, permeant-rich feed will require more membrane stages whereas a permeant-dilute feed will require fewer stages thereby leading to a small feed preheat requirement. Furthermore, industrial grade membranes usually have a large lifespan of approximately 3 years (Van Hoof et al., 2004) if employed correctly. According to Van Hoof *et al.* (2004), pervaporation also offers an ecological advantage since the process is more environmentally friendly than distillation.

1.3 Overview of thesis

This thesis includes 9 chapters and supporting information presented in Appendices A to E. The focus of the work is presented in two parts, i.e., Part 1: Experimental studies, and Part 2: Modelling and Simulation. Chapter 2 provides a literature review on the separation of binary homogeneous azeotropic mixtures comparing conventional techniques to the proposed method of pervaporation. The effect of crucial operating conditions on membrane separation is explained and recent work highlighting the simulation of pervaporation is discussed.

Thermodynamic fundamentals are reported in Chapter 3. The transport mechanisms of permeation are explained along with derived equations for the solution-diffusion model. Key parameters, such as flux and separation factor, used to assess the performance of membrane separation are introduced and equations are derived from first principles. Mathematical models developed for the simulation of pervaporation are described using thermodynamic and kinetic properties.

The investigation of this report was conducted in two parts. Part 1 presents the experimental undertakings for the ethanol and water system which were performed on the apparatus described in Chapter 4. Due to the experimental results presented in Chapter 5, a more accurate method was required to assess the separation ability of pervaporation. This led to the simulation study presented

in Part 2 wherein the modelling and simulation of a pervaporation system for three alcohol-water systems; ethanol-water, propan-1-ol−water, and propan-2-ol−water is reported.

The simulation study was conducted to develop a more realistic representation of the pervaporation process for the alcohol-water systems and to fully explore the advantages and limits of pervaporation in industry. Chapter 6 of Part 2 details the method used to develop working models of pervaporation with Aspen Custom Modeler® as well as the manner in which simulations were set up in Aspen Plus®. Chapter 7 details the simulated results of three systems (ethanol-water, propan-1-ol−water and propan-2-ol−water) as well as the design of an industrial unit for the dehydration of propan-2-ol. The latter also included a feasibility study to determine the optimal design and a cost comparison to traditional methods of separation.

Chapter 8 provides the conclusions drawn from the extensive study conducted. Finally, further improvements based on observations made during the model compilation are explained in Chapter 9.

CHAPTER 2

Literature Review

This chapter presents a concise summary of the methodologies applied in separating alcohol-water mixtures, the experimental methods and the pervaporation models reported in literature for alcohol/water systems.

Enhanced distillation techniques are generally used to separate azeotropic mixtures of alcohols and water. This is usually branched into six methods namely, extractive distillation, homogeneous and heterogeneous azeotropic distillation, salt distillation, pressure-swing distillation, as well as reactive distillation. Each technique has the advantage of being able to overcome/avoid the azeotrope present in a mixture. However, there are disadvantages with respect to the quality of the feed applicable/product obtained and the specific operating conditions and costs.

Extractive distillation is usually limited to employing high-boiling solvents. This differs when applying the method of homogeneous azeotropic distillation. Salt distillation is limited by several operational challenges that include corrosion, malfunction of the mechanism used to meter the salt into the column, as well as increased foaming of the fluids. Pressure swing distillation requires two-column operation and strict control measures. In some cases, the azeotrope may not be pressure sensitive, which makes this option unviable. Reactive distillation is energy saving since the heat of reaction can be integrated for the energy requirement of the column. The method is also not hindered by chemical equilibrium since products are removed as they are formed. Each of these methods are described in detail by Sinnott and Towler (2009) and Seader, Henley and Roper (2011).

In consideration of the techniques described above, extractive distillation, azeotropic distillation and reactive distillation are the most widely used in industry. Due to its comparable performance with pervaporation, a detailed description of the manner in which these methods are employed in industry is contained within this chapter. Sections A.1 and A.2 of Appendix A can be consulted for the application of salt distillation and pressure-swing distillation, respectively as performed in industry.

2.1 Conventional methods of separating the alcohol/water systems in industry

There is great interest in the separation of ethanol and water due to the industrial versatility of ethanol. Apart from using ethanol as a raw material, it can be used as an additive to gasoline (octane enhancer) and as a complete substitute of gasoline (gasoline replacement) (Gomis et al., 2007; Weiss et al., 1992). Ethanol has a higher-octane number than gasoline and when used as an octane enhancer in fuel, it improves the blending properties (Ahmed et al., 1989). Hence, the most important function of ethanol is the ability to be used as a clean burning fuel and its potential of being a renewable energy source. For this use and numerous other solvent applications, the ethanol must be dehydrated (Weiss et al., 1992).

Similarly, propan-1-ol is known for its ability to be converted to a diesel biofuel by an esterification reaction (Pla-Franco et al., 2015). The biodiesel produced from propan-1-ol has a cetane number comparable to that of commercial diesel. It has low toxicity and is biodegradable creating a clean fuel (Farobie et al., 2016). However, the dehydration of propan-1-ol is difficult due to the presence of the azeotrope with water. In addition, propan-2-ol can be used in the transesterification process for the development of biodiesel and is a common disinfectant. Propan-2-ol has a low polarity enhancing the miscibility with oil which makes it a better reactant during catalysed conversion (Karmakar et al., 2020). Although propanol isomers can be used in biofuel production, these components are widely used as solvents in many other industries including those producing personal care items and pharmaceuticals (Urtiaga et al., 2006).

2.1.1 Extractive distillation

Extractive distillation of ethanol and water is usually performed with the use of two columns; an extractive distillation column and a solvent recovery column. The extractive column serves the purpose of removing anhydrous ethanol as a distillate. A mixture of water and solvent is then fed to the recovery column where a water distillate is separated from the bottoms solvent to be recycled to the main distillation column. The most common solvent used for an ethanol-water separation is ethylene glycol (Black and Ditsler, 1974; Gil et al., 2008; Lynn and Hanson, 1986; Rojas et al., 2016; Weiss et al., 1992). The limitation of extractive distillation is the high energy consumption which translates to a high process cost (Weiss et al., 1992). According to Weiss, Herfurth and Meirelles (1992), favourable process parameters can reduce the energy consumption for the

system. It was found that the energy consumption of the main extraction column was strongly dependent on reflux ratio while the solvent-to-feed ratio had a smaller effect. In this case, the feed concentration controlled the reflux ratio without causing a disturbance to the operating conditions. In addition, a feed mixture in the vapour phase was found to further reduce the energy consumption. The latter posed an issue of a lower ethanol purity which was accommodated for by raising the solvent-to-feed ratio (Weiss et al., 1992).

Conventional extractive distillation processes consist of two columns. However, Li & Bai (2012) proposed a three-column sequence to create a thermally coupled distillation arrangement. In this arrangement the extractive distillation column produced a distillate of nearly pure ethanol. The solvent recovery column separated an ethanol-water distillate from the pure solvent. Finally, the separation of the third column, known as the concentrator, resulted in a pure bottoms product of water and an azeotropic mixture being recycled as a main feed. Unlike conventional 2-column methods, the extractive distillation strategy proposed by Li and Bai (2012) found it is not necessary to withdraw ethanol completely from the extractive distillation column for two reasons; ease of operation, and at least a 50% reduction in the energy consumed as compared to technologies with alternative solvents such as gasoline and ethylene glycol–potassium acetate.

The extractive distillation and solvent recovery columns operated with lower reflux ratios (0.1 and 0.5) in comparison to the two-column arrangement (0.5 and 1.0) which affected the heat duties and ethanol quality. Although the three-column sequence was able to produce a higher ethanol concentration of 99.95 mol%, the conventional arrangement resulted in an energy saving of 0.3 MJ/kg ethanol for the production of 99.5 mol% ethanol in the distillate. The solvent used in both cases was ethylene glycol. Despite the above, the total annual cost of both methods is the same. This is due to the difference in the reflux ratios, recycle flow rates and usage of entrainer implemented into the strategy of Li & Bai (2012).

Pla-Franco et al. (2015) focused on the dehydration of propan-1-ol using various environmentally friendly solvents in the extractive distillation process. Previously, a series of studies were conducted by the authors using solvents such as 2-methoxyethanol and n-propyl acetate (Pla-Franco et al., 2014, 2013). Ethylene glycol, however, was of particular interest since it is commonly used as an entrainer to separate ethanol-water mixtures. This is due to its low toxicity and reduced vapour pressure (Pla-Franco et al., 2015). In the study, a two-column distillation

sequence was simulated with Aspen Hysys® wherein pure propan-1-ol was obtained as a distillate in the extractive column while the recovery column separated water in the distillate from ethylene glycol in the bottoms. The study reported an optimum solvent-to-feed ratio of 3 and confirmed that a preconcentration column was not required for the separation of the components using ethylene glycol.

The research performed by Jia et al. (2018) simulated extractive distillation using Aspen Plus® and designed two sequences: one implementing N-methyl-2-pyrrolidone (NMP) as the solvent and the other using ethylene glycol. The latter resembled the sequence configured by Pla-Franco et al. (2015). However, the use of NMP as a solvent required a 3-column arrangement inclusive of a preconcentration-distillation step (Jia et al., 2018). This resulted in an 85.5% increase in TAC when compared to the use of ethylene glycol.

An energy-efficient approach to separating propan-2-ol−water mixtures using dimethyl sulfoxide (DMSO) as the entrainer was suggested by Liang et al. (2014). In the study, a two-column process was proposed whereby the preconcentration column and entrainer recovery column were combined. This is known as decomposition and is commonly implemented when a sidestream column is implemented. Therefore, the complex first column consisted of two feed streams and three product streams. It was found that a 20 mol% propan-2-ol feed could be separated to provide pure product streams with 99.99 mol% propan-2-ol, water and DMSO. The process was compared to a conventional 3-column approach and a 12.1% saving in TAC was observed (Liang et al., 2014). This was due to the elimination of a condenser and the reduced heat transfer area of the sidestream reboiler which led to a 10.7% reduction in capital investment as well as a 13.7% saving in energy consumption.

The rising interest in sustainable development has caused many companies to become environmentally conscious and go green with their operations. The recent literature also shows this trend, as seen with the work of De et al. (2019) and Hartanto et al. (2019) both of which investigate the use of environmentally friendly solvents for the dehydration of propan-2-ol with extractive distillation. Hartanto et al. (2019) proposed the use of glycerol, a by-product of biodiesel production, as a solvent since it is inexpensive, sustainable, eco-friendly and has a low vapour pressure. De et al. (2019) compared the performance of a conventional organic solvent: glycerol, a saline entrainer: a blend of glycerol and magnesium chloride, and a deep eutectic solvent (DES):

choline chloride-glycerol. The saline entrainer outperformed the conventional and DES solvent-based operations with a TAC saving of 32.5 and 21.4% respectively (De et al., 2019). In addition, only two columns were required for the distillation sequences simulated. Therefore, the number of columns required for extractive distillation is clearly dependent on the type of solvent used for the binary system.

Table 2.1 briefly summarizes some important applications of extractive distillation for alcohol-water systems from the literature. These have been selected based on lowest energy requirements. It is evident that alternative solvents can replace pure ethylene glycol for the separation of ethanol/water. This can reduce the number of stages in the main distillation column. According to Gil *et al.* (2008), a solvent mixture of ethylene glycol and calcium chloride significantly reduces the energy requirement from 4853 kJ/kg using a benzene entrainer (Chianese and Zinnamosca, 1990) to 1204 kJ/kg ethanol with an 18-stage extractive column. Although the energy requirements for the extractive distillation of propan-1-ol− and propan-2-ol−water systems are not extensively available in the literature, literature sources indicate that mixtures can be separated with various solvents to produce a highly concentrated alcohol of approximately 99 mol%. The solvent selection, reflux ratio and solvent-to-feed ratio contribute to the overall process design and energy consumption (Gil et al., 2008) thereby impacting the cost.

Table 2.1. Extractive distillation for various aqueous alcohol mixtures.

System	Solvent	Main Column							Recovery Column		Reference
		S/F	Solvent stage location	Feed stage location	Total theoretical plates	Product alcohol (mol%)	R	Energy requirement (kJ/kg)	R	Energy requirement (kJ/kg)	
ethanol-water	Ethylene glycol	0.6	2	12	24	99.5	0.5	1528	0.2	232	(Weiss et al., 1992)
	Ethylene glycol	0.62	3	24	32	99.4	2	-	2	-	(Rojas et al., 2016)
	Benzene	-	4	-	29	99.3	-	4853	-	-	(Chianese and Zinnamosca, 1990)
	Ethylene glycol and calcium chloride	0.3	3	12	18	99.5	0.35	1204	0.25	221	(Gil et al., 2008)
propan-1-ol–water	Ethylene glycol	3	25	3	30	99	1.32	-	0.426	-	(Pla-Franco et al., 2015)
	1-Methylpyrrolidin-2-one (NMP)	1.1	6	44	57	99.9	2	5114	0.97	1851	(Jia et al., 2018)
propan-2-ol–water	Glycerol	0.27	2	20	25	99.27	0.5	-	2	-	(Hartanto et al., 2019)
	(Methanesulfinyl)methane (DMSO)	0.88	6	40	48	99.9	0.52	1324	0.72	720	(Liang et al., 2014)
	Choline chloride-Glycerol (1:2)	1	3	15	23	99.9	-	1794	-	513	(De et al., 2019)

R – reflux ratio.

2.1.2 Homogeneous azeotropic distillation

Although homogeneous azeotropic distillation can be economically feasible and has the ability to outperform heterogeneous distillation, the latter can be used when the entrainer forms an additional azeotrope in the system to shift the distillation boundary. In this case, the choice of entrainer is extremely important. A good entrainer will shift the azeotrope and raise the relative volatilities between the two constituents with a small entrainer loading. Furthermore, efficient entrainers will produce the lowest total annualised cost which is assessed with the use of minimum trade-off curves (Lionel Laroche et al., 1991). Minimum trade-off curves are constructed with the minimum reflux ratios as a function of feed ratio. The minimum reflux ratio determines the operating expenses which is estimated to contribute to half of the total annualised cost in the separation sequence. Entrainer screening is followed by determination of the separation sequence arrangement (Lionel Laroche et al., 1991). Application of homogeneous azeotropic distillation for ethanol-water separation is limited and heterogeneous separation is generally more economical. Some potential entrainers for the homogeneous azeotropic distillation of ethanol-water systems is presented in Table 2.2. Similar data for propanol isomer-water systems is not readily available.

Table 2.2. List of possible entrainers for homogeneous azeotropic distillation of ethanol/water system (Doherty et al., 1991).

Entrainer	T_{bp} (K)	Entrainer	T_{bp} (K)
ethylene glycol	470.55	acetic acid	391.15
meso-2,3-butanediol	456.15	n-butyl alcohol	390.15
2-aminoethanol	443.65	ethyl butyl ether	365.35
N,N-dimethylformamide (DMF)	426.15	cyclohexene	355.90
2-ethoxyethanol	406.15	isopropyl alcohol	355.65
isoamyl alcohol	405.15	N-butylamine	350.95

T_{bp} – Normal boiling point.

2.1.3 Heterogeneous azeotropic distillation

The separation of an ethanol-water mixture using heterogeneous azeotropic distillation is often carried out using a non-polar hydrocarbon such as benzene or cyclohexane as the entrainer (Gomis et al., 2007) as they are immiscible with water and create a heterogeneous azeotrope in the system.

Due to the carcinogenic properties of benzene, alternative entrainers such as carbon tetrachloride, trichloroethylene and ethyl acetate have also been considered. These components exhibit similar trends in the residue curve map to benzene and generally perform equally as well (Pham and Doherty, 1990). Again, a two-column sequence is required, with the first column being the pre-concentrator which is followed by the main extraction column. A third and, in some cases, fourth column is added to the separation to recover the entrainer. Although heterogeneous mixtures may decrease the mass transfer efficiency on column trays, heterogeneous azeotropic distillation has been shown to be a feasible technique for a wide range of operating conditions.

A study conducted by Gomis *et al.* (2007) attempted to reduce the energy demands of purifying ethanol for gasoline purposes. Instead of completely dehydrating ethanol, isooctane was used to obtain a "dry" mixture of ethanol and hydrocarbon to be employed directly as a gasoline additive. The reboiler heat duty of this heterogeneous distillation was the most critical parameter. Although a sequence with low heat duties produced a mixture of ethanol and isooctane, an excess amount of water was found in the bottoms product stream. High duties caused malfunction of the azeotropic distillation column by condensing the top stream producing only one liquid phase (Gomis et al., 2007). The major concern was that the reboiler duties must be straddled between the given range to produce a mixture suitable to be used as a carburant. A list of entrainers for heterogeneous azeotropic distillation from the literature is presented in Table 2.3.

Table 2.3. Heterogeneous azeotropic distillation for various binary alcohol systems.

System	Entrainer	Reference	System	Entrainer	Reference
Ethanol-water	Benzene	(Pham and Doherty, 1990)	n-Propanol-water	Isooctane	(Pienaar et al., 2013)
Ethanol-water	Butanol		n-Propanol-water	Cyclohexane	(Lee and Shen, 2003)
Ethanol-water	Carbon tetrachloride		n-Propanol-water	n-Propyl acetate	(Janakey Devi et al., 2017a)
Ethanol-water	Cyclohexane		Propanol-water	Butanol	(Pham and Doherty, 1990)
Ethanol-water	Ethyl acetate		Isopropanol-water	Benzene	
Ethanol-water	Ethyl ether		Isopropanol-water	Cyclohexane	
Ethanol-water	Isooctane		Isopropanol-water	Isooctane	(Font et al., 2004)
Ethanol-water	Pentane		Isopropanol-water	n-propyl acetate	(Janakey Devi et al., 2017b)
Ethanol-water	Trichloroethylene		Isopropanol-water	isopropyl acetate	

2.1.4 Reactive distillation

Catalytic reactive distillation describes the process of when a homogeneous or heterogeneous catalyst is used to carry out a reaction within the distillation vessel. It was previously found that catalytic distillation of ethanol-water with the use of isobutylene could remove 90% of the water whilst providing a final product suitable to be used as a fuel additive (Dirk-Faitakis and Chuang, 2004).

A study conducted by An *et al.* (2014) proposed a reactive distillation column capable of overcoming the azeotrope limitation and producing anhydrous ethanol. The reaction kinetics included two reactions; a hydration reaction and an ethoxylation reaction. The former produced ethylene glycol by hydration of ethylene oxide. By-products, diethylene glycol (DEG) and triethylene glycol (TEG), were formed. However, the process was designed for selectivity to ethylene glycol. The ethoxylation reaction described the reaction between ethanol and ethylene oxide which produced short-chain polymers such as ethylene glycol monoethyl ether (EGME) and diethylene glycol monoethyl ether (DEGME). A single column was operated with dehydrated ethanol being recovered as a distillate and the bottoms stream contained a mixture of the heavier components. Natural heat integration was achieved by absorbing the heat of reaction into the heat required for separation in the column (An et al., 2014). This offers an improvement to the conventional reactive distillation methods used to separate ethanol and water. A reboiler duty of 5.32 MJ/kg anhydrous ethanol was required. Although the energy requirement to produce absolute ethanol is far greater compared to the 0.8 MJ/kg ethanol presented by Dirk-Faitakis and Chuang (2004), the by-products such as EG, DEG, TEG, EGME and DEGME are widely used in the industry of fine-chemicals (An et al., 2014) and can offer economic advantages. Table 2.4 presents a list of reactive distillation applications involving alcohols.

The hydration of propylene to produce propan-2-ol is a common process implemented in the solvent industry. Reactive distillation combines the reversible reaction with distillation to improve the efficiency of the process. This can be achieved with two methods; using excess propylene (molar ratio of propylene to water being 1.5:1) as reported by Wang and Wong (2006) or using excess water (molar ratio of propylene to water being 1:2.05) as outlined by Chua et al. (2017). Both methods were optimized for 99.9 mol% propan-2-ol and resulted in comparable reboiler

duties of 19.4 and 18.7 MJ/s for excess propylene and excess water in the feed, respectively. However, row 4 and 5 of Table 2.4 indicate a substantial difference in the total number of stages in the reactive distillation column which was expected to impact the total annual costs. According to the cost comparison performed by Chua et al. (2017) for both reactive distillation methods, the unit cost of production for propan-2-ol was only 1.7% lower for the method of excess water as compared to the method of excess propylene. This was due to the use of DMSO as an entrainer and additional distillation column implemented in the method of excess water (Chua et al., 2017).

Table 2.4. Reactive distillation involving alcohols.

System	Chemical addition	Total number of stages	Feed stage location	Column pressure (kPa)	D/F	R	Liquid holdup (m^3)	Reference
Ethanol-water	Ethylene oxide	22	17	600	0.8	7	1.1	(An et al., 2014)
Ethanol	Dimethyl carbonate (DMC)	30	20	101.3	-	6	0.00001	(Luo and Xiao, 2001)
Methanol*	Acetic acid	10	3	101.3	0.6275	5	-	(Sakhre, 2019)
Propylene*	Water	28	5	2026.5	-	30	-	(Wang and Wong, 2006)
Propylene	Propane	17	4	2000	0.07	15	-	(Chua et al., 2017)

* For the production of isopropanol.
D/F – Distillate-to-feed ratio.
R – Reflux ratio.

2.1.5 Energy consumption of separation techniques

The separation techniques discussed above report the optimal design and configuration to obtain high purity outlet streams whilst minimising the energy requirement. All methods listed above employ at least one reboiler and condenser for the stripping and rectifying sections respectively of the column.

Reactive distillation is the only method that can be operated using a single column since the reaction takes place in the upper portion of the column and desired products are removed whilst being formed (Sinnott and Towler, 2009). An *et al.* (2014) reported a 45 – 75% reduction in energy

consumption compared to azeotropic and extractive distillation for an ethanol-water system. However, there are a few limitations to the abovementioned technique. Additional cost for a catalyst may be incurred to facilitate a reaction. This may prove to be expensive depending on the reaction and components involved (Mueanmas et al., 2010). Furthermore, the pressure of the reactive distillation column controls the column temperature which is vital. A low temperature would result in a poor reaction rate. Since these chemical reactions generally take place in the liquid phase, the temperature is set as close as possible to the boiling point of the mixture (An et al., 2014). Undesirable by-products may have to be separated and discarded or sold.

Iqbal and Ahmad (2016) suggested that pressure-swing distillation is the most economical of the enhanced distillation methods for aqueous alcohol systems. However, the process requires two columns to obtain purity of both components in a binary mixture. This raises the capital cost of the process. In addition, the process is governed by the effect of pressure on the azeotrope. If the azeotrope composition does not change considerably with a change in pressure, the separation scheme cannot be employed. Therefore, the use of pressure-swing distillation is limited.

The use of a solvent, salt or an entrainer is imperative for the operation of the remaining separation processes. Each of these additives are fed separately from the feed to the column with both inlet streams requiring heating. This immediately increases the operational cost. Homogeneous and heterogeneous azeotropic distillations require the use of at least two columns (Seader et al., 2011). The use of a decanter for the latter technique raises the capital cost further. Laroche *et al.* (1991) stated that decanting may be included in the condenser to create a more economically feasible process. However, this is difficult to operate, and a disturbance would be likely to cause phase separation within the column thereby reducing the efficiency (Lionel Laroche et al., 1991).

The issue of maintaining one liquid phase in the column for heterogeneous azeotropic distillation can be overcome by manipulating the operating conditions of the condenser or using a mixture of aqueous and organic phases from the decanter as a reflux, so that the heterogeneous mixture only exists when approaching the decanter. Water can be added to the decanter or the temperature of the decanter can be reduced for a system with a minimum-boiling azeotrope (Chemstations Inc., 2020). Alternatively, the high cost and phase maintenance can be avoided by implementing a dividing-wall column to replace the two-column operation. In a study conducted by Kiss and

Suszwalak (2012), ethanol was dehydrated with an azeotropic dividing-wall column with the use of n-pentane as the entrainer and an energy saving of 20.2% was obtained.

Pervaporation poses an economically feasible process due to low utility costs incurred. Feed temperature has a significant impact on permeate flowrate. However, the temperature is optimized to reduce cost and avoid boiling of the retentate in the cell. This is in contrast to reactive distillation which operates as close to the boiling point as possible. In addition, a feasible heat network may be devised since the permeate is required to be condensed before collection and sampling. Table 2.5 provides an economic analysis of the energy consumption across the various methods discussed. Pressure-swing distillation has the highest energy consumption with heterogeneous azeotropic and salt distillation being a tenth lower, extractive distillation moderately lower and pervaporation significantly lower than all mentioned techniques. The high energy cost implication of pressure-swing distillation deems the method unfavourable to industry, and therefore, was not discussed in detail for the separation techniques considered in this report. It is far more plausible to compare pervaporation to extractive distillation since it has a greater likelihood of being implemented in large-scale operations.

Table 2.5. Comparison of energy requirement for various ethanol-water separation processes (compiled in this study).

Separation method	Specific energy consumption kJ/kg ethanol	Concentration mol% ethanol	Reference
Extractive distillation	1390	99.5	(Weiss et al., 1992)
Salt distillation	1998	99.998	(Llano-Restrepo and Aguilar-Arias, 2003)
Pressure-swing distillation	25262	99.7	(Mulia-Soto and Flores-Tlacuahuac, 2011)
Heterogeneous azeotropic distillation	2200	38.93	(Gomis et al., 2007)
Reactive distillation	5320	98.983	(An et al., 2014)
Pervaporation	472	99.8	(Mulder, 1994)

2.2 Pervaporation

Membrane separation has become increasingly popular in industry due to its reduced energy consumption and substantial reduction in operating and capital cost (Aminabhavi et al., 2006). The method employs a semipermeable barrier to separate a mixture containing two or more miscible

components into a retentate and permeate. The feed can exist either as a gas or liquid phase. Some liquid feed membrane-separation process applications include dialysis, reverse osmosis, and pervaporation (Seader et al., 2011).

Pervaporation is a separation method in which a heated liquid feed is separated using a membrane. This results in two outlet streams in continuous operation; a liquid retentate and a vapour permeate. The vapour phase of the permeate is a result of the downstream vacuum. The pressure differential created across the membrane acts as a driving force for pervaporation facilitating the permeation of the favourable component. The feed and retentate maintain a liquid phase since the feed compartment of the pervaporation cell is exposed to a high enough pressure (Seader et al., 2011). Phase change across the membrane sets pervaporation apart from the other barrier separations mentioned above (Roizard and Favre, 2012). Figure 2.1 represents a typical pervaporation cell with $P_1 > P_2$. A membrane separates the feed compartment from the permeate-side and separates the components in the feed mixture. The resulting permeate stream is highly concentrated with the preferentially permeating specie. Consequently, the non-selective specie enriches the retentate stream (Seader et al., 2011). The type of membrane employed, either hydrophilic or hydrophobic, determines the component to permeate preferentially. Seader et al. (2011) emphasized that although a membrane is selective to one component, finite permeation of the remaining components will occur.

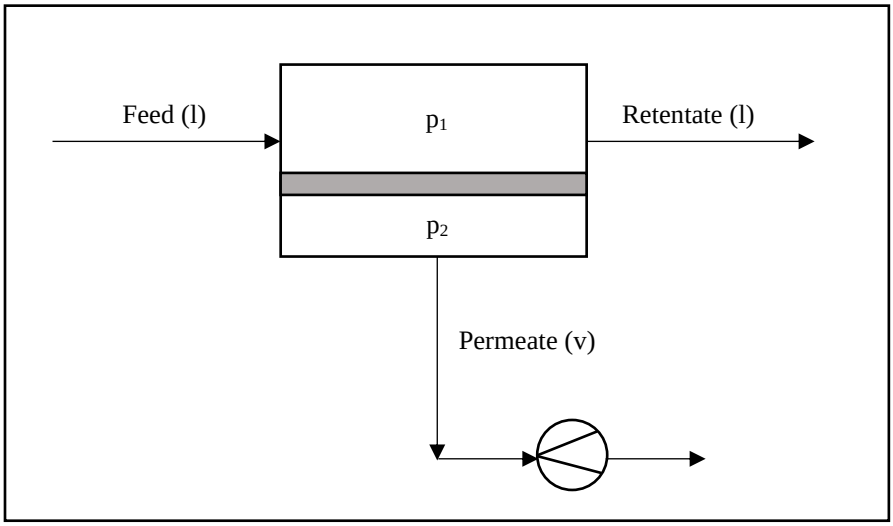

Figure 2.1. Schematic of a typical pervaporation process.

The concept of pervaporation was first described by Kober (1917) to explain the disappearance of liquid contained within a tightly sealed collodion bag. Further experiments were then carried out to investigate the effects of spontaneous and heat-induced pervaporation (Kober, 1917). Another prominent leader in membrane-separation is Binning and co-workers (Binning et al., 1961). The energy crisis of the 1970's precipitated interest in pervaporation technology. This led to the investigation and implementation of pervaporation-assisted distillation in the late 1980's (Scharzec et al., 2017). Finally, as reported by Lipnizki et al. (1999), economics and applications of these hybrid systems were realised and employed in pilot plants as well as on an industrial scale. These early findings made the commercial application of pervaporation techniques possible.

There are many industrial operations that make extensive use of pervaporation today. GFT of Sulzer Chemtech, previously owned by Deutsche Carbone, design and manufacture pervaporation systems that use non-porous membranes to separate azeotropic mixtures such as alcohols or esters in water (Process Engineering, 2000). In addition, pervaporation membranes developed at the BP Research Centre were commercialised by Kalsep, BP's Separation Company which was acquired by Smith & Loveless, for the dehydration of alcohols and other organic liquids (Naylor, 1996). However, it was the first Lurgi commercial-scale pervaporation plant which was designed for the dehydration of alcohols using PVA composite membranes that revolutionized the ethanol dehydration industry. This plant was located at a pulp and paper mill in Germany. The spent liquor from the pulping process ferments to produce ethanol which requires dehydration (Sander and Soukup, 1988).

2.2.1 Types of membranes

Membranes are generally made from either processed natural polymers or synthetic polymers both of which can be classified as amorphous or crystalline. Amorphous polymers display a glassy appearance in contrast to the opaquer crystalline polymer (Seader et al., 2011). In addition, membranes are characterised as macroporous, microporous or non-porous (dense).

Microporous membranes have high permeability but low selectivity for small molecules making separation difficult. Thin-film composite membranes are a means to combat the problem. A thin dense skin, known as a permselective layer, is layered overtop a thick supporting microporous layer. Pervaporation uses a composite membrane that is selective to one component with partial

finite permeability to the second component. The liquid feed of the pervaporation system is exposed to the dense, thin-film side of the membrane (Seader et al., 2011).

Two transport mechanisms are generally used to describe membrane separation namely; the solution-diffusion model and the pore flow model. Porous membranes can be described using the pore-flow mechanism whilst solution-diffusion adequately represents the design of dense membranes. Pore-flow suggests that a pressure-driven convective flow separates the permeating species through the membrane pores. In contrast, the solution-diffusion model proposes that the permeants dissolve into the membrane and diffuse through due to a concentration gradient (Wijmans and Baker, 1995).

The solution-diffusion model describes mass transport in pervaporation in three steps. The first step is sorption of the permeating species through the upstream surface of the membrane. Step two is the diffusion through the membrane material. The third and final step is desorption of the permeant as a vapour on the downstream surface of the membrane (Zhang and Driol, 1995). Wijmans and Baker (1995) mention the main model assumption that the feed and permeate chemical potentials are in equilibrium with the upstream and downstream sides of the membrane respectively.

The driving force of the permeants through a membrane can be pressure, temperature, concentration and/or electromotive force. These parameters are interrelated and represented by chemical potential for the solution-diffusion model which is based on Fick's Law. Flux of a component is measured as a function of chemical potential. The phase of the membrane influences the chemical potential. For an incompressible phase (liquid or solid), the volume is independent of pressure influences. However, the volume of a compressible gas is subjected to pressure changes which will alter the chemical potential function (Wijmans and Baker, 1995).

The key factors for assessing the separation effectiveness of a membrane are flux and selectivity. Process compatibility, longevity, cost, etc. are also key factors. The choice of membrane and feed conditions ultimately play a significant role in the degree of separation to be achieved.

2.2.2 Experimental measurements for pervaporation at the laboratory scale

Numerous standard setups for laboratory pervaporation experiments have been proposed in the literature. The main components of all setups include a pervaporation cell, cold traps and a vacuum pump. Table 2.6 presents a summary of the various arrangements. A revision of the schemes proposed in the literature are described below.

Neel *et al.* (1986) separated water-tetrahydrofuran mixtures using hydrophilic regenerated cellulose membrane and a cooling agent other than liquid nitrogen was suggested. The stainless-steel pervaporation cell designed by Neel *et al.* (1986) consisted of a steel sintered disk inserted between two half-cells and secured with a Teflon gasket. The feed compartment of the pervaporation cell had a magnetic stirrer, and the thermostatic conditions were carefully controlled. A dryer column placed after the cold receivers serve to protect against humidity. In addition, the cold traps were arranged in parallel to condense the permeate alternately so that each could be disconnected separately from the setup. According to Wee, Tye and Bhatia (2008), a parallel arrangement is implemented to perform pervaporation experiments in continuous mode using the equipment setup.

The pervaporation of various alcohol mixtures using polyamide membranes were investigated by Teng *et al.* (2000). In most vertically orientated pervaporation units, the feed is fed above the membrane and the vapour permeate is withdrawn to a condensing cold trap using a vacuum pump. Teng *et al.* (2000) proposed a process having 3 cold traps; 2 arranged in parallel with the remaining cold trap placed in series afterwards.

Alternatively, Lv and Xiao (2011) suggested the use of a glass pervaporation cell with flanges designed to keep the membrane place. The cell also contained a stainless-steel support for the membrane. A heating mantle surrounded the pervaporation cell such that isothermal conditions could be maintained. A PID controller was used to maintain temperature. The permeate vapour was condensed with liquid nitrogen in parallel arranged cold traps to remove permeate alternately. This facilitated continuous sampling at regular intervals. The study investigated the dehydration of water/pyridine mixtures with a cellulose acetate/polyacrylonitrile (CA/PAN) membrane (Lv and Xiao, 2011).

In a recent study by Singha et al. (2013), the standard pervaporation cell was equipped with a stirrer preventing possible concentration and temperature gradients. Additionally, the cell itself

was surrounded by a jacket of circulating water to maintain a constant temperature during the experiment. The membrane was held in place by a sinter disk within the pervaporation cell. The cold traps were arranged in series unlike the literature sources of Neel *et al.* (1986); Teng *et al.* (2000); Lv and Xiao (2011); Rozicka *et al.* (2014). This was due to experiments being performed under batch operation for 2 – 3 hours before permeate collection and analysis was carried out. Therefore, continuous sampling was not required. The study focused on the recovery of pyridine from water/pyridine mixtures using filled and crosslinked EPDM membranes (Singha et al., 2013).

Rozicka *et al.* (2014) assessed the performance of PDMS-based membranes for various binary aqueous mixtures. In the study, the use of a stainless-steel support and an o-ring to provide a seal was employed. The thermostatic condition of the feed was maintained by a jacketed feed tank. The standard pervaporation rig of parallel cold traps was implemented into this setup since the experiments were run in continuous operation mode.

Table 2.6. Summary of various schematic arrangements for pervaporation from literature (compiled in this study).

Reference	Cell specification	Membrane support	Feed heat (Method or Maintenance)	Cold traps			Other differences
				No.	Arrangement	Cooling agent	
(Neel et al., 1986)	Stainless-steel, 110 ml feed capacity. Effective membrane area of 20 cm^2.	Membrane is held by a sintered steel disk	Feed chamber under thermostatic control. Magnetic stirrer to avoid temperature gradients.	2	Parallel	Chilled water or organic solvent, liquid air	● Dryer column to protect against humidity ● No feed tank. Feed heated within pervaporation cell.
(Teng et al., 2000)	Material of construction not reported. Effective membrane area of 10.2 cm^2.	Not stated	Feed was vaporised. Actual method not disclosed.	3	Parallel and series	Liquid nitrogen	● Feed tank separated from membrane module
(Lv and Xiao, 2011)	Glass test cell with effective membrane area of 14.4 cm^2	Membrane supported by highly porous stainless-steel with specially designed flanges	Heating mantels wrapped around feed cell to maintain isothermal conditions. PID controller to maintain temperature.	2	Parallel	Liquid nitrogen	● Feed tank separated from membrane module
(Singha et al., 2013)	Material of construction not reported. Feed compartment capacity of 150 cm^3. Effective membrane area of 19.6 cm^2.	Membrane supported on a Sinter Disk	Jacket around cell with circulating water of constant temperature. Stirrer in feed compartment to avoid temperature/concentration gradients.	2	Series	Liquid nitrogen	● No feed tank. Feed heated in pervaporation cell.
(Rozicka et al., 2014)	Stainless-steel membrane module	Membrane supported by porous stainless-steel	Thermostated feed from jacketed tank is circulated in module.	2	Parallel	Liquid nitrogen	● Feed tank separated from membrane module

2.3 Pervaporation experiments for ethanol (1) + water (2) system

2.3.1 Membrane selection

Membrane separation requires the use of either a hydrophilic or hydrophobic membrane depending on the component to be separated from the binary mixture. A hydrophilic membrane dehydrates the organic feed such that a water-rich permeate is produced. Natural polymers for dehydration purposes include cellulose and its derivatives (Fu et al., 2014). Water soluble polymers with good mechanical integrity are used to create hydrophilic membranes (Singha et al., 2013). Hydrophobic membranes allow organic compounds to preferentially permeate through the membrane. According to Singha et al. (2013), the polymer used to prepare this membrane must possess a similar solubility parameter to the preferentially permeating component.

Zhang and Drioli (1995) suggested numerous hydrophilic membranes that are capable of dehydrating alcohol-water mixtures, which include PAN, PC, PI, polysulfones, PPO, PVA and PVC. The first large-scale plant for the dehydration of ethanol operated in 1988 by GFT Co., Ltd at Betheniville, France employed a PVA membrane (Zhang and Driol, 1995)**.** Previously, it was reported by Kujawski, Nguyen and Neel (1991) that PVA was gaining increasing popularity for industrial dehydration in the 90's. Since then, the most commonly used hydrophilic membrane has been poly(vinyl alcohol) (Win and Friedl, 2012).

The solution-diffusion mechanism, explained in detail in the upcoming Chapter 3, describes permeability as a function of solubility and diffusivity (Feng and Huang, 1996). The solubility of a component in a membrane is determined by the chemical affinity between the penetrating component and the membrane. Diffusion, however, favours the transport of small molecules through a dense membrane. According to Zhang and Driol (1995), in a mixture consisting of two components with a large difference in molecular size, permeation of the specie with the smaller molecule may be preferential despite the bigger molecule having a high solubility. Consequently, water preferentially permeates through many polymeric membranes due to water molecules being much smaller in size than organic molecules. This means that the membrane selectivity of organic over water is less than unity. In order for a hydrophobic membrane to remove organic compounds from a dilute aqueous solution, the material must have a high affinity for organic molecules (Zhang and Driol, 1995). Many hydrophobic membranes exist among which include PDMS, zeolite-filled PDMS, EPDR, SBR, PMS, POMS and PEBA (Rozicka et al., 2014). An organophilic membrane

commonly employed in an alcohol-water system is poly(dimethyl siloxane) (Leppäjärvi et al., 2015). Table 2.7 extracted from Zhang and Driol (1995) provides a summary of the various membrane options available and their applications. The separation that can be achieved using these membranes will depend on the operating conditions and binary system being separated.

Table 2.7. Summary of membrane types and their uses (Zhang and Driol, 1995).

Polymer	Application
Cellulose and derivatives	Extraction of water from an aqueous solution of ethanol, separation of benzene/cyclohexane mixtures
Chitosan	Extraction of water from an aqueous solution of ethanol
Collagen	Extraction of water from aqueous solutions of alcohols and acetone
Cuprophane	Extraction of water from an aqueous solution of ethanol
Ion-exchange resins (Nafion, etc.)	Extraction of water from an aqueous solution of ethanol
LDPE	Separation of C_8 isomers
NBR	Separation of benzene/n-heptane
Nylon-4	Extraction of water from an aqueous solution of ethanol
PA	Extraction of water from an aqueous solution of ethanol, acetic acid
PAA	Extraction of water from an aqueous solution of ethanol, acetic acid
PAN	Extraction of water from an aqueous solution of ethanol
PAN-co-AA	Extraction of water from an aqueous solution of ethanol
PB	Extraction of 1-propanol, ethanol from an aqueous solution
PC	Extraction of water from an aqueous solution of ethanol, acetic acid
PDMS filled with silicalite, molecular sieves, etc.	Extraction of alcohols from an aqueous solution, separation of butanol from butanol/oleyl alcohol mixture
PEBA	Extraction of alcohols and phenol from an aqueous solution, recovery of natural aromas
PI	Extraction of water from an aqueous solution of ethanol. acetic acid: separation of benzene/cyclohexane and acetone/cyclohexane mixtures
Plasma polymerized fluorine-containing polymers	Extraction of ethanol from an aqueous solution
Plasma polymerized PMA	Separation of organic/organic mixtures
Polyion complexes	Extraction of water from an aqueous solution of ethanol
Polysulfones	Extraction of water from an aqueous solution of ethanol, acetic acid
POUA	Separation of benzene/n-hexane mixtures
PP	Separation of xylene isomers
PPO	Extraction of water from an aqueous solution of alcohols, separation of benzene/cyclohexane mixtures
PTMSP/PDMS composite	Extraction of ethanol from an aqueous solution
P'TMSP and derivatives	Extraction of ethanol from an aqueous solution
PUR	Extraction of ethanol from an aqueous solution
PVA	Extraction of water from an aqueous solution of alcohols, acetic acid, ethers, pyridine, etc.
PVC	Extraction of water from an aqueous solution of ethanol
Silicone rubber (PDMS, etc.)	Extraction of alcohols, ketones, hydrocarbons, halogenated hydrocarbons, amines, acetic acid, natural aromas, etc., from an aqueous solution

2.3.2 Operating conditions

(a) Pressure and Temperature

A partial-vapour-pressure difference is the driving force of pervaporation (Wijmans and Baker, 1993). A pressure difference across the membrane must be maintained by creating a vacuum downstream of the membrane while the feed is exposed to atmospheric or elevated pressures (Wee et al., 2008) to maintain the feed in the liquid phase (Vane, 2020). The partial pressure of the desired component must be lower than the equilibrium vapour pressure in order to facilitate the diffusion of the relevant component through the membrane (Wee et al., 2008). Table 2.8 displays the partial pressures for water and various alcohols which are of interest in this study. These values were obtained using the process simulation software Aspen Plus® V9 and the Non-Random Two-Liquid (NRTL) model was applied. The driving force required for specie transport in pervaporation decreases in the order of decreasing partial pressure (propan-1-ol < water < propan-2-ol <ethanol). Absolute pressures are reported in this work.

Table 2.8. Liquid vapour pressure (bubble point pressure) for pure components at 298.15 K and 101.3 kPa.

Component	Ethanol	Water	Propan-1-ol	Propan-2-ol
Partial Pressure (kPa)	7.92405	3.17038	2.80795	5.82111

As demonstrated in the study of Vane (2020), a high feed temperature elevates the partial pressure of individual species, hence a greater pressure driving force is created. This would ultimately result in an increased flux. Therefore, the feed temperature is of particular importance in pervaporation. Multiple literature sources were consulted to determine the operating conditions for the experimental method presented in Chapter 4. This information is summarised in Table 2.9. All sources utilized PVA-based membranes in the ethanol/water separation experiments conducted.

Table 2.9. Summary of ethanol-water systems under different operating conditions.

Reference	Feed temperature (K)	Permeate pressure (kPa)
(Sander and Soukup, 1988)[a]	363.15 – 373.15	1 – 1.5
(Wesslein et al., 1990)	298.15, 333.15, 348.15	2, 10, 20
(Huang et al., 2010)	348.15	< 0.1
(Win and Friedl, 2012)	338.15 – 348.15	2 – 5

[a]LURGI pervaporator developed for research into industrial pervaporation plant.

(b) Feed composition

The separation of alcohol-water systems containing azeotropes are investigated in this study. Separation techniques attempt to obtain high purity output streams from a mixture lying before the azeotropic point. Azeotropic composition is specific to the system being studied. Hence, the feed range considered may differ from one system to another. Table 2.10 illustrates the minimum boiling azeotrope for each system studied at atmospheric feed conditions and a suitable feed range for investigation. T-x-y diagrams for the investigated systems are presented in Chapter 3.

Table 2.10. Suitable feed composition range for various alcohol-water systems.

System	Azeotrope composition at 101.3 kPa (wt.% alcohol)	Feed range (wt.% alcohol)
Ethanol-water	95.62	90 – 100
Propan-1-ol–water	69.23	60 – 100
Propan-2-ol–water	87.27	74 – 100

2.3.3 Effect of operating conditions on membrane performance

The operating conditions of a pervaporation process plays a vital role in the degree of separation achieved. Membrane performance is assessed with the permeate flux, separation factor and selectivity. Three parameters are controlled namely; feed concentration, operating temperature and downstream pressure. The use of a hydrophilic membrane warrants the use of a feed in the upper concentration range for the alcohol (above the azeotrope) to assess membrane performance. Since the type of membrane employed dictates the separation quality obtained, a list of the literature

sources mentioned in this section along with the respective membranes used is presented in Table 2.11.

Table 2.11. Summary of various literature sources examined, and membranes employed.

Reference	Membrane
(Sander and Soukup, 1988)	composite poly(vinyl alcohol)
(Wesslein et al., 1990)	slightly crosslinked, composite poly(vinyl alcohol)
(Huang et al., 2010)	composite perfluoro polymer
(Win and Friedl, 2012)	composite poly(vinyl alcohol)/polyacrylo nitrile

Temperature changes may result in possible changes to the membrane structure and interaction between components in the feed. The maximum operating temperature must be determined from the thermal stability of the membrane material. Permeate flux is dependent on temperature. The temperature function is described with an Arrhenius relation (Sander and Soukup, 1988). It was reported by Win and Friedl (2012) that elevated operating temperatures led to significantly higher permeation fluxes. Alternatively, a decline in the separation factor may be observed (Win and Friedl, 2012).

The use of a vacuum downstream of the membrane maintains the driving force for mass transfer. However, the pressure must be operated below dewpoint to prevent condensation downstream of the membrane (Sander and Soukup, 1988). The influence of permeate pressure on flux and separation factor for an ethanol-water system was reported by Win and Friedl (2012). It was found that increasing pressure produced a decline in both the permeate flux as well as the separation factor.

Early pervaporation studies conducted by Sander and Soukup (1988) investigated the design and operation of a commercial-scale ethanol dehydration pervaporation plant. A poly(vinyl alcohol) composite membrane with three layers, each made from a different polymer and having distinct structure, was used. The selective skin layer was pore-free PVA and had a thickness of 0.5 μm. Flux and selectivity were determined by this layer. The remaining two layers formed the porous substructure beneath the skin layer. First, an asymmetric open-pore polyacrylonitrile layer with 100 μm thickness provided membrane support. Thereafter, a 200 μm thick non-woven polyester

fibre formed the underlining of the composite membrane (Sander and Soukup, 1988). The latter had two purposes; to provide mechanical strength and to allow easy dissipation of permeate vapour. Operating conditions, as reported by Sander and Soukup (1988), can be found in Table 2.9. As the ethanol feed concentration increased from 90 – 100 wt.%, the ethanol concentration in the permeate increased steeply while the water flux decreases linearly. A study later conducted by Wijmans and Baker (1993) presented similar behaviour of feed concentration on permeate flux by creating a model to represent the solution-diffusion with the influence of permeate pressure gradient as the driving force. In addition, the separation factor of an ethanol-water system increases with increasing ethanol feed concentration (Win and Friedl, 2012). Selectivity of permeate ethanol remains constant for a wide feed range with a steep increase at 98 – 99 wt.% ethanol feed (Sander and Soukup, 1988).

Wesslein et al. (1990) investigated the separation of 11 binary mixtures containing water using pervaporation. Temperature and pressure influences were assessed by total flux, partial fluxes and separation factor. The experiments performed made use of a slightly crosslinked, composite PVA membrane produced by GFT-Homburg. The structure of each layer contained within the membrane was not disclosed. The operating conditions applied by Wesslein et al. (1990), as shown in Table 2.9, revealed the membrane was water-selective except when low ethanol feed concentrations and high permeate pressures were applied.

Research conducted by Huang et al. (2010) described the dehydration of ethanol using hydrophilic and hydrophobic perfluoro polymer (PFP) membranes. The membrane used was a multilayer composite membrane in which each layer served to perform a different function. A non-woven paper layer made from polyester or polyolefin acted as a base to provide mechanical strength to the composite membrane (Lokhandwala et al., 2010). A microporous ultrafiltration layer then provided support while a finely microporous layer with a pore diameter in the range of 100 – 500 Å sat above it (Huang et al., 2010). Thin selective perfluoro polymer was layered onto the support for protection.

The performance of PFP coated membranes was compared to that of uncoated hydrophilic cellulose ester membranes. The results indicated that a coated membrane maintained a relatively high selectivity for the full composition range while the uncoated membrane declined in selectivity as the feed water concentration increased. The cellulose ester membrane displayed low selectivities

at high feed water concentrations unlike the PFP coated membranes. This was due to the perfluoro layer providing protection against high water concentrations and thereby, preventing plasticization which allowed the membrane to maintain selective properties for a longer period.

A more recent study by Win and Friedl (2012) investigated the separation of ethanol-water mixtures using pervaporation and compared the results to a modelled separation performance. The composite membrane used consisted of a polyvinyl alcohol based active layer supported by polyacrylo nitrile. As previously mentioned, the study revealed that an increase in permeate pressure leads to a decrease in both flux and separation factor. An increase in feed water concentration and feed temperature both produced an enhanced flux and reduced separation factor (Win and Friedl, 2012). The solution-diffusion model successfully predicted the pervaporation flux when applied to the correlated experimental results.

2.4 Pervaporation experiments for propan-1-ol− and propan-2-ol−water mixtures

Although ethanol-water is the most common system investigated in membrane studies, the dehydration of C3 alcohols is also of particular importance due to its widespread application in industry.

An early study conducted by Nieuwenhuis et al. (1987) investigated the pervaporation of propan-1-ol−water mixtures using water selective membranes composed of poly(vinylpyrrolidone)-poly(methacrylic acid) (PVP-PMAA) complexes. The membranes employed in experiments were cast using varying ratios of PVP and PMAA. Nieuwenhuis et al. (1987) reported that PMAA-rich membranes possessed greater mechanical strength with less swelling and hence, this was the preferred membrane. Maximum swelling occurred at 40 wt.% feed propan-1-ol. In addition, the flux was observed for a feed composition range of 0 – 100 wt.% propan-1-ol. The water flux was found to be dependent on the concentration of feed propan-1-ol whereas the alcohol flux was independent of the presence of water.

Chan et al. (1997) investigated the dehydration of methanol, ethanol, propan-1-ol and propan-2-ol using poly(amide-sulfonamide)s (PASAs). PASAs were used to synthesize a hydrophilic membrane due to the sulfonamide and amide functional groups which enable hydrogen bonding between the polymer and water molecules. The greatest selectivity was observed when exposing

the membrane to propan-1-ol−water mixtures suggesting that selectivity is dependent on the size of the alcohol molecules. Similarly, the various alcohol-water mixtures mentioned above were explored by Will and Lichtenthaler (1992) but with the use of PVA/PAN membranes. GFT mbH supplied the membranes for experiments undertaken and the focus of the research was to compare the performance of vapor permeation to pervaporation. The effect of feed temperature, composition, permeate pressure and membrane temperature were observed. This particular study utilized a full composition range of 0 – 100 wt.% alcohol which resulted in a polynomial trend for the permeate quality and flux.

Dehydration of propan-1-ol using a PVA/PAN membrane was also studied by Teleman et al. (2006). The influence of feed concentration, temperature and permeate pressure were observed during experiments. Flux increased with increasing feed water concentration and temperature whereas an opposite effect was observed for increasing permeate pressures. The feed composition range was limited to 5 – 20 wt.% water (Teleman et al., 2006). Nevertheless, research findings indicated that a PVA-based membrane is highly selective and can produce a good quality permeate of 96 – 100 wt.% water given the feed range which lies beyond the azeotropic composition.

Despite earlier studies investigating the dehydration of propan-2-ol using PVA/PAN (Will and Lichtenthaler, 1992) and PASAs (Chan et al., 1997), Naidu and Aminabhavi (2005) attempted to improve membrane performance by employing sodium alginate (NaAlg) membranes blended with (hydroxyethyl)cellulose (HEC). The mass of HEC was varied between 5 – 20 wt.% when casting the crosslinked membranes to determine the best concentration for optimal selectivity. The membrane consisting of 10 wt.% HEC displayed the greatest selectivity of 30000 with a feed water content of 10 wt.%. This translated to a permeate water content of 99.97 wt.%. However, the selectivity dropped significantly when the azeotropic region was considered. The findings of this study also indicated that zeolite-filled membranes enhanced the water flux whilst maintaining selectivity. The increased water permeation was reportedly due to membrane pores allowing zeolite particles to possess greater capacity for absorption of water.

Pervaporation of C3 alcohols using hydrophilic membranes is not extensively studied in literature. Although PVA is a well-known membrane, the research available for its employment in dehydrating the abovementioned alcohols is still limited. Therefore, the simulation exercises for propan-1-ol−water and propan-2−ol−water reported later in Chapters 6 and 7 were imperative for

an improved understanding of these systems and the separation capability using a PVA-based membrane.

2.5 Simulation of pervaporation units

To address the need for the development of processes for pervaporation studies with C3 alcohols, rigorous simulation and costing studies were conducted in this work to assess the feasibility and potential of these processes.

The concept of laboratory scale pervaporation as a separation technique has become increasingly popular since early studies conducted by Kober in 1912. However, membrane units are still unavailable as standard unit operations on simulator programs. Modelling and simulation tools are currently utilised to create user models from experimental data thereby, creating semi-empirical models for the simulation of membrane modules and pervaporation plants. This is a complex procedure with limited studies to describe the comprehensive development of modelling especially on an industrial scale.

Schiffmann (2014) developed a three-step modelling approach (shortcut, discrete and rigorous) and implemented a user interface to describe the separation of 2-butanol/water for a wide feed composition and temperature. The models were developed and implemented with Microsoft Excel (for the shortcut and discrete models) and Aspen Custom Modeler® (for the rigorous model). Schiffmann (2014) described the models as successive since the calculated results of one model were set as initial values for the next model. The purpose of the user interface, programmed on Microsoft Visual Studio, was to specify operating conditions/parameters and to display the results as diagrams or to allow the user to save the results in a Microsoft Excel file.

Research conducted by Haaz and Toth (2018) investigated the dehydration of an aqueous methanol mixture using experiments and modelling. The experiments were performed with the use of a composite PVA membrane purchased from Sulzer Chemtech Ltd. to estimate parameters for the pervaporation model. The pervaporation subroutine was written and rigorously modelled using the software of ChemCAD. The parameters were validated by comparing the modelled data to measured data. Thereafter, the dewatering process was optimized with a dynamic programming method.

In a recent study, the separation of 2-methylpropan-1-ol/water with a hybrid process of distillation and pervaporation was modelled and simulated by Hassankhan and Raisi (2020). Mathematical models were prepared based on the solution-diffusion mechanism: feed components are absorbed into the membrane, species diffuse through the membrane material and thereafter, the components desorb the membrane as a permeate. This theory is described in detail in Chapter 3 and these procedures were applied in this work. The models were coded using FORTRAN, and Aspen Custom Modeler® was used to integrate the model with Aspen Plus® for further simulation. Hassankhan and Raisi (2020) employed the UNIFAC thermodynamic model to describe the activity of feed components so that the model was applicable to a wider range of temperature and pressure (limited in correlative models like NRTL for the system of 2-methylpropan-1-ol/water). In addition to the UNIFAC model, Lee's equation and Flory-Huggins, with the latter describing the activity of the membrane, were also implemented by Hassankhan and Raisi (2020).

CHAPTER 3

Thermodynamic Fundamentals

3.1 Description of azeotropic mixtures

An azeotrope exists in a mixture when the mole fraction of each species in the liquid phase is equal to that in the vapour phase thereby producing a constant-boiling solution (Smith et al., 2005). This is an indication that the like and unlike interactions differ greatly or that the vapour pressures of the pure components intersect in the region considered. Two types of azeotropes exist depending on the deviation from Raoult's law namely; minimum- and maximum-boiling azeotropes. These extremes are exhibited on phase diagrams in the figures presented below.

A positive deviation from Raoult's law is observed when like interactions are stronger than unlike interactions. The total system pressure is higher than the saturation pressure of the lightest component. This is known as a minimum-boiling azeotrope and is illustrated in the T-x-y of Figure 3.1 (a). Figure 3.1 (b) illustrates the maximum pressure of the same system on a P-x-y diagram.

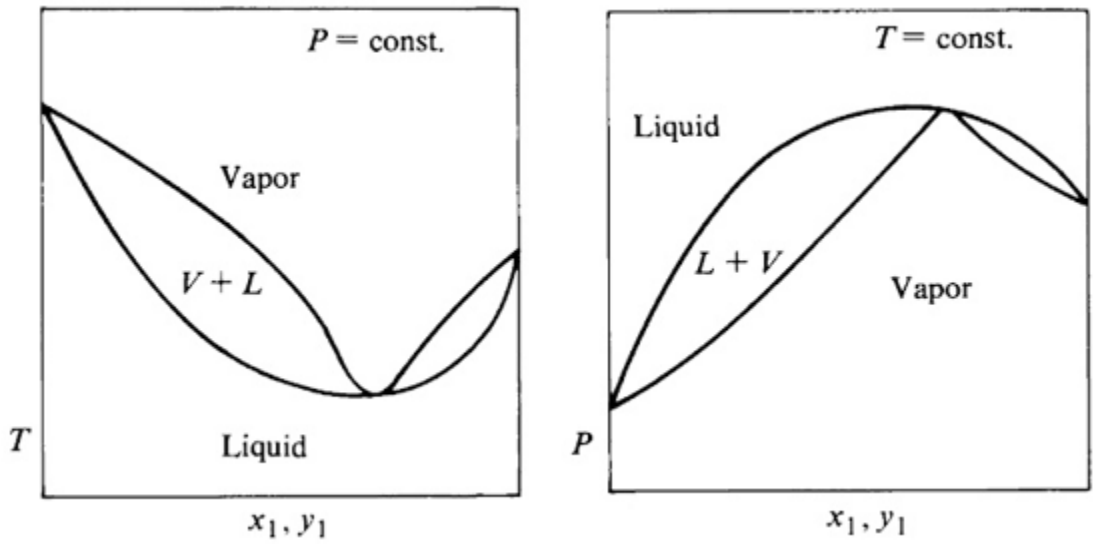

(a) **(b)**

Figure 3.1. Vapour-liquid behaviours of a system containing a minimum-boiling azeotrope (Walas, 1985): (a) Temperature profile; (b) Pressure profile.

A negative deviation from Raoult's law occurs when unlike interactions are stronger than the like interactions. In this case, the total system pressure lies below the saturation pressure of the heaviest component. This is known as a maximum-boiling azeotrope as shown in Figure 3.2 (a). Similarly, the P-x-y of Figure 3.2 (b) displays the point of minimum pressure.

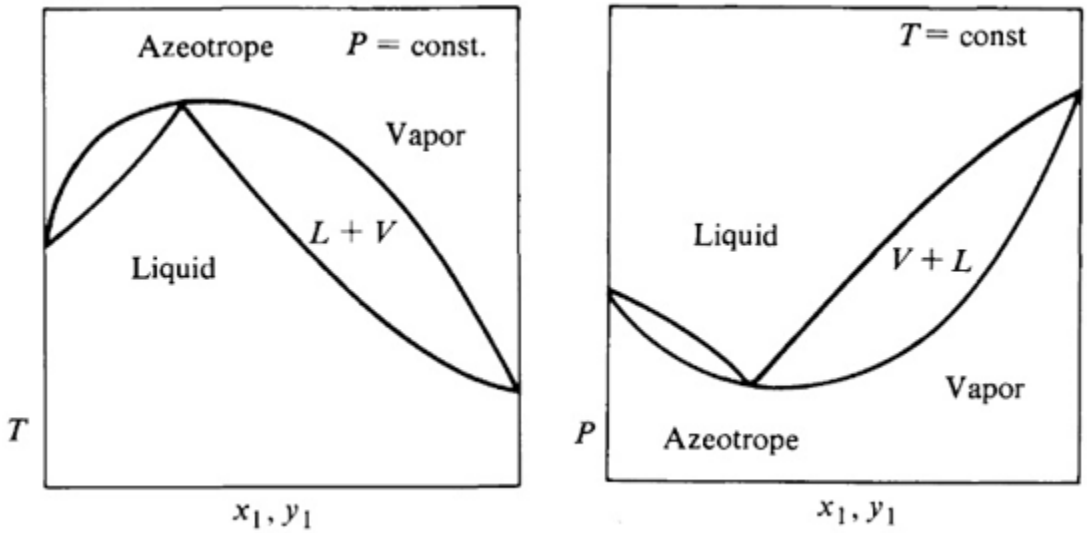

(a) **(b)**

Figure 3.2. Vapour-liquid behaviours of a system containing a maximum-boiling azeotrope (Walas, 1985): (a) Temperature profile; (b) Pressure profile.

3.1.1 Phase diagram of test system

An ethanol and water system exhibits a homogeneous minimum-boiling azeotrope of 95.62 wt.% (89.52 mol%) ethanol at 351.3 K and 101.325 kPa as shown in Figure 3.3. The Non-Random Two-Liquid (NRTL) model was applied to plot the predictive phase behaviour for the ethanol-water system using Aspen Plus® V11.

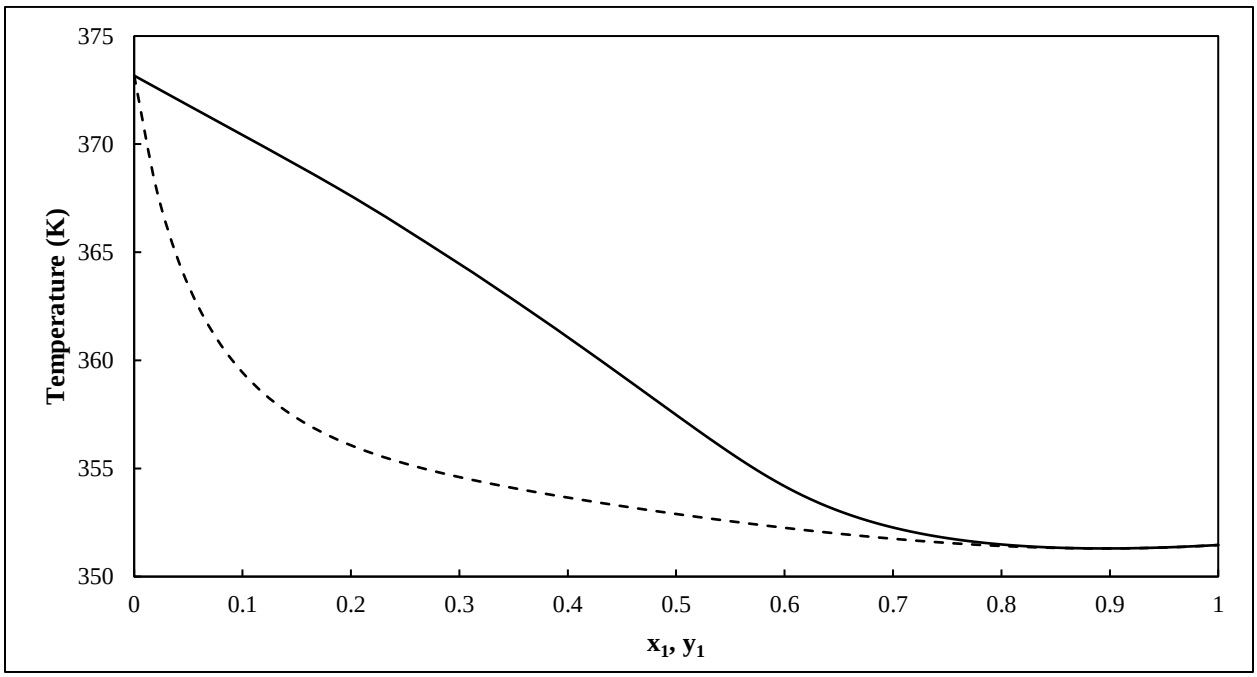

Figure 3.3. T-x-y phase diagram for the ethanol (1) + water (2) system at 101.3 kPa. Solid line (-), dewpoint; dashed line (---), bubble-point.

3.1.2 Phase diagram of C3 alcohol systems

The two main systems investigated in this study included propan-1-ol–water and propan-2-ol–water. The composition at which the azeotrope exists determined the feed composition for the experimental work as mentioned in Section 2.3.3. The Non-Random Two-Liquid (NRTL) model was applied to plot the predictive phase behaviour for the C3-water systems using Aspen Plus®.

The propan-1-ol–water system exhibits a homogeneous minimum-boiling azeotrope of 69.23 wt.% (40.28 mol%) propan-1-ol at 360.82 K and 101.325 kPa. Propan-2-ol and water form a homogeneous minimum-boiling azeotrope of 87.27 wt.% (67.28 mol%) propan-2-ol at 353.33 K and 101.325 kPa. These azeotropes were predicted from the Aspen Plus® software using the NRTL

model. Figure 3.4 and Figure 3.5 illustrate the temperature profiles for the propan-1-ol– and propan-2-ol–water systems respectively.

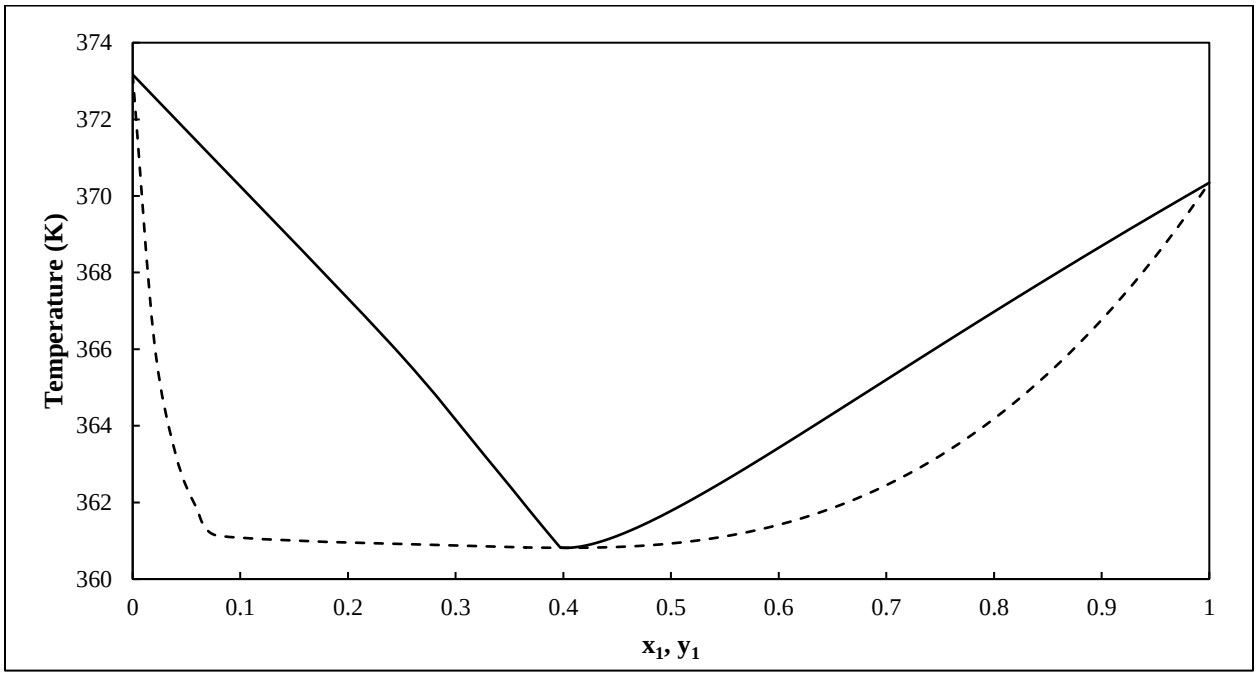

Figure 3.4. T-x-y phase diagram for the propan-1-ol (1) + water (2) system at 101.3 kPa. Solid line (-), dewpoint; dashed line (---), bubble-point.

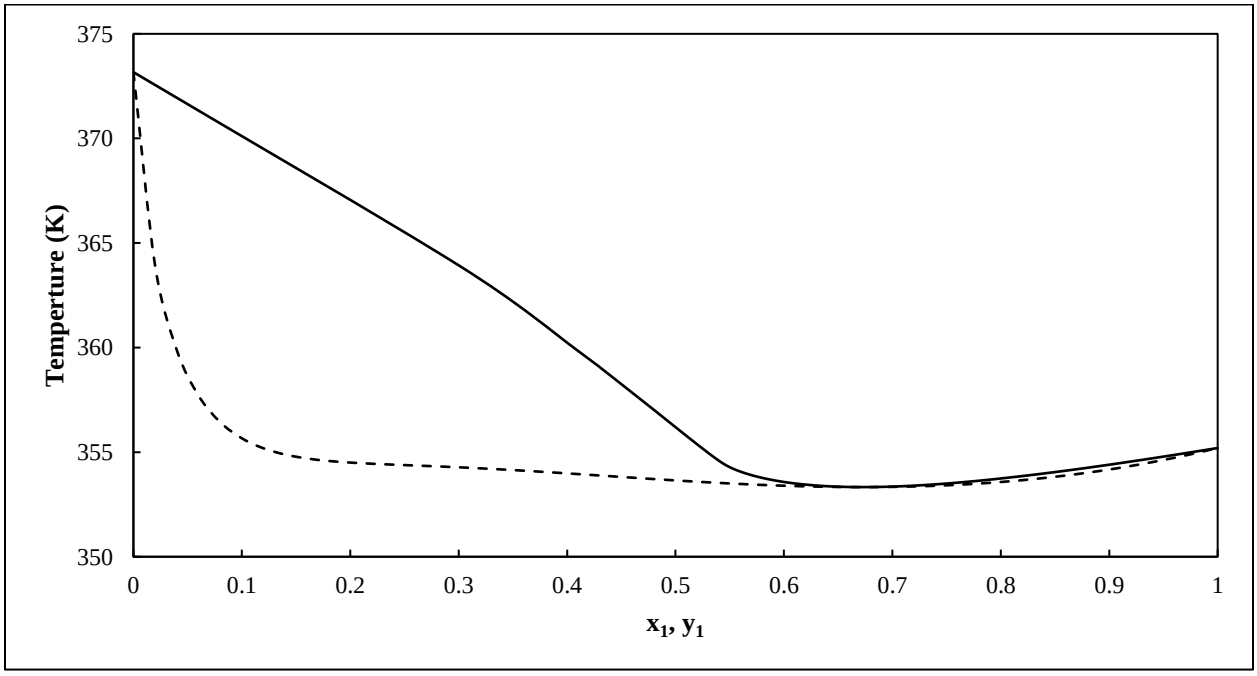

Figure 3.5. T-x-y phase diagram for the propan-2-ol (1) + water (2) system at 101.3 kPa. Solid line (-), dewpoint; dashed line (---), bubble-point.

3.2 Transport mechanism

Two transport mechanisms can be used to describe the permeation process; the pore-flow model and the solution-diffusion model. The pore-flow model describes permeation as a process in which the permeating species are separated from the mixture by pressure-driven convective flow through tiny pores (Wijmans and Baker, 1995). The solution-diffusion model assumes the permeating species dissipate into the material of the membrane before diffusing through the membrane creating a concentration gradient (Wijmans and Baker, 1995).

The main difference between both models is the gradient of the chemical potential within the membrane. The pore-flow model describes chemical potential as a pressure gradient while solute and solvent concentrations are assumed to be uniform. In contrast, solution-diffusion is governed by uniform pressure within the membrane and a chemical potential gradient (Wijmans and Baker, 1995). Figure 3.6 summarizes the above with respect to the membrane boundaries.

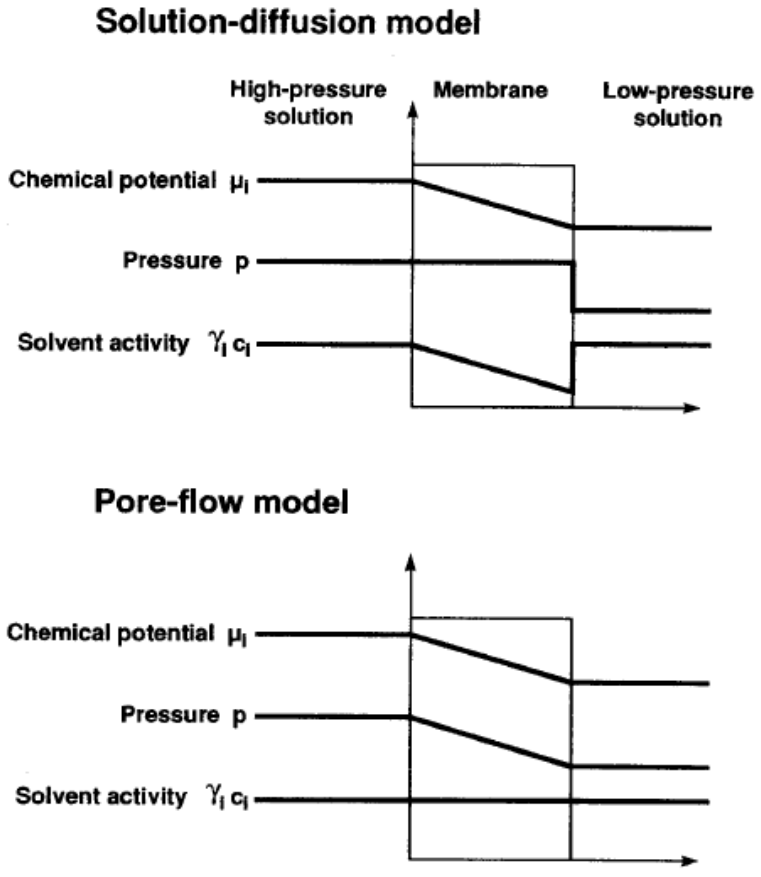

Figure 3.6. Comparison between transport mechanisms for pressure-driven permeation of a single component (Wijmans and Baker, 1995).

Kruczek (2015) advised that the solution-diffusion model correctly describes separation in a dense and microporous membrane often used in processes such as gas separation, pervaporation and reverse osmosis. The pore-flow model was said to better represent meso- and macroporous membranes typically utilized in ultrafiltration and microfiltration (Kruczek, 2015).

Wijmans and Baker (1995) developed equations from fundamental first principles to describe the solution-diffusion transport model. The model was then validated against experimental data by observing the effect of permeate pressure on specie flux. The model fitted strongly with the experimental data providing a decreasing gradient and sensitivity at the specie saturation pressure as expected from the equations developed by Wijmans and Baker (1995). Therefore, the solution-diffusion model adequately described pervaporation separation.

Similarly, Okada and Matsuura (1991) developed equations to describe the pore-flow mechanism and the model was compared to pervaporation experimental data. A plot of specie permeation rates versus downstream pressure yielded minor deviations between the model and experimental data. In addition, there were a few parameters which did not correlate to those from experiments. It was concluded that the equations could be improved upon (Okada and Matsuura, 1991).

As a result, the former was selected to describe the separation method investigated in this report. The solution-diffusion model is the most widely accepted model for pervaporation since it accurately describes the transport effect in pervaporation.

3.2.1 Development of solution-diffusion model equations

Pervaporation through a membrane is considered an open system since mass flows into and out of the membrane boundary due to some type of driving force such as pressure, temperature, concentration or electromotive force. These are interrelated and reduced to chemical potential gradients. Fundamentally, a gradient in the chemical potential is proportional to flux thereby facilitating permeant movement.

The flux of the permeating species, i, is described by the equation as given by Wijmans and Baker (1995):

$$J_i = -L_i \frac{d\mu_i}{dx} \tag{3.1}$$

where L_i is a coefficient of proportionality and $\frac{d\mu_i}{dx}$ is the gradient in chemical potential. Temperature and electromotive force gradients are assumed negligible for membrane transport producing a function for chemical potential:

$$d\mu_i = RTd\ln(\gamma_i c_i) + v_i dp \tag{3.2}$$

where γ_i is the activity coefficient, c_i is the molar concentration of component i, v_i is the molar volume of component i, and p is the pressure. The above is integrated and expressed in two forms; compressible and incompressible phases:

For liquids and solids (incompressible phases), volume is independent of pressure. Equation (3.2 is integrated to give:

$$\mu_i = \mu_i{}^o + RT\ln(\gamma_i c_i) + v_i(p - p_i{}^o) \tag{3.3}$$

For gases (compressible phases), molar volume is dependent of pressure. Integration of Equation (3.2 using this condition together with ideal gas laws gives:

$$\mu_i = \mu_i{}^o + RT\ln(\gamma_i c_i) + RT\ln\frac{p}{p_i{}^o} \tag{3.4}$$

The following assumptions were made to define the solution-diffusion model:

a) At the interface of the membrane, fluids on both sides of the membrane are in equilibrium with the membrane itself
b) Uniform pressure exists within the membrane material
c) The chemical potential gradient across the membrane is expressed only as a concentration gradient

(i) Feed/Membrane interface

The above assumptions indicate that the chemical potential of the liquid feed is in equilibrium with the membrane at constant pressure. Using Equation (3.3

$$\begin{aligned}\mu_i{}^o + RT\ln(\gamma_{io}c_{io}) + v_i\left(p_o - p_{i_{sat}}\right) \\ = \mu_i{}^o + RT\ln\left(\gamma_{io(m)}c_{io(m)}\right) + v_i\left(p_o - p_{i_{sat}}\right)\end{aligned} \tag{3.5}$$

$$RT\ln(\gamma_{io}c_{io}) = RT\ln(\gamma_{io(m)}c_{io(m)}) \tag{3.6}$$

$$\ln(c_{io(m)}) = \ln\left(\frac{\gamma_{io}c_{io}}{\gamma_{io(m)}}\right) \tag{3.7}$$

$$c_{io(m)} = \frac{\gamma_{io}c_{io}}{\gamma_{io(m)}} = K_i c_{io} \tag{3.8}$$

where K_i is defined as the liquid-phase sorption coefficient.

(ii) Membrane/Permeate interface

The pressure drops from p_o to p_l in the permeate vapour at the interface. Using Equation (3.3 and (3.4 to represent the membrane and permeate vapour respectively:

$$\mu_i{}^o + RT\ln(\gamma_{il(m)}c_{il(m)}) + v_i(p_o - p_{i_{sat}}) = \mu_i{}^o + RT\ln(\gamma_{il}c_{il}) + RT\ln\frac{p_l}{p_{i_{sat}}} \tag{3.9}$$

$$RT[\ln(\gamma_{il(m)}) + \ln(c_{il(m)})] = RT\left[\ln(\gamma_{il}c_{il}) + \ln\frac{p_l}{p_{i_{sat}}}\right] - v_i(p_o - p_{i_{sat}}) \tag{3.10}$$

$$\ln(\gamma_{il(m)}) + \ln(c_{il(m)}) = \ln\left(\frac{\gamma_{il}c_{il}p_l}{p_{i_{sat}}}\right) - \frac{v_i(p_o - p_{i_{sat}})}{RT} \tag{3.11}$$

$$\ln(c_{il(m)}) = \ln\left(\frac{\gamma_{il}c_{il}p_l}{p_{i_{sat}}\gamma_{il(m)}}\right) - \frac{v_i(p_o - p_{i_{sat}})}{RT} \tag{3.12}$$

$$c_{il(m)} = exp\left[\ln\left(\frac{\gamma_{il}c_{il}p_l}{p_{i_{sat}}\gamma_{il(m)}}\right)\right] \times exp\left[-\frac{v_i(p_o - p_{i_{sat}})}{RT}\right] \tag{3.13}$$

$$c_{il(m)} = \frac{\gamma_{il}p_l c_{il}}{p_{i_{sat}}\gamma_{il(m)}} exp\left[-\frac{v_i(p_o - p_{i_{sat}})}{RT}\right] \tag{3.14}$$

with the exponential term close to 1 and $p_l c_{il} = p_{il}$ which represents a partial pressure term, the above expression becomes

$$c_{il(m)} = \frac{\gamma_{il}}{\gamma_{il(m)}} \frac{p_{il}}{p_{i_{sat}}} = {K_i}^G p_{il} \tag{3.15}$$

where ${K_i}^G$ is defined as the gas-phase sorption coefficient.

At this point, the flux of Equation (3.1 can be modified. As reported by Wijmans and Baker (1995), the chemical potential of the solution-diffusion model is expressed as a smooth gradient in solvent activity, $\gamma_i c_i$, with the absence of a pressure gradient. Substitution of Equation (3.8 and (3.15 into (3.1 gives

$$J_i = -L_i \frac{RTd\ln(\gamma_i c_i)}{dx} \tag{3.16}$$

$$J_i = -L_i RT \left(\frac{1}{c_i}\frac{dc_i}{dx}\right) \tag{3.17}$$

$$J_i = -\frac{RTL_i}{c_i}\frac{dc_i}{dx} \tag{3.18}$$

$$J_i = -D_i \frac{dc_i}{dx} \tag{3.19}$$

where D_i is defined as the diffusion coefficient is analogous to Fick's law. The above is integrated over the thickness of the membrane to give

$$\int_0^L J_i = -D_i \int_{c_{io(m)}}^{c_{il(m)}} dc_i \tag{3.20}$$

$$J_i = \frac{D_i\left(c_{io(m)} - c_{il(m)}\right)}{L} \tag{3.21}$$

The absorption coefficient of Equation (3.8 is in the liquid phase whereas Equation (3.15 presents a gas-phase coefficient. Interconversion of liquid- and gas-phase coefficients is performed using the assumption of a vapour in equilibrium with a feed solution:

$${\mu_i}^o + RT\ln({\gamma_{io}}^L {c_{io}}^L) + v_i\left(p_o - p_{i_{sat}}\right) = {\mu_i}^o + RT\ln({\gamma_{io}}^G {c_{io}}^G) + RT\ln\frac{p_o}{p_{i_{sat}}} \tag{3.22}$$

And rearranging:

$$RT\ln({\gamma_{io}}^{L}{c_{io}}^{L}) = RT\left[\ln\left(\frac{{\gamma_{io}}^{G}p_o{c_{io}}^{G}}{p_{i_{sat}}}\right)\right] - v_i\left(p_o - p_{i_{sat}}\right) \tag{3.23}$$

$$\ln({\gamma_{io}}^{L}{c_{io}}^{L}) = \ln\left(\frac{{\gamma_{io}}^{G}p_o{c_{io}}^{G}}{p_{i_{sat}}}\right) - \frac{v_i\left(p_o - p_{i_{sat}}\right)}{RT} \tag{3.24}$$

$${\gamma_{io}}^{L}{c_{io}}^{L} = exp\left[\ln\left(\frac{{\gamma_{io}}^{G}p_o{c_{io}}^{G}}{p_{i_{sat}}}\right) - \frac{v_i\left(p_o - p_{i_{sat}}\right)}{RT}\right] \tag{3.25}$$

$${\gamma_{io}}^{L}{c_{io}}^{L} = \frac{{\gamma_{io}}^{G}p_o{c_{io}}^{G}}{p_{i_{sat}}}exp\left[\frac{-v_i\left(p_o - p_{i_{sat}}\right)}{RT}\right] \tag{3.26}$$

The exponential term is approximated to 1 since the term $\frac{-v_i(p_o - p_{i_{sat}})}{RT}$ is small. The above then becomes:

$${c_{io}}^{L} = \frac{{\gamma_{io}}^{G}p_o}{{\gamma_{io}}^{L}p_{i_{sat}}}{c_{io}}^{G} \tag{3.27}$$

where $p_o{c_{io}}^{G} = {p_{io}}^{G}$ represents the partial vapour pressure which gives:

$${c_{io}}^{L} = \frac{{\gamma_{io}}^{G}}{{\gamma_{io}}^{L}p_{i_{sat}}}{p_{io}}^{G} \tag{3.28}$$

Substitution of Equation (3.28 in (3.8 and remembering the gas-phase sorption coefficient gives:

$$c_{io(m)} = \frac{{\gamma_{io}}^{G}}{\gamma_{io(m)}}\frac{{p_{io}}^{G}}{p_{i_{sat}}} \tag{3.29}$$

$$c_{io(m)} = {K_i}^{G}p_{io} \tag{3.30}$$

Equations (3.15 and (3.30 relates to concentrations which are substituted into the flux of Equation (3.21 to provide the final solution-diffusion model for pervaporation:

$$J_i = \frac{D_i}{L}\left({K_i}^{G}p_{io} - {K_i}^{G}p_{il}\right) \tag{3.31}$$

where $D_i{K_i}^{G} = {p_i}^{G}$ which is the permeability coefficient and allows the driving force to be expressed in terms of vapour pressure as:

$$J_i = \frac{{p_i}^G}{L}(p_{io} - p_{il}) \tag{3.32}$$

Finally, the driving force can be expressed in terms of concentration differences using Henry's law coefficient as follows:

$$J_i = \frac{{p_i}^G}{L}\left(\frac{c_{io}{\gamma_{io}}^L {p_i}_{sat}}{{\gamma_{io}}^G} - p_{il}\right) \tag{3.33}$$

$$J_i = \frac{{p_i}^G}{L}(c_{io}H_i - p_{il}) \tag{3.34}$$

$$J_i = \frac{{p_i}^G H_i}{L}\left(c_{io} - \frac{p_{il}}{H_i}\right) \tag{3.35}$$

$$J_i = \frac{p_i}{L}\left(c_{io} - \frac{p_{il}}{H_i}\right) \tag{3.36}$$

3.3 Evaluation of pervaporation membrane performance

The performance of a membrane is assessed by two main parameters namely; flux and separation factor. The flux is known as the rate of mass transfer across the membrane (Galiano et al., 2016). The following expression is used to represent the partial permeate flux:

$$J_i = \frac{m_i}{At} \tag{3.37}$$

where J_i is the permeation flux of component i [g.m^{-2}h^{-1}]

m_i is the mass of the permeating species, i, in the permeate [g]

A is the effective membrane area [m^2]

t is the permeation time [h]

Separation factor depicts the separation characteristics of the membrane in terms of weight ratios as:

$$\alpha_{ij} = \frac{{y_i}/{y_j}}{{x_i}/{x_j}} \tag{3.38}$$

where α is the dimensionless separation factor

i is the preferentially permeating species

j is the non-preferentially permeating species

y is the weight fraction of the species in the vapour permeate

x is the weight fraction of the species in the liquid feed

Equations (3.37 to (3.38) provide an analysis that is strongly dependent on operating conditions Rozicka *et al.* (2014). According to Baker, Wijmans and Huang (2010), the influence of operating conditions on the membrane performance can be eliminated with the use of intrinsic membrane properties; permeance and selectivity.

The computation of permeance requires molar partial flux. Therefore, Equation (3.37 is modified to give:

$$j_i = \frac{J_i {v_i}^G}{M_i} \tag{3.39}$$

where j_i is the molar flux of component i [cm^3(STP).$cm^{-2}s^{-1}$]

${v_i}^G$ is the molar volume of gas i [22.4 l(STP).mol^{-1}]

M_i is the molecular weight of component i

Equation (3.15 is implemented into a recast version of Equation (3.10 to give the permeation expression:

$$j_i = \frac{{P_i}^G}{L}\left({\gamma_{io}}^L {X_{io}}^L {p_i}_{sat} - Y_{il} p_l\right) \tag{3.40}$$

where $\frac{{P_i}^G}{L}$ is the permeance [gpu]

${\gamma_{io}}^L$ is the activity coefficient of component i

${X_{io}}^L$ is the mole fraction of component i in the liquid feed

${p_i}_{sat}$ is the saturated vapour pressure of pure component i [cmHg]

Y_{il} is the mole fraction of component i in the permeate

p_l is the permeate pressure [cmHg]

Selectivity is the ratio of component permeances (Baker et al., 2010) and is found using the expression below:

$$\beta_{ij} = \frac{{P_i}^G/_L}{{P_j}^G/_L} \tag{3.41}$$

It is important to note:

${P_i}^G$ is the membrane permeability [Barrers]. Barrers is a non-SI unit used for gas permeability and it is equated as 1 Barrer = 1×10^{-10} cm^3(STP).cm.cm^{-2}.s^{-1}.$cmHg^{-1}$ (Baker et al., 2010).

3.4 Effect of temperature on membrane performance

Membrane flux can be adjusted whilst maintaining separation factor by manipulating the feed temperature (Sander and Soukup, 1988). In addition, Kujawski *et al.* (2007) explained that an exponential increase in flux due to raised feed temperatures indicate that the temperature effect on pervaporation must be described by an Arrhenius-type relation.

The solution-diffusion model was used as a starting point. According to Equation (3.32, the permeability coefficient depends on two key aspects; partition in and diffusion through the membrane. Therefore, the following relation was developed to describe permeability in terms of diffusivity, a kinetic property, and solubility, a thermodynamic property (Feng and Huang, 1996):

$$P = DS \tag{3.42}$$

The temperature dependence of diffusivity and solubility are expressed in Equations (3.43) and (3.44) respectively (Feng and Huang, 1996):

$$D = D_o \exp\left(-\frac{E_D}{RT}\right) \tag{3.43}$$

$$S = S_o \exp\left(-\frac{\Delta H}{RT}\right) \tag{3.44}$$

Consequently, the above gives rise to

$$P = P_o \exp\left(-\frac{E_p}{RT}\right) \tag{3.45}$$

Equation (3.45) as reported by Feng and Huang (1996) is used in combination with Equation (3.40) which clearly depicts flux is directly dependent on permeance. According to Win and Friedl (2012), the Arrhenius-type relationship between feed temperature and permeance can be represented as follows:

$$\frac{P_i{}^G}{L} = \frac{P_{i,ref}{}^G}{L} exp\left[\frac{E_{p_i}}{R}\left(\frac{1}{T_{ref}} - \frac{1}{T_f}\right)\right] \tag{3.46}$$

where E_{p_i} is the activation energy inclusive of heat of adsorption and diffusion energy

R is the gas constant

T_{ref} refers to the reference temperature of 333 K

T_f is the temperature of the feed

Equation (3.46) is then modified to give the logarithmic form as follows:

$$\ln\frac{P_i{}^G}{L} = \ln\frac{P_{i,ref}{}^G}{L} + \frac{E_{p_i}}{R}\left(\frac{1}{T_{ref}} - \frac{1}{T_f}\right) \tag{3.47}$$

A plot of Equation (3.47) with $\ln\frac{P_i{}^G}{L}$ as the ordinate and the inverse of temperature as the abscissa should dictate a linear relationship. Constants E_{p_i} and $P_{i,ref}{}^G$ are found by means of the slope and y-intercept, respectively.

3.5 Modelling equations for simulation study

As previously mentioned, the solution-diffusion mechanism describes permeation rate as a function of solubility and diffusivity (Equation 3.42 to 3.46). According to Mulder et al. (1985), solubility is categorized as a thermodynamic property whereas diffusivity is a kinetic property. Therefore, mathematical models developed for simulation of pervaporation must be based on one of these two key mass transport steps. Several thermodynamic models which can be used to predict the equilibrium sorption of pervaporation have been outlined in literature (Kamesh et al., 2018;

Lipnizki and Trägårdh, 2001). These include the Flory-Huggins theory, UNIQUAC model, UNIFAC model, modified NRTL, as well as a combination of these models. The classic Flory-Huggins model is described in Appendix A. The activity of components can be predicted using a thermodynamic model, making it suitable for membrane development (Lipnizki and Trägårdh, 2001). However, a crucial limitation is the inability to predict component fluxes. This can only be overcome by combining one of the abovementioned thermodynamic models with the free volume theory (a kinetic model) or the Stefan-Maxwell theory (similar to the solution-diffusion model which incorporates sorption, diffusion, and desorption) (Lipnizki and Trägårdh, 2001).

Conversely, kinetic models can predict component fluxes and selectivity. Thus, making the approach more suitable for practical processes and module design (Lipnizki and Trägårdh, 2001). Models representing membrane diffusion focus on the non-linearity of concentration profiles as well as the temperature-dependence of diffusivities. Since membrane separation and module configuration were of particular importance in this project, a kinetic approach was followed in developing the pervaporation models of Chapter 6. The custom semi-empirical models created for the three unique alcohol-water systems, as outlined in Chapter 7, were based on concentration-dependent diffusion coefficients. This technique along with other kinetic models such as the free volume theory, dual sorption model and molecular simulations for diffusion were reviewed in detail by Lipnizki and Trägårdh (2001).

In this work, the simulation model consisted of four key parts (A, B, C and D) to prepare the model script code.

A. Temperature-dependent diffusivities
B. Flux expressed in terms of concentration gradient
C. Concentration of a component entering the membrane
D. Concentration of a component leaving the membrane

Part A and B have already been developed and were presented earlier represented by Equations (3.43) and (3.21 respectively. The solution-diffusion model equations explained that the concentration gradient can be expressed in terms of pressure. However, the basis of the model developed for simulation stems from Equation (3.21. This was done to simplify the structure of equations presented in the ACM model script.

Part C was developed from the standard chemistry definition of concentration for a liquid incorporating density and molecular weight. A liquid phase is assumed at the membrane entry boundary since this corresponds with the phase of the feed mixture fed to a pervaporation cell. The result is as follows:

$$c_{io(m)} = \frac{\rho_l \, x_i}{M_i} \tag{3.48}$$

Where $c_{io(m)}$ is the concentration of specie i entering the membrane [kmol.m^{-3}]

ρ_l is the liquid density [kg.m^{-3}]

x_i is the weight fraction of component i in the liquid feed

M_i is the molecular weight of component i [kg.kmol^{-1}]

Part D represents the concentration of a component in the permeate. The exit boundary of the membrane is in direct contact with the permeate. Since the permeate is a vapour due to the pressure gradient, the following relation was developed from the ideal gas equation:

$$c_{il(m)} = \frac{p_{il} \, Y_i}{RT_p} \tag{3.49}$$

Where $c_{il(m)}$ is the concentration of specie i exiting the membrane [kmol.m^{-3}]

p_{il} is the permeate-side pressure [atm]

Y_i is the mole fraction of component i in the permeate

R is the gas constant [atm.L.mol^{-1}.K^{-1}]

T_p is the temperature of permeate [K]

The above equations were developed into the model script along with material balances around the cell to provide a complete set of equations that can be solved. The algorithm outlining the model computation using the above equations can be seen in Chapter 4.

PART 1: EXPERIMENTAL WORK

The investigation was conducted in two parts. Part 1 presents the experimental undertakings for the ethanol and water system which were performed on the apparatus described in the following chapter, Chapter 4. Due to the quality of experimental results presented in Chapter 5, a more accurate simulation method based on high-quality experimental data from the literature, was implemented to assess the separation ability of pervaporation. This led to the simulation study presented in Part 2. Part 2 presents the modelling and simulation of a pervaporation system for three alcohol-water systems; ethanol-water, propan-1-ol−water, and propan-2-ol−water.

CHAPTER 4

Experimental Methodology

This chapter provides an overview of the equipment and materials used to perform experiments. The pervaporation system was the first membrane separation apparatus to be setup in the Thermodynamics Research Unit at the institution. The equipment commissioned was based on literature research presented in Chapter 2. A detailed account of equipment assembly as well as modifications made to adapt to the required operating conditions is described. To gain an understanding of the effect of some of the properties on membrane performance, preliminary pervaporation experiments using the common PVA membrane were conducted as part of this study for a test system of ethanol and water. A commercial composite PVA membrane supplied by DeltaMem AG was used for these experiments. This experience was used to inform the design and costing of pervaporation separation routes via simulation in the remainder of the study. The experimental procedure, including leak testing and product analysis, is discussed in this chapter.

4.1 Materials

Ethanol was purchased from Honeywell. Distilled, deionized water was obtained from the Chemical Engineering laboratories at UKZN. The ethanol and water purities were confirmed with gas chromatography analysis and refractive indices which are reported in Chapter 5. The conductivity of distilled water was measured as 19 $\mu S.m^{-1}$. In addition, the water content of ethanol

was determined using the Karl Fischer titration method. This was found to be less than 0.005 mass fraction.

4.2 Description of apparatus

In this study a pervaporation unit was required to be commissioned as there was no such membrane separation device available in the Thermodynamics Research Unit. The equipment shown in Figure 4.1 was set up using guidance from the literature sources discussed in Chapter 2. The inventory of items required to assemble a pervaporation unit are listed as follows:

1. A 400 ml cell (height of 120 mm; inner diameter of 70.53 mm and outer diameter of 76.05 mm) fitted with a membrane plate.
2. Composite PVA-based membrane sheets of three types namely; PERVAP^{TM} 4100, PERVAP^{TM} 4101 and PERVAP^{TM} 4155-80 were considered for the dehydration of alcohols.
3. A teflon magnetic stirring bead (length of 50.60 mm and width of approximately 8.00 mm).
4. A stirring plate.
5. Cold traps to condense the vapour permeate.
6. A RNF Neuberger (Type NSE 800) vacuum pump.
7. A 14L Scientific (Model 130) water bath with dimensions 38.20 mm × 25.50 mm × 24 mm.
8. A FMH Instruments (FMH 110) temperature controller with a temperature control range of 253 – 373 K.
9. A WIKA stainless-steel Pt-100 (Class A) temperature probe and a Shinko ACS (13A – S/M) display.
10. A P-10 WIKA pressure transducer (0 – 10 bar abs with 4 – 20 mA).
11. A computer with LabVIEW™ installed to control and monitor pressure.

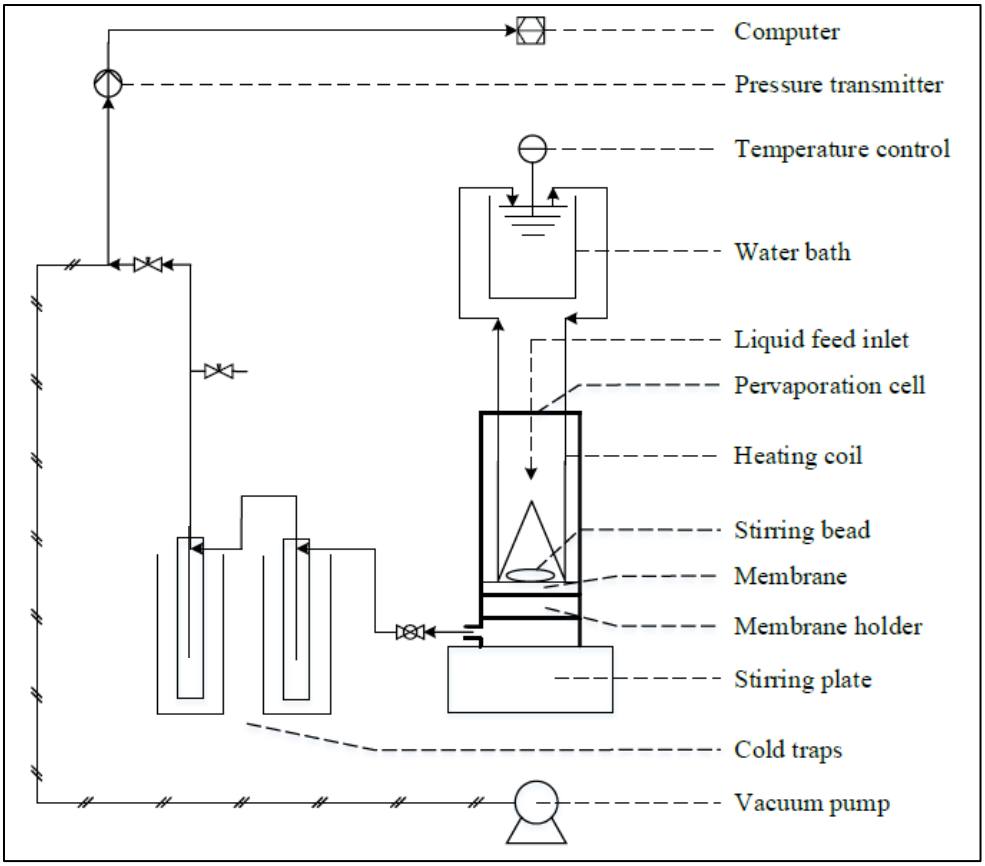

Figure 4.1. Schematic diagram of pervaporation setup.

A cell constructed of polysulfone was used for the purpose of this experiment. The Millipore stirred ultrafiltration cell (Model 8400) was repurposed such that it could be used as a pervaporation cell. The cylindrical cell had a capacity of 400 ml and an effective membrane area of 41.8 cm^2. The cell was equipped with a magnetic stirring bead which provided continuous mixing upstream of the membrane to prevent gradients in the feed concentration and temperature, similar to the procedure described by Singha et al. (2013). All experiments were performed under semi-batch operation.

The laboratory-scale pervaporation cell separated the binary mixture with the use of a PVA-based membrane. DeltaMem AG supplied three PVA-based membranes namely; PERVAP^{TM} 4100, PERVAP^{TM} 4101 and PERVAP^{TM} 4155-80. These membranes were recommended for dehydration of volatile organic mixtures by the supplier.

The temperature of the feed was raised by inserting a stainless-steel heating coil into the pervaporation cell. Heated water was circulated through the coil before being returned to a bath. The bath was fitted with a CAHO H481 digital temperature control which was used to regulate the temperature of water passing through the coil. Due to the indirect heating method applied, the feed temperature was monitored with the use of a Pt-100 probe with a supplier uncertainty of 0.02 K.

An Edwards vacuum pump was connected to the second cold trap using vacuum tubing to reduce the pressure downstream of the membrane. A pressure transducer (P-10, supplied by WIKA) rated for operations between 0 to 10 bar abs with a current output of 4 to 20 mA was used to convert the applied pressure. The pressure gauge in combination with LabVIEW™ was used to control and monitor the permeate side pressure. Originally, the set-up consisted of a pressure gauge valve and Agilent 34972A LXI Data Acquisition/Switch Unit to log the pressures during an experiment. However, this method of pressure control was inadequate. A precise pressure control system such as LabVIEW™ was required due to the instability of maintaining a low pressure with 2 – 5 kPa. Therefore, pressure was regulated in the system via solenoid valves connected to both the vacuum pump and a vent to the atmosphere.

Vapour permeate was withdrawn from the bottom of the cell and condensed using two cold traps connected in series. A series arrangement of the cold traps ensures all permeate were condensed and collected. A slurry of water, ice and NaCl was used to condense the vapour permeate. The condensed permeate was collected from both cold traps for sampling and analysis. Permeate samples were analysed using a Shimadzu GC-2014 gas chromatograph. This was equipped with a thermal conductivity detector and a POROPAK-Q column (2 m × 2.2 mm) for separation.

Silicon tubing was used to connect the cell to the cold traps. The pressure control system consisting of the transmitter, vacuum pump, solenoid valves and the output computer was linked via stainless-steel tubing. In addition, stainless-steel hose clamps were used to secure all tube fittings.

4.3 Experimental method

The materials and apparatus described above were used to execute the required pervaporation experiments. In order to prepare the equipment for experiments, the following steps were performed:

i. Calibration of sensors.
ii. A leak test was undertaken after connecting all the lines and fittings in the setup.
iii. The experiment was performed using the pervaporation unit.
iv. The permeate product was analysed using gas chromatography.

4.3.1 Calibration of sensors

The system pressure was measured using a WIKA P-10 pressure transmitter. Pressure was effectively controlled using LabVIEW^{TM} which utilized a solenoid valve connected to a vacuum pump as well as a vent to the atmosphere. The transmitter employed during experiments was calibrated against a standard WIKA Mensor CPC 3000 device over the range of 1 – 6 kPa. Although this range is narrow, it encompassed the range of experimental pressures considered in this work. The readings of both transmitters were recorded to produce the calibration curves presented in Chapter 5. The standard uncertainty of the transmitter and standard instrument were 0.1 and 0.01 kPa as reported by the suppliers.

A Pt-100 temperature sensor was used to measure the temperature of the feed in the pervaporation cell. This was calibrated by placing the probe in a calibration bath together with a standard temperature probe. The setpoint temperature was varied between 323.15 – 343.15 K and the temperatures of the standard probe (WIKA CTB 9100 and WIKA CTH 6500 kit, <0.02 K uncertainty) as well as the experimental temperature sensor recorded. Results of the calibration are reported in Chapter 5. The standard uncertainty of the standard probe was reported as 0.03 K by the manufacturer.

4.3.2 Leak detection

Leaks within a system lead to inadequate operation of equipment due to compromised pressure measurement and control. Leaks can result from a pre-existing weakness in the materials of construction, poorly sealed joints, from occasional maintenance and repair performed or simply due to wear and tear from stress placed on the operating equipment. Routine leak tests can prevent small leaks from causing continuous damage to a system. The solvent method was implemented for leak detection in which a solvent, such as acetone, was sprayed on all joints and suspected

problem areas while the system was under vacuum and observing any spikes in the vacuum pressure due to the acetone vapour pressure. All identified leaks were corrected with vacuum seal, or the tubing replaced when required.

4.3.3 Experimental Procedure

(i) Start-up procedure

a. The alcohol/water mixture was prepared in a gas-tight storage vessel and stored in an ice bath to reduce any evaporation.
b. The membrane disk was prepared and inserted in the membrane holder of the pervaporation cell with an o-ring (RMT 3×72 viton) placed above the membrane to provide rigid support. The membrane holder was placed in the cell body such that the tabs alongside the holder line up with the base of the cell body. The base was screwed into the cell body to ensure a tight seal was created.
c. All pipes were inspected to ensure correct fitting and to avoid possible leakages.
d. The heating coil was placed in the cell. The level in the water bath was inspected for safe operation. The water bath controller was switched on, the setpoint entered, and the required temperature was reached for heating of the sample feed. This took approximately 40 minutes.
e. The release valve was closed, and the vacuum pump was switched on.
f. The LabVIEW™ programme was initiated and the setpoint for the operating pressure was entered into the programme.
g. Enough time, approximately 5 minutes, was allowed for the setpoint to be reached and for the system to stabilize. The upstream pressure was maintained at atmospheric pressure.
h. The stirring bead was placed in the cell body and the sample feed was poured into the cell. A time of 15 minutes was allowed for the feed to heat up. A temperature probe was used to ensure the desired feed temperature was obtained.
i. The needle valve was turned to the open position and the stirring plate was switched on. The stirring rate was adjusted until the vortex created was one-third the depth of the liquid volume. This ensured thorough mixing and maintained a homogeneous liquid phase on the retentate side.

j. The stopwatch was started. Each experiment was allowed to proceed for a duration of 60 minutes as suggested by Win and Friedl (2012).
k. The permeate from both cold traps was collected and weighed.
l. The composition of the collected permeate was analysed using a gas chromatograph.
m. Three or more runs were performed to verify that the composition results were consistent and reproducible.

(ii) Test run

The test experiment was performed with an ethanol-water mixture to confirm the procedure used. As mentioned in Chapter 2, the literature sources of Table 2.9 were consulted to determine the operating conditions for the experiments conducted. Three variables were studied namely; pressure, feed concentration and temperature. Pressure was investigated within the range from 2 to 5 kPa using a constant feed temperature of 338 K and feed composition of 5 wt.% water. Thereafter, the temperature effect was investigated between the range of 328 and 338 K at a constant pressure of 2 kPa and using a maximum feed water concentration of 5 wt.%. Finally, the effect of feed concentration on permeation was studied (permeate pressure of 2 kPa, feed temperature of 338 K) by varying the water concentration of the feed in the range from 95 to 98 wt.% ethanol.

(iii) Shutdown procedure

a. The pressure control of LabVIEW^{TM} was stopped and the programme was closed.
b. The vacuum pressure pump was switched off and the release valve was opened.
c. The stirring plate was switched off.
d. A time of 5 minutes was allowed to ensure all condensed vapours were collected.
e. The water bath was switched off and the heating coil was allowed to cool.
f. The stirring bead and heating coil were removed from the pervaporation cell.
g. The remainder feed was disposed.
h. The base of the cell was opened to remove the membrane from the membrane holder.
i. The membrane was placed on a clean flat surface.

(iv) Cleaning procedure

a. The cell was disassembled.
b. All components were washed with a cleaning agent.

c. The cell was put together and dried under vacuum.
d. The cell was inspected to ensure it was ready for the next use.
e. The cold traps were washed and dried with acetone.

4.3.4 Composition analysis

Permeate samples were analysed by gas chromatography using the Shimadzu 2014 model equipped with a thermal conductivity detector. The GC used helium as the carrier gas and contained a POROPAK-Q column. Operating conditions for the Shimadzu 2014 GC are presented in Table 4.1.

Table 4.1. Operating conditions for gas chromatograph.

Carrier gas flowrate (ml/min)	80
Injector profile (K)	473.15
Column temperature (K)	513.15
TCD detector temperature (K)	513.15

The GC detector was calibrated for the ethanol and water dilute regions using the area ratio method of Raal and Mühlbauer (1998). In the procedure outlined by Raal and Mühlbauer (1998), a proportionality constant termed the response factor (F_i) related the GC peak area (A_i) to the number of moles (n_i) passing the detector.

$$n_i = A_i F_i \tag{4.1}$$

Although the sample size injected into the GC is known to govern the area of the peak, it is also difficult to reproduce. Hence, area ratios in the form of Equation (4.2 were suggested by Raal and Mühlbauer (1998) to overcome errors of irreproducibility.

$$\frac{n_1}{n_2} = \left(\frac{A_1}{A_2}\right)\left(\frac{F_1}{F_2}\right) = \frac{x_1}{x_2} \tag{4.2}$$

According to Raal and Mühlbauer (1998), the calibration of a mixture must be performed at both ends of the composition spectrum for pairs of components. Calibration plots of this manner avoid

cases where the response factor ratios may not be constant for a large composition range. Therefore, the calibration of a binary mixture consisted of two plots, at the dilute regions of both component 1 and 2, of areas ratios versus mole fraction ratios. Standard mixtures were gravimetrically prepared and analysed using the GC to plot the calibration curves. An Ohaus Pioneer mass balance with a readability of 0.0001 g was used to prepare the mixtures. A linear relationship in both dilute regions represented a good calibration procedure. The results for the calibrations are presented and discussed in Chapter 5. The composition of the permeate was evaluated using measured area ratios and corresponding mole fraction ratios from the calibration curves.

CHAPTER 5

Experimental Results & Discussion

This chapter presents the results from the experimental investigation. A binary mixture of ethanol and water was fed to the pervaporation unit described in Chapter 4. The effect of varying permeate pressures, feed temperatures and feed compositions were tested in the apparatus set up and compared to literature sources with similar operating conditions. Three factors were used to assess the performance of pervaporation: flux, permeate composition and separation factor. In addition, calibration plots for the temperature probe, pressure transmitter and gas chromatograph detector are presented.

5.1 Experimental Setup

A few minor modifications to the equipment were performed while initial experiments were conducted. Firstly, the cell base was reconstructed to provide stronger support to the membrane plate. This also stopped leakages of feed which were found to be an issue during runs. Due to the high temperatures required, the water from the bath evaporated quickly and needed to be replenished often. As a result, a stainless-steel sheet was placed over the bath to avoid loss of water to the atmosphere. These changes ensured improved, easier operation of equipment.

Experiments were conducted in three parts. The first set consisting of 4 permutations were performed with a varying pressure of 2 -5 kPa for a feed of 5 wt.% water heated to 338 K. The second set consisted of 3 permutations which were conducted by heating the feed of 5 wt.% water to various temperatures in the range of 328 – 338 K for experiments with a constant permeate pressure of 2 kPa. Lastly, 4 permutations were performed by passing a feed of different compositions (in the range of 95 – 98 wt.% ethanol) through the pervaporation cell. Each experiment was repeated twice to ensure the apparatus performed reliably and to confirm reproducibility of measurements. After each part was conducted, the optimal condition was chosen and applied to the next set of experiments in a factorial approach. A pressure of 2 kPa and feed temperature of 338 K were applied to the final third set of experiments.

The maintenance of a set pressure throughout a run became increasingly difficult as experiments progressed, especially at 2 kPa. After performing all 3 sets of experiments for the test system of

ethanol and water, a few major issues were encountered with the equipment. The nozzle at the base of the pervaporation cell, which was responsible for passing permeate to the cold traps, began to weaken and developed fractures. Therefore, the pressure setpoint of LabVIEW^{TM} could no longer be maintained resulting in a severe pressure leak. The fractured length of the nozzle was removed, and a sleeve inserted to provide additional strength and support to the nozzle. However, other hairline fractures began to develop on the membrane plate. Despite best efforts to modify the existing membrane plate as well as remake an entirely new membrane plate, it was difficult to obtain a tight seal with the original cell and the pressure leak persisted. This would require over 18 months of design and testing of novel equipment which was beyond the scope of this work, and not feasible under COVID-19 induced lockdown restrictions. Due to the importance of pressure in pervaporation, it was decided to conclude experiments with the test system and to explore simulation of pervaporation units for various alcohol-water systems as presented in Part 2 (Chapters 6 and 7).

5.2 Pure component properties

The chemical properties of all components were analysed using a refractometer (Atago 7000α), densitometer (DSA 5000) and gas chromatograph (Shimadzu GC2014). The measured densities and refractive indices were compared to literature. The results are presented in Table 5.1. Ethanol was purchased from Sigma-Aldrich. Distilled deionized water with a conductivity of 19 μS.m^{-1} was obtained from the laboratories of the School of Engineering at the University of KwaZulu-Natal.

Table 5.1. Chemical properties and refractive indices.

Component	CAS no.	Supplier	RI (293.15 K)[a]		ρ (kg.m^{-3})[c] (298.15)		GC Analysis (Peak area %)	Minimum Purity[#] (Mass %)
			Exp.	Lit.[b]	Exp.	Lit.		
Ethanol[d]	64-17-5	Sigma-Aldrich	1.3609	1.3611	785.17	785.21[e] 785.10[f] 785.22[g]	99	99
Water	7732-18-5	Merck	1.3334	1.33336	997.09	997.04[h] 997.04[i] 997.0[j]	99	99

[a]At sodium D-line = 589 nm. Standard uncertainties are $u_c(RI) = 0.0001$, $u_c(T) = 0.01K$, $u_c(P) = 0.001\ MPa$; [b](Haynes, 2014); [c] Standard uncertainties $u_c(T) = 0.01K$, are $u_c(P) = 0.001\ MPa$ and $u_c(\rho) = 0.54\ kg.m^{-3}$; [d]Purified by molecular

sieve; [e](García-Abuín et al., 2009); [f](Zafarani-Moattar and Majdan-Cegincara, 2008); [g](Arce et al., 2006); [h](Makarov et al., 2015); [i](Egorov et al., 2013); [j](Han et al., 2012); [#]As stated by the supplier.

5.3 Calibration of sensors

5.3.1 Pressure transmitter calibration

The P-10 pressure transmitter was calibrated using a standard WIKA Mensor pressure controller (model CPC 8000) connected to the apparatus. Figure 5.1 shows a plot of the actual pressure versus the display pressure. A linear response was fitted to the data points. The deviation plot of Figure 5.2 was used to find the standard uncertainty of the measurement. The expanded combined uncertainty of the measured pressure was estimated to lie within ±0.1 kPa. This included the standard uncertainty of the transducer in combination with the standard uncertainty of the Mensor pressure controller.

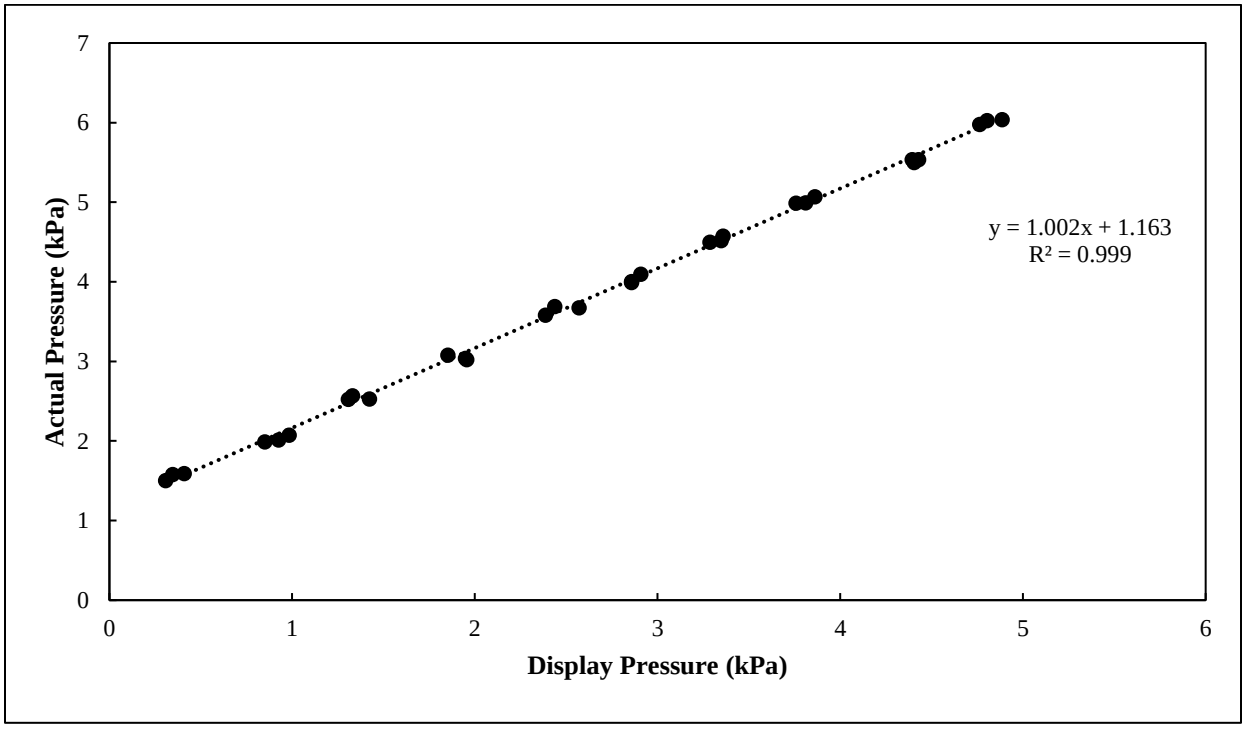

Figure 5.1. Pressure sensor calibration (symbols are experimental; --- linear trendline).

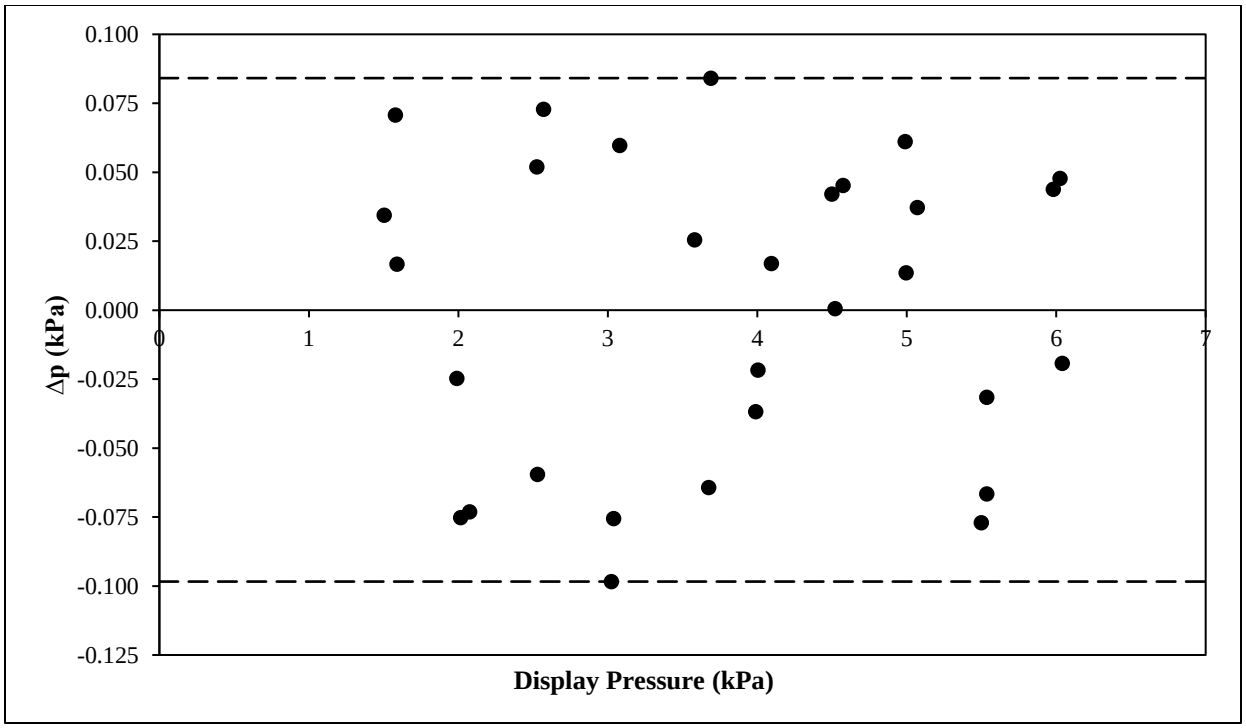

Figure 5.2. Deviation plot for pressure measurement.

5.3.2 Temperature sensor calibration

The calibration of the temperature probe was performed by measuring and comparing the actual temperature and the display temperature (Section 4.3.1). A linear trendline was fitted to the data points to give the function displayed in Figure 5.3.. The deviation plot of Figure 5.4 was used to find the standard uncertainty of the measurement. The expanded combined uncertainty of the measured temperature was estimated to lie within ±0.1 K. This was evaluated by considering the uncertainty of the temperature calibration and the standard uncertainty of the temperature standard.

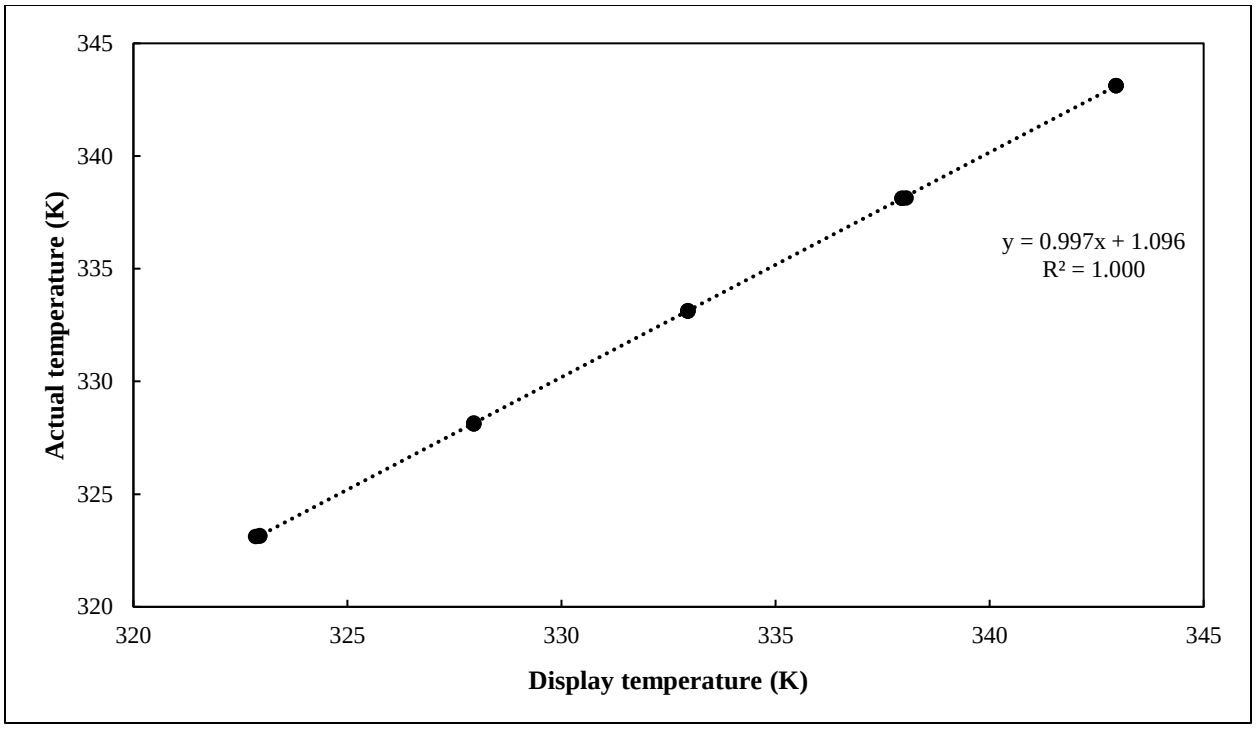

Figure 5.3. Temperature sensor calibration (symbols are experimental; --- linear trendline).

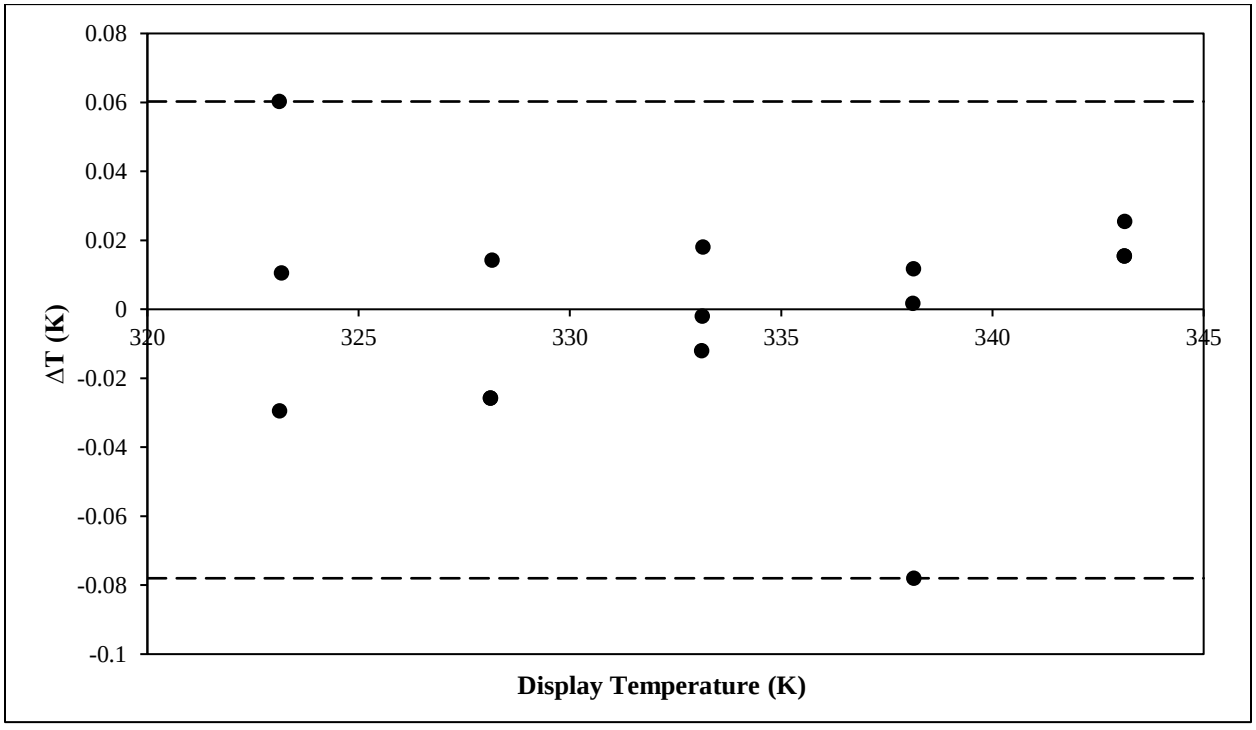

Figure 5.4. Deviation plot for temperature measurement.

5.3.3 Gas chromatograph detector calibration

The gas chromatograph detector was calibrated for the ethanol-water system across both dilute regions by employing the area ratio method suggested by Raal and Mühlbauer (1998). This is explained in Chapter 4.3.4. Figure 5.5 represents the calibration curve for the ethanol-dilute region whereas Figure 5.7 represents the calibration curve for the water-dilute region. In addition, the deviation plot for the dilute ethanol and water regions can be found in Figure 5.6 and Figure 5.8 respectively. The accuracy for the ethanol mole fraction composition was estimated to lie within ±0.006 whereas for water the range is within ±0.02. The expanded combined standard uncertainty for composition considered the errors associated with weighing (use of the mass balance), repeatability and GC detector calibration. The latter was established from the calibration deviation plots.

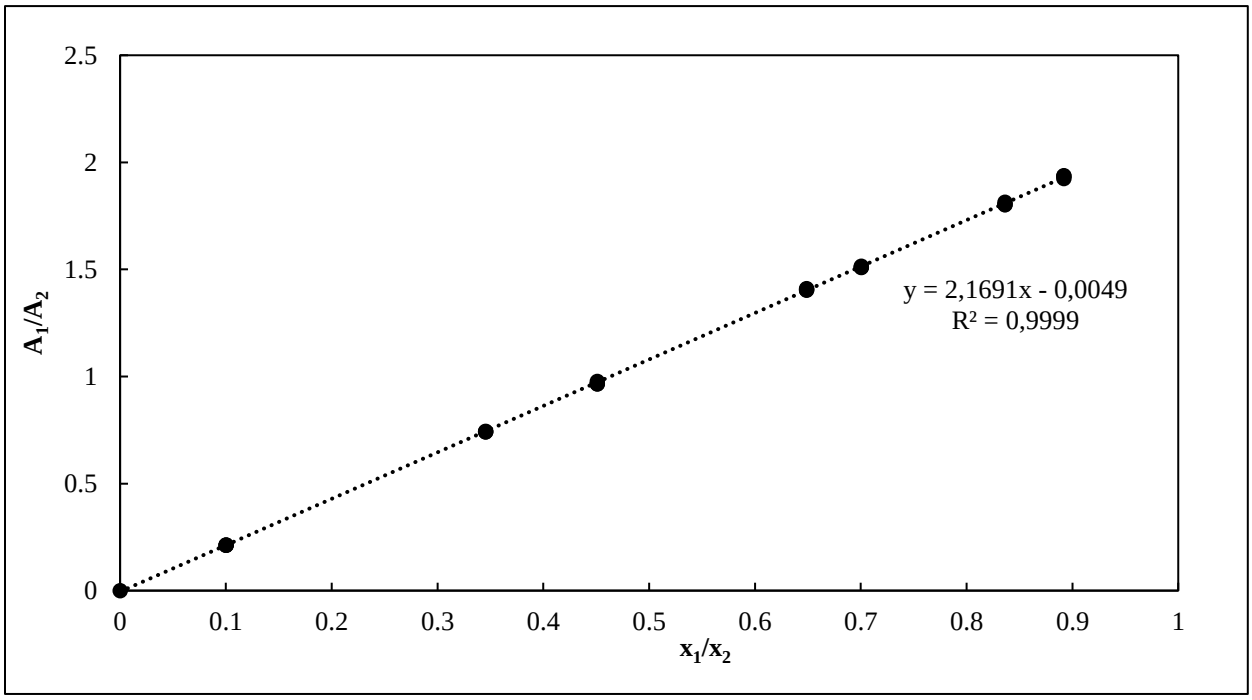

Figure 5.5. GC detector calibration for the ethanol (1) + water (2) system in the dilute ethanol composition range (symbols are experimental; --- linear trendline).

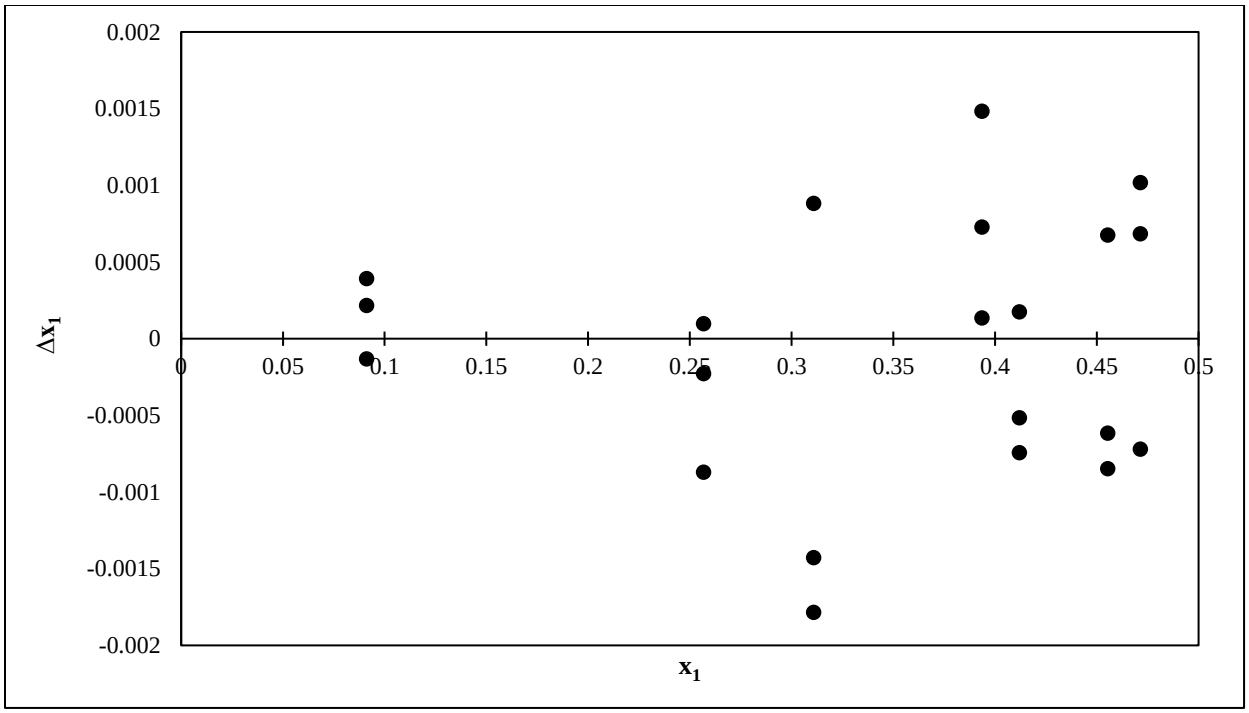

Figure 5.6. Deviation plot for the ethanol (1) + water (2) system in the dilute ethanol composition range.

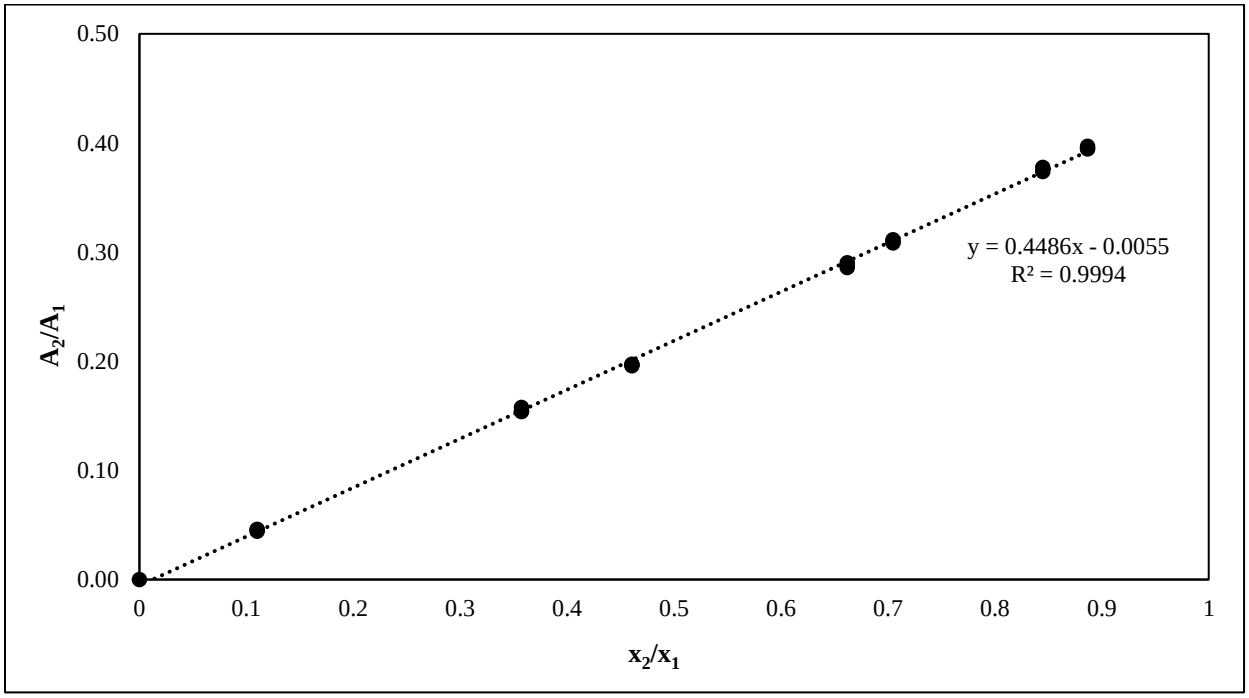

Figure 5.7. GC detector calibration for the ethanol (1) + water (2) system in the dilute water composition range (symbols are experimental; --- linear trendline).

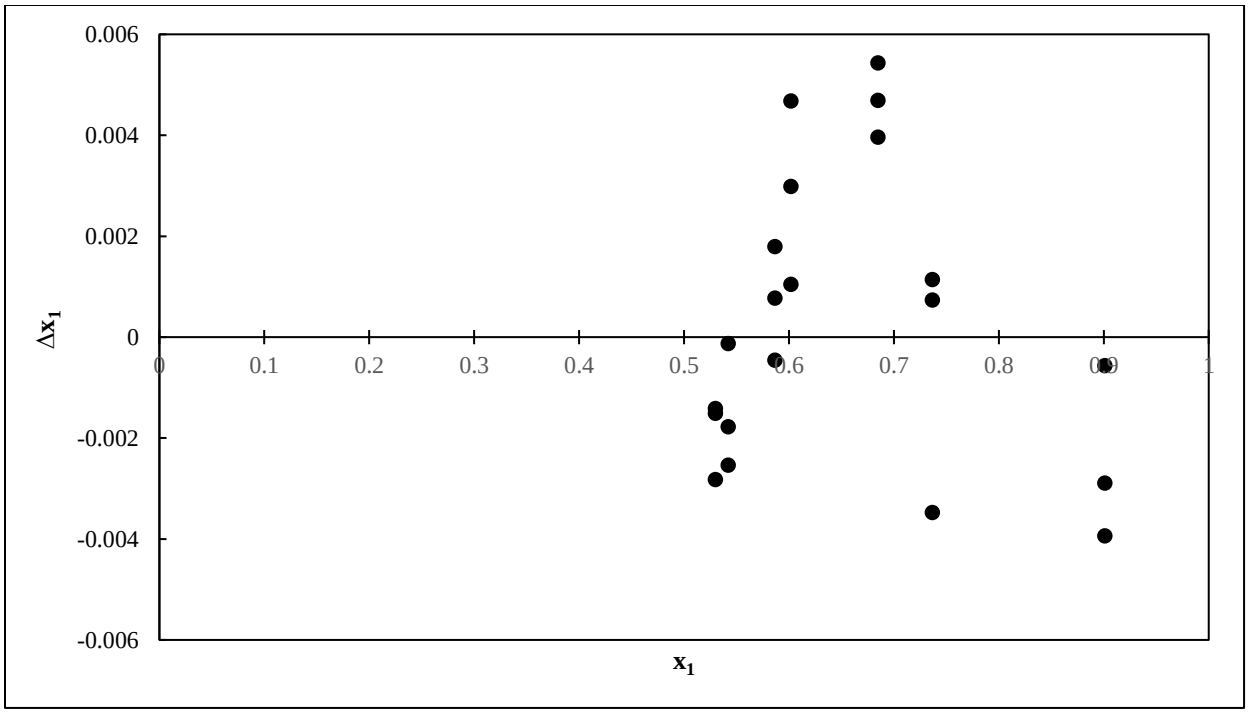

Figure 5.8. Deviation plot for the ethanol (1) + water (2) system in the dilute water composition range.

5.4 Pervaporation results for the ethanol/water separation

The purpose of the experimental study was to determine the effect of permeate pressure, feed temperature and concentration on the permeate quality obtained from a pervaporation unit. This was performed by analysing the total and specie flux for the ethanol-water system. The total and specie flux were adequate to assess the separation performance of the system since composition of the permeate is essentially incorporated into the specie flux. Appendix B contains additional plots of the permeate quality and separation factor (Figure B.1 to Figure B.5) as described in Chapter 3. The measured and calculated data for all experiments conducted is tabulated in Appendix B (Table B.1 to Table B.3). Furthermore, an example of the calculations performed for a sample set of experimental data is included towards the end of Appendix B for further guidance.

The membrane used in this work was a crosslinked PVA-based hydrophilic membrane supplied by DeltaMem AG which allowed partial permeation of water. The experimental results in this work were compared to the data of Sander and Soukup (1988); Wesslein et al. (1990) & Win and Friedl (2012). These references reported the use of similar pervaporation units to dehydrate ethanol

and water mixtures with slight differences in operating pressures and feed temperatures (as reported in Table 2.9 of Chapter 2). Although literature sources and the experimental measurements in this work were both performed using PVA-based membranes, minor differences between the membranes may have directly affected the selectivity and flux.

In the study of Sander and Soukup (1988), a composite PVA membrane with 3 layers of different polymer components were used. Each layer had a distinct structure and function. The pore-free PVA layer was responsible for selectivity and permeate flux. The asymmetric open-pore polyacrylonitrile layer provided support whereas the non-woven polyester fibre layer allowed permeate vapour to dissipate easily and also provided additional mechanical strength to the membrane.

Win and Friedl (2012) employed a composite membrane having a PVA-based active layer and a polyacrylonitrile (PAN) support layer. This was supplied by GKSS Research Center Geesthacht GmbH, Germany. The membrane utilized by Wesslein et al. (1990) was supplied by GFT-Homburg. This membrane was not only composite but also crosslinked unlike that of Sander and Soukup (1988) & Win and Friedl (2012). The type of crosslinking agent, reaction time and quantity of agent for commercial membranes are not disclosed due to intellectual property limitations. A study conducted by Yeom and Huang (1991) indicated the impact of the abovementioned factors on the mechanical and thermal strength of a PVA membrane crosslinked with amic acid. This provided insight with respect to the difference in performance seen in the experiments conducted versus the results of Wesslein et al. (1990).

5.4.1 Effect of permeate pressure on membrane performance

The effect of permeate pressure on the PVA-based membrane was investigated at a feed water composition of 5 wt.% and a feed temperature of 338 K. Four different pressures (2, 3, 4, 5 ± 0.1 kPa) were considered to provide the flux and permeate quality. The plots of these variables with respect to changing pressure is presented in Figure 5.9 to Figure 5.10 and compared to the results taken from literature.

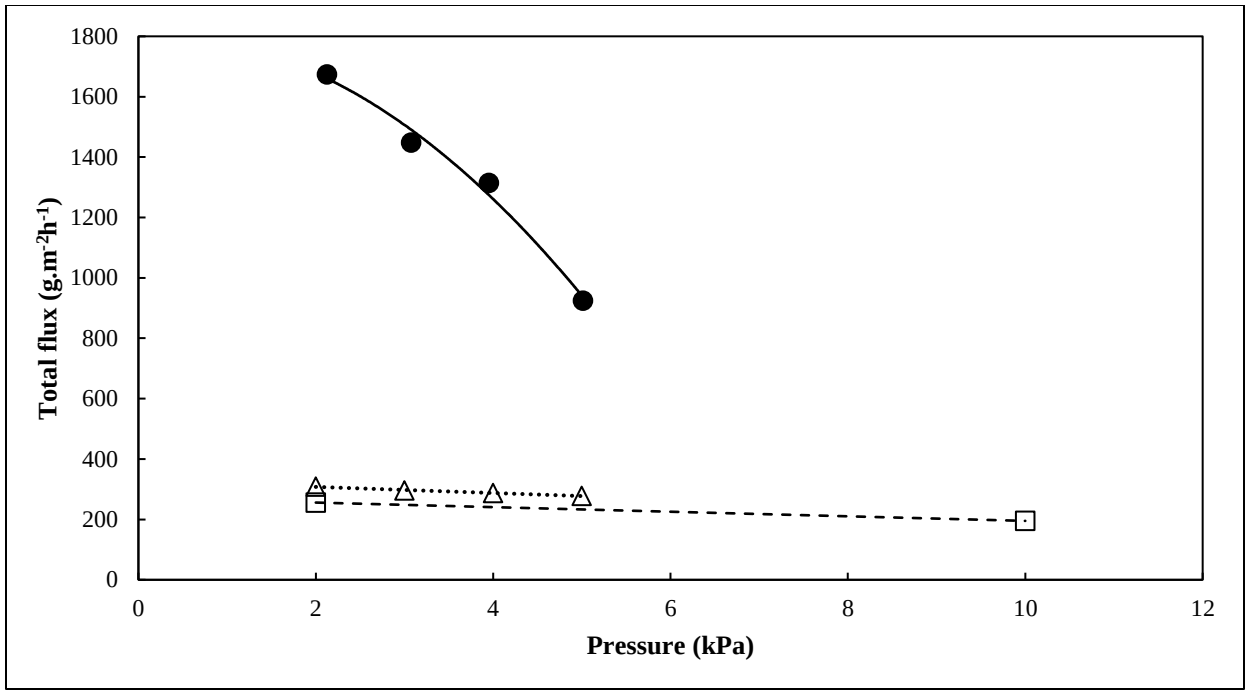

Figure 5.9. Total flux versus permeate pressure for the ethanol (1) + water (2) system. ●, Exp, This work; ∆, Win et al. (2012); □, Wesslein et al. (1990). Lines represent a smooth polynomial fit.

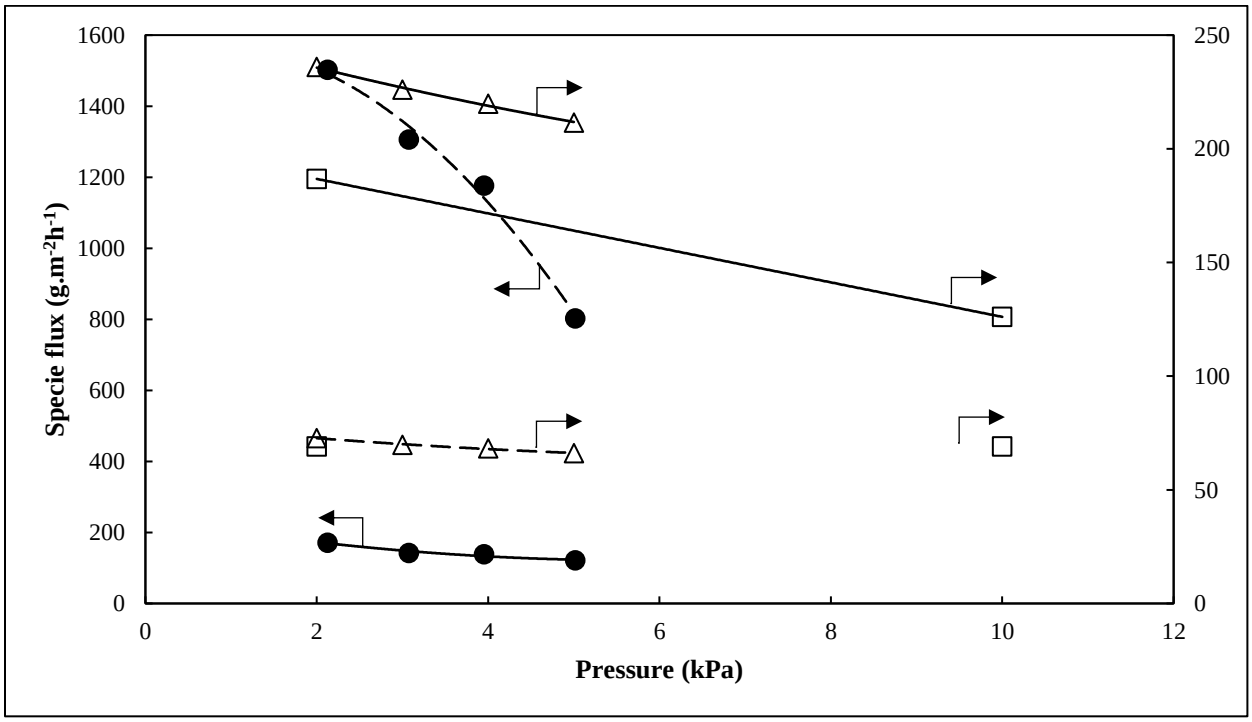

Figure 5.10. Permeation fluxes versus permeate pressure for ethanol (1) + water (2) system. ●, Exp, This work; ∆, Win et al. (2012); □, Wesslein et al. (1990). Solid lines (-) are water; dashed lines (---) are ethanol. Lines represent a smooth polynomial fit.

For the experimental data measured in this work a decline in the total and partial flux was observed with increasing permeate pressure. Figure 5.9 indicates that the flux is directly proportional to the downstream pressure which is the driving force for the pervaporation. This is an expected behaviour. A maximum total flux of 1673.88 $g.m^{-2}h^{-1}$ is observed at 2 kPa in Figure 5.9 since a greater mass of permeate is collected when a strong vacuum is applied to the system. Contrary to the data reported by Wesslein et al. (1990) and Win and Friedl (2012), the ethanol flux is higher than that of water indicating an ethanol-rich permeate was obtained during experiments. (Wijmans and Baker (1993) transformed the data of Wesslein et al. (1990) to calculate normalized fluxes, and it was found that although the pervaporation process appeared to be water-selective for most operating conditions, the separation was ethanol-selective at low feed ethanol concentrations and high permeate pressures. Since the experiments performed in this work were conducted at a high concentration of 95 wt.% ethanol, it is far more likely that higher ethanol fluxes may be due compromised structure and selectivity of the membrane caused by the stirring bead making direct contact with the membrane. The difference in specie flux can be attributed to the differences in the structure and type of membranes employed across literature and in the experiments performed. Although the purpose of the PAN layer is for membrane support according to Win and Friedl (2012), PAN is known to be a suitable polymer to extract water from aqueous solutions of ethanol (Zhang and Driol, 1995). Hence, it is possible the PAN layer provided an additional separation layer in the membrane itself facilitating a higher water flux. In addition, the difference in specie flux between Wesslein et al. (1990) and the experimental data can be attributed to the details of crosslinking employed by the respective companies which manufactured the membranes. Both crosslinking agents modified the chemical structure of the polymer membrane. However, the membrane supplied by GFT – Homburg enhances water selectivity to a much greater degree than DeltaMem AG.

Yeom and Huang (1991) performed a study which investigated the effect of amic acid as a crosslinking agent for poly(vinyl alcohol). Two factors alter the performance of a crosslinked membrane; the reaction time and the amount of crosslinking agent used. A two-step reaction occurs between PVA and amic acid. The first part is the crosslinking reaction which occurs over 30 minutes, and the second part is imidization which occurs after 90 minutes. However, both reactions must reach completion to ensure a strong crosslinking effect. The study also found that greater quantities of amic acid improves the PVA membrane properties as well as the selectivity of the

membrane to water. However, a critical amic acid content exists above which membrane performance is poor. An excess quantity of amic acid causes a steep decline in the tensile strength, tensile modulus and elongation of the membrane. Unreacted crosslinking agent disperses in the film and thereby, leads to brittleness of the film. Therefore, it is possible to create a membrane which outperforms another based on the crosslinking reaction of the manufacturing process.

Since a higher water content was anticipated in the permeate when a lower permeate pressure was set, the separation factor was expected to decrease with increasing downstream pressure (Win and Friedl, 2012). However, a different trend is observed (Figure B.3). This may be explained by the order of the runs performed. A higher-pressure run was executed before one at a lower pressure. Repeated experiments were performed in a similar manner. It is possible the ethanol content of the feed was higher than reported resulting in swelling of the membrane which proceeded until the 2 kPa run was carried out. According to Mixa and Staudt (2008), swelling components increase the chain mobility which in turn leads to more rearrangement of polymer chains. The diffusion coefficients of permeating components change. Thus, the diffusion rate of ethanol accelerates more than the diffusion rate of water. It is also likely the ethanol flux at the low pressures considered is high enough (as indicated in Figure 5.10) to reduce the effective separation factor to a significant degree. Figure 5.10 also implies that ethanol flux may approach zero at permeate pressures greater than 7 kPa. According to Wijmans and Baker (1993), as the permeate pressure approaches the feed pressure, the composition of the permeate vapour approaches that which is obtained by simple evaporation of the liquid feed. Since ethanol is more volatile than water, a steeper decline in flux is observed. It was however found upon analysis of the feed and permeate compositions using a gas chromatograph, that the permeate did show an improved water concentration of 89.82 wt.% ethanol compared to the initial feed (95 wt.% ethanol).

5.4.2 Effect of feed temperature on membrane performance

The effect of feed temperature on the PVA-based membrane was investigated at a feed water composition of 5 wt.% and a permeate pressure of 2 kPa. Three different temperatures (328, 333, 338 ± 0.1 K) were considered to observe the variation in flux and permeate quality as shown in Figure 5.11 to Figure 5.12. An Arrhenius representation of the system energies is presented in Figure 5.13.

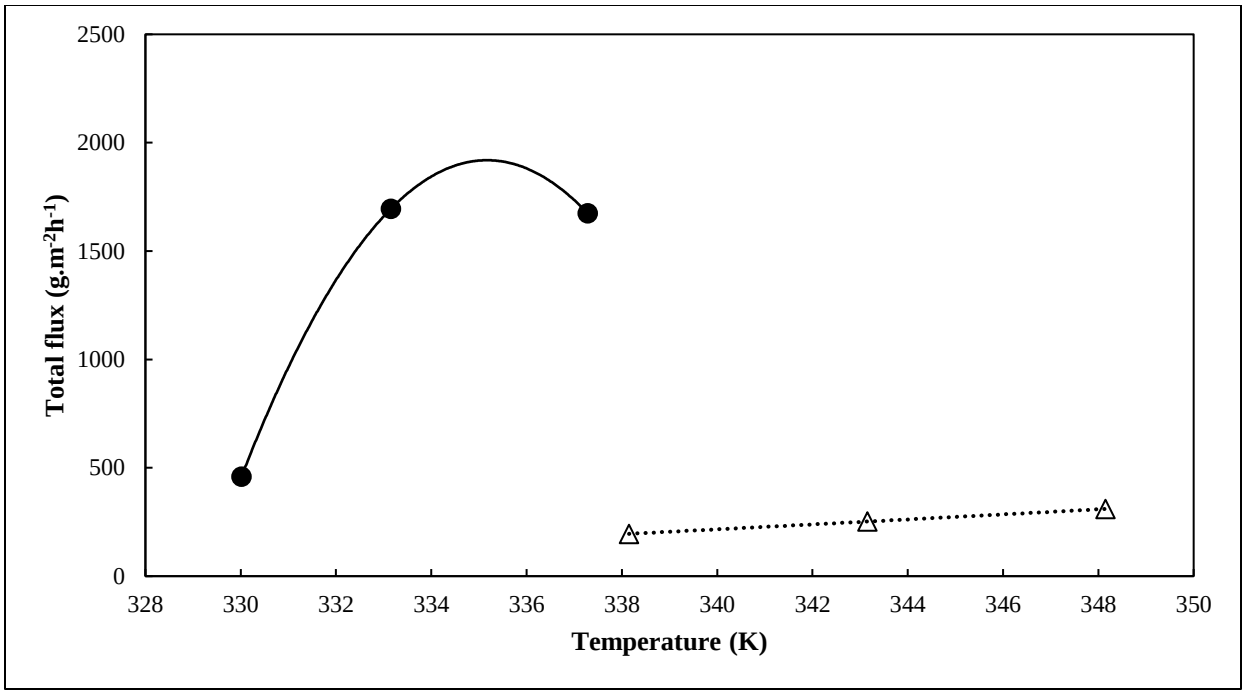

Figure 5.11. Total flux versus feed temperature for ethanol (1) + water (2) system at a permeate pressure of 2 kPa. ●, Exp, This work; ∆, Win et al. (2012). Lines represent a smooth polynomial fit.

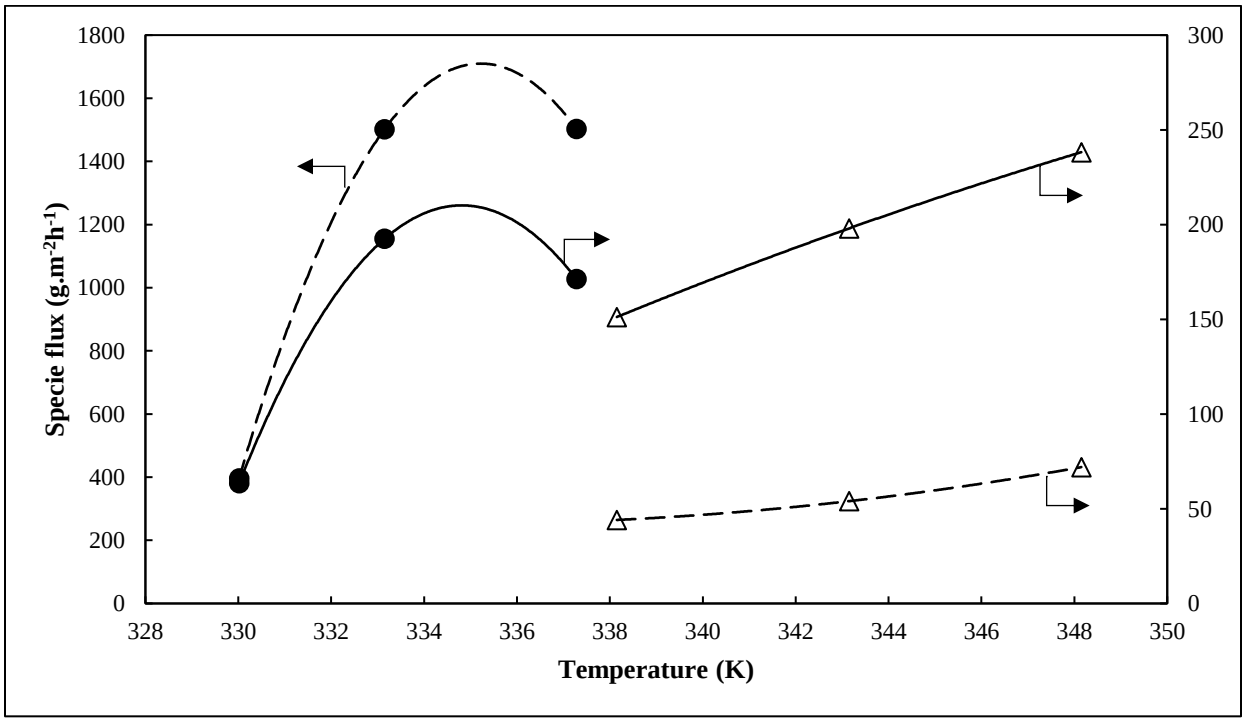

Figure 5.12. Permeation fluxes versus feed temperature for ethanol (1) + water (2) system at a permeate pressure of 2 kPa. ●, Exp, This work; ∆, Win et al. (2012). Solid lines (-) are water; dashed lines (---) are ethanol. Lines represent a smooth polynomial fit.

High temperatures cause polymer chains to possess more energy. This creates larger free volumes to exist due to an increase in the frequency and amplitude of the polymer chain movement (Yeom and Huang, 1991). More ethanol and water molecules can then diffuse through the membrane resulting in a greater mass of permeate collected in the cold traps. Since the flux is proportional to the permeate mass, the total flux of Figure 5.11 and partial fluxes of Figure 5.12 seem to increase with increasing feed temperature. Additionally, as mentioned in Chapter 2, an increase in feed temperature results in higher partial pressures for both ethanol and water. This increases the partial pressure driving force thereby resulting in a higher flux.

Experimental data differs from literature in that an optimum temperature and higher flux range is observed. The unusual maximum temperature may be a reflection of a compromised membrane. It is possible the stirring bead contacting the membrane surface may have impacted the integrity of the membrane to a greater degree during the experiments carried out at 333 K. Alternatively, the difference between the experimental results and literature may be due to the differences in the membrane structure. As previously mentioned, Win and Friedl (2012) used a composite PVA/PAN membrane. Different structures of the supporting layers in a composite membrane affect the degree of swelling (Rozicka et al., 2014). Polyacrylonitrile provides strength and support to the membrane preventing deformation during high temperatures.

The membrane supplied by DeltaMem AG was reported to have thermal stability for feed temperatures of up to 378 K for short term operation and 373 K for long term operation. However according to the trend of Figure 5.11, it is evident that a peak operating temperature of approximately 335 K exists for this system. At this temperature, a maximum total flux of 1721.31 $g.m^{-2}h^{-1}$ is observed. It is possible the temperatures investigated in this set of experiments were excessively high and compromised the strength of the membrane used in the experiments.

Thermal properties of a membrane are directly influenced by crosslinking. As previously mentioned, Yeom and Huang (1991) investigated the effect of amic acid as a crosslinking agent. Sufficient time must be allowed for both parts of the reaction to reach completion. Failure to do so results in membranes being dissolved or heavily swollen when exposed to room temperature feed. In addition, the amount of crosslinking agent influences the glass transition temperature (T_g), melting point (T_m) and thermal decomposition temperature (T_d) of the membrane. A higher

crosslinking density reduces the free volume within the material and hence, a higher T_g exists. The same effect on T_d was observed except at the critical crosslinking content which caused a decline in the value. Glass transition and thermal decomposition temperatures rely on both the crosslinking and imidization reactions. The melting temperature is solely dependent on the extent of the crosslinking reaction. A high conversion reduces the content of unreacted crosslinking agent acting as diluents. This means allowing a longer reaction time will increase the T_m of the membrane.

The ethanol flux of the experiments conducted is significantly higher than that of water. The permeate concentration can be seen to increase from 85.30 to 89.82 wt.% ethanol. This may be due to the membrane swelling greatly thereby allowing permeation of the larger ethanol molecule. Therefore, the crosslinking agent employed by DeltaMem AG is thought to have reacted insufficiently and compromised the thermal stability of the membrane. It is also possible the quantity of crosslinking agent lies at the threshold of the critical content. Crosslinking must be carefully controlled to produce a favourable separation result. Despite the better separation achieved by Win and Friedl (2012), the feed ethanol was raised from 22.58 to 23.21 wt.%. This was explained by the free volume theory in which free volume is created in a membrane due to the thermal motion of polymer chains in amorphous regions. At elevated temperatures, the diffusion of isolated and associated permeating molecules are high (Win and Friedl, 2012). Therefore, one can conclude temperature has a significant effect on the separation achieved by composite and crosslinked membranes.

In this set of experiments with a permeate pressure of 2 kPa, although this pressure displayed slight instabilities as compared to higher pressures, the control system was expected to maintain minor deviations in the setpoint. However, the results indicate that the pressure control system may not have been sufficient to maintain the apparatus at a low pressure for extended periods of time. It is likely the unstable operating pressure in combination with high temperatures ultimately led to the poor separation observed in Figure 5.12.

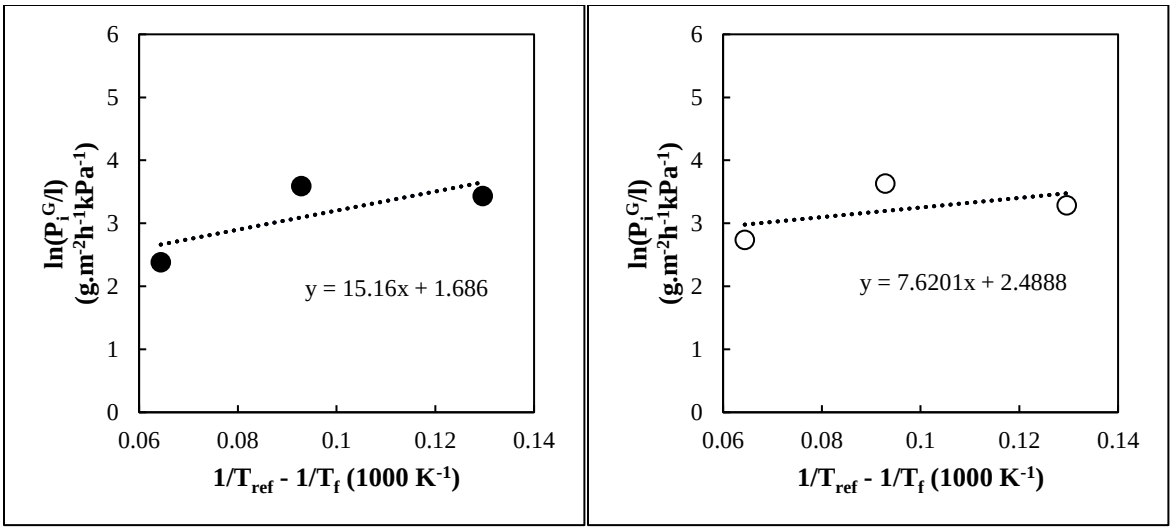

(a) **(b)**

Figure 5.13. Effect of feed temperature on permeance for the ethanol (1) + water (2) system at the permeate pressure of 2 kPa. (a) ●, ethanol; (b) ○, water, (This work).

Table 5.2. Activation energy and pre-exponential factor of ethanol and water.

	Activation energy of permeation, E_p ($kJ.mol^{-1}$)	**Pre-exponential factor, $\ln(P_{i,ref}^G/l)$ ($g.m^{-2}h^{-1}kPa^{-1}$)**
Ethanol	126.04	1.6860
Water	63.354	2.4888

The permeance of ethanol and water can be expressed in terms of the Arrhenius relation. Figure 5.13 (a) and (b) were plotted using Equation (3.47). As previously mentioned, the slope of the Arrhenius relation represents the activation energy whereas the y-intercept can be used to determine the pre-exponential factor. The activation energy of ethanol exceeds that of water in Table 5.2. This supports the notion that more ethanol molecules permeate through the membrane during conditions of elevated temperatures. Water has a lower activation energy which means fewer water molecules permeated through the membrane. This correlates with the literature of Win and Friedl (2012) and Yeom and Huang (1991).

The activation energy of permeation, E_p, is the summation of the activation energy of diffusion, E_D, and the enthalpy of dissolution, ΔH. The former provides a positive energy contribution

whereas the latter represents an exothermic reaction. Since the activation energy of permeation is positive for both ethanol and water, the permeability coefficient can be confirmed to increase with rising temperatures (Win, et al., 2012).

5.4.3 Effect of feed composition on membrane performance

The effect of feed composition on the PVA-based membrane was investigated at a feed temperature of 338 K and a permeate pressure of 2 kPa. Four different compositions in the range from 95 to 98 wt.% ethanol were considered to provide the flux and permeate quality observed in Figure 5.14 to Figure 5.15.

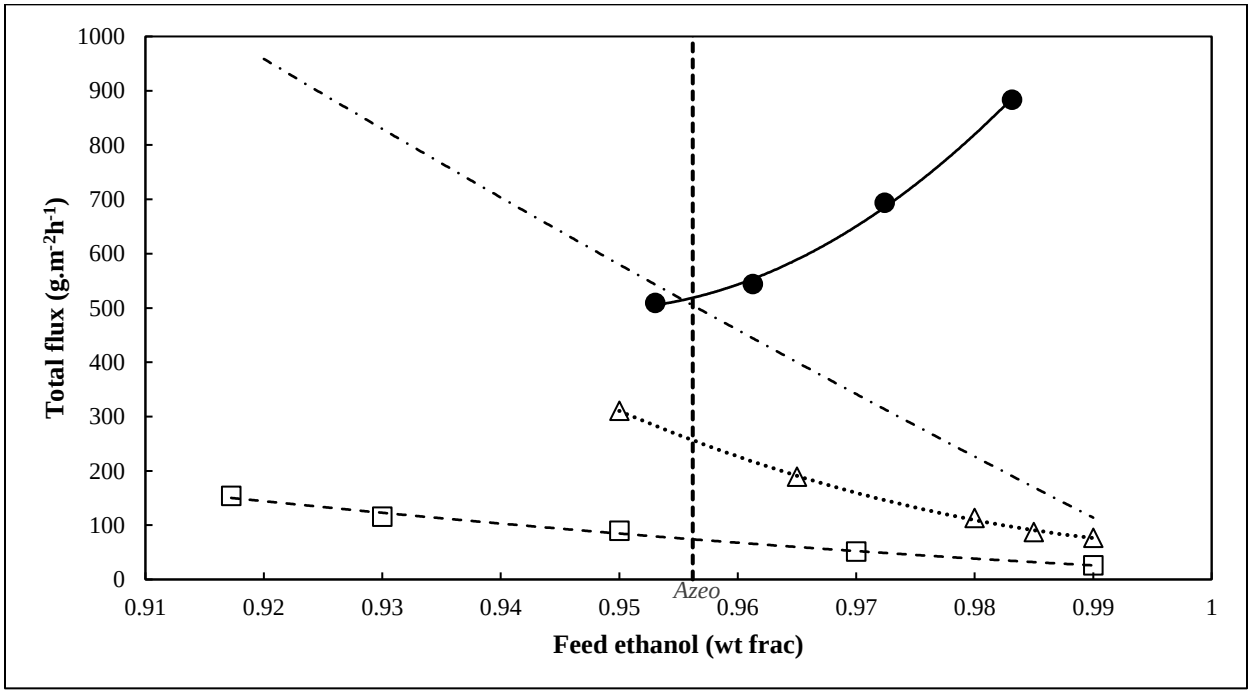

Figure 5.14. Total flux versus feed composition for ethanol (1) + water (2) system at a permeate pressure of 2 kPa. ●, Exp, This work; ∆, Win et al. (2012); □, Wesslein et al. (1990); , Sander & Soukup (1988). Lines represent a smooth polynomial fit.

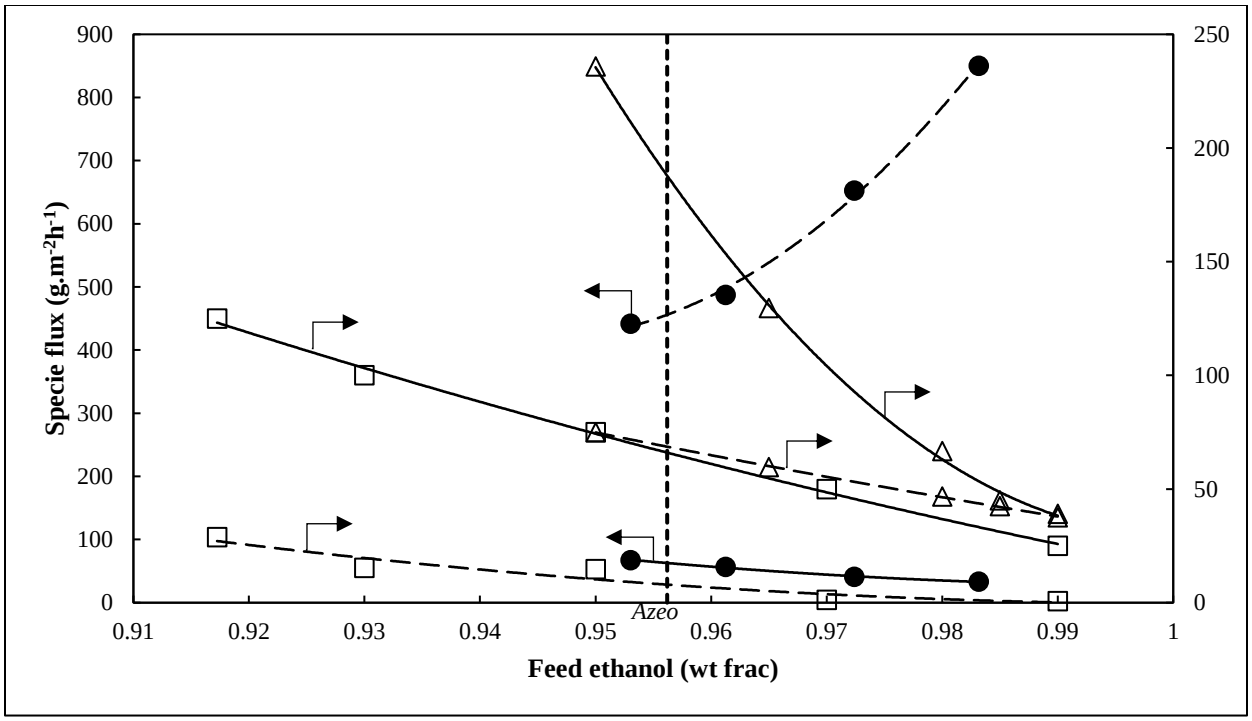

Figure 5.15. Partial flux for ethanol (1) + water (2) system at a permeate pressure of 2 kPa. ●, Exp, This work; Δ, Win et al. (2012). Solid lines (-) are water; dashed lines (---) are ethanol. Lines represent a smooth polynomial fit.

The rising total flux with feed ethanol in Figure 5.14 is contrary to the trend suggested by literature. This can be attributed to the measured specie flux of Figure 5.15. Although PVA is a dehydrating membrane and known to be soluble in water, it is also slightly soluble in ethanol and insoluble in other organic compounds. This effect coupled with an impaired membrane selectivity due to the stirring bead resulted in partial permeation of ethanol in the experiments conducted. Therefore, the trend of the total flux is governed by the ethanol permeation rate.

Figure 5.15 indicates the water flux decreases with increasing ethanol concentration as expected. A feed with 95.30 wt.% ethanol has a slightly higher water flux of 72.39 $g.m^{-2}h^{-1}$ compared to a feed of 98.32 wt.% ethanol having a flux of 33.25 $g.m^{-2}h^{-1}$. Therefore, a higher water content in the feed allows amorphous regions of the membrane to hold more water thereby, possibly swelling the membrane. Membrane swelling causes the polymer chains to become more flexible allowing greater sorption of water.

Experiments indicated a reduced ethanol flux was obtained at a higher feed water content. This means fewer ethanol molecules are available to permeate the membrane. It also suggests that a higher feed water content did not severely swell the PVA-based membrane used as compared to Win and Friedl (2012). Win and Friedl (2012) rationalized that an elevated ethanol permeation rate at a larger feed water content is due to the plasticization of the membrane. Plasticization signifies weakening of thermal and mechanical properties. Since the experimental data illustrates an opposite effect, one can conclude it is unlikely that plasticization occurred from a high feed water content in the experimental work. In this case, the membrane supplied by DeltaMem AG proved to have superior strength to the PVA/PAN membrane reportedly used by Win and Friedl (2012) with respect to water swelling in a membrane. Efficient separation can be obtained with higher water concentrations before significant swelling can occur.

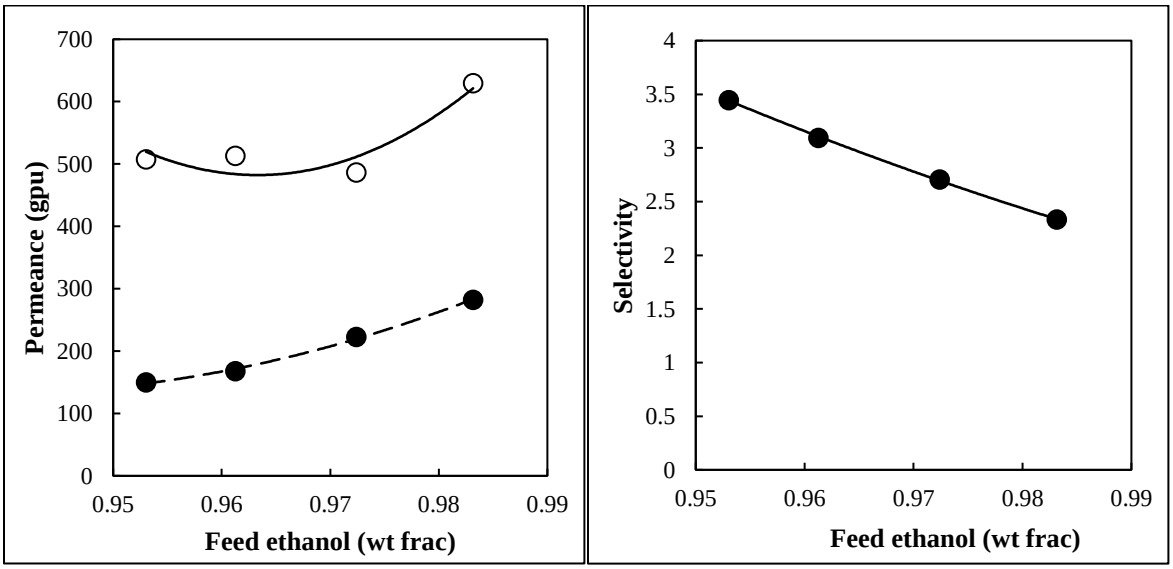

(a) **(b)**

Figure 5.16. Normalised form of pervaporation results for ethanol (1) + water (2) system at a permeate pressure of 2 kPa for varying feed compositions: (a) Permeances. ●, ethanol; ○, water, This work; (b) Selectivity. ●, This work.

The root cause of swelling in the membrane can be more clearly explained using the permeances and selectivity plotted against feed ethanol concentration as shown in Figure 5.16 (a) and (b). As the ethanol concentration increases, the ethanol and water permeances both increases. The resulting swelling and plasticization enhance the permeance of water from 507.44 gpu to 629.54

gpu. This can be translated as a 24.06% increase. Ethanol permeance was boosted by 88.54% as the permeance increased from 149.71 gpu to 282.27 gpu. It is evident the feed ethanol content has a much greater effect on ethanol permeance. As a consequence, the water/ethanol selectivity drops to 2.33 at a high ethanol concentration of 98.32 wt.%. Since the permeances and selectivity shifted with an increase in ethanol content, one can conclude that ethanol does cause the membrane to swell at very high ethanol concentrations.

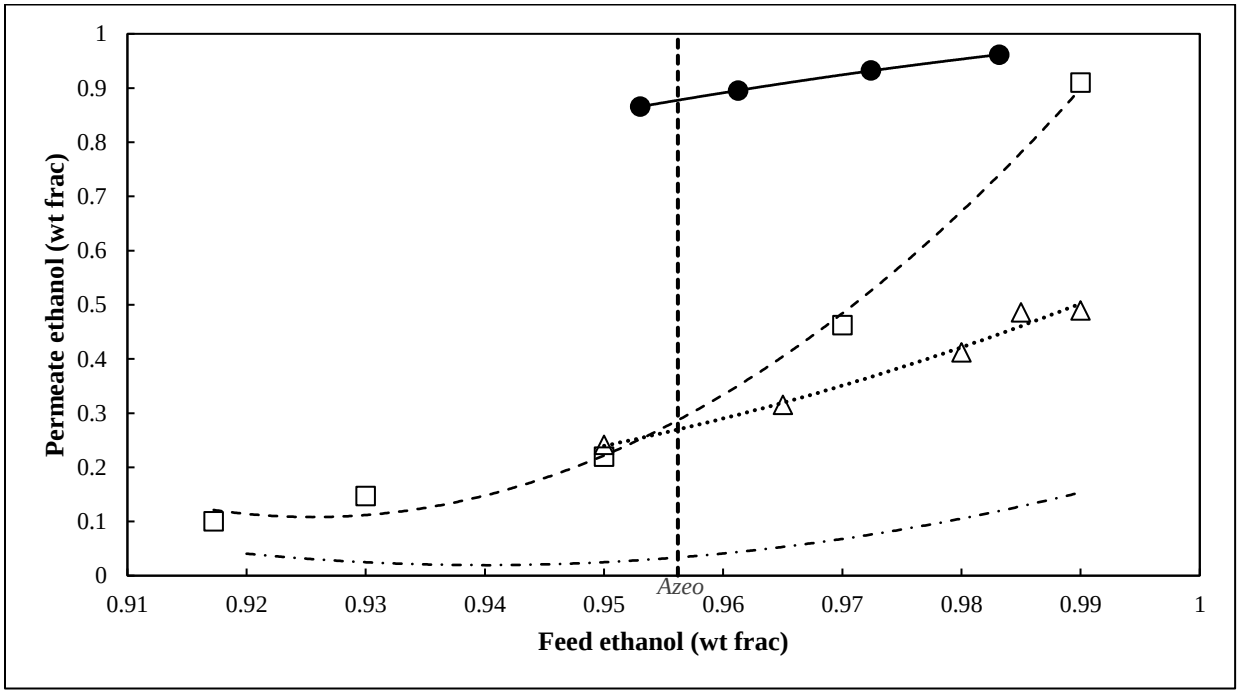

Figure 5.17. The effect of feed composition on permeate quality for the ethanol (1) + water (2) system at a permeate pressure of 2 kPa. ●, Exp, This work; Δ, Win et al. (2012); □, Wesslein et al. (1990); , Sander & Soukup (1988). Lines represent a smooth polynomial fit.

Figure 5.17 provides a representation of the changes in the permeate composition in relation to the ethanol feed content. A common effect was observed across the membranes. It is interesting that the separation achieved by Sander and Soukup (1988) and Win and Friedl (2012) are fairly similar to each other in that the permeate composition deviates greatly from ethanol purity even with a feed composition of 99 wt.% ethanol. Both literature sources reported the use of a composite membrane.

Wesslein et al. (1990) utilized a crosslinked membrane as in this study. It is possible the crosslinking effect becomes less significant when separating mixtures approaching pure ethanol composition. However, it is still worth noting that a feed containing 97.24 wt.% ethanol was separated past the azeotropic composition to give a permeate of 93.21 wt.% ethanol during experiments conducted in this work (Figure 5.17).

In summary, although the results obtained from these experiments were not comprehensive and most trends, including the relative water and ethanol fluxes being contradictory, do not correlate with the comparative reportings from literature, the experiments proved that membrane separation with PERVAP^{TM} 4100 can break the azeotrope present in ethanol-water mixtures. Many recommendations for the modification of the equipment and membrane cell are proposed, along with the experimental method to be changed. Due to the restricted access for measurements during 2020, no further modifications or experiments could be undertaken. Hence, the supervisors and student agreed to focus on the simulation exercises.

PART 2: MODELLING & SIMULATION

A simulation study was conducted to develop a realistic representation of a pervaporation process for the alcohol-water systems and to fully explore the technoeconomic feasibility of an industrial scale pervaporation process. Chapter 6 presents Part 2 of the study in which details of the method used to develop working models of pervaporation with Aspen Custom Modeler® V11 are discussed. This also includes discussion of the manner in which simulations were set up in Aspen Plus® V11. Chapter 7 reported on the simulation results of three systems with a single pervaporation unit (ethanol-water, propan-1-ol–water and propan-2-ol–water) as well as the design of an industrial process to dehydrate an aqueous propan-2-ol process stream. The latter also includes the feasibility study to determine the optimal design and a cost comparison to traditional methods of separation.

CHAPTER 6

Modelling & Simulation Methodology

Aspen Plus® is generally used to simulate processes with a library of pre-designed conventional unit operations available such as distillation, flash, reactor. However, units for specialised techniques such as membrane separation are not available in the software package libraries. Instead, a pervaporation user model can be designed using several options to customize the simulator. These include Fortran, Excel, COM models or Aspen Custom Modeler®.

In each of the methods mentioned above, three important steps are required: code development, compilation and linkage to Aspen Plus®. Most methods require separate programs to write the code and compile. However, Aspen Custom Modeler® (ACM) allows code to be written using modelling language while being compiled on the same program. Therefore, this was the chosen method for the pervaporation model design.

As discussed in Chapter 3, the mathematical model for the simulation of pervaporation can be carried out using either a thermodynamic or kinetic approach. The latter is favoured for the modelling of practical processes and module configuration since no additional models are required to be incorporated to predict selectivity and flux. The kinetic model applied in this work relies on

concentration-dependent diffusivities. Diffusion coefficients were calculated using the experimental data of literature. Each of the three alcohol-water systems considered requires a unique model code since permeation rates, and therefore predicted diffusivities, depend on component-component as well as component-membrane interactions (Lipnizki and Trägårdh, 2001).

Due to successful model development, dehydration of an industrial propan-2-ol stream was investigated. The design and optimization of the process was performed using Aspen Plus®. Basic calculations of the upscaled separation were attempted and this is presented in Appendix D.

6.1 ACM user model development

A model was created by employing a semi-empirical approach. A summary of the procedure used is provided in Figure 6.2. Initial independent variables such as feed flowrate, feed temperature (T_f), pressures of the feed (p_o) and permeate (p_l), membrane area (A) and number of cells were obtained from literature which had previously undertaken pervaporation experiments. The pervaporation performance is typically described using plots of permeate composition (reported as a wt.%) and flux (reported as a mass flowrate for a specified membrane area and duration of time). These characteristic curves were used to develop diffusion coefficients for both components of the binary system. The modelled pervaporation process was based on temperature-dependent diffusion equations, mass balances and energy balances which were solved using the developed model code.

The temperature-dependent diffusion equations were derived from component-specific diffusivities, also known as diffusion coefficients (D_i). Since literature reports feed (x_i) and corresponding permeate compositions (y_i), the model utilized the difference in concentration to describe diffusion across the membrane. According to Equation (3.21), flux (J_i) is dependent on diffusion coefficients and the concentration difference between the retentate and permeate $\left(c_{io(m)} - c_{il(m)}\right)$. Hence from measurements of flux and concentration difference, diffusion coefficients may be inferred. The feed composition was assumed as the initial estimate for the retentate composition. This was based on the solution-diffusion model, as described in Chapter 3, which assumes the retentate membrane interface is in direct contact with the stirred liquid feed

(Wijmans and Baker, 1995). Hence, although there would be some degree of a concentration boundary on the feed side, as the membrane is selectively permeable, it will likely not cause a significant limiting effect on the transport through the membrane due to the vigorous mixing on the feed side. It's effect will however likely become more significant as the feed approaches one of the pure species concentrations.

Molar concentrations of the liquid retentate ($c_{io(m)}$) and vapour permeate ($c_{il(m)}$) for each component were calculated (according to Equations (3.48) and (3.49)) using specie properties as well as operating conditions. Alcohol and water diffusivities were then calculated using the difference in retentate and permeate concentrations in combination with the reported flux from literature. For a given input of feed composition, a component-specific diffusivity was obtained as an output.

This procedure was then repeated for multiple feed compositions by employing the data available in literature. Appendix C (Table C.1 to Table C.3) provides tabulated calculated diffusivities for the feed composition range of the three systems investigated in this study. A detailed account of the calculation carried out for diffusivities is also provided under Section C.2 of Appendix C.

Average diffusivity values for both alcohol and water were then found based on the calculations described above. A best fit between the diffusion model and the experimental data was determined by analysing the full feed composition range for the lowest deviation in diffusion coefficient. It was imperative that the azeotropic point was present in the chosen feed composition range since this is the critical region for separation. The area near the azeotrope was weighted so that the model fitted the region well. This procedure is outlined under Section C.3 of Appendix C.

According to Sander and Soukup (1988), membrane flux in these processes is known to approximately double with a 10 K increase in temperature. Since Equation (3.21) illustrates that diffusivity is directly proportional to flux, the same relation was applied to the diffusivities. As a result, the relationship between component diffusivities and temperature could then be plotted using a line of best fit to describe the behaviour at various operating conditions. The line of best fit was incorporated into the diffusion equation required for a simulation user model code.

Diffusion expressions for each component were coded into the model script together with the concentration terms (Equations (3.48) and (3.49)) as a starting point for the simulation computation.

The permeate flowrate was calculated using the summation of permeate flux of each component. The permeate compositions were calculated iteratively across the flux and by applying the mass balances. Model calculations, inclusive of iterative steps for the permeate composition, were validated by manual hand calculations using Microsoft Excel. This is detailed in Section C.4 of Appendix C. A simple mass balance around a pervaporation cell provided the retentate flowrate. This is illustrated in Figure 6.1 below.

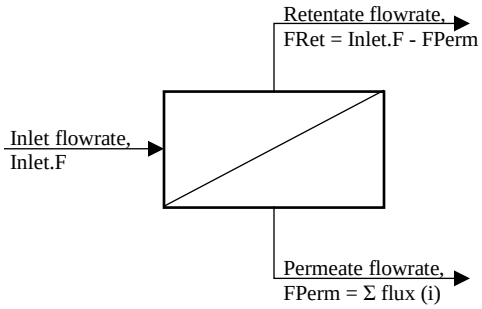

Figure 6.1. Mass balance around a single membrane cell.

The above methodology was repeated to create a user model for each of the three alcohol + water systems investigated: water + ethanol, propan-1-ol, or propan-2-ol. Models were then specified by fixing independent variables such as feed flowrate, temperature, pressures of the feed and permeate as well as the membrane area before running the model within ACM. Thereafter, the files were converted using Microsoft Visual Studio before exporting to Aspen Plus® for simulation and specifically, optimization. The model and streams required additional specification when simulating on the flowsheet.

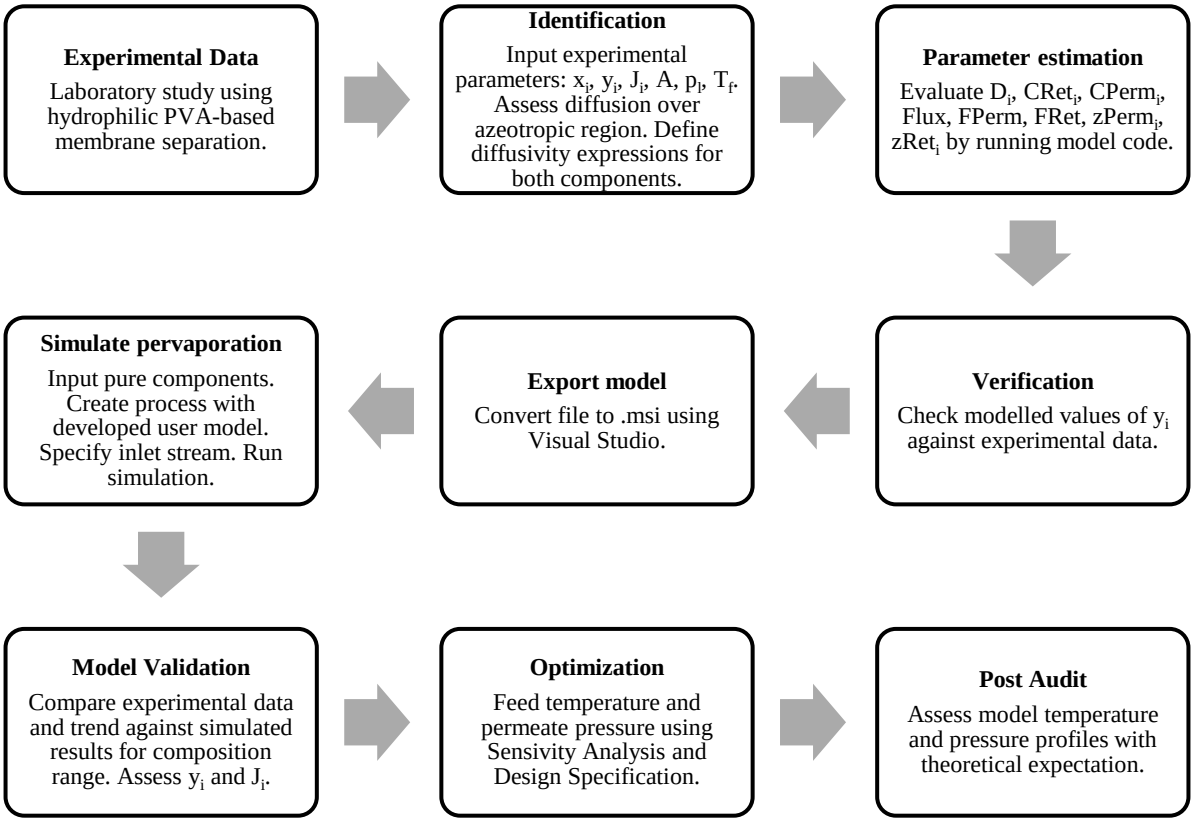

Figure 6.2. Algorithm for modelling and simulation of pervaporation.

6.2 Simulation method

In order to set up these simulations, the following steps were performed:

(i) Aspen Custom Modeler®

a. A component list containing the alcohol and water was configured using Aspen Properties® (Figure 6.3).

b. The property method of NRTL was chosen.

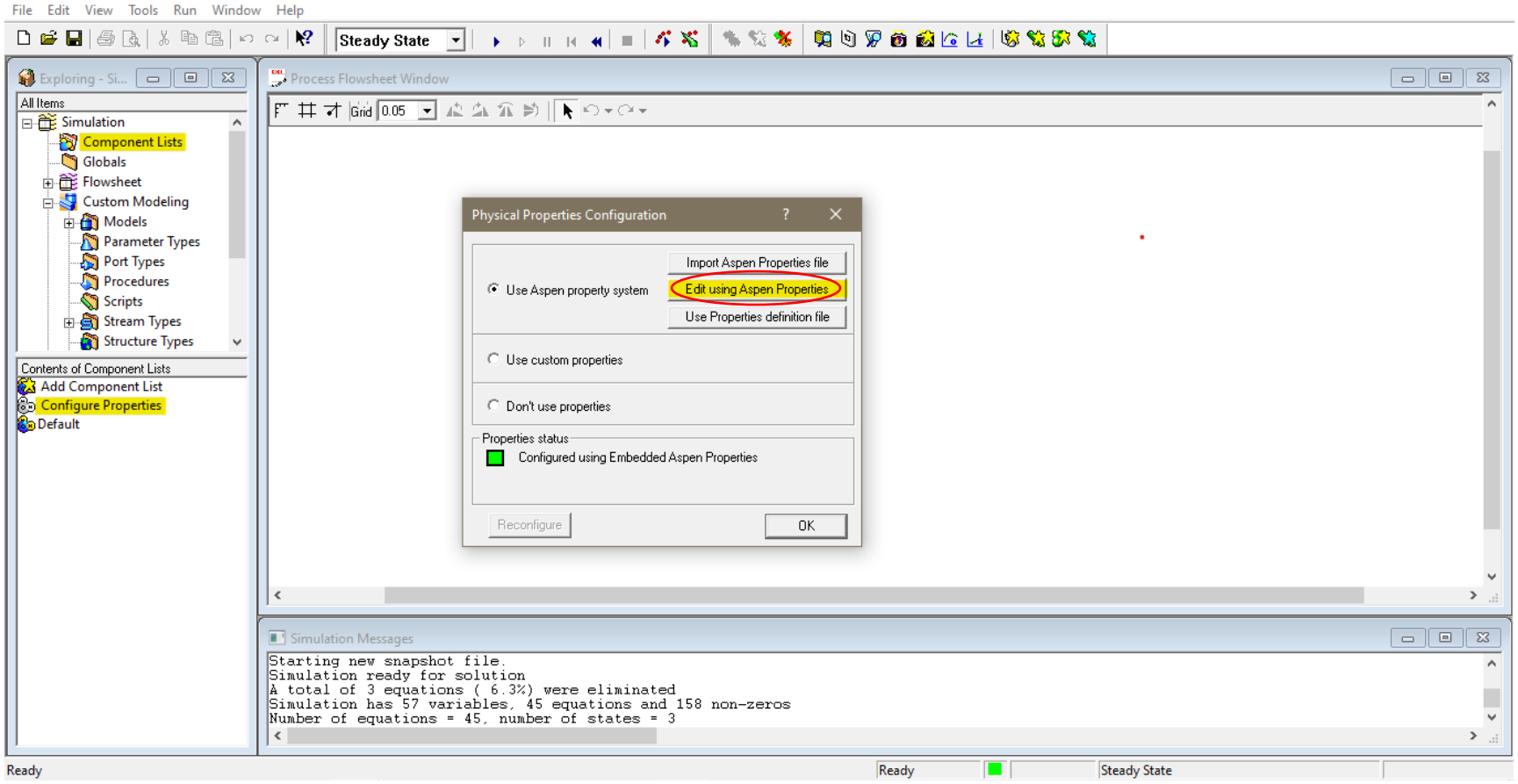

Figure 6.3. Component list configuration.

c. In the Explore Window under “Custom Modeling”, “Add model” was selected to develop the user model script for the unit (Figure 6.4). The code was scripted by first listing variables/parameters. Thereafter, the ports and streams were identified. Finally, a series of equations (including those mentioned in Chapter 3.5) were used to describe a pervaporation unit.

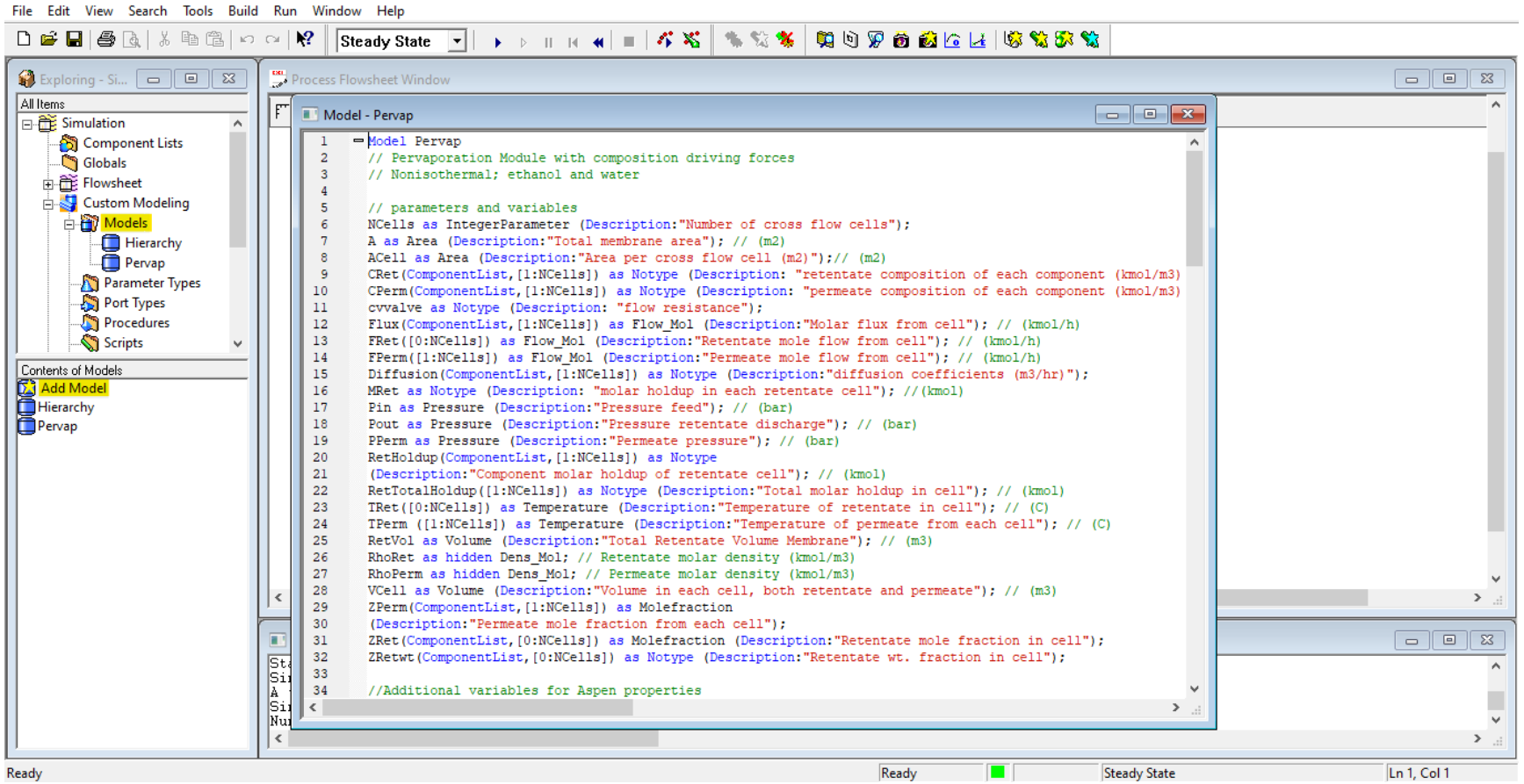

(a)

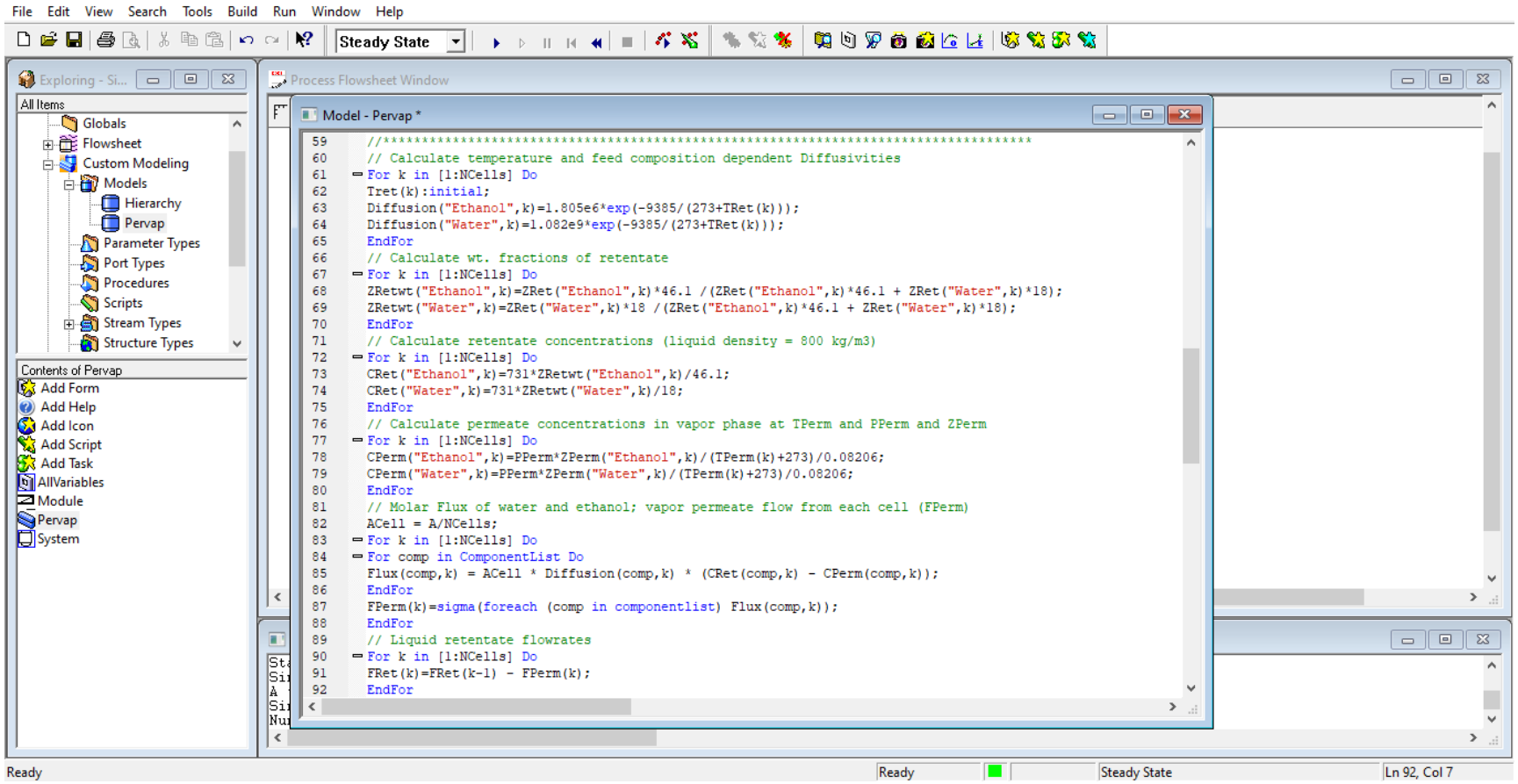

(b)

Figure 6.4. Scripted model code with (a) variables/parameters and (b) model equations.

d. The unit icon was modified (Figure 6.5). It was ensured that inlet port contained the inlet feed stream while retentate and permeate streams belonged to the outlet port. Ports are linked to streams in the user model script.

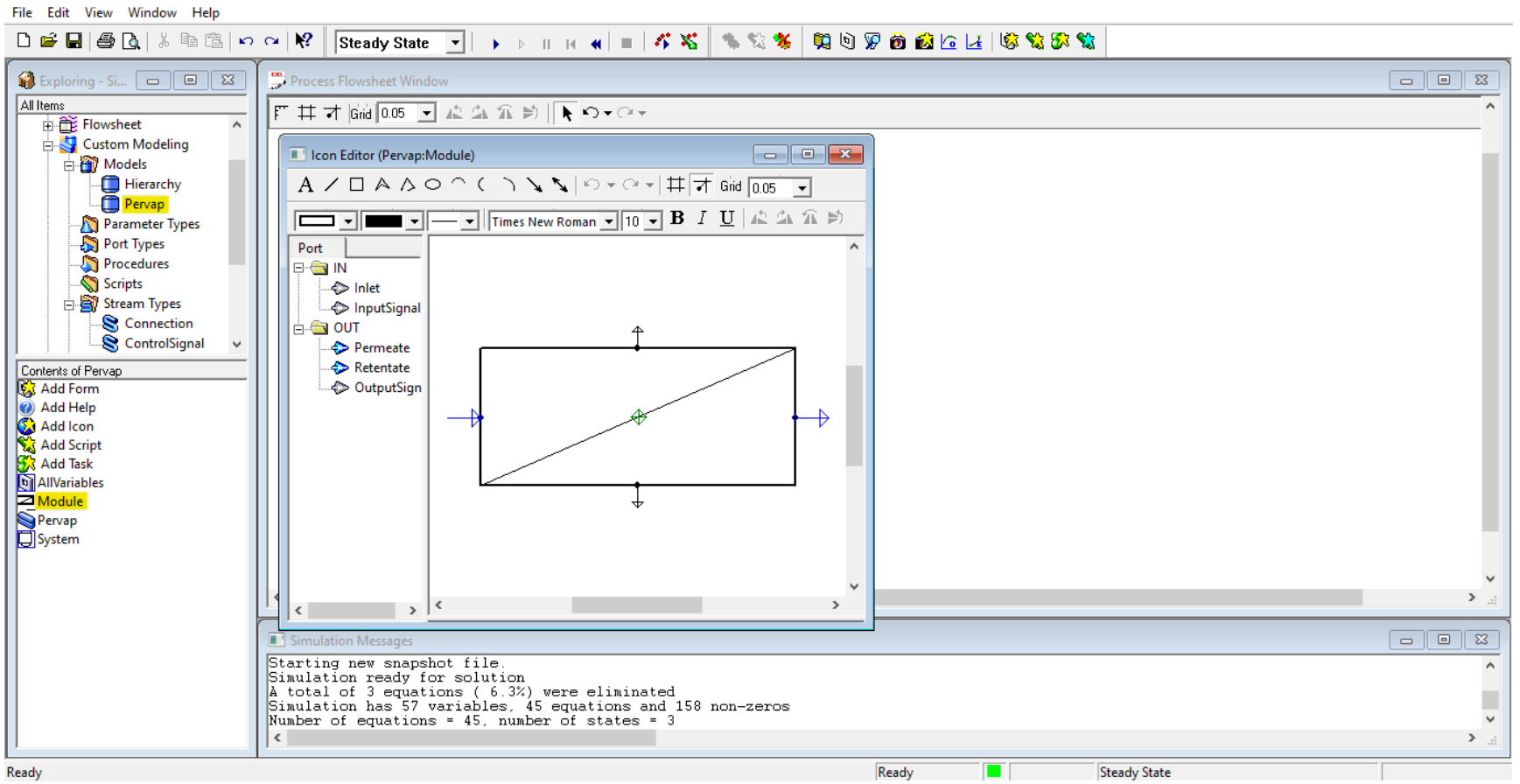

Figure 6.5. Pervaporation unit icon and ports.

e. A process flow diagram was created on the Process Flowsheet Window using the model that was compiled and under “Stream Types” in the Explore Window, “Connection” was selected for the inlet and outlet streams on the flowsheet (Figure 6.6).

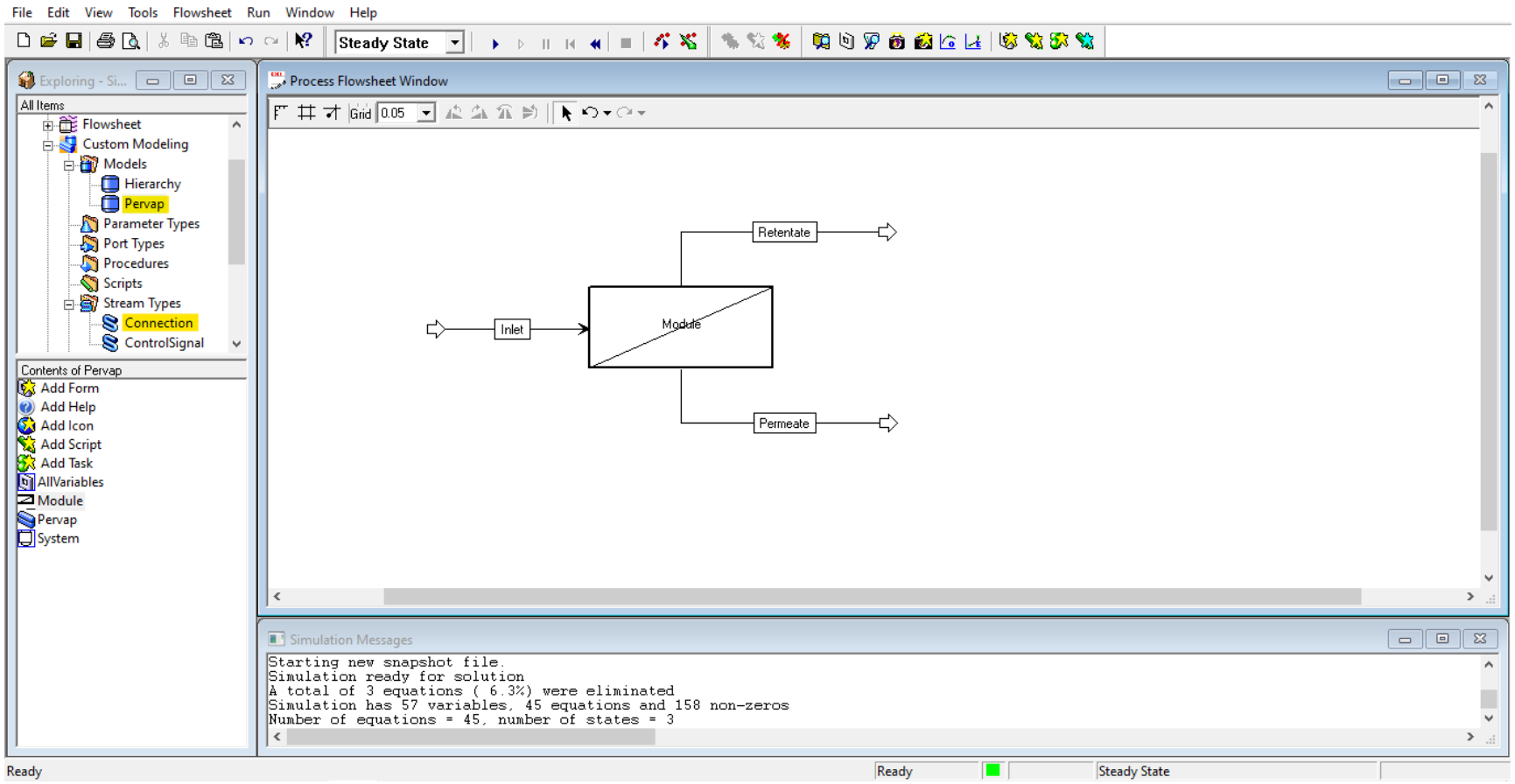

Figure 6.6. ACM flowsheet of pervaporation module.

f. The "All Variables" table for the model was accessed and the fixed and free variables were identified therein.

g. Fixed variables such as feed flowrate, temperature, pressures of the feed and permeate as well as the membrane area were specified according to the literature source used to create the corresponding diffusion expressions (Figure 6.7).

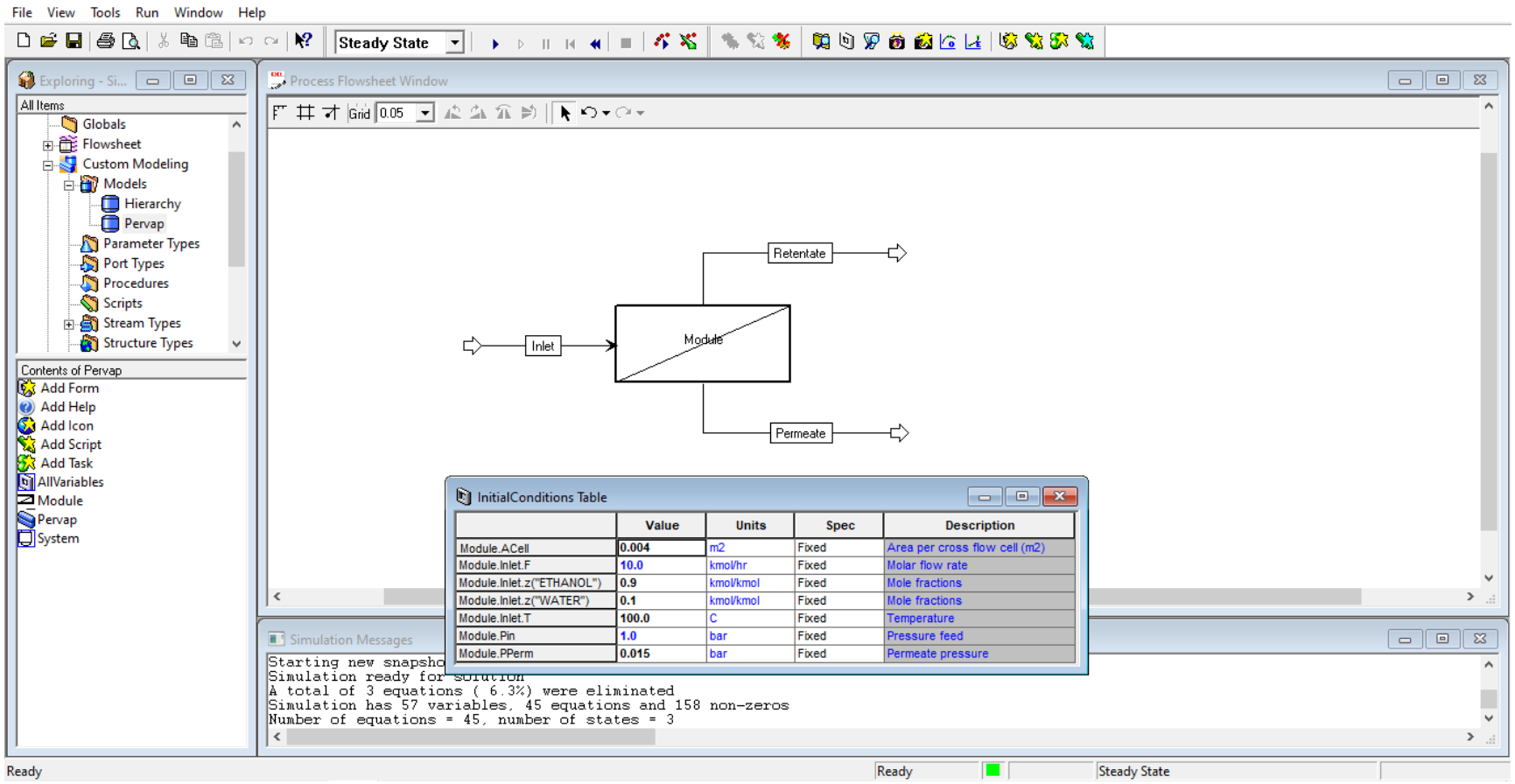

Figure 6.7. Input fixed variables.

h. The model was confirmed to be fully specified when a green square icon appeared on the bottom right of the configuration screen.

i. The model was run, and the Simulation Messages Window was monitored to ensure no errors were obtained. The results of the free variables were observed in the “All Variables” table.

(ii) Aspen Plus®

It was noticed that optimization tools such as Sensitivity Analysis and Design Specification were not available on Aspen Custom Modeler®. Therefore, ACM models were exported to Aspen Plus® following these steps:

a. The user model script was modified by removing lines of code that contained the calculation of enthalpy, heat capacity and density for mixtures.
b. The model from ACM was exported by right clicking on the model name under the Model Explorer and the file was saved as an .msi version. This can only be done by installing Microsoft Visual Studio onto the desktop.
c. A package for the model was then created.
d. The model was installed.
e. A new Aspen Plus® file was created. The components were entered and the property method was selected.
f. On the Simulation tab of Aspen Plus®, Manage Libraries on the Customize ribbon was selected and the ACM Models checkbox was ticked.
g. The .msi file was imported.
h. An ACM Model tab then appeared on the flowsheet window with the list of units available. This tab should contain all units imported from ACM for simulation and optimization.
i. Model and stream variables were specified as previously done on ACM.
j. The process was fully specified by identifying a green square on the bottom right corner of the screen before running the simulation.

6.3 Model validation

The first model created utilised the data of Luyben and I-Lung (2010) to represent an ethanol-water system. Results of the model were compared against literature flux and permeate composition to determine the accuracy of the model. The developed model was then adapted to represent a second set of data by Wesslein, Heintz and Lichtenthaler (1990). This was performed by modifying the diffusion equations for both ethanol and water using the characteristic curves of the literature source. In addition, independent variables such as feed flowrate, feed temperature, feed and permeate pressures as well as the membrane area were specified according to the

experimental conditions outlined by Wesslein, Heintz and Lichtenthaler (1990). Once again, the modelled data was compared to the literature data to judge the accuracy of the method.

The purpose of the above was to validate the method of deriving diffusivities and to ensure multiple data sets can be implemented in the developed model code. Similarly, the pervaporation of C3 alcohols, namely propan-1-ol and propanol-2-ol, were investigated by adjusting the abovementioned parameters to fit the chosen data set from literature. The effect of temperature and permeate pressure was assessed with each modified model. All systems investigated focused on dehydration exercises utilizing a PVA-based membrane.

It is important to note that the method outlined in this chapter is not limited strictly to hydrophilic PVA-based membranes. It can be used to represent various membrane types, hydrophobic membranes included, provided the pervaporation results are reported in terms of flux, feed and permeate compositions. Essentially, the characteristic curves define the performance of pervaporation with respect to the binary system and membrane of interest. The basic structure of the model code remains unchanged. However, the diffusion equations within the user model code of Aspen Custom Modeler® were replaced for each set of experimental data thereby creating new models specific to the system studied. Four main models were created namely, ethanol-water (Model 1-A and 1-B), propan-1-ol–water (Model 2) and propan-2-ol–water (Model 3). These will be discussed in Chapter 7.

6.4 Industrial implementation

Although the models were proved to represent lab-scale experiments, the application to process and separate an industrial-scale feed using a pervaporation process to replace traditional methods of separation was investigated. A pervaporation unit generally consists of a series of membrane cells grouped together in modules with interstage heating applied to the feed of subsequent modules. That is, generally, there is no heat exchange between the cells of a module. The model was used to design and configure membrane module variations for the dehydration of an industrial propan-2-ol stream of 15 wt.% water. The basis, variations in operating conditions and arrangements considered to provide the most feasible membrane separation, and general performances are discussed further in Chapter 7.

CHAPTER 7

Modelling and Simulation Results & Discussion

7.1 Developed alcohol-water models

The design and optimization of unit operations through simulation is an important engineering tool as it provides a methodology to perform rigorous analysis quickly with reliable results. Although many newer processes such as pervaporation cannot be readily simulated using simulation software such as Aspen Plus® V11, the simulator can be customized by developing user models with Aspen Custom Modeler® (ACM) V11 as described in Chapter 6.

Custom models and processes were designed for three unique alcohol-water systems namely, ethanol-water, propan-1-ol–water and propan-2-ol–water. Each of these systems exhibit a homogeneous minimum-boiling azeotrope. The simulated studies investigate pervaporation units equipped with a PVA-based membrane, with variations in conditions based on the available data to model the systems. Since the permeation of various alcohols through the membrane differ, three separate models were created to represent each system. The models were customized by modifying the diffusion equations, for both the alcohol and water, within the user model code of ACM. Due to the nature of the alcohols studied, their behaviour in varying membranes based on the interactions and diffusion properties differ. Therefore, diffusion relations were derived from characteristic curves (flux and permeate composition) presented in literature experimental studies which classifies the models as semi-empirical.

7.1.1 Property method

The non-random two-liquid (NRTL) activity coefficient model (Seader et al., 2011) was implemented to predict the properties of the pure components and the mixture. The NRTL model is recommended for chemical systems at low pressures and in particular processes involving azeotropic separations. The feed pressure for the pervaporation processes considered in this study did not exceed atmospheric pressure while the permeate pressure was significantly lower than the atmospheric pressure, creating the pressure differential which served as the driving force to facilitate permeation. The NRTL model is also commonly used for alcohols and water since the components are polar by nature (Weiss et al., 1992). The NRTL model predictions, using in-built

Aspen Plus® model parameters, were compared to available VLE data for the alcohol + water systems and were found to represent the data within experimental uncertainty.

7.2 The ethanol (1) + water (2) system

Two models (Model 1-A and 1-B) were created for the ethanol-water system in order to validate the custom model development procedure by comparison to the available experimental studies from the literature. The first model (Model 1-A) was based on findings reported by Luyben and I-Lung (2010) whereas the second model (Model 1-B) was based on the data presented by Wesslein, Heintz and Lichtenthaler (1990). Figure 7.1 and Figure 7.2 compare the results of both models developed in this work to experimental data from various literature sources (Luyben and I-Lung, 2010; Sander and Soukup, 1988; Wesslein et al., 1990; Win and Friedl, 2012).

Luyben and I-Lung (2010) reported the water flux and composition of the permeate vapour for the ethanol (1) + water (2) system. These plots were used to derive diffusion equations (7.1) and (7.2) for ethanol and water, respectively. The temperature-dependent diffusivities characterize the developed model. Operating conditions in this study included a feed temperature of 373 K and a permeate pressure of 1.5 kPa. It must be noted that the feed had to be held at an elevated pressure for this feed temperature to be achieved. The laboratory test cells comprised a membrane with a surface area of 0.002 or 0.004 m^2. Both cells were available and used during experiments. Since the model required a constant membrane area, 0.004 m^2 was chosen as a simulation input to specify the system for consistency.

The equations for the ethanol and water diffusivities ($m.h^{-1}$) as derived for Model 1-A are provided below in which temperature is in (K):

$$D_1 = 1.805 \times 10^6 \, e^{\left(-\frac{9385}{T}\right)} \tag{7.1}$$

$$D_2 = 1.082 \times 10^9 \, e^{\left(-\frac{9385}{T}\right)} \tag{7.2}$$

For the second model (Model 1-B), Wesslein, Heintz and Lichtenthaler (1990) performed experiments with a feed temperature of 333 K and a permeate pressure of 2 kPa. The experimental setup consisted of 4 cells with a total membrane area of 0.016 m^2. The reported flux and permeate composition diagrams provided sufficient data to create the second model. Equations (7.3 and (7.4 represent the diffusivities for ethanol and water, respectively using the data from Wesslein, Heintz and Lichtenthaler, (1990).

The equations for the ethanol and water diffusivities ($m.h^{-1}$) as derived for Model 1-B are provided below, in which temperature is in (K):

$$D_1 = 6.555 \times 10^5 \, e^{\left(-\frac{3650}{T}\right)} \tag{7.3}$$

$$D_2 = 3.517 \times 10^8 \, e^{\left(-\frac{3650}{T}\right)} \tag{7.4}$$

It is clear that the diffusivities for both models differ to a great degree. This is due to the operating temperature and structure of the membrane employed during experiments. Model 1-A (Luyben and I-Lung, 2010) represented a composite membrane separation at a relatively high feed temperature of 373 K which boosted the total flux (895.14 $g.m^{-2}h^{-1}$ for a feed ethanol of 92 wt.%). Alternatively, Model 1-B (Wesslein et al., 1990) was based on experiments conducted with a crosslinked membrane which is known to provide extra strength and prevent excessive swelling. The feed was heated to 333 K which is lower than that of Model 1-A and hence, a considerably lower flux of 186.41 $g.m^{-2}h^{-1}$ was obtained for a feed composition of 92 wt.% ethanol. Both literature sources also displayed a difference in membrane selectivity. Therefore, the variance between the diffusivities, from Model 1-A and 1-B, was expected.

7.2.1 Effect of feed concentration

A comparison must first be made between the model and the experimental data to validate the accuracy and reliability of the model. As previously mentioned, the semi-empirical model is based on two inputs, namely, concentration of ethanol in the permeate and the water flux. The model validation permits the comparison to additional literature sources reporting on ethanol-water separations using PVA membranes.

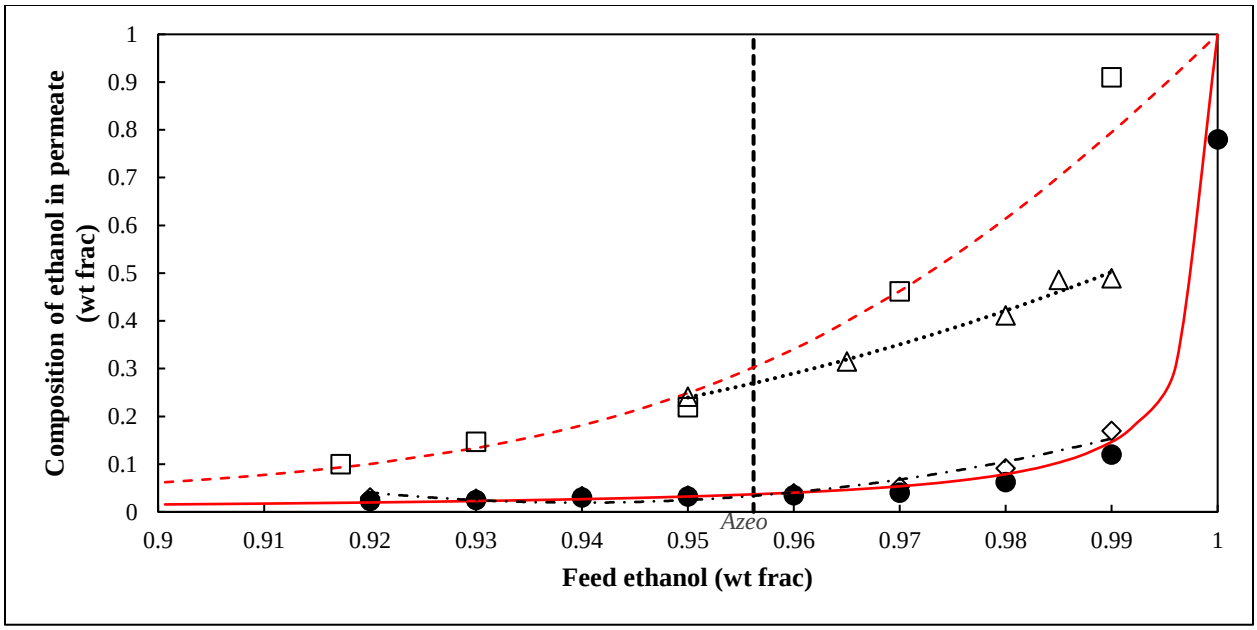

Figure 7.1. The effect of feed composition on permeate quality for simulated ethanol (1) + water (2) system. ●, Luyben and I-Lung (2010); Δ, Win et. al (2012); □, Wesslein et. al (1990); ◊, Sander and Soukup (1988). Red lines are the developed models; black lines represent a smooth polynomial fit of literature data. Solid line (-) represents Model 1-A; dashed line (---) represents Model 1-B.

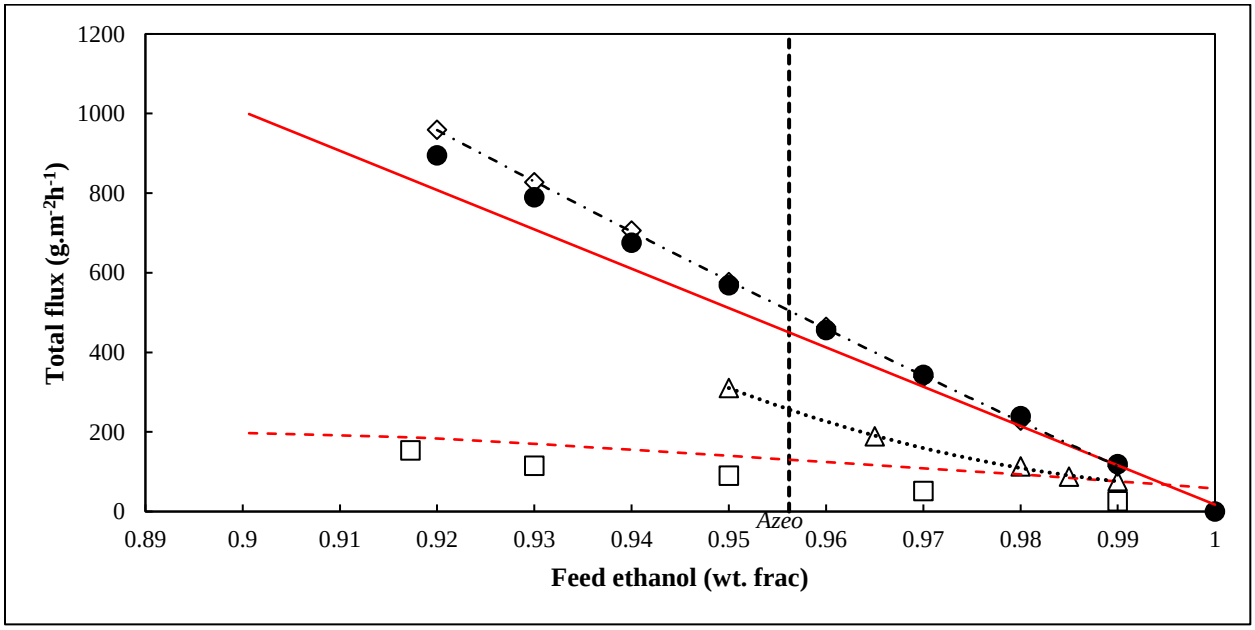

Figure 7.2. Total flux versus feed composition for simulated ethanol (1) + water (2) system. ●, Luyben and I-Lung (2010); Δ, Win et. al (2012); □, Wesslein et. al (1990); ◊, Sander and Soukup (1988). Red lines are the developed models; black lines represent a smooth polynomial fit of literature data. Solid line (-) represents Model 1-A; dashed line (---) represents Model 1-B.

It can be observed in Figure 7.1 and Figure 7.2 that a similar trend between the models and the reported literature data was observed. An increase in feed ethanol concentration translates to the permeate having a higher composition of ethanol. As previously explained in Chapter 5, ethanol permeation is raised when the feed approaches ethanol purity. PVA-based membranes dehydrate the feed sufficiently to create a high quality permeate. However, ethanol may diffuse into the permeate in small proportions and the model adequately represents this realistic behaviour found during experiments.

Figure 7.1 illustrates a strong correlation between the two models and the experimental data extracted from Wesslein, Heintz and Lichtenthaler (1990) and Luyben and I-Lung (2010). The permeate purity obtained from the models compare with the results reported from the experiments. It was noted that Model 1-B (Wesslein et al., 1990) displayed a 12.63% deviation in permeate composition from the experimental data of literature at 99 wt.% feed ethanol. This was due to the feed range selected to derive the diffusion equations. Since this report focuses on the separation of azeotropic mixtures, the model and diffusion equations were weighted to obtain the least deviation for the permeate composition near the azeotrope. A 2.85% deviation between Model 1-B and experimental data of Wesslein, Heintz and Lichtenthaler (1990) was observed at the azeotrope composition of 95.62 wt.% ethanol. Rather than compromising the accuracy at the azeotrope, a separate model for highly concentrated ethanol mixtures can be designed. However, this may not be required for industry purposes and is beyond the scope of this work.

Both models indicate a slight deviation for total flux as shown in Figure 7.2 over the composition range (0.9 – 1.0) ethanol feed mole fraction. Model 1-A provided a fair representation of flux for the experimental data of Luyben and I-Lung (2010). However, it was observed that Model 1-A (Luyben and I-Lung, 2010) displayed a deviation of 7.87% compared to the experimental data at the azeotropic feed. This can be attributed to the assumption of the membrane area stated earlier, as the membrane area was reported to be within a range of values. The permeate flowrate of the model was calculated as the sum of specie flux through a pervaporation cell and the flux computation included the membrane area. Experiments were performed in cells with either 0.002 or 0.004 m^2 while the model implemented a constant membrane area of 0.004 m^2.

However, further analysis of the modelled system revealed a minor deviation of 1% in total flux (Table D.1 of Appendix D) when implementing a membrane area of 0.002 m^2 for the range of 90

– 100 wt.% ethanol. The deviation was projected to increase with a wider composition range (Figure D.1 of Appendix D). Since all other parameters such as feed flowrate, feed temperature and permeate pressure were tested realistic values from the literature, a significant factor in the 7.87% deviation in flux may have been due to the assumed timespan (1 hour) of each pervaporation experiment. It is possible experiments were performed slightly under 60 minutes which would have led to the model possessing a lower permeate flowrate and subsequently, a lower flux than the literature source used to derive the model.

The trend of Model 1-B in Figure 7.2 is in agreement with the experimental data of Wesslein, Heintz and Lichtenthaler (1990). The slight discrepancy may be due to values of the feed flowrate which was estimated, true active area, and the temperature dependence of the model implemented in the simulation. The permeate flowrate is directly dependent on the quantity of feed fed to the pervaporation cell. As a result, the permeate flowrate and flux deviated from the experimental data. Nevertheless, Figure 7.2 illustrated systems exhibiting low range flux can also be modelled.

Overall, the flux was expected to decrease with a high feed ethanol concentration due to the permeation effect as less water molecules are present to diffuse into the permeate. This translates to a steep decline in the total flux. In addition, the data of Sander and Soukup (1988) and Model 1-A displayed an increased flux in comparison to the remaining literature sources. This can be explained by two factors; operating temperature and membrane structure. Wesslein, Heintz and Lichtenthaler (1990) used a crosslinked membrane which provided additional strength and support. This prevented membrane swelling; hence the flux was maintained.

Temperature-dependent diffusivities for Model 1-A were modelled using the reported feed temperature of 373 K (Luyben and I-Lung, 2010). Sander and Soukup (1988) employed temperatures between 363 – 373 K whereas Model 1-B based on data from Wesslein, Heintz and Lichtenthaler (1990), and Win and Friedl (2012) used a feed heated to 333 and 348 K respectively. Due to the closely related feed temperatures, the data from Luyben and I-Lung (2010) and Sander and Soukup (1988) display similar behaviour as do Wesslein, Heintz and Lichtenthaler (1990) and Win and Friedl (2012). Elevated temperatures may cause polymer chains to move more freely facilitating greater diffusion resulting in a higher flux. Therefore, a different range of flux was reported in the literature for the ethanol-water systems.

The ability of a membrane to separate a feed mixture which lies in the azeotropic region is of particular importance when modelling a pervaporation unit. According to Figure 7.1, a feed concentrated with 96.28 wt.% ethanol can be separated to provide a permeate with 95.67 and 62.84 wt.% water with Model 1-A and 1-B, respectively. Repeatable results for these experiments are difficult to control in batch experiments, due to transport effects to the membrane, active surface area, membrane swelling and defects from wear, temperature variations etc. Hence, the modelling procedure can be used to simulate the continuous process considering a range of results that correlate well with realistic experimental data. For example, Model 1-A shows that a yield permeate concentration of 81.98 wt.% water with a feed containing 99.21 wt.% ethanol could principally be obtained in the continuous process.

7.2.2 Effect of feed temperature

It was expected that a rise in feed temperature will produce a higher flux with more ethanol in the permeate since a greater quantity of molecules pass through the membrane. As mentioned in Chapter 3, the mathematical models in this work are developed using a kinetic approach. An increase in feed temperature, increases the partial vapour pressure of components thereby, leading to a raised flux. Therefore, the driving force of partial vapour pressure difference is being incorporated into the model. Sander & Soukup (1988) stated the flux generally doubles with a 10 K increase in temperature. This assumption was used to develop diffusion equations for the continuous process model.

The study conducted by Wesslein, Heintz and Lichtenthaler (1990), represented by Model 1-B, consisted of rigorous analysis with varying feed temperatures (298 – 348 K). However, the experimental data of Luyben and I-Lung (2010) did not present a plot for the effect of varying temperature on pervaporation. In addition, the feed temperature (373 K) implemented in the experiments performed was at the normal boiling point of the less volatile component being water. Therefore, it was decided to perform an analysis of the temperature effect of Model 1-A to extend the applicable range of the original experimental data. Figure 7.3 and Figure 7.4 represent a sensitivity analysis of the model for the effect of feed temperature on the ethanol permeate weight fraction and the component fluxes, with comparisons to literature for both parameters.

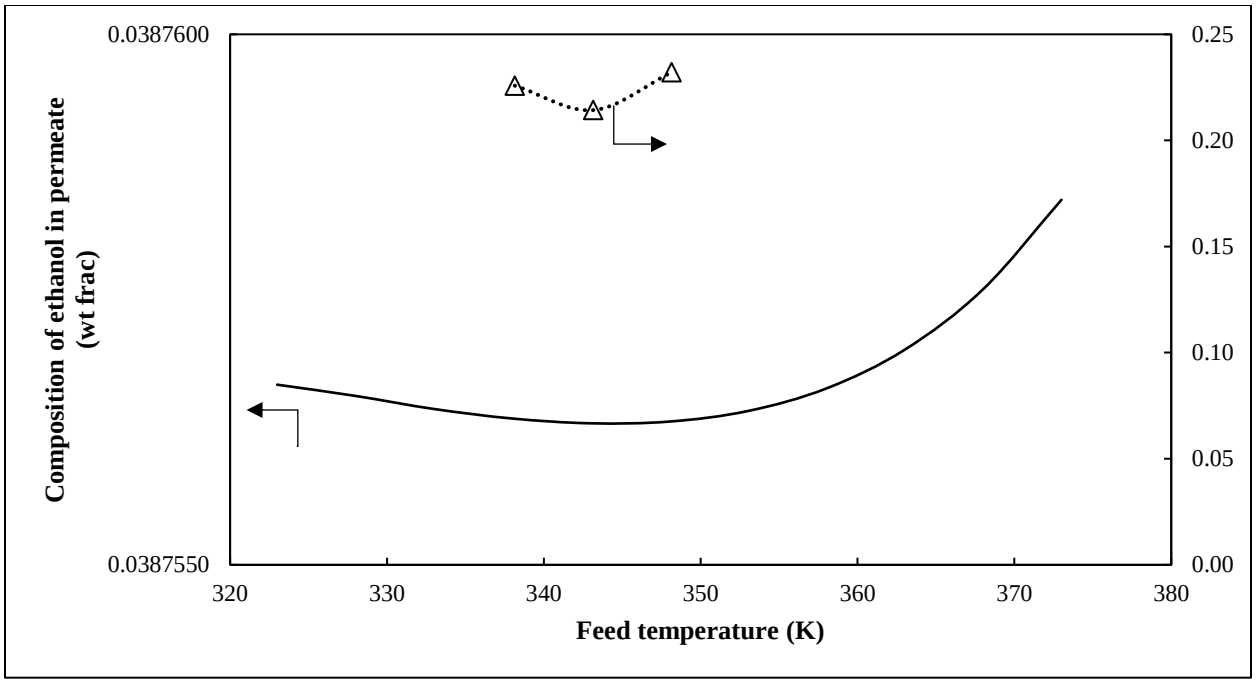

Figure 7.3. The effect of feed temperature on permeate quality for simulated ethanol (1) + water (2) system. Solid line (-), Model 1-A based on Luyben and I-Lung (2010); Δ & dotted line (…), Win et. al (2012).

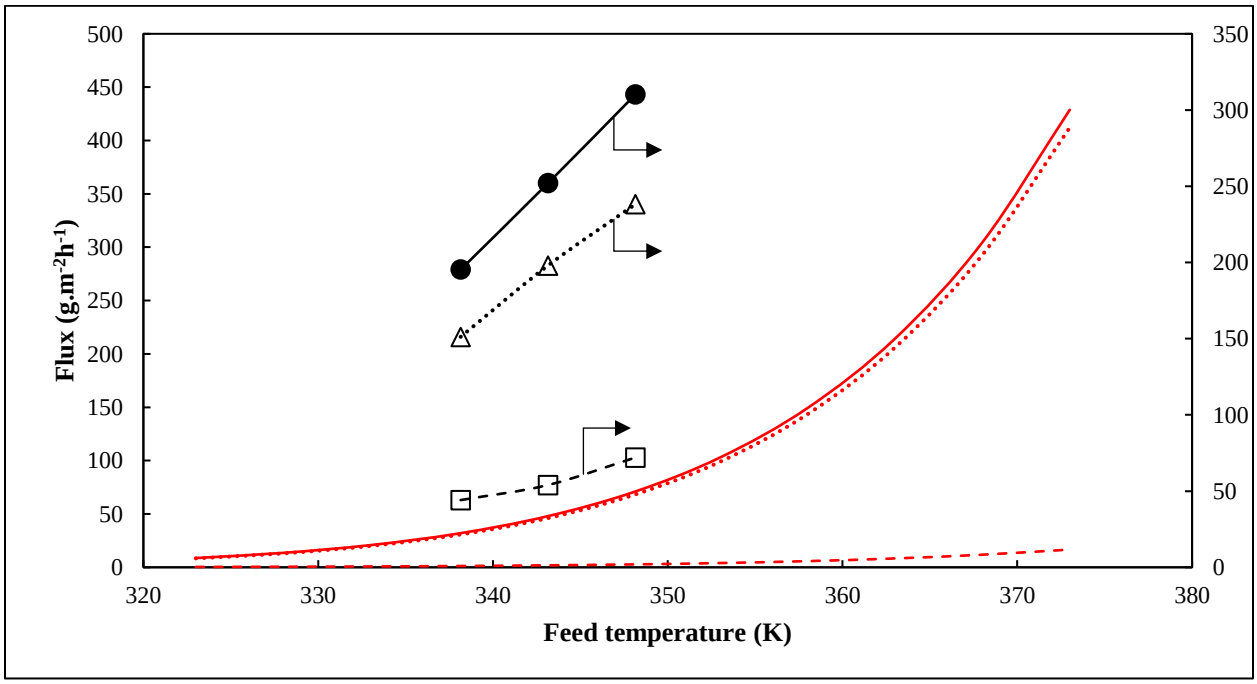

Figure 7.4. Flux versus feed temperature for simulated ethanol (1) + water (2) system. ● & solid line (-), total flux; □ & dashed line (---), ethanol flux; Δ & dotted line (…), water flux. Red lines represent Model 1-A; black lines represent literature source of Win and Friedl (2012).

Figure 7.3 illustrates that the model and literature temperature trend behave in a similar manner, namely the minimum ethanol composition observed experimentally by Win and Friedl (2012) for the given temperature range, although spurious, was effectively replicated by the model. The minimum permeate composition (3.88 wt.% ethanol) of Model 1-A was observed at 348 K. A temperature range of 338.15 – 348.15 K was investigated by Win and Friedl (2012) with the minimum permeate ethanol of 21.43 wt.% displayed at 343 K. The minimum temperature of the experimental study is lower than that of Model 1-A. This is attributed to variations in the membrane properties and relative fluxes obtained which will also influence the optimal temperature for the membrane. However, the model validation against the achievable purity in Figure 7.1 provides sufficient confidence in the result obtained.

It is important to note the permeate composition remained relatively constant with increasing feed temperature. This highly sensitive behaviour was modelled according to two conclusions made by Sander and Soukup (1988): the permeate composition is dependent on the alcohol feed rate, and the composition of the permeate from a PVA composite membrane remains constant for a wide range of feed compositions. The latter was true except at 98 – 99 wt.% ethanol according to the characteristic curves of Luyben and I-Lung (2010). Hence, the requirements of Sander and Soukup (1988) were met by implementing a constant feed of 10 $kg.h^{-1}$ with 95.84 wt.% ethanol as a specification for Model 1-A. This led to the temperature effect on flux (Figure 7.4) being more prominent than the effect on the composition of ethanol in the permeate (Figure 7.3).

The effect of temperature on flux is more apparent as shown in Figure 7.4. An exponential increase in flux was observed with increasing temperature. This correlates with the temperature assumption of Sander and Soukup (1988) employed in the model within 2%. Although the experiments of Win and Friedl (2012) and Luyben and I-Lung (2010) both employed composite membranes, the flux calculated in the literature exceeds that of the model. This indicated that the PVA/PAN membrane of Win and Friedl (2012) had a greater sensitivity to temperature and possibly experienced more swelling in the experimental study.

Table 7.1. Feed temperature and corresponding water flux for optimization.

Feed temperature (K)	Water flux ($g.m^{-2}h^{-1}$)
323	8.36
328	13.02
333	20.02
338	30.38
343	45.56

The feed temperature of Model 1-A was optimized to lower energy costs and produce a feasible process configuration with the lowest possible heat requirement. An initial temperature of 373.15 K was specified by Luyben and I-Lung (2010). Although this produces a high quality permeate of a reasonable quantity (3.88 wt.% ethanol and 412.12 $g.m^{-2}h^{-1}$), the retentate would boil which results in a mixture of liquid and vapour which is undesirable in non-hybrid pervaporation operations. This was expected since feed temperatures should not exceed 351.55 K which is the boiling point of ethanol, and which is lower as the azeotrope is approached. A design specification was conducted at a fixed pressure of 100 kPa using Aspen Plus® to determine the maximum feed temperature required to maintain a liquid phase of the retentate. A temperature of 343.89 K, producing a permeate with 98.45 wt.% water, was obtained as the upper limit for the temperature range. The lower limit was then determined by selecting the lowest temperature capable of maintaining 98.45 wt.% water in the permeate. Thus, the sensitivity analysis revealed a minimum feed temperature of 323.15 K could be implemented for the ethanol-water separation method. Given that the permeate composition was not significantly impacted by a heated feed, the temperature profile of Figure 7.4 was studied. Table 7.1 shows the proportional relationship between feed temperature and water flux. Since it is evident a trade-off between energy consumption and water flux exists, a satisfactory compromise was made. Therefore, it was decided that a feed temperature of 333 K was low enough to reduce energy costs while providing a reasonable water flux of 20.02 $g.m^{-2}h^{-1}$ at the retentate condition.

7.2.3 Effect of permeate pressure

Permeate-side pressure creates the driving force for any pervaporation process. The semi-empirical model assumed that diffusion was influenced by the concentration gradient between the retentate and permeate. The concentration of the permeate incorporates permeate pressure to correctly model its impact. Luyben and I-Lung (2010) specified a downstream pressure of 1.5 kPa. Once again, due to the lack of experimental data from Luyben and I-Lung (2010) to describe the effect of varying pressure, an analysis of the pressure effect was carried out using Model 1-A. Model sensitivities and comparison to other existing literature sources are provided in Figure 7.5 and Figure 7.6.

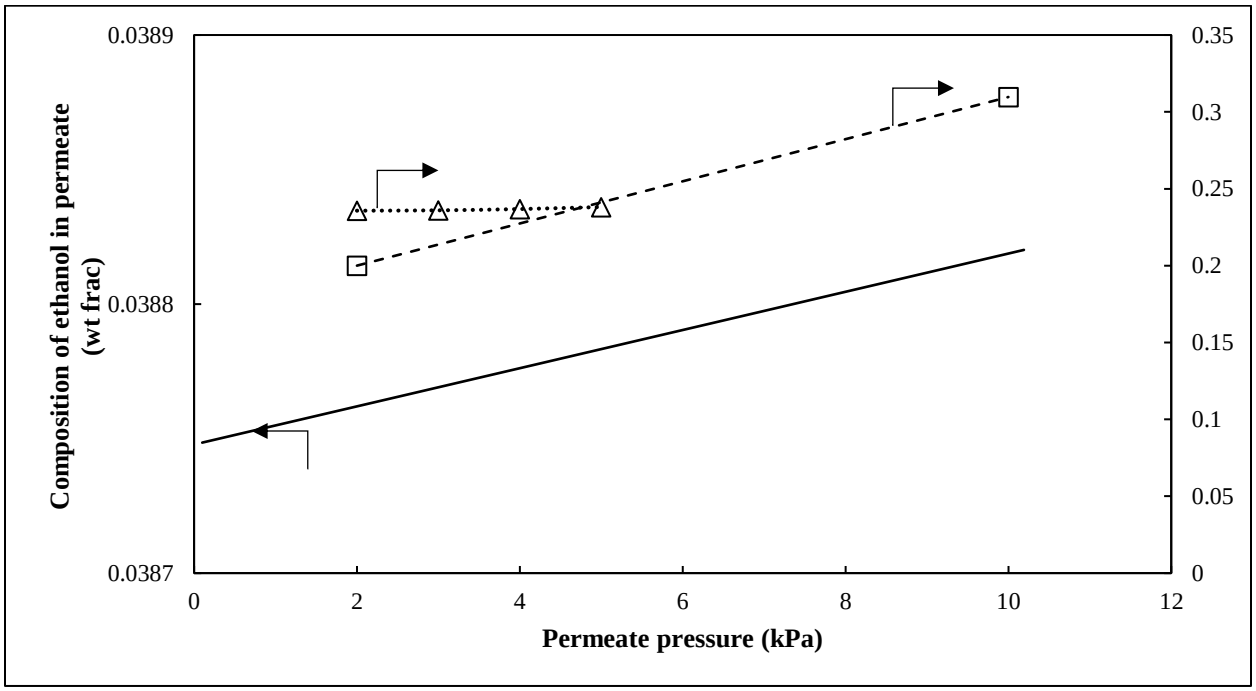

Figure 7.5. The effect of permeate pressure on permeate quality for simulated ethanol (1) + water (2) system. Solid line (-), Model 1-A based on Luyben and I-Lung (2010); Δ & dotted line (…), Win et. al (2012); □ & dashed line (---), Wesslein et. al (1990).

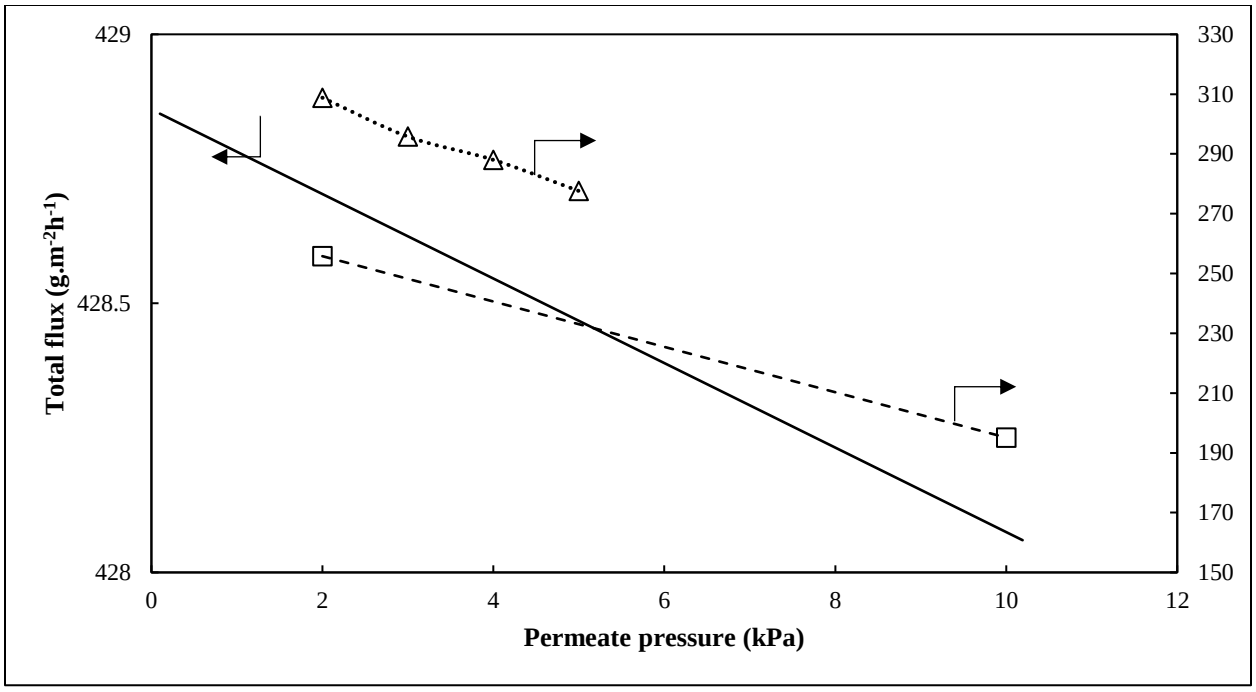

(a)

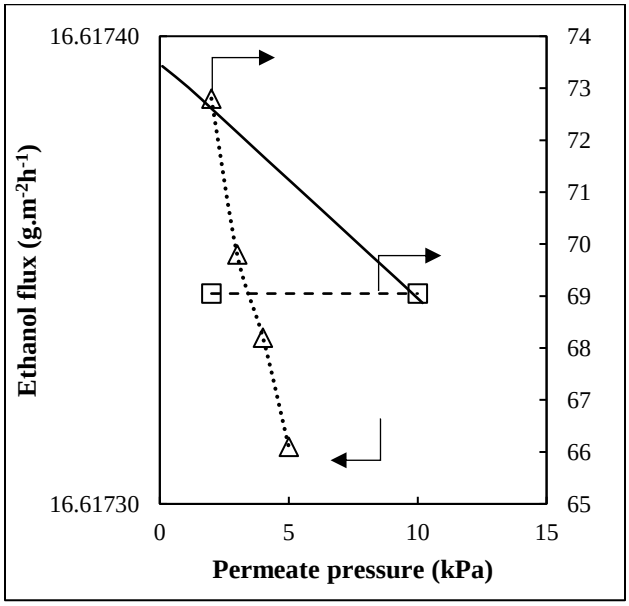

(b)

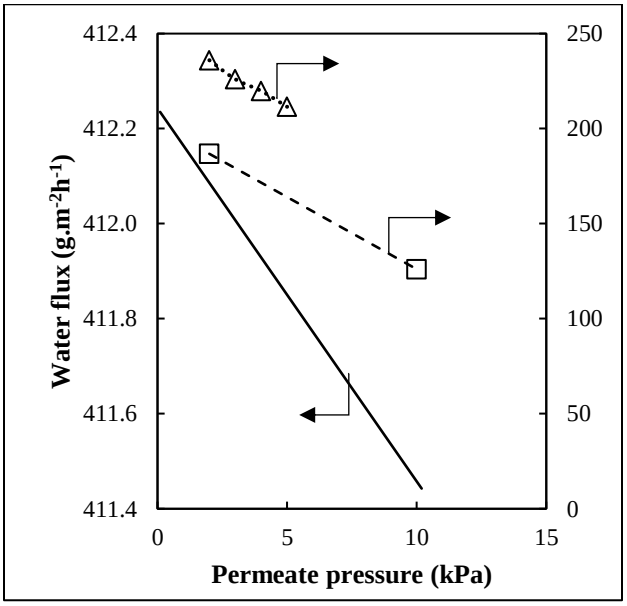

(c)

Figure 7.6. Flux versus permeate pressure for simulated ethanol (1) + water (2) system: (a) Total flux; (b) Ethanol flux; (c) Water flux. Solid line (-), Model 1-A based on Luyben and I-Lung (2010); Δ & dotted line (…), Win et. al (2012); □ & dashed line (---), Wesslein et. al (1990).

In Figure 7.5 the effect of pressure on the quality of the permeate was studied. As predicted by literature, the permeate ethanol composition increased with increasing pressure. The elevated composition exhibited by the model and data of Win and Friedl (2012) presents a gradual increase. This is in contrast to the steep gradient shown in results presented by Wesslein, Heintz and Lichtenthaler (1990). It is worth noting that the experimental study of Wesslein, Heintz and Lichtenthaler (1990) proposed the use of a crosslinked membrane. Hence, the membrane properties and the resulting pressure threshold differs by a significant degree when compared to the composite membrane which seems to offer greater stability for varying pressures.

An increased pressure creates a weaker driving force for pervaporation thereby hindering the movement of permeating species. This theory was reflected in the total flux decline observable in Figure 7.6 (a). Ethanol flux was generally stable across the range of pressures studied in Figure 7.6 (b) with the data of Win and Friedl (2012) exhibiting a slightly greater pressure dependence of the ethanol permeation compared to the other sources. The water flux of Figure 7.6 (c) replicates the behaviour of total flux since water is the preferentially permeating specie for a PVA-based membrane. The increased water and total flux of the model can be substantiated by the temperature of the heated feed. Luyben and I-Lung (2010) used a feed temperature of 373 K. A temperature difference of up to 40 K exists between the model and literature sources. As a result, at a pressure of 2 kPa, the flux from Model 1-A (428.69 $g.m^{-2}h^{-1}$) was almost double that of Wesslein, Heintz and Lichtenthaler (1990) (255.79 $g.m^{-2}h^{-1}$).

Pressure optimization was performed by studying the various pressures in the range of 0.1-10 kPa using a sensitivity analysis. The optimum case obtained by simulations that maintained a reasonable flux without compromising the permeate quality was found to be 1.5 kPa. This is in accordance with the operating pressure initially proposed by both Luyben and I-Lung (2010) and Sander and Soukup (1988). A pressure of 0.1 kPa yielded a maximum water flux of 412.24 $g.m^{-2}h^{-1}$. However, it was not necessary to operate at the lower limit. A permeate pressure of 1.5 kPa was still capable of maintaining a water flux of 412.13 $g.m^{-2}h^{-1}$ which is suitable as it does not deviate significantly from the maximum flux achievable (412.24 $g.m^{-2}h^{-1}$).

7.3 The propan-1-ol (1) + water (2) system

Pervaporation studies on higher alcohol-water systems such as propan-1-ol + water are limited in the literature with only 4 reported sources in the open literature (Chan et al., 1997; Nieuwenhuis et al., 1987; Teleman et al., 2006; Will and Lichtenthaler, 1992). The work presented in Section 7.2 demonstrated the ability of the developed model to replicate results of experimental data that was practicably suitable for simulation purposes. In the model development, it was confirmed that one set of experiments was sufficient to provide a working model of the system. In this section, the dehydration of propan-1-ol–water was investigated by developing a pervaporation model using the method outlined in Chapter 6 and observing the effect of feed concentration, temperature and permeate pressure on the achievable separation. The research performed in this section of the report will contribute towards membrane studies not fully explored and provide better insight to industrial applications, and uptake of the technology.

Model 2 which was designed for the propan-1-ol–water system was based on the experimental results reported by Will and Lichtenthaler (1992). Operating conditions for the propan-1-ol–water system included a feed temperature of 348 K and permeate-side pressure of 3 kPa. The effective membrane area for a cell was stated to be 0.0039 m^2. A PVA-based composite membrane with a PAN supporting layer was applied in the study to obtain experimental data.

The equations for the propan-1-ol and water diffusivities ($m.h^{-1}$) as derived for Model 2 are provided below, in which temperature is in (K):

$$D_1 = 3.111 \times 10^7 \, e^{\left(-\frac{8636}{T}\right)} \tag{7.5}$$

$$D_2 = 1.026 \times 10^9 \, e^{\left(-\frac{8636}{T}\right)} \tag{7.6}$$

7.3.1 Effect of feed concentration

The impact of varying feed compositions on the separation performance was described in terms of the permeate weight fraction and component flux. This was studied using the plotted data of Figure 7.7 and Figure 7.8. Initial conditions of the experiments such as feed temperature and permeate pressure were optimized separately to improve performance.

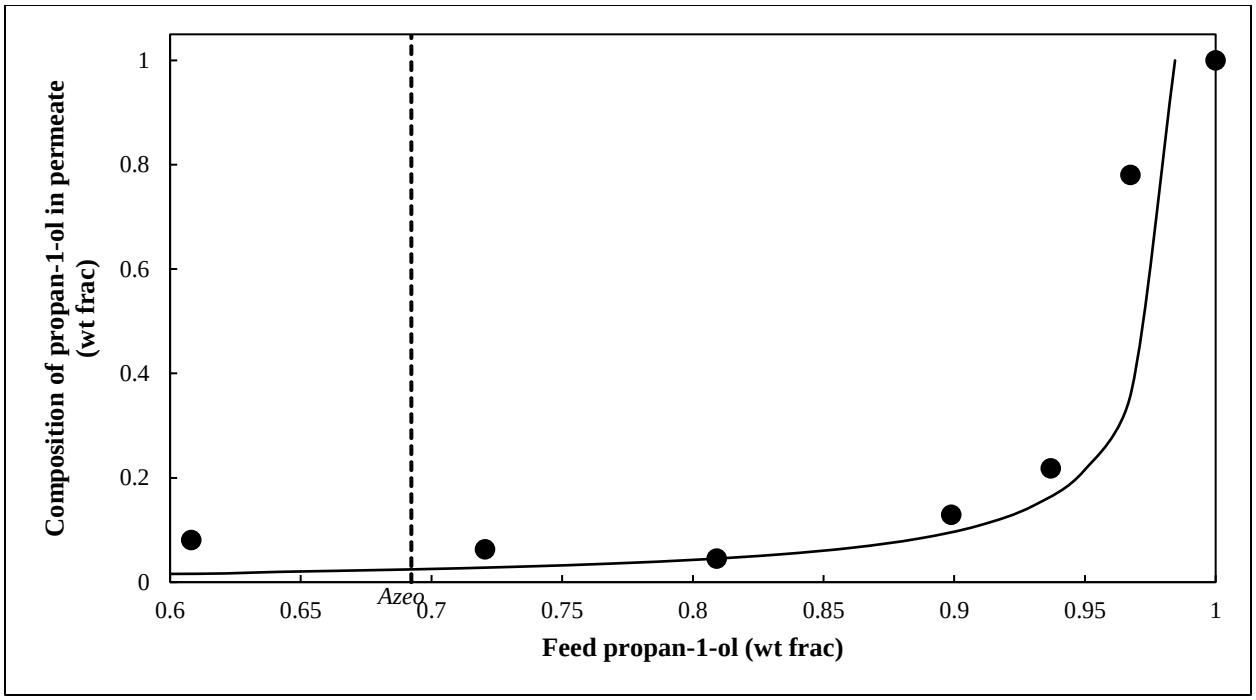

Figure 7.7. The effect of feed composition on permeate quality for simulated propan-1-ol (1) + water (2) system. ●, Will and Lichtenhaler (1992). Solid line (-) represents Model 2.

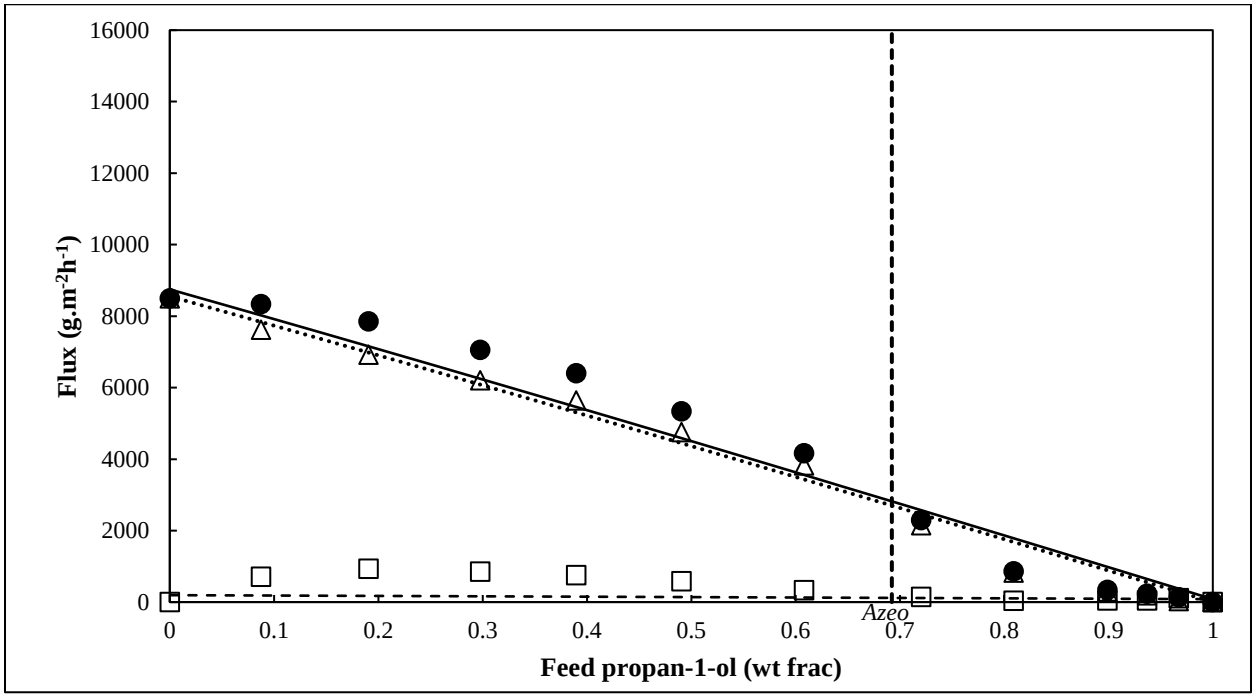

Figure 7.8. Flux versus feed composition for simulated propan-1-ol (1) + water (2) system. ● & solid line (-), total flux; □ & dashed line (---), 1-propanol flux; Δ & dotted line (…), water flux. Symbols represent experimental data points by Will and Lichtenhaler (1992); lines represent Model 2.

A comparison between the model and experimental data was made to validate the accuracy and reliability of the model results. Will and Lichtenthaler (1992) presented the results of their study in the form of a separation diagram with the composition of propan-1-ol in permeate and a total flux curve. The azeotrope for the propan-1-ol–water system lies at 69.23 wt.% propan-1-ol. The ethanol-water system of Section 7.2 displayed a linear relationship between the feed composition and the permeate quality and for the water flux. In contrast, the propan-1-ol–water system reported by Will and Lichtenthaler (1992) displayed a substantial variation in the results plotted across the feed composition likely due to experimental uncertainty. This increased the possibility for deviation between the model and the experimental data. However, Figure 7.7 illustrates that the model correlated well with the experimental data (within 5%). The expected exponential relationship between feed composition and permeate quality was also achieved. Therefore, the permeate concentration obtained with the simulation was assumed to be well replicated by the model.

Figure 7.8 shows the influence of feed compositions on component flux. Once again, the model adequately described the flux behaviour with slight differences between the model and literature. As previously mentioned, the nonlinearity of the experimental flux may have caused the deviation of approximately 50% at 80.91 wt.% propan-1-ol. However, given the variation in the values of experimental flux reported by Will and Lichtenthaler (1992), the model presented a fair replication of the data. In addition, the flux decreased with increasing feed propan-1-ol, as expected, due to fewer molecules of the preferentially permeating specie being present.

7.3.2 Effect of feed temperature

The effect of temperature on separation was not investigated by Will and Lichtenthaler (1992). However, feed temperature is necessary in creating the user model since the diffusivities are temperature dependent. Using the estimation of Sander & Soukup (1988) wherein the flux is doubled for every 10 K increase in temperature, the flux-temperature relation for the propan-1-ol–water system was established. The temperature-flux approximation reported by Sander and Soukup (1988) describes the general characteristic of a PVA-based membrane, not that of a specific system such as ethanol-water. Therefore, the rule was extended to the C3 alcohol-water systems modelled in this work.

A rise in feed temperature caused an increased mass of alcohol to pass through the membrane, which was also observed by Burshe et al. (1997). This can be seen in Figure 7.9. Elevated temperatures cause polymer chains to possess more energy thereby creating free volume spaces facilitating the movement of both species. The diffusion rate of both components increases and as a result, the temperature profile of Figure 7.10 displayed an escalated flux.

Once again, the permeate composition displays highly sensitivity for varying feed temperatures due to the conclusion drawn by Sander and Soukup (1988) which states that permeate concentration, when employing a PVA composite membrane, remains relatively constant for a wide feed range. This was observed in literature apart from the feed composition range of 82 – 100 wt.% propan-1-ol according to the characteristic curves of Will and Lichtenthaler (1992). Hence, the specifications of Sander and Soukup (1988) were met by implementing 73.19 wt.% feed propan-1-ol as a specification for Model 2.

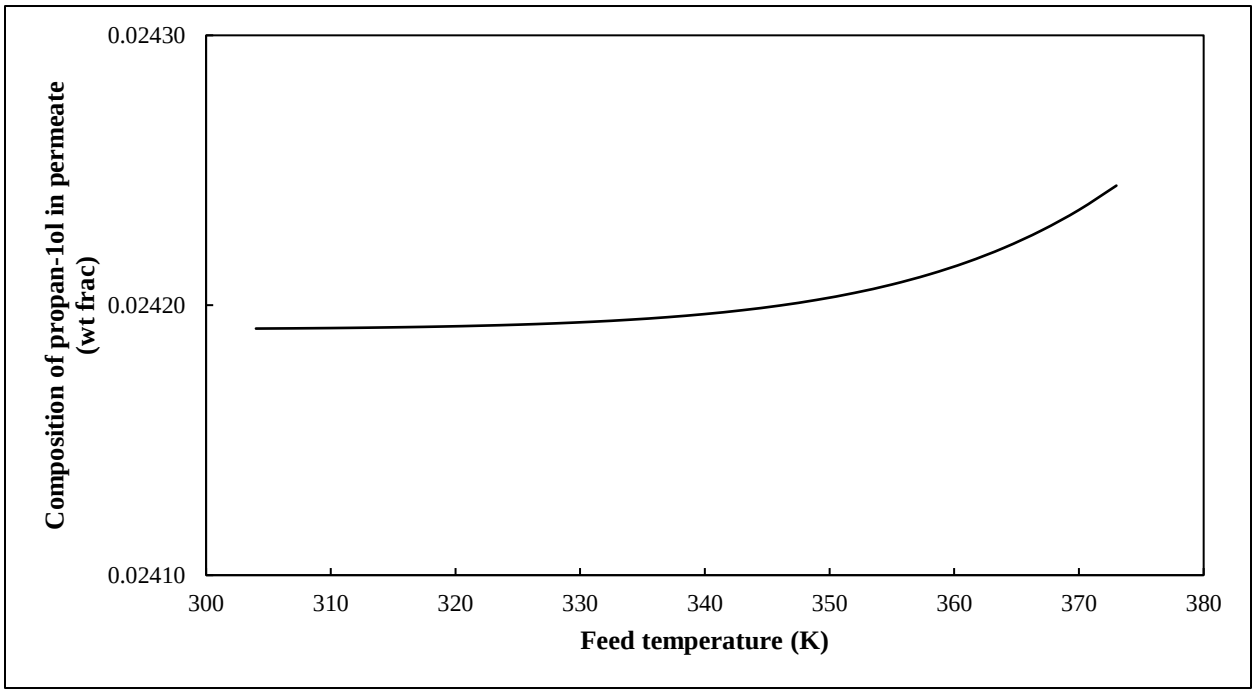

Figure 7.9. The effect of feed temperature on permeate quality for simulated propan-1-ol (1) + water (2) system. Solid line (-), Model 2 based on Will and Lichtenhaler (1992).

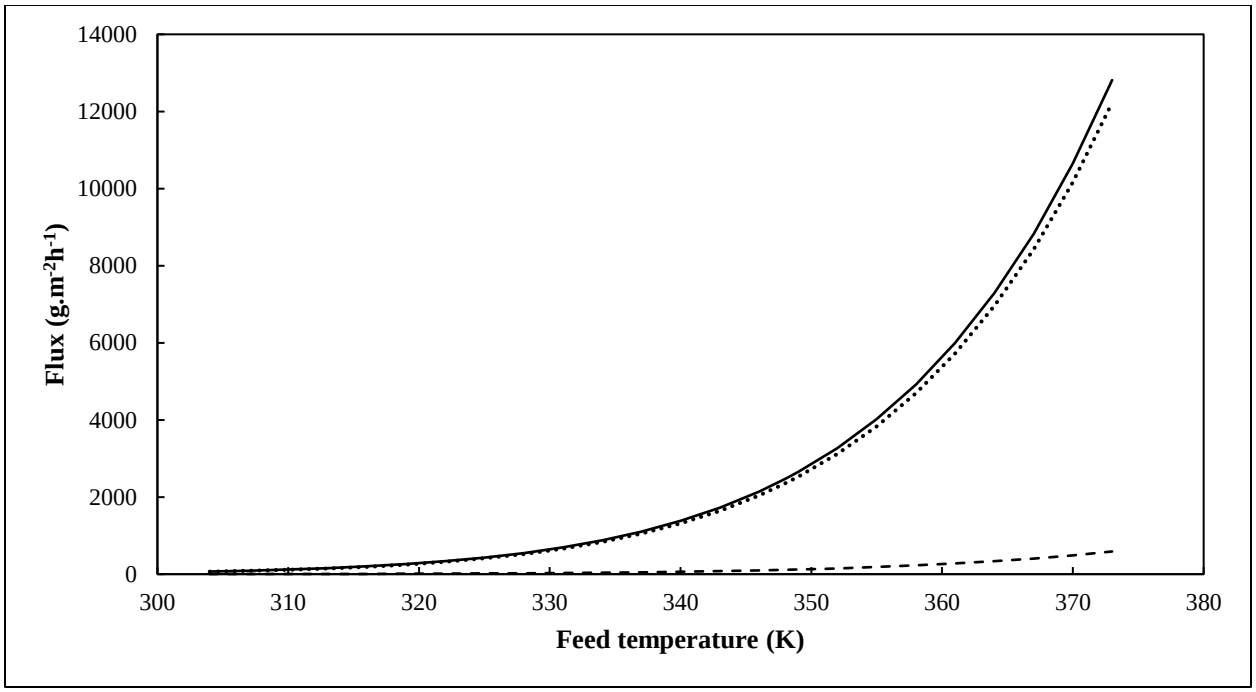

Figure 7.10. Flux versus feed temperature for simulated propan-1-ol (1) + water (2) system. Solid line (-), total flux; dashed line (---), propan-1-ol flux; dotted line (…), water flux. Lines represent Model 2 based on Will and Lichtenhaler (1992).

Although the experimental work of Will and Lichtenthaler (1992) did not include a temperature evaluation, the model can be used to optimize the feed temperature of the pervaporation experiments performed, using the procedure applied previously to the ethanol + water system. The upper limit for the temperature range was estimated from the normal boiling point of propan-1-ol which is 370.35 K. A feed temperature exceeding the boiling point of propan-1-ol would result in partial vaporization of the retentate. The results of the sensitivity analysis revealed that a minimum feed temperature of 304 K can be employed for the system with viable fluxes. In addition, a design specification was performed to determine the maximum operating temperature of 348 K to maintain a liquid retentate. It was found that an optimal feed temperature of 337 K with the alcohol feed composition being 73.19 wt.% will maintain a permeate quality of 97.58 wt.% water whilst providing a reasonable water flux of 1050.63 $g.m^{-2}h^{-1}$.

7.3.3 Effect of permeate pressure

Permeate pressure is considered to be the driving force of pervaporation. However, the designed model focused on the concentration gradient between the retentate and the permeate simply due to

the model being semi-empirical. This signifies direct outputs from the experiment, such as permeate concentration and flux, were used to develop diffusion expressions to correctly describe the performance of a pervaporation setup. The permeate pressure was still incorporated into the model with the permeate concentration term. A downstream pressure of 3 kPa was implemented during experiments and this was optimized using the pressure profiles of Figure 7.11 and Figure 7.12.

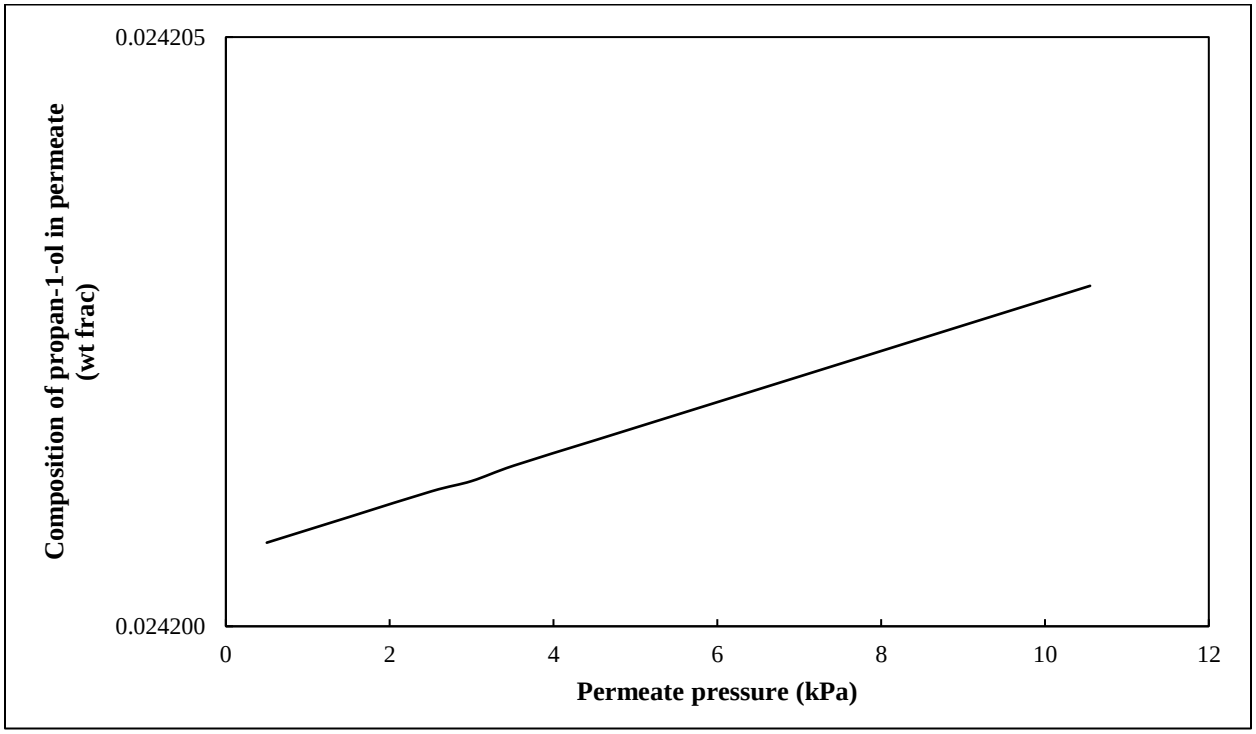

Figure 7.11. The effect of permeate pressure on permeate quality for simulated propan-1-ol (1) + water (2) system. Solid line (-), Model 2 based on Will and Lichtenhaler (1992).

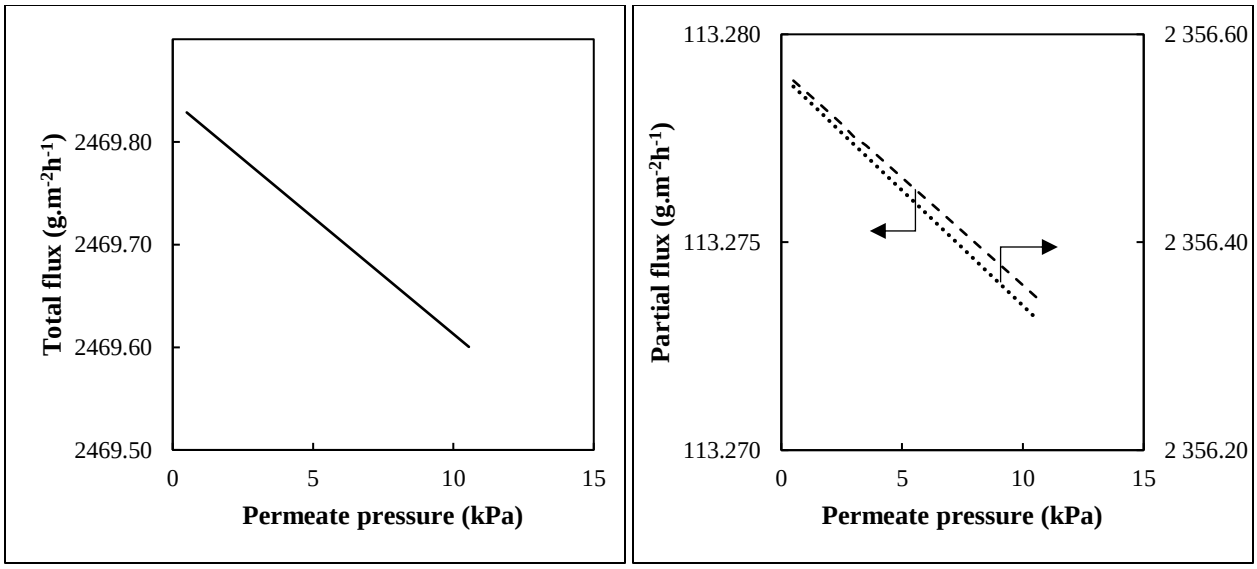

(a) **(b)**

Figure 7.12. Model results for the flux versus permeate pressure for simulated propan-1-ol (1) + water (2) system: (a) Total flux. Solid line (-); (b) Partial fluxes. Dashed line (---), propan-1-ol; dotted line (…), water. Lines represent Model 2 based on Will and Lichtenhaler (1992).

Figure 7.11 illustrates a gradual increase of permeate propan-1-ol composition with an increase in permeate pressure. Moreover, the highly sensitive permeate concentration displays an almost constant trend when subjected to varying downstream pressure. This is due to the model being developed from characteristic curves such as flux and permeate compositions for varying feed concentrations. The semi-empirical models were based on the manipulation of concentration gradients rather than using pressure-sensitive data. This is also in line with the solution-diffusion model of Chapter 3 which assumes the chemical potential gradient is expressed as a concentration gradient. Therefore, a minor impact on the alcohol composition in the permeate was expected.

A low pressure is often desirable since a stronger driving force is created for diffusion to take place. This is demonstrated with the maximum total flux of 2469.83 $g.m^{-2}h^{-1}$ obtained at 0.5 kPa as shown in Figure 7.12 (a). The partial fluxes of Figure 7.12 (b) decrease at a slower rate as the pressure increases. It is possible that greater pressures can be tolerated by the propan-1-ol–water system before severely impacting the flux and separability.

The experiments of Will and Lichtenthaler (1992) were performed at 3 kPa. A sensitivity analysis on Aspen Plus® was performed to determine the optimal pressure in the range of 0 – 10 kPa. It was

found that a maximum flux and permeate water content were obtained at a minimum pressure of 0.5 kPa. However, very low pressures should be avoided for safety, operability and cost implication. It was possible to maintain the separation with the alcohol feed composition being 73.19 wt.% and obtain an acceptably high flux by implementing a more reasonable permeate pressure of 5 kPa. This results in a water flux of 2356.45 $g.m^{-2}h^{-1}$.

7.4 The propan-2-ol (1) + water (2) system

There is very little data available in the literature for the dehydration of propan-2-ol + water systems using pervaporation. To explore these processes further with the aim of contributing predictive solutions to the literature, the dehydration of propan-2-ol–water was investigated by developing a pervaporation model using the method outlined in Chapter 6. Once again, the effect of feed concentration, temperature and permeate pressure was observed. Despite propan-2-ol being an isomer of propan-1-ol, these two components have different thermophysical properties such as boiling points and densities which indicate that their behaviours in pervaporation systems would be different. Therefore, a unique model (Model 3) was developed for the propan-2-ol–water system. The research performed in this section of the report will contribute towards membrane studies not fully explored and provide better insight to industry.

Model 3 created for the propan-2-ol–water system was based on experimental findings reported by Will and Lichtenthaler (1992). The basis of the model formulation remained the same in that temperature-dependent diffusivities were implemented. This is represented by Equations (7.7) and (7.8) below. Operating conditions for the propan-2-ol–water measurements included a feed temperature of 333 K and permeate-side pressure of 3 kPa. The effective membrane area for a cell was stated to be 0.0039 m^2. A PVA/PAN composite membrane was implemented in the experimental study performed to obtain data.

The equations for the propan-2-ol and water diffusivities ($m.h^{-1}$) as derived for Model 3 are provided below in which temperature is in (K):

$$D_1 = 7.522 \times 10^5 \, e^{\left(-\frac{7917}{T}\right)} \tag{7.7}$$

$$D_2 = 5.097 \times 10^7 \, e^{\left(-\frac{7917}{T}\right)} \tag{7.8}$$

7.4.1 Effect of feed concentration

Figure 7.13 and Figure 7.14 shows the model and experimental data that describe the effect of feed weight fraction on the performance of the pervaporation module (permeate composition and flux) and were used to select the appropriate feed composition.

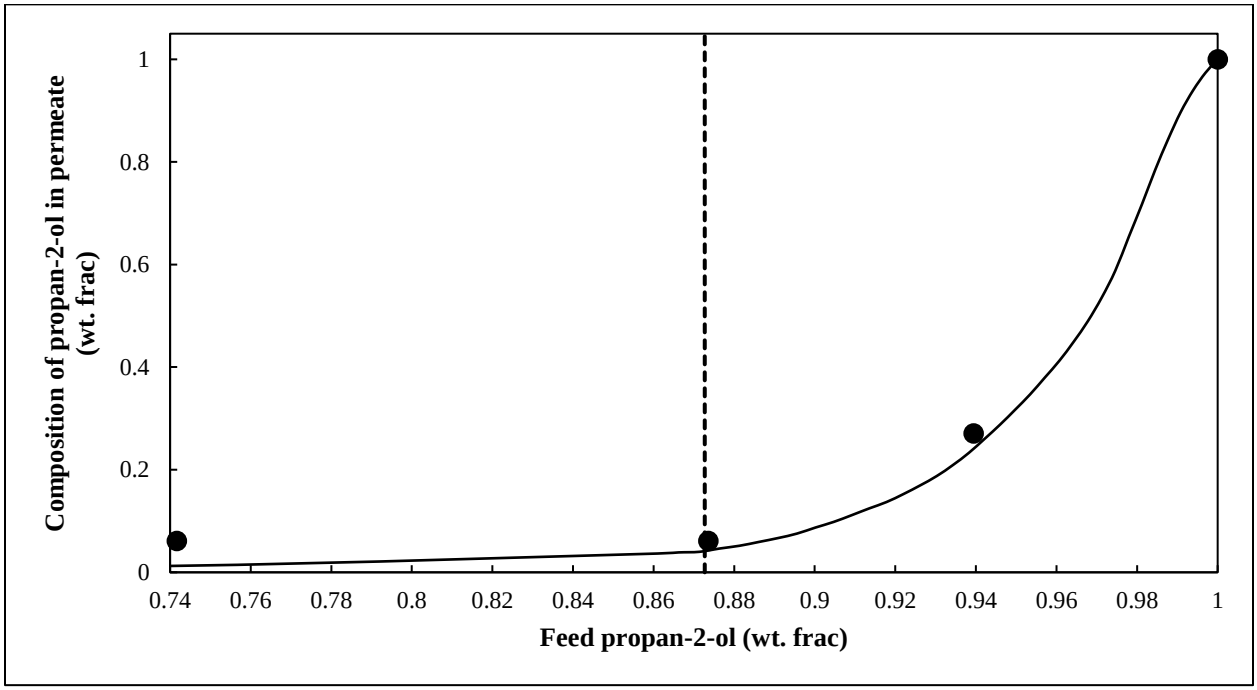

Figure 7.13. The effect of feed composition on permeate quality for simulated propan-2-ol (1) + water (2) system. ●, Will and Lichtenhaler (1992). Solid line (-) represents Model 3.

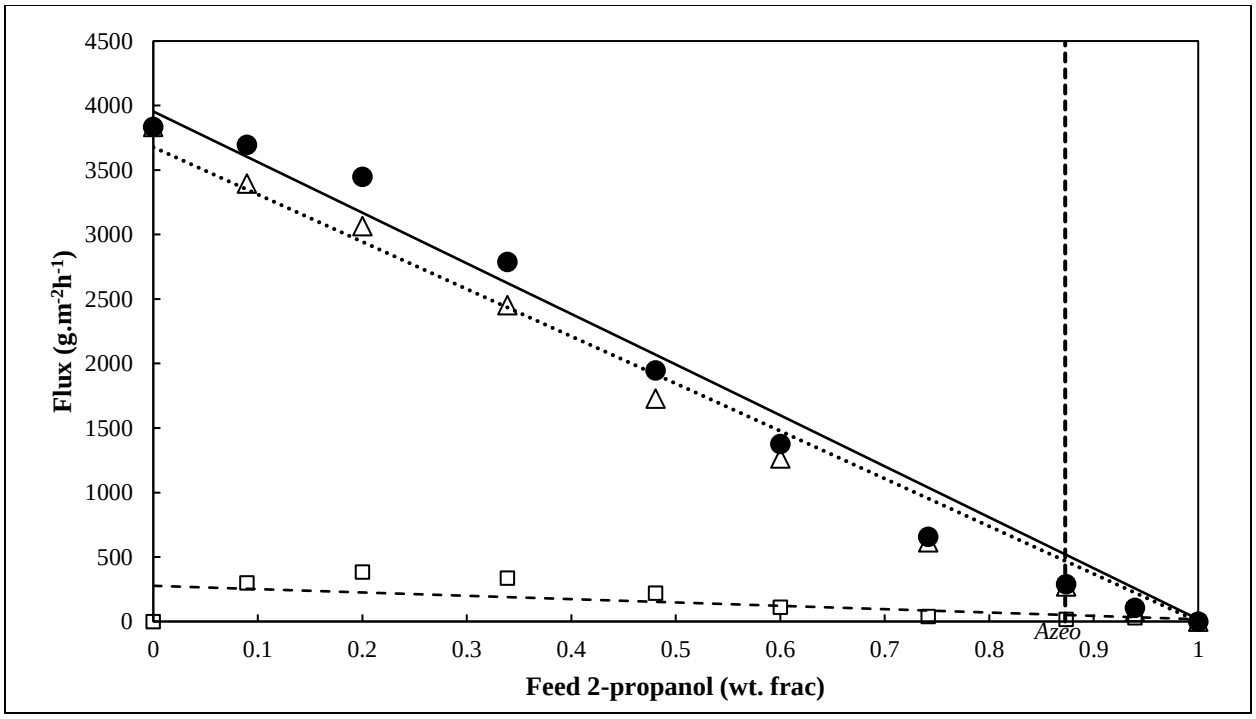

Figure 7.14. Flux versus feed composition for simulated propan-2-ol (1) + water (2) system. ● & solid line (-), total flux; □ & dashed line (---), propan-2-ol flux; Δ & dotted line (…), water flux. Symbols represent experimental data points by Will and Lichtenhaler (1992); lines represent Model 3.

The model was compared to experimental data to validate the accuracy and reliability of results. Two imperative factors (a phase diagram with the composition of propan-2-ol in the permeate and the flux) were presented by Will and Lichtenthaler (1992) for model development. These included the propan-2-ol composition in the permeate and the total flux at various feed compositions. The azeotrope for the system is present at 87.27 wt.% propan-2-ol. According to Figure 7.13, the model developed correlates very well with the experimental permeate composition data for varying feed compositions. A deviation in the permeate quality was noted at a feed of 74.00 wt.% propan-2-ol of approximately 80%. This may be due to the variation in the experimental permeate composition reported by Will and Lichtenthaler (1992) which are likely due to uncertainties. Unlike the ethanol-water system investigated, the permeate quality near the azeotrope composition fluctuates to a greater degree. One could have forced a linear relationship into the developed model for a concentration of 87.36 wt.% propan-2-ol and greater. However, this would restrict the use of the model only to azeotropic mixtures. The wider feed composition range considered in Figure 7.13 provides the best description of the system yielding a model with improved versatility.

Will and Lichtenthaler (1992) reported a non-linear relationship between flux and feed composition. Figure 7.14 illustrates that the total and specie flux of the model correlates reasonably well with the experimental data. The total flux is constituted mainly by the permeation of water which is the preferentially permeating specie. As expected, the decrease in water flux with increasing propan-2-ol fraction is due to fewer water molecules being present in the feed at higher increasing propan-2-ol concentrations for transport through the membrane. A minor deviation was observed near the propan-2-ol -rich region. This may be attributed to the nonlinearity of the experimental flux particularly near the azeotropic point as well as experimental uncertainties from the literature study. In addition, a maximum deviation of 12% at 20.00 wt.% propan-2-ol was noted. Again, this could be attributed to experimental uncertainties. Despite these discrepancies, the model adequately describes the propan-2-ol–water separation using a PVA-based membrane.

7.4.2 Effect of feed temperature

Will and Lichtenthaler (1992) did not investigate the effect of temperature on the degree of separation achievable. However, the model created in Aspen Custom Modeler® expressed diffusivities as temperature dependent using an assumed temperature gradient. Experiments performed by Will and Lichtenthaler (1992) utilized a composite membrane similar to Sander and Soukup (1988) who reported the flux doubled with a 10 K increase in temperature. Due the membrane structure of both membranes being alike, the above assumption was used to model the temperature effect in the propan-2-ol−water system.

It is evident that the separation behaviour of all alcohol-water mixtures at elevated feed temperatures is very similar. A high feed temperature increases the energy of the polymer chains enabling greater flexibility. This allows larger molecules such as propan-2-ol to diffuse into the permeate as illustrated in Figure 7.15. Diffusion rates ultimately influence the flux. Therefore, Figure 7.16 indicates a non-linear growth in flux at increased feed temperatures.

Once more, the permeate composition displays highly sensitivity for varying feed temperatures due to the conclusion drawn by Sander and Soukup (1988) which states that permeate concentration, when employing a PVA composite membrane, remains relatively constant for a wide feed range. This was observed in literature apart from the feed composition range of 89 – 100

wt.% propan-2-ol according to the characteristic curves of Will and Lichtenthaler (1992). Hence, the requirements of Sander and Soukup (1988) were met by implementing 88.62 wt.% feed propan-1-ol as a specification for Model 3.

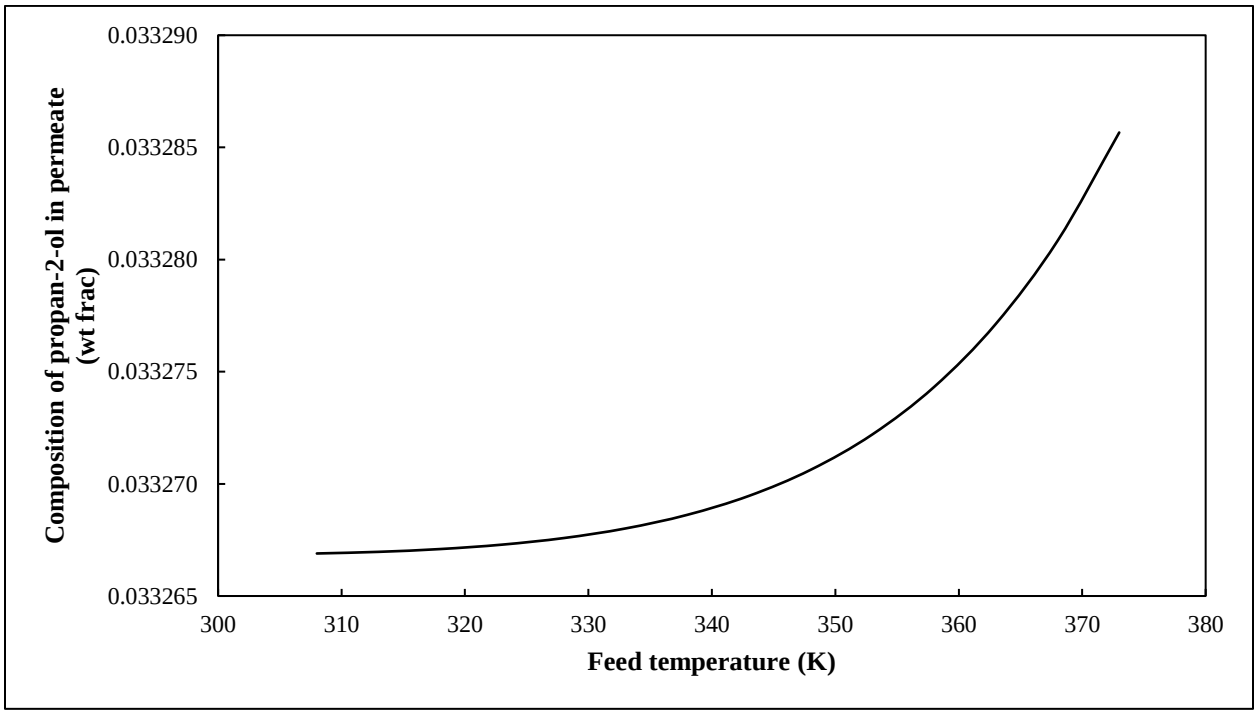

Figure 7.15. The effect of feed temperature on permeate quality for simulated propan-2-ol (1) + water (2) system. Solid line (-), Model 3 based on Will and Lichtenhaler (1992).

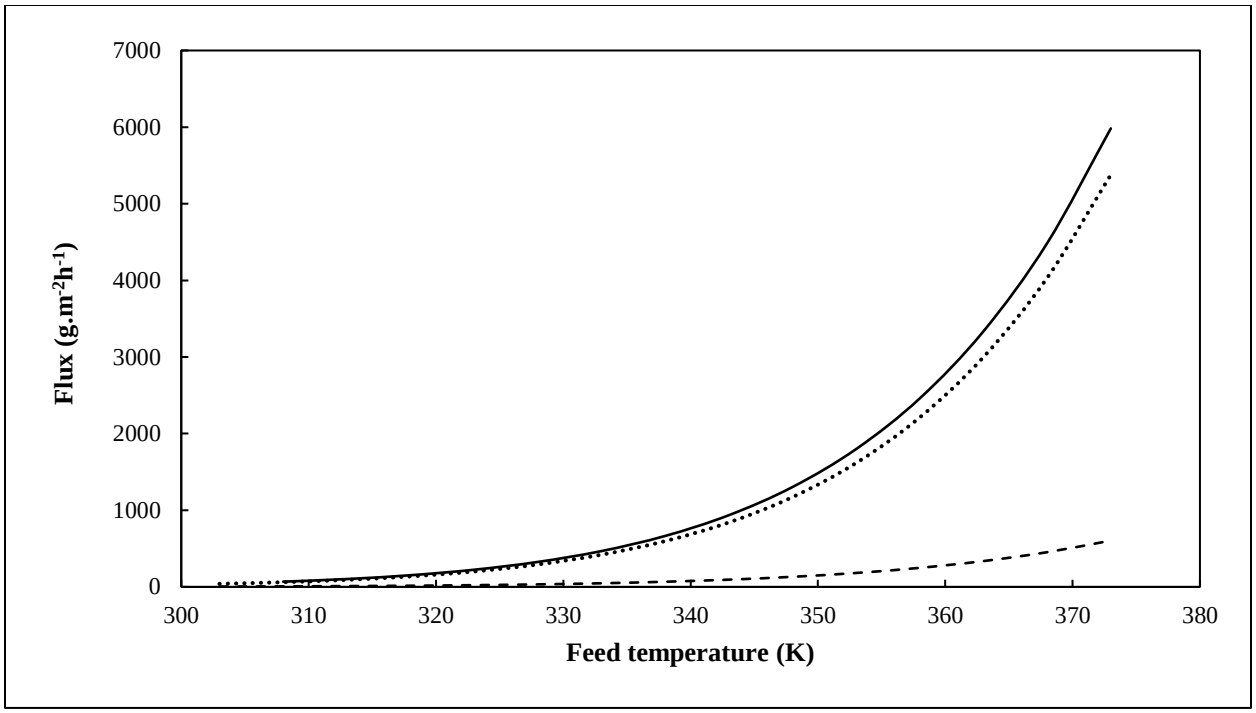

Figure 7.16. Flux versus feed temperature for simulated propan-2-ol (1) + water (2) system. Solid line (-), total flux; dashed line (---), propan-2-ol flux; dotted line (…), water flux. Lines represent Model 3 based on Will and Lichtenhaler (1992).

The feed temperature was optimized with the use of the model. The feed should not be heated above the boiling point of the more volatile component to avoid phase change. The boiling point of propan-2-ol is 355.41 K. A design specification revealed that the feed with alcohol composition being 88.62 wt.% could be heated to a maximum of 333 K to avoid vaporizing the contents of retentate. It was found that a minimum feed temperature of 303 K can be implemented in the separation of propan-2-ol–water and achieve a separation of 96.67 wt.% water in the permeate. Figure 7.16 indicates that the flux was influenced greatly by feed temperature. Using this information in combination with a sensitivity analysis, an optimum operating temperature of 325 K was selected.

7.4.3 Effect of permeate pressure

The permeate-side pressure creates the driving force for the pervaporation separation. The impact of pressure is incorporated in the computation for permeate concentration. Will and Lichtenthaler (1992) specified a downstream pressure of 3 kPa in their experimental study. The permeate pressure effect on permeate composition and fluxes are presented in Figure 7.17 and Figure 7.18.

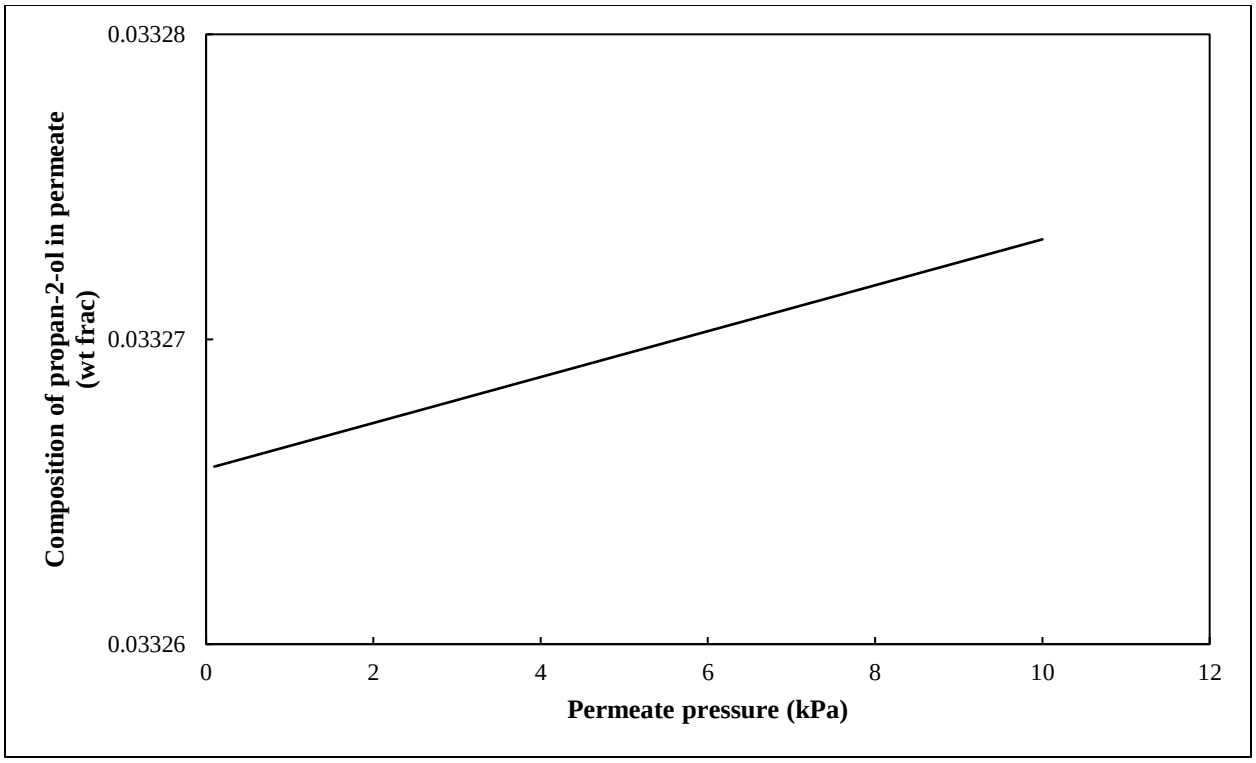

Figure 7.17. The effect of permeate pressure on permeate quality for simulated propan-2-ol (1) + water (2) system. Solid line (-), Model 3 based on Will and Lichtenhaler (1992).

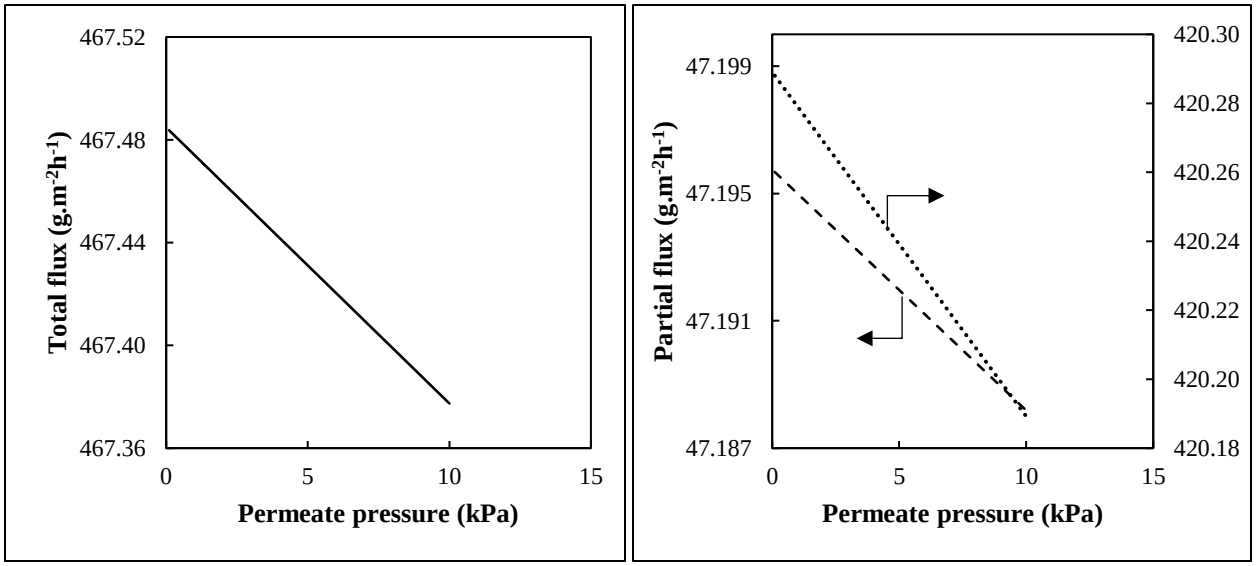

(a) **(b)**

Figure 7.18. Model results for the flux versus permeate pressure for simulated propan-2-ol (1) + water (2) system: (a) Total flux. Solid line (-); (b) Partial fluxes. Dashed line (---), propan-2-ol; dotted line (…), water. Lines represent Model 3 based on Will and Lichtenhaler (1992).

Figure 7.17 illustrates a highly sensitive, almost constant, permeate concentration when subjected to varying permeate pressures. This is due to the model being developed from characteristic curves such as flux and permeate compositions for varying feed concentrations. The semi-empirical models were based on the manipulation of concentration gradients rather than using pressure-sensitive data. This is also in line with the solution-diffusion model of Chapter 3 which assumes the chemical potential gradient is expressed as a concentration gradient. Therefore, a minor impact on the alcohol composition in the permeate was expected.

An increase in the permeate pressure translates to a decrease in the driving force needed to facilitate the movement of water. Although the composition of the permeate was not significantly influenced by pressure, the resulting permeate propan-2-ol composition for permeate pressure above 10 kPa was taken as the acceptable limit in Figure 7.17. Additionally, Figure 7.18 describes a relatively stable flux as the permeate pressure increased. Although pressures higher than 10 kPa may be tolerated, the permeate quality would eventually be compromised.

Initial experiments by Will and Lichtenthaler (1992) were performed at 3 kPa. A sensitivity analysis on Aspen Plus® was completed to determine the optimum permeate pressure in the range of 0 – 10 kPa. It was found that a maximum flux and permeate water compositions were obtained at a minimum pressure of 0.5 kPa. However, very low operating pressures should be avoided for safety, operability and cost implication. It was possible to maintain the separation and obtain a reasonable flux with the alcohol feed composition being 88.62 wt.% by implementing a permeate pressure of 5 kPa. This would result in a water flux of 420.24 $g.m^{-2}h^{-1}$.

The permeate pressure of the experiments can be optimized using Model 3. The experiments performed by Will and Lichtenthaler (1992) applied a reasonable pressure of 3 kPa to provide good separation. However, the sensitivity analysis revealed that a pressure as high as 5 kPa can still maintain good separation whilst providing the pressure differential needed for pervaporation. At this pressure, a water flux of 420.24 $g.m^{-2}h^{-1}$ will be obtained with an alcohol feed composition of 88.62 wt.%.

It is known that the propanol isomers (propan-1-ol and propan-2-ol) differ in chemical structure and nature. Since pervaporation using a PVA membrane is governed by permeate pressure and

molecule size, it is expected that the flux for the different isomeric mixtures will differ. A comparison between the two systems reveal that the flux obtained from the dehydration of propan-1-ol is almost five times that of propan-2-ol for a similar hydrophilic membrane. This proves and confirms that each alcohol system requires individual modelling even for variations in the alcohol isomers.

7.5 Simulation of an industrial propan-2-ol (IPA) dehydration process using PVA membrane

Aqueous waste streams of pharmaceutical industries commonly contain a moderate to high quantity of solvents, inorganic salts and organic compounds. Propan-2-ol (IPA) is extensively used as a solvent in such industries (Urtiaga et al., 2006; Yu et al., 2011). As a result, pharmaceutical industries often employ high-energy extractive and heterogeneous distillation for the dehydration of propan-2-ol in waste streams for re-use/disposal.

The purpose of this section is to investigate the pervaporation membrane separation of an industrial propan-2-ol–water stream using the simulated model prepared in Section 7.4 to assess the applicability on the industrial scale. Two main variables were considered for an optimized configuration, namely, interstage heating and the number of cells in each membrane module. An economic feasibility study was conducted by assessing the operating, investment, and maintenance cost for the various arrangements. A final configuration was then chosen based on the economic evaluation.

7.5.1 Simulated designs

(i) Operating parameters

Yu *et al.* (2011) described an industrial facility built for the dehydration of IPA using sodium acetate (NaA) zeolite membranes. The IPA solvent was first pre-treated before being fed to the membrane unit. The pre-treatment steps included the removal of salts and other coloured substances before neutralizing the pH of the solvent with sulphuric acid. A rectifying plate column was thereafter used to remove the sulphuric salts and residual impurity organics. The resulting stream containing IPA and water was fed into a membrane separation unit for dehydration.

The membrane unit was simulated and optimized using an alternate PVA membrane which was incorporated in the model developed as per Section 6.2. The specification set for the product requirements was a permeate water content of approximately 80 wt.% to meet the specification of the existing industrial facility.

The pervaporation unit was designed to dehydrate a feed IPA solvent from 15 wt.% water to less than 2 wt.% in the retentate. According to Yu *et al.* (2011), it can be assumed that the IPA solvent stream exited the pre-treatment step at a flowrate of 306.77 $kg.h^{-1}$ and at a temperature of 353.01 K. A design specification was conducted on Aspen Plus® to obtain the latter temperature required to maintain a liquid phase. A permeate pressure of 2 kPa was implemented to provide a sufficient driving force. This vacuum pressure can be achieved more readily and safely on the industrial scale using steam ejectors. Each cell membrane area was fixed at 5 m^2 as per the industrial-scale unit specification suggested by Yu *et al.* (2011). This is in accordance with the standard mounted unit specification outlined by Merry (1996).

Typically, a pervaporation unit consists of a series of membrane cells grouped together in modules. The retentate from each cell becomes the feed for the subsequent cell (Luyben and I-Lung, 2010). Pervaporation experiments of Chapter 5 proved that feed temperature drastically impacts the separation performance of a membrane. An elevated flux at high feed temperatures was observed due to greater permeation of the partially permeating specie. The heat lost in each module due to evaporation is replaced by interstage heating (Feimer et al., 1990). Therefore, an industrial pervaporation unit can be designed to meet the water purity requirement specified earlier by varying two main factors, interstage heat and maximum number of cells per module. Each of these parameters were varied in a factorial design on 3 levels resulting in a total of 9 cases, as seen in Figure 7.19 , for simulation and analysis.

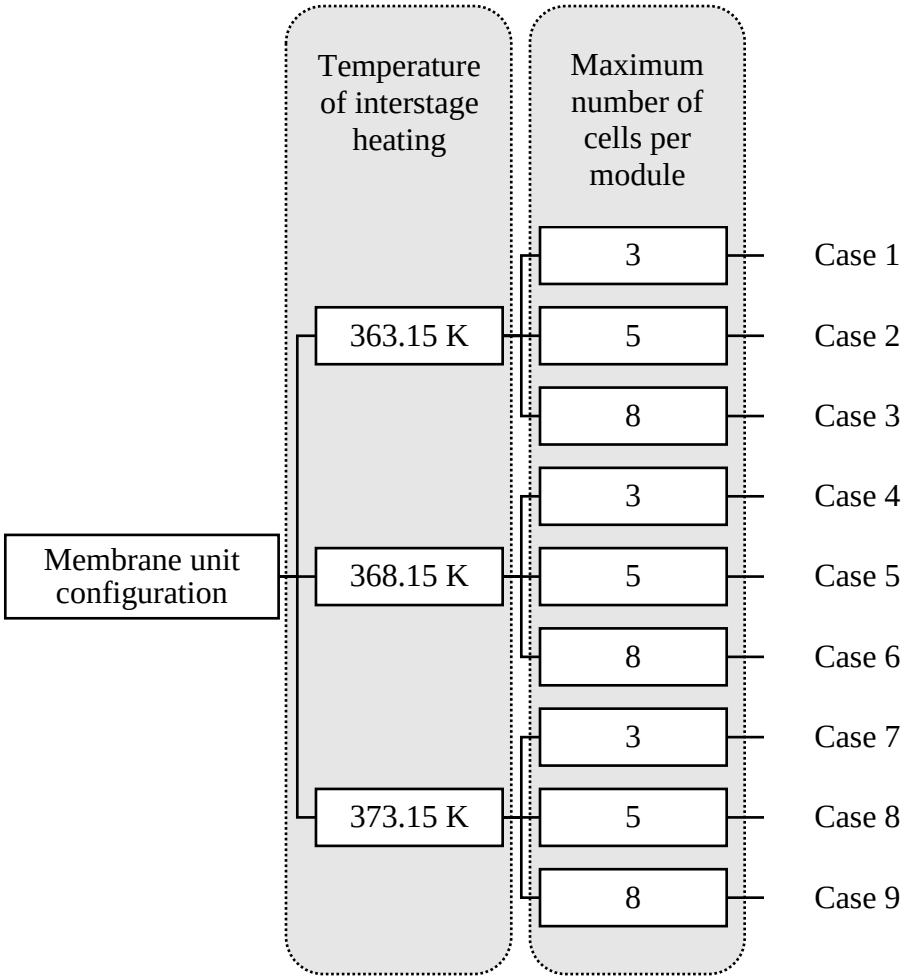

Figure 7.19. Design variations for membrane unit.

Initially, a base simulation case with interstage heating omitted was run using Aspen Plus®. The number of cells were increased, without the use of modules, whilst observing the retentate water composition. The purpose was to determine an effective range for the number of cells to be employed within each module. This is the process presented in Figure 7.20. As a result of the initial bulk uptake in retentate water and subsequent tapering-off, a maximum of 8 cells per module was considered. It can be seen in Figure 7.20 that the retentate contained 6.67 wt.% water after a 20-cell sequence. This would require an unreasonable total membrane area while still not meeting the industrial specification. Hence, the method of interstage heating between modules was investigated to improve the separation.

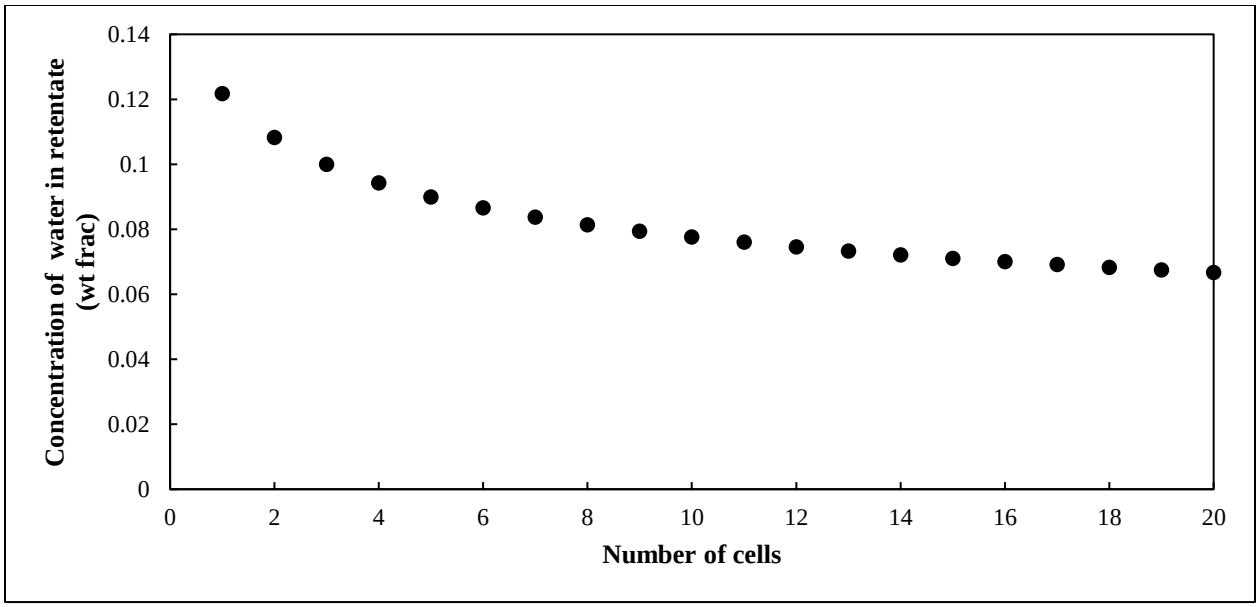

Figure 7.20. Effect of number of cells on membrane performance in industrial process.

(ii) Comparison of designs

The final design cases presented in this industrial application study employed interstage heating for the pervaporation modules. Chou and Hellmuth (1994) recommended that the charge liquid of a propan-2-ol dehydration process be heated in the temperature range of 313.15 – 393.15 K before being passed into contact with a membrane. This formed the basis for the range of temperature selected for the simulation study. The work presented in Section 7.4 was used to establish the effect of temperature on flux in the propan-2-ol + water systems. However, elevated temperatures were likely to vaporize the feed when the boiling point of the propan-2-ol–water mixture was exceeded (which approaches a minimum below the pure component boiling points). Feed liquid phases were maintained with a slight increase in the pressure of the heated feed.

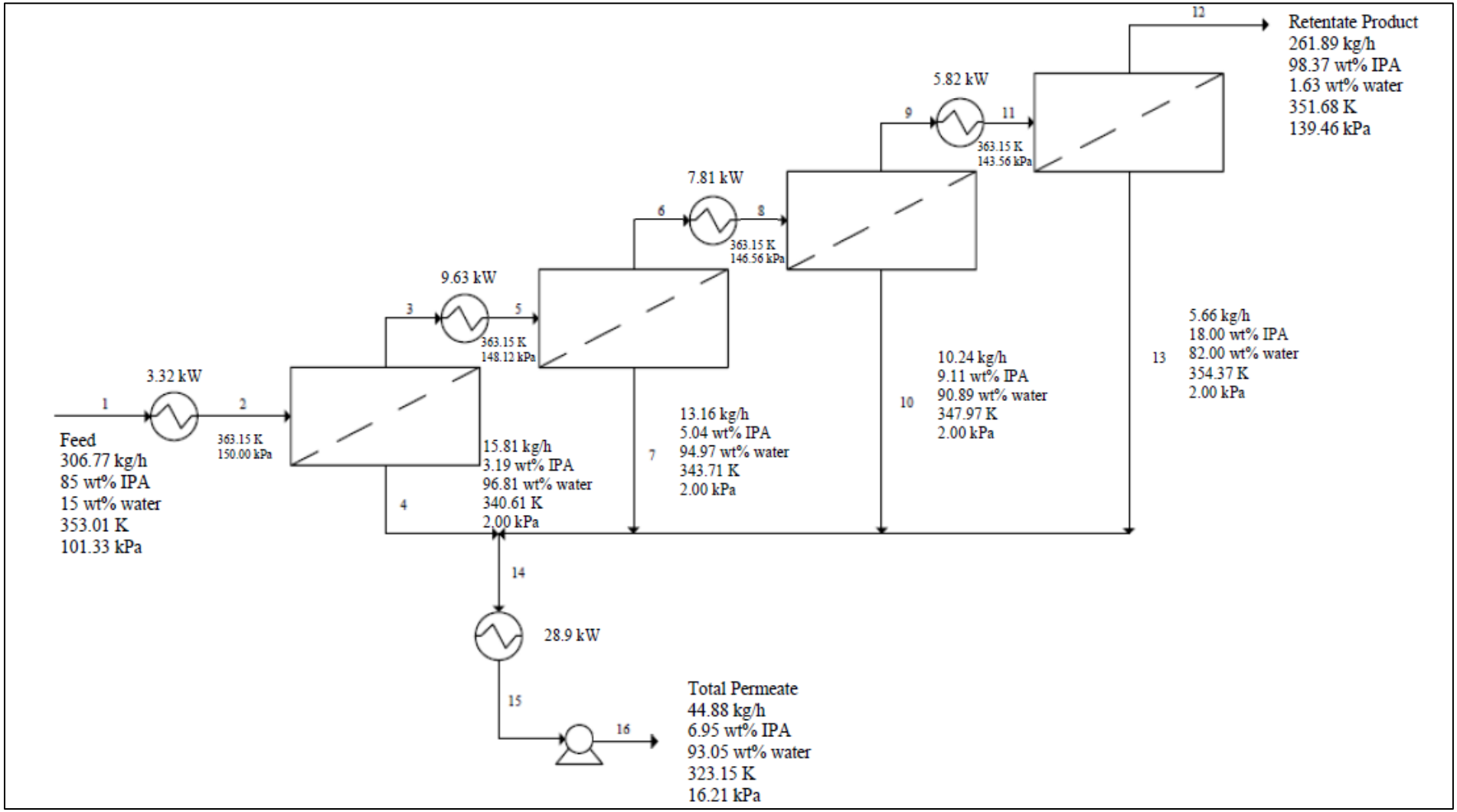

Figure 7.21. (a) Process flow diagram of the pervaporation system with 363.15 K interstage heat: Case 1 (3 cells per module; 4 modules).

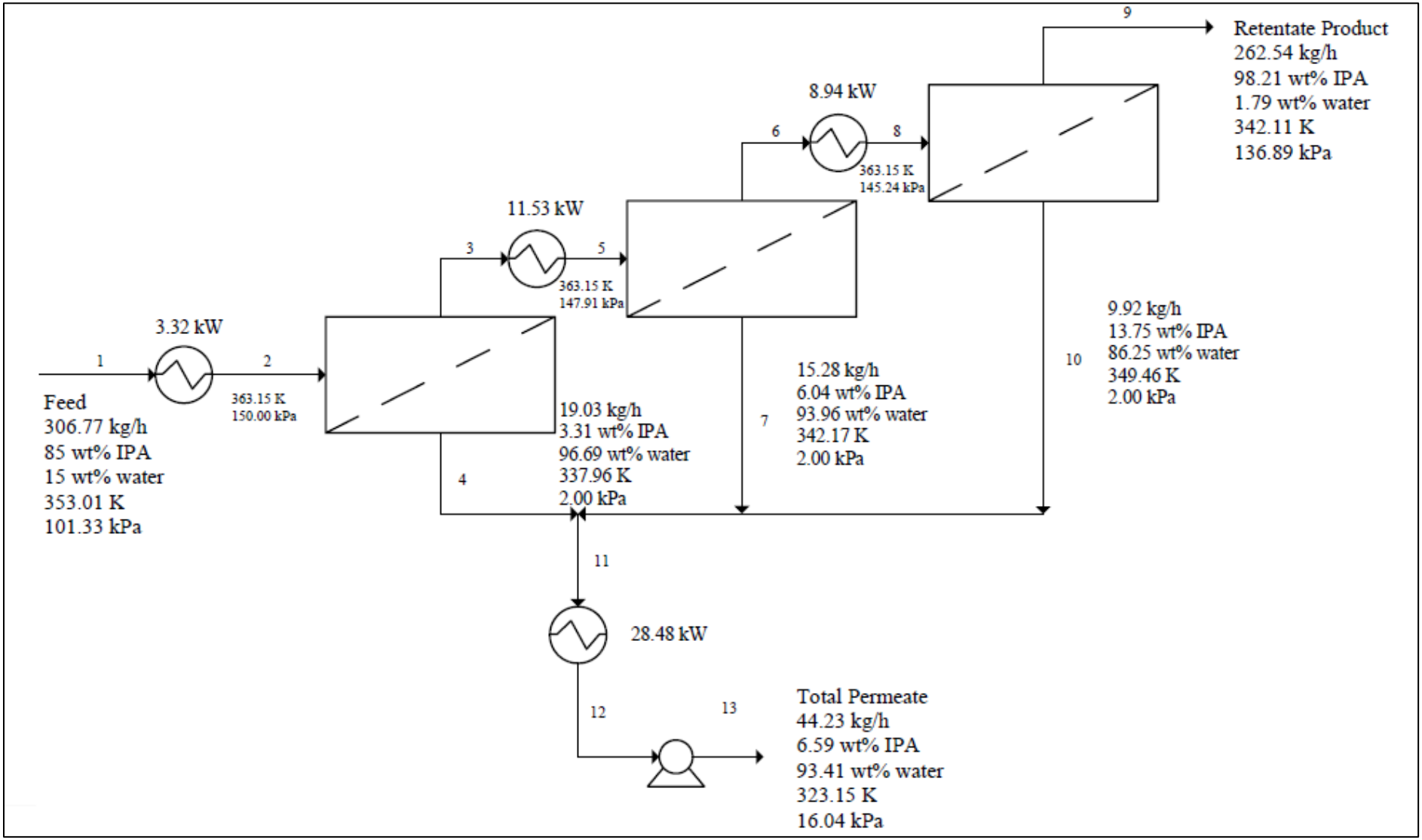

Figure 7.21. (b) Process flow diagram of the pervaporation system with 363.15 K interstage heat: Case 2 (5 cells per module; 3 modules).

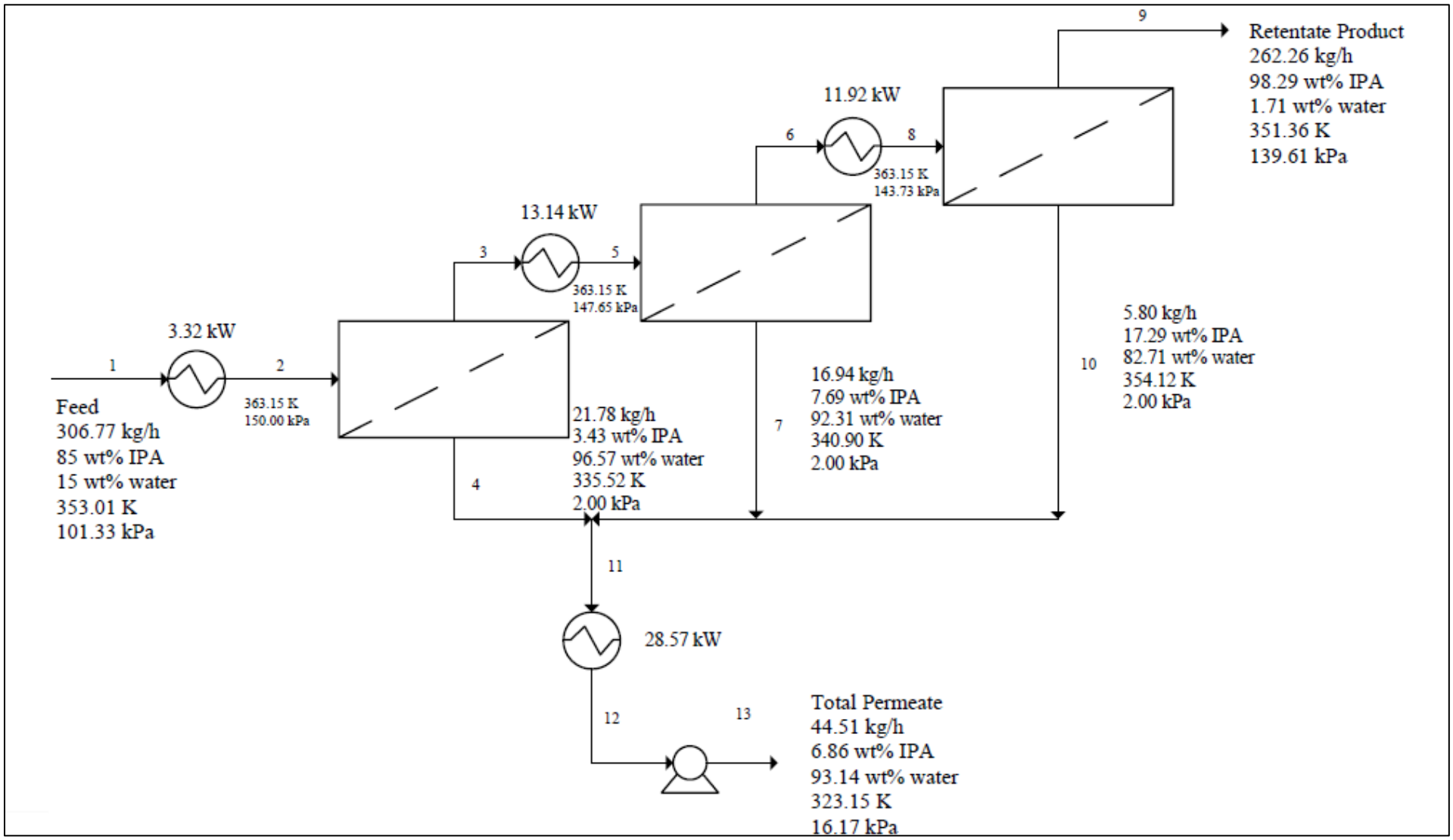

Figure 7.21. (c) Process flow diagram of the pervaporation system with 363.15 K interstage heat: Case 3 (8 cells per module; 3 modules).

Figure 7.21 (a) – (c) gives an overview of Cases 1 – 3 which employed an interstage heating to 363.15 K. The final retentate composition of Case 1 (4 modules with 3 cells per module; and 11 cells out of a maximum of 12 cells) was 98.37 wt.% IPA and a final retentate flowrate of 261.89 $kg.h^{-1}$ was obtained. Case 2 (3 modules with 5 cells per module; and 14 cells out of a maximum of 15 cells) and Case 3 (3 modules with 8 cells per module; and 18 cells being the maximum) had approximately the same retentate purity (98.21 and 98.29 wt.% IPA). The retentate flowrates were 262.54 and 262.26 $kg.h^{-1}$ for Cases 2 and 3 respectively. A design specification was conducted to obtain the pressure required to maintain a liquid phase in stream 2. A feed pressure of 150 kPa (absolute) was necessary, which is commonly achievable on an industrial scale. Multiple membrane modules were arranged in a series until a retentate of 2 wt.% water was achieved. Although Case 1 utilized a smaller total membrane area, an extra heater was required in comparison to Cases 2 and 3. Therefore, a lower maintenance cost but higher operational cost for a 3-cell arrangement was expected, and a difference in the capital and operating costs.

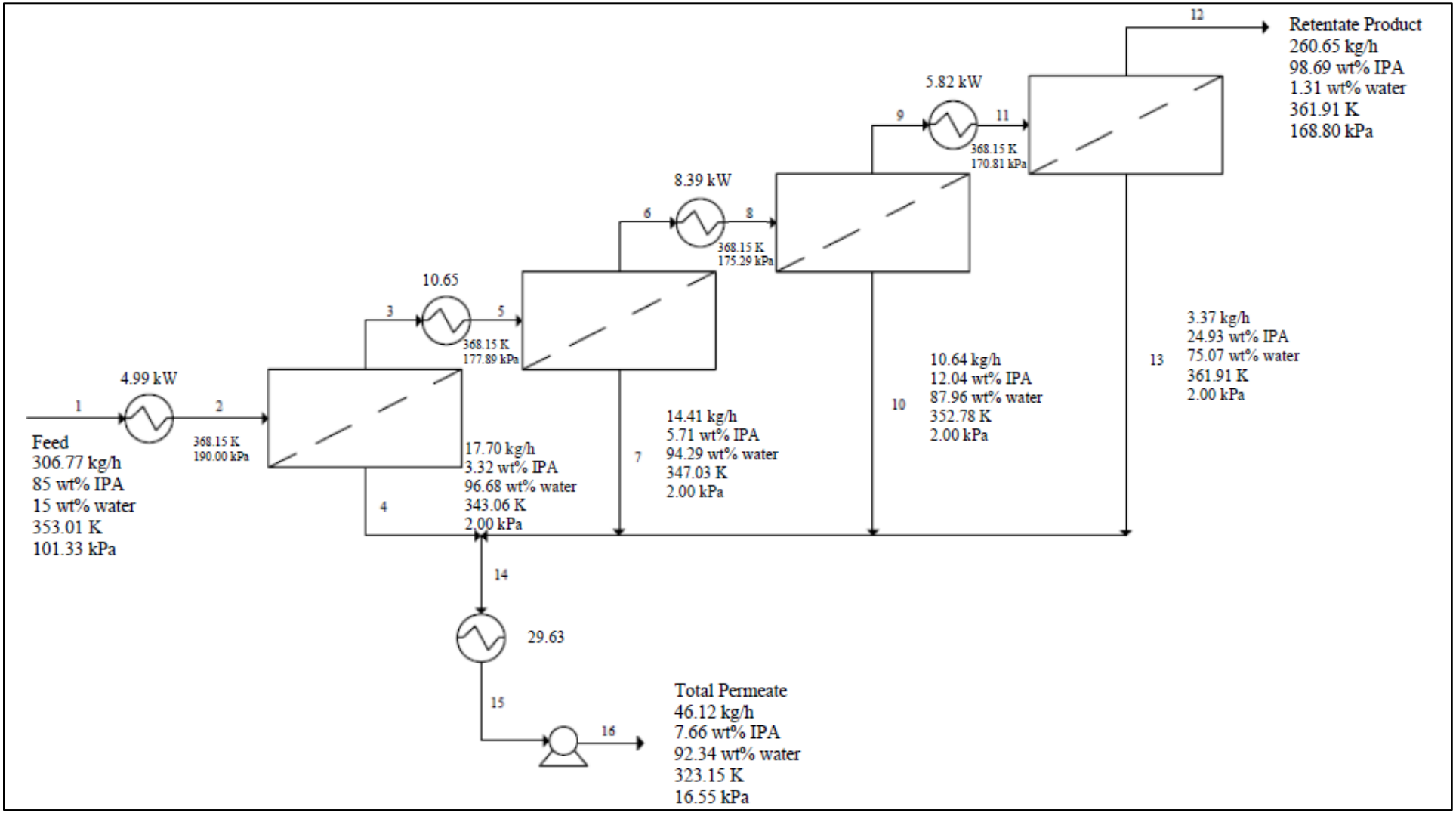

Figure 7.22. (a) Process flow diagram of the pervaporation system with 368.15 K interstage heat: Case 4 (3 cells per module; 4 modules).

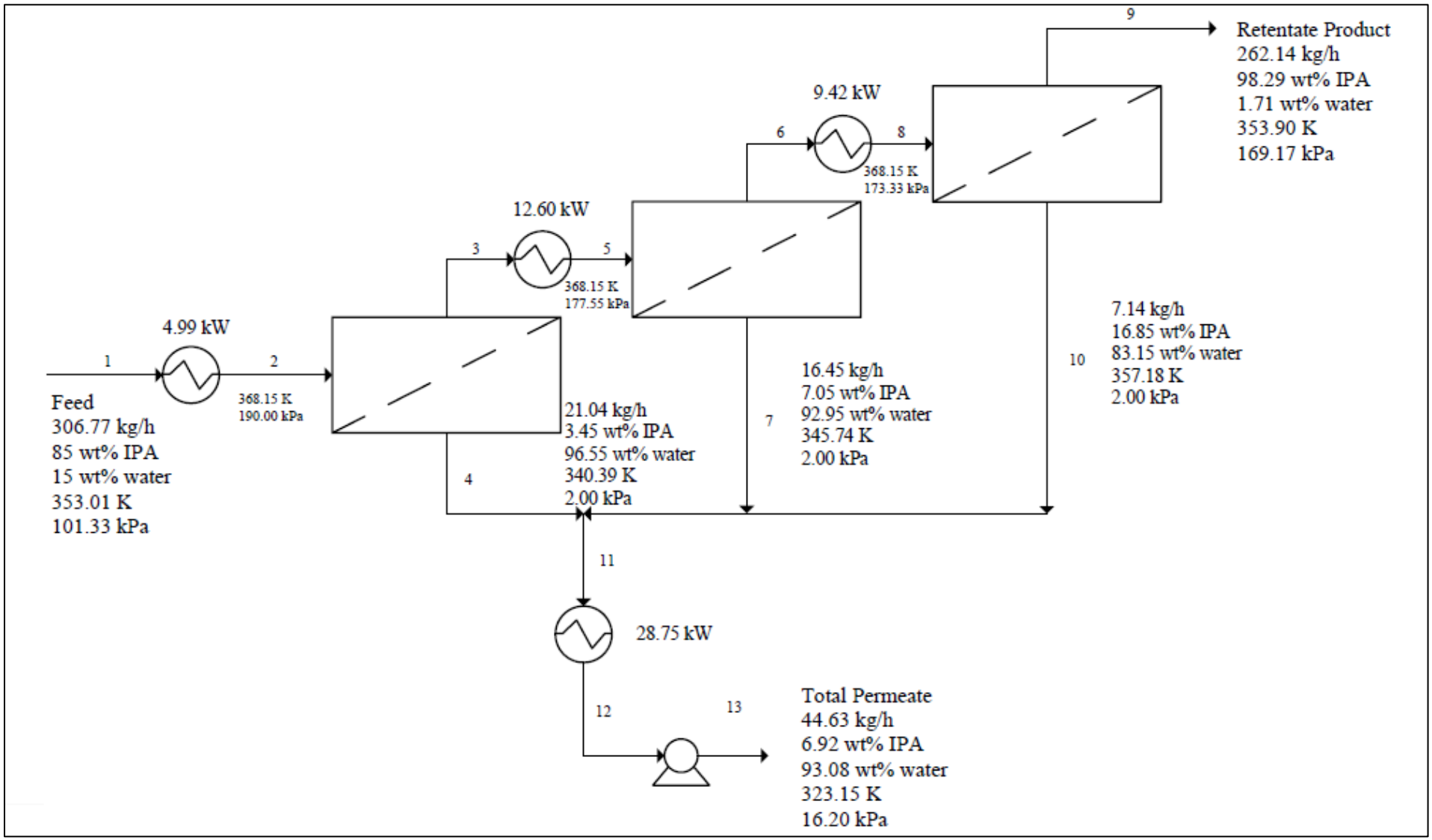

Figure 7.22. (b) Process flow diagram of the pervaporation system with 368.15 K interstage heat: Case 5 (5 cells per module; 3 modules).

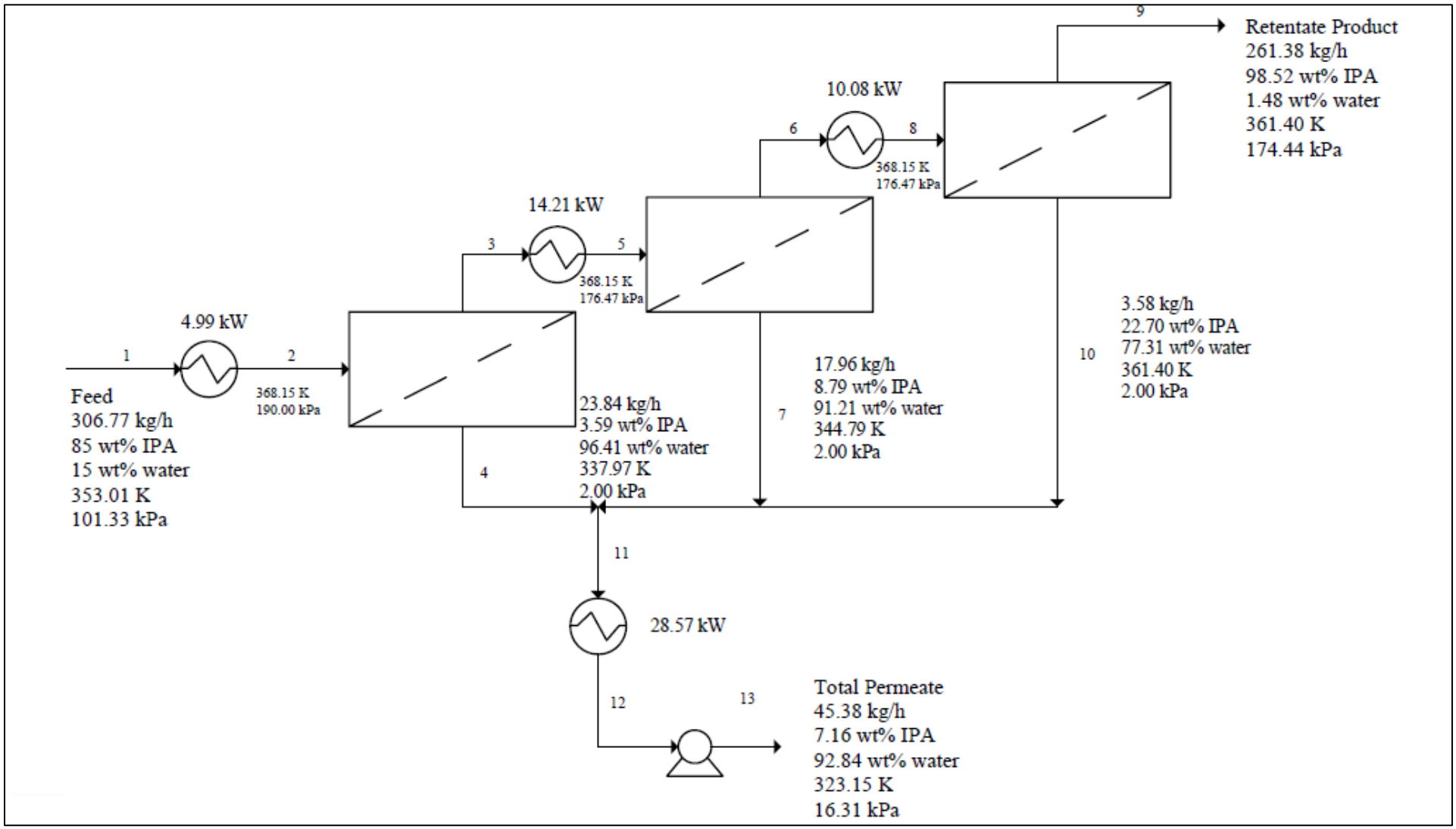

Figure 7.22. (c) Process flow diagram of the pervaporation system with 368.15 K interstage heat: Case 6 (8 cells per module; 3 modules).

Figure 7.22 (a) – (c) above gives stream conditions and heat duties for Cases 4 – 6 which employed an interstage heating to 368.15 K. The final retentate composition of Case 4 (4 modules with 3 cells per module; and 10 cells out of a maximum of 12 cells) was 98.69 wt.% IPA and a final retentate flowrate of 260.65 $kg.h^{-1}$ was obtained. Case 5 (3 modules with 5 cells per module; and 12 cells out of a maximum of 15 cells) and 6 (3 modules with 8 cells per module; and 17 cells out of a maximum of 24) had retentate purities of 98.29 and 98.52 wt.% IPA. The retentate flowrates were 262.14 and 261.38 $kg.h^{-1}$ respectively. The design specification conducted found a feed pressure of 190 kPa was required to maintain the liquid phase in stream 2. Once again, the 3-cell per module network of Case 4 had the smallest membrane area requirement and required one additional heater. The latter may increase the operating and capital cost similar to that observed in the comparison of Cases 1-3.

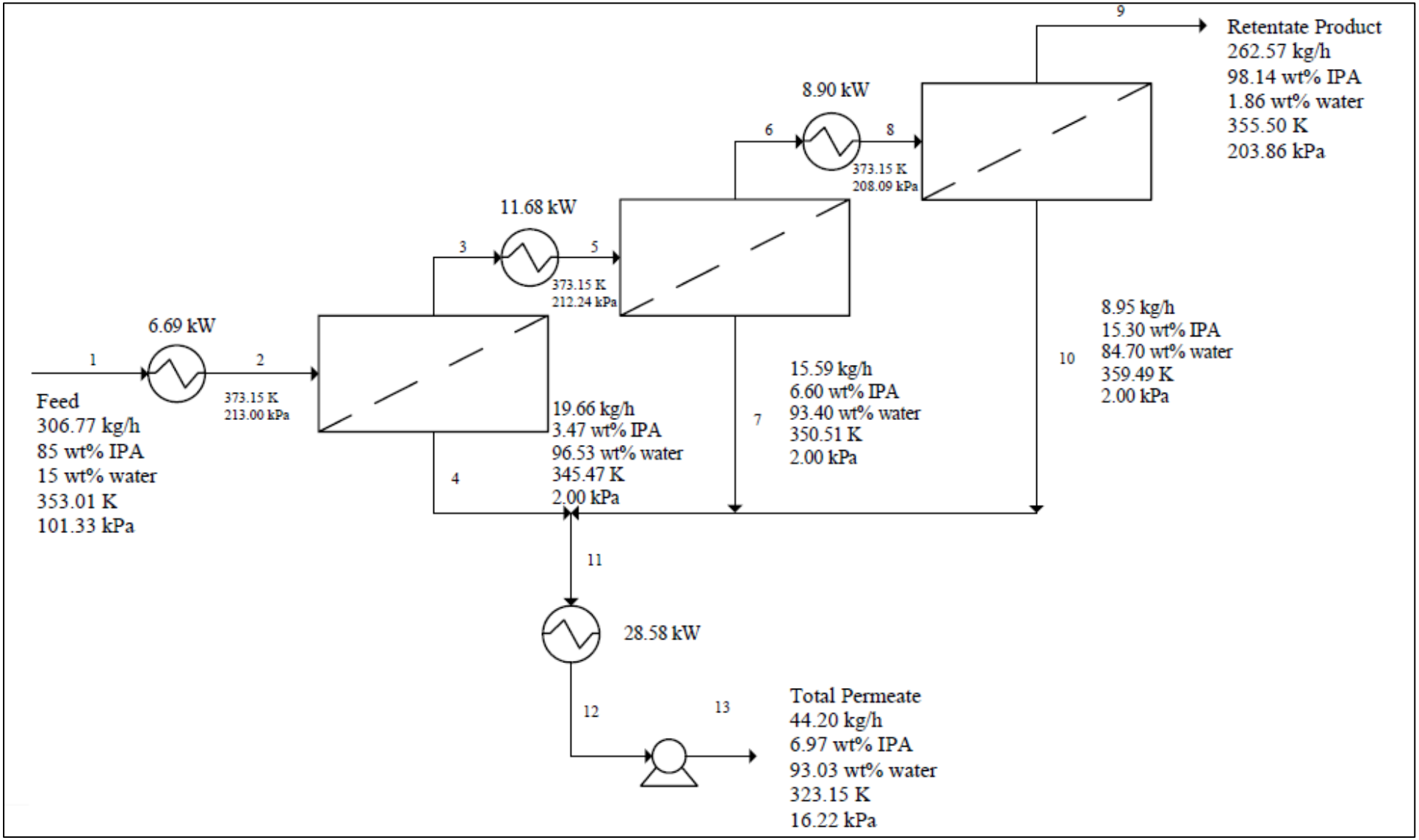

Figure 7.23. (a) Process flow diagram of the pervaporation system with 373.15 K interstage heat: Case 7 (3 cells per module; 3 modules).

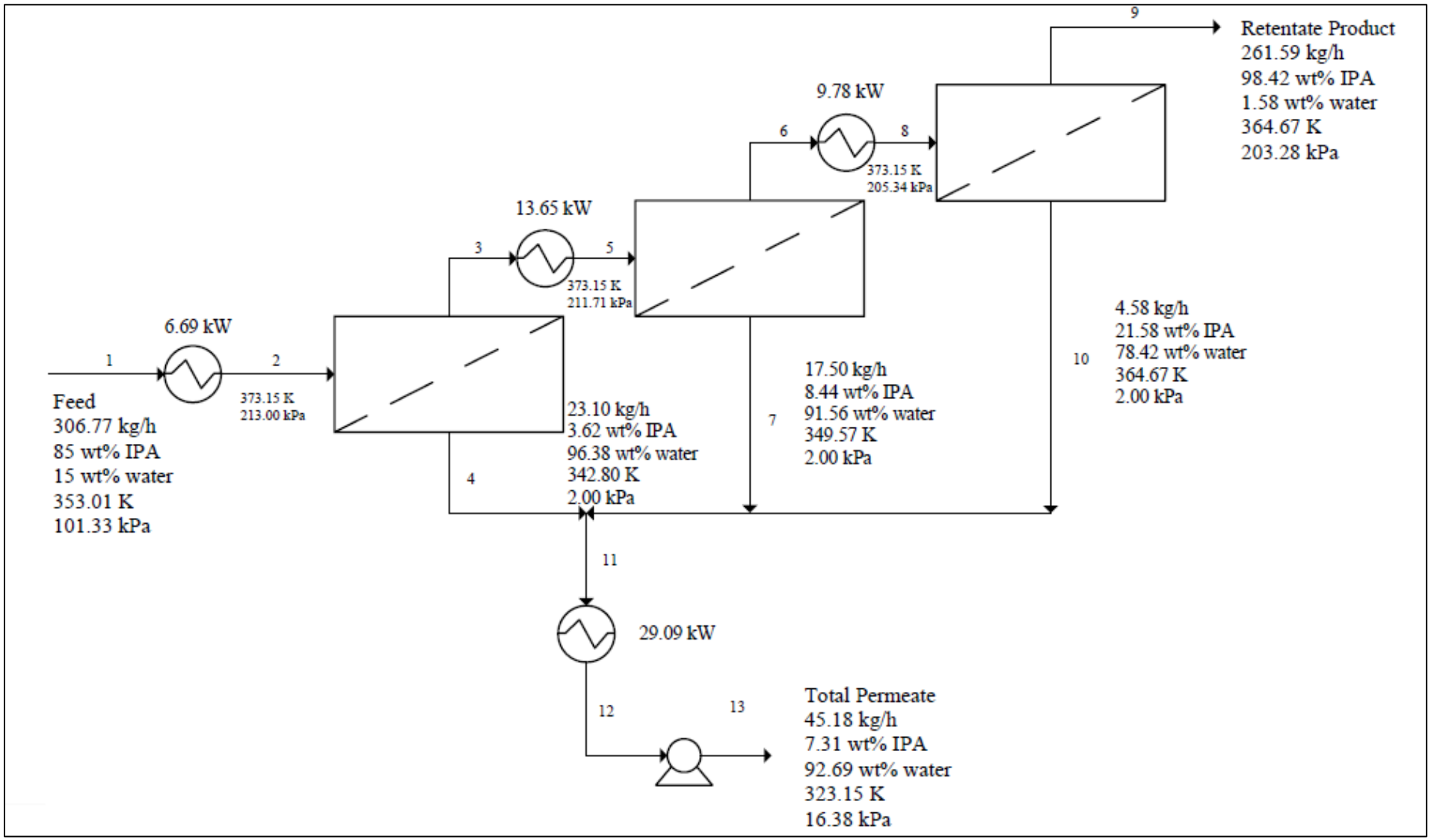

Figure 7.23. (b) Process flow diagram of the pervaporation system with 373.15 K interstage heat: Case 8 (5 cells per module; 3 modules).

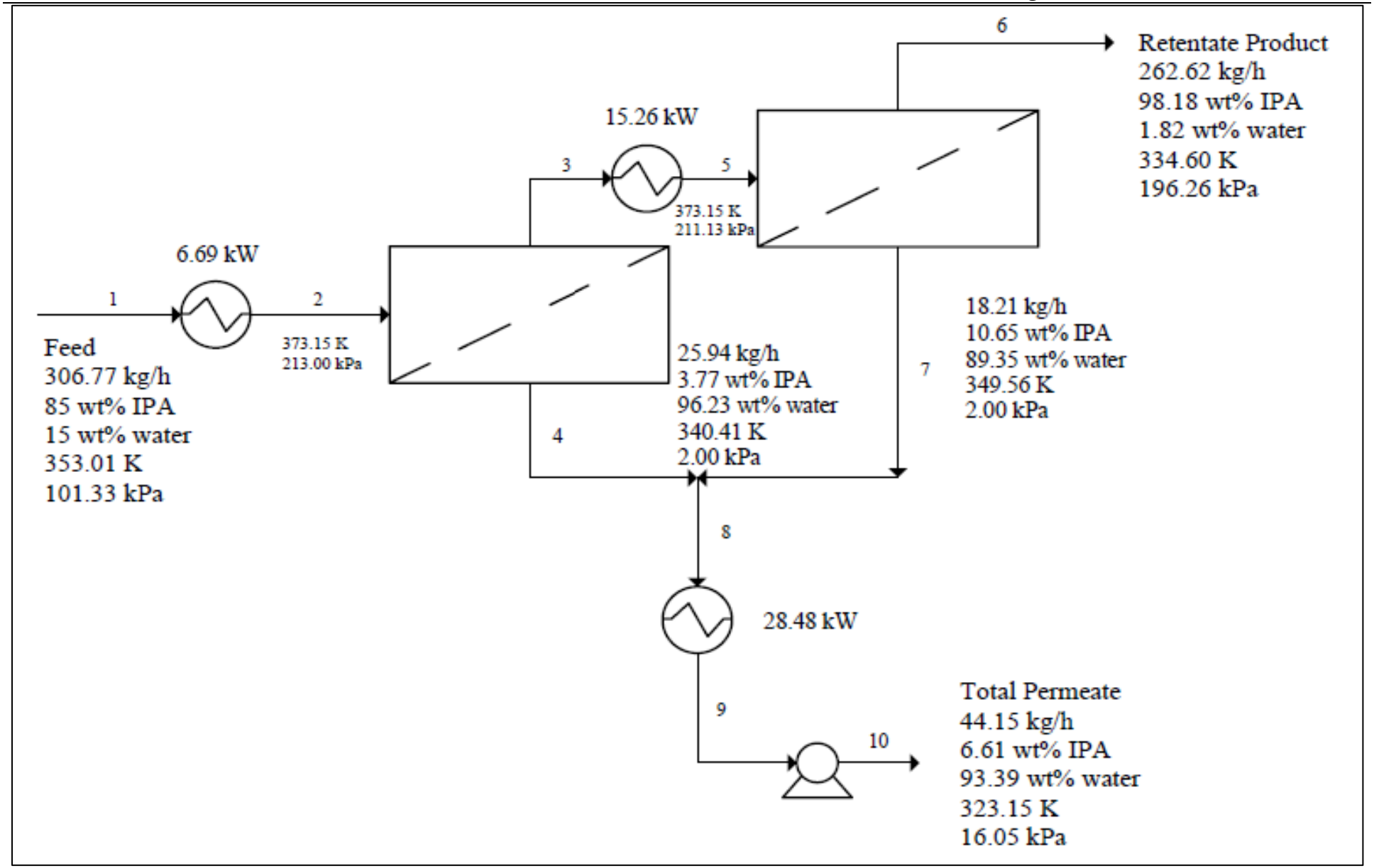

Figure 7.23. (c) Process flow diagram of the pervaporation system with 373.15 K interstage heat: Case 9 (8 cells per module; 2 modules).

Figure 7.23 (a) – (c) above reports the stream conditions and heat duties for Cases 7 – 9 which employed an interstage heating to 373.15 K. Case 7 (3 modules with 3 cells per module; and 8 cells out of a maximum of 9 cells) and 8 (3 modules with 5 cells per module; and 11 cells out of a maximum of 15 cells) had retentate purities of 98.14 and 98.42 wt.% IPA, respectively. The retentate flowrates were approximately the same with 262.57 and 262.59 $kg.h^{-1}$ respectively. The final retentate composition for Case 9 with (2 modules with 8 cells per module; and 15 cells out of a maximum of 16 cells) was 98.18 wt.% IPA and a final retentate flowrate of 262.62 $kg.h^{-1}$ was obtained. A design specification was performed to obtain the pressure required to maintain a liquid phase in stream 2. A feed pressure of 213 kPa was determined. Note that an elevated inlet pressure would have a slight impact on the process cost in general, in comparison to feed at atmospheric conditions.

Membrane modules were arranged in series in an attempt to meet the 2 wt.% water purity specification in the final retentate product stream. It is clear that the total number of cells and the resulting maintenance costs would be the lower for a network with higher interstage heating. Hence the interstage heating to 373.15 K may be the most favourable from a capital cost perspective. However, utility costs will be higher. Cases 7 and 8 had a design requirement of 3 heaters which have capital and utility cost implications. In addition, Case 9 had 15 cells which was almost double the number of cells required in Case 7. This would significantly impact the membrane cost of the unit designed. Therefore, Case 7 may be the most viable theoretical design.

7.5.2 Economic evaluation

The design variations were simulated and optimized to meet the industry purification requirements mentioned above. This prompted a cost comparison between all 9 cases to determine the most feasible configuration. Table 7.2 presents the results of the economical evaluation conducted in this work. The total cost of a pervaporation unit was assessed and included the operating cost, investment cost and the maintenance cost. The industrial facility to implement the membrane unit was assumed to operate for 24 hours a day and 300 days a year (Van Hoof et al., 2004). This accounted for shutdowns, maintenance and chemical cleaning of the membrane module.

Chemical cleaning is carried out when productivity begins to decrease. The clean-in-place (CIP) technique is implemented in which modules remain within the membrane unit for the duration of the cleaning process (Merry, 1996; Minnesota Rural Water Association, 2001). A cleaning solution is circulated through the module at high velocities and temperatures after which a soak cycle proceeds. This is repeated several times using different chemicals until all forms of fouling is expelled. Manufacturers may recommend quick routine maintenance cleans once every few days to reduce possible fouling (Minnesota Rural Water Association, 2001). However, since most membrane plants are fully automated, the plant should start up, run and perform a cleaning sequence with manual intervention only required to charge CIP chemicals into storage tanks (Merry, 1996).

(i) Operating cost

The operating cost was directly linked to the energy intensive aspects of the pervaporation process. This included the energy required to heat feed streams before entering the next membrane module as well as the utilities for permeate condensation and vacuum pressure. Steam at 100 psi (689.48 kPa) was used to heat the feed streams to the desired temperature. The cost of low pressure steam was found to be 58.04 $/t using the method outlined by Sinnott and Towler (2009) which considered the current price of fuel, 25.96 $/GJ. Cooling water was used in condensers at a cost of 0.40 $/kL. The cost of electricity was taken as 0.13 $/kWh. All prices were obtained as of March 2021 and where the time value of money was required for recent price adjustment, an inflation rate of 28.55% for the period of 2004 – 2021, specific to the eurozone, was applied. Detailed calculations for the energy cost are presented in Appendix E.

A comparison of operational costs for the different membrane networks indicated that the arrangements with 3 cells per module were the most energy demanding. A decrease of 20.45% was observed from Case 1 at 363.15 K to Case 7 at 373.15 K. In addition, Case 4 to Case 7 illustrated a 20.71% cost decrease. This significant decline is due to the additional fourth heater employed in Cases 1 and 4. However, the lowest operating cost was for Case 9 due to the requirement of only 2 heaters in the design. Minor differences in operating cost between the module arrangements may be due to slight variations in production rate of the final product, the retentate composition, and the retentate temperature (Van Hoof et al., 2004).

(ii) Investment cost

The investment cost considered for the pervaporation process included the main units such as the membrane modules, piping, heaters, condensers, and vacuum pumps. The cost of a membrane module for the required capacity and conditions of 1192 $/m^2 was provided by the membrane supplier, DeltaMem AG. The installation cost for auxiliary units were calculated by applying the inflation rate of 28.55% to the installation cost provided herein (Alzate, 2006; Van Hoof et al., 2004). The installation rate was found to vary depending on the number of modules. The pervaporation units were depreciated at a rate of 5% per annum. According to Van Hoof *et al.* (2004), a period of 10 years is a reasonable assumption for the useful life of the asset.

It is clear from Table 7.2 that investment costs are the highest for arrangements with 8 cells per module. It is almost double the amount incurred with the use of 3 cells per module. This is due to the fact that several cells are required to meet the retentate specification of 2 wt.% water. Since extra membrane area was implemented into these pervaporation units, the investment cost increased. Although the concern of a heat increase to 373 K raised the operational cost, the high temperature designs of Case 7 and 8 yielded lower investment costs compared to those designed with temperatures of 363.15 and 368.15 K for interstage heating. This was due to a reduction in the total number of cells. Moreover, the design preference of Case 7 over Case 9 yielded a saving of up to 145.84%.

(iii) Maintenance cost

Maintenance costs were inclusive of membrane replacement as well as the maintenance on installed pervaporation units. It was assumed that membranes were replaced in cells twice before the useful life of the asset expired. The cost of a PVA-based membrane as per the membrane supplier of DeltaMem AG was 608.34 $/m^2. Van Hoof *et al.* (2004) described that the additional maintenance cost on installation was 2.5% of the total installation cost. As expected, the total maintenance cost was highest and approximately the same for the Cases 3, 6 and 9 due to the excess number of cells required to produce an acceptable quality retentate. Notably, savings between the range of 84.86 – 122.71 % can be made by implementing 3 cells per module in each temperature bracket.

(iv) Cost comparison

The total cost per ton was calculated from the sum of the operating cost, investment cost and the maintenance cost. It was found that Case 7 (8 cells in total) simulated with an interstage heating temperature to 373.15 K and inclusive of 3 cells per module presented the lowest total cost of 174.27 $/t product.

Case 7 illustrated the lowest installation and maintenance cost. Despite Case 9 (15 cells in total) presenting the lowest operating cost, this was one of the most expensive designs with a total cost of 205.44 $/t product. This was due to 8 cells being implemented in each module. The excessive installation cost of Case 9 does not compensate for the decrease in operating cost. It is notable that Case 8 with 5 cells per module (11 cells in total) is also a reasonable option with a saving of 14.75% compared to Case 1 (11 cells in total) which is the most expensive design.

Cases 8 (11 cells in total) and 5 (12 cells in total) were the preferred alternatives in design configurations following Case 7. It was interesting to note that the 3 cost-effective designs all possess less than 8 cells per module. Therefore, a crude estimation is that the number of cells per module governs the economic aspect to a substantial degree. The 19.40% savings obtained with Case 7 over Case 1 yielded the most feasible design from an economic point of view and was selected as the best design for the industrial dehydration of propan-2-ol using PVA membranes.

The pervaporation process designed in this work was then compared to conventional azeotropic distillation techniques used for propan-2-ol–water systems to determine the cost effectiveness of membrane separation. The total cost of the processes presented in various literature sources (Chen et al., 2017; Harvianto et al., 2015; Van Hoof et al., 2004) were assessed. Both Van Hoof *et al.* (2004) and Harvianto *et al.* (2015) employed 3 distillation columns with a benzene entrainer to break the propan-2-ol–water azeotrope. A decanter was also used. Final products of 501.51 $kg.h^{-1}$ IPA (Van Hoof et al., 2004) and 497.50 $kg.h^{-1}$ IPA (Harvianto et al., 2015) were obtained from the initial feed of 1000 $kg.h^{-1}$ (50 wt.% IPA). In the study conducted by (Chen et al., 2017), an extractive distillation process using dimethyl sulfoxide as the entrainer was presented. A feed of 3488.62 $kg.h^{-1}$ with 65 wt.% IPA and 2 distillation columns resulted in a product stream of 3003.98 $kg.h^{-1}$ IPA.

In order to perform a comparative economic analysis across the different processes, the total cost per ton of propan-2-ol product was calculated to account for differences in feed and product

flowrates. An operational time of 300 days a year and 24 hours a day was assumed. The developed pervaporation simulated design employed a significantly lower feed flowrate to produce 257.69 $kg.h^{-1}$ IPA. Therefore, this was used as the standard to compare the total costs presented by literature.

It was evident that the processes with a benzene entrainer were the most expensive. Harvianto *et al.* (2015) determined a cost of 504.93 $/t whereas Van Hoof *et al.* (2004) followed closely with a cost of 393.65 $/t. This is due to the additional distillation column used in both processes. The cost comparison is presented in Figure 7.24, where the pervaporation system of Case 7 is shown to yield a saving of at least 34% assuming a pre-concentrator cost of 1/3 of the total process costs from the literature studies of azeotropic distillation. Therefore, it can be concluded that the pervaporation process is not only a suitable technique to obtain high purity propan-2-ol, but it also competes strongly with conventional distillation methods due to the cost effectiveness of the technique. The limitation of the economic evaluation performed here is that relative equipment/maintenance costs for the separation alternatives have not been evaluated, which is beyond the scope of the work.

Table 7.2. Cost comparison of 9 design variations for an industrial propan-2-ol dehydration simulated in this study.

		Case 1	Case 2	Case 3	Case 4	Case 5	Case 6	Case 7	Case 8	Case 9
Total number of cells	-	11	14	18	10	12	17	8	11	15
Membrane area	m^2	55	70	90	50	60	85	40	55	75
Production rate	t/year	1854,95	1856,41	1855,94	1851,98	1855,17	1854,03	1855,23	1853,64	1856,41
1. Operating cost										
Cooling water	$/year	6382,80	6296,40	6307,20	6544,80	6350,40	6436,80	6318,00	6426,00	6296,40
Steam @100psi										
Heater 1	$/year	2,42	2,42	2,42	3,63	3,63	3,63	4,87	4,87	4,87
Heater 2	$/year	7,01	8,39	9,56	7,75	9,17	48,06	8,50	9,93	11,10
Heater 3	$/year	5,68	6,50	7,09	6,11	6,85	0,02	6,48	7,12	0,00
Heater 4	$/year	4,23	0,00	0,00	4,24	0,00	0,00	0,00	0,00	0,00
Electricity										
Heater 1	$/year	55765,21	55765,21	55765,21	55765,21	55765,21	55765,21	55765,21	55765,21	55765,21
Heater 2	$/year	55765,21	55765,21	55765,21	55765,21	55765,21	49687,26	55765,21	49687,26	49687,26
Heater 3	$/year	55765,21	55765,21	55765,21	55765,21	55765,21	55765,21	55765,21	55765,21	49687,26
Heater 4	$/year	55765,21	0,00	0,00	55765,21	0,00	0,00	0,00	0,00	0,00
Condenser	$/year	49687,26	49687,26	49687,26	49687,26	49687,26	49687,26	49687,26	49687,26	49687,26
Vacuum pump	$/year	49922,78	49922,78	49922,78	49922,78	49922,78	49922,78	49922,78	49922,78	49922,78
Total operating cost	***$/t product***	***177,40***	***147,18***	***147,22***	***177,78***	***147,30***	***144,18***	***147,28***	***144,19***	***140,63***
2. Investment cost										
PV unit	$	324900,45	511879,83	658131,21	295364,04	438754,14	621568,36	292502,76	402191,29	719637,97
Depreciation	$/year	42076,23	66291,00	85231,28	38251,12	56820,85	80496,21	37880,57	52085,78	93196,72
Total investment cost	***$/t product***	***22.68***	***35.71***	***45.92***	***20.65***	***30.63***	***43.42***	***20.42***	***28.10***	***50.20***
3. Maintenance cost										
Membrane cost	$/year	6691,73	8516,74	10950,10	6083,39	7300,06	10341,76	4866,71	6691,73	9125,08
Maintenance installation	$/year	8122,51	12797,00	16453,28	7384,10	10968,85	15539,21	7312,57	10054,78	17990,95
Total maintenance cost	***$/t product***	***7,99***	***11,48***	***14,77***	***7,27***	***9,85***	***13,96***	***6,56***	***9,03***	***14,61***
TOTAL COST	**$/t product**	**208.07**	**194.37**	**207.91**	**205.70**	**187.78**	**201.56**	**174.27**	**181.32**	**205.44**

- *Case 7 is the most economical design.

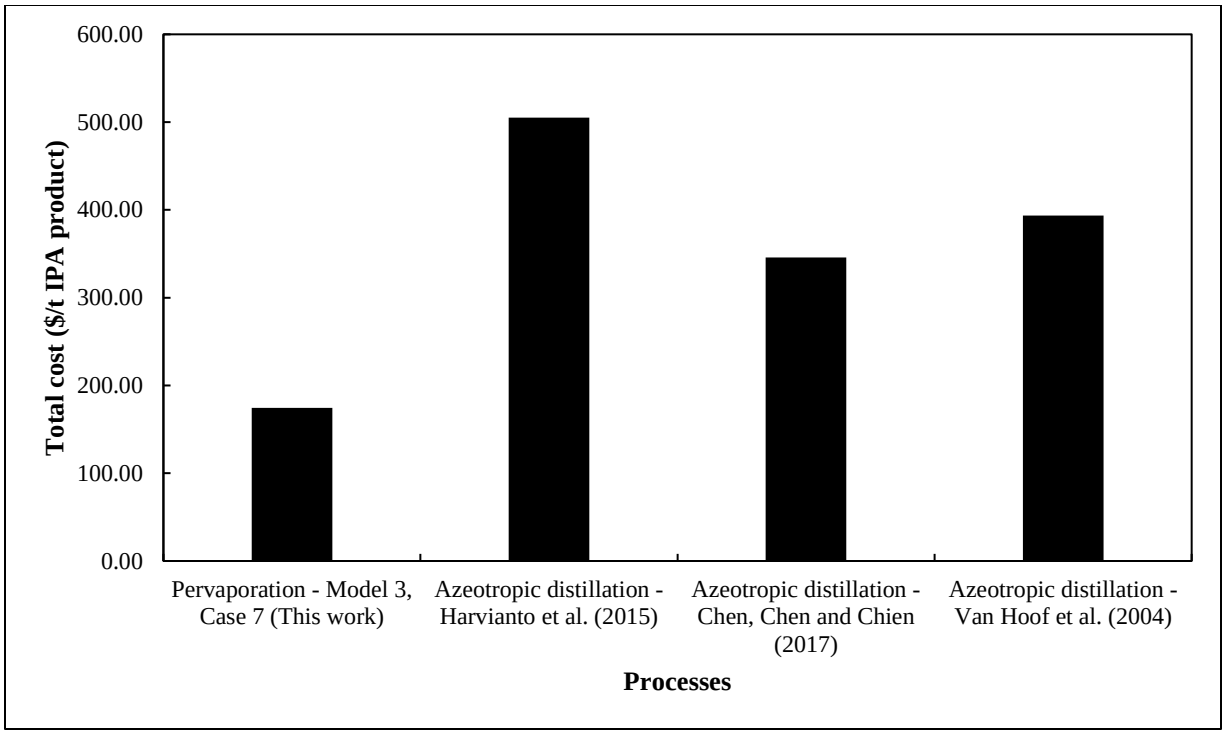

Figure 7.24. Cost comparison between pervaporation and azeotropic distillation for propan-2-ol (1) + water (2) system.

The rising cost of energy and recent call for reduced pollution in industrial practices renders pervaporation a viable separation technique. Yu *et al.* (2011) described an industrial facility with 8 membrane modules having a total membrane area of 52 m^2 to dehydrate propan-2-ol. However, the preferred design of Case 7 utilized 3 modules with a total membrane area of 40 m^2 to meet the product specification of approximately 80 wt.% water in the permeate and less than 2 wt.% water in the retentate. Yu *et al.* (2011) employed a NaA zeolite membrane. The design configuration presented in this work proves that an entry-level membrane, such as PVA, can dehydrate binary homogeneous azeotropic mixtures with a substantial reduction in cost compared to extractive distillation. Therefore, pervaporation not only provides a sharp separation, but also offers an economic and environmentally friendly resolution for the separation of azeotropic mixtures in industry.

CHAPTER 8

Conclusions

i. An apparatus for pervaporation was successfully set up for the test system of ethanol + water. However, after prolonged use and due to time constraints in 2020, no further modifications and experiments could be performed. The equipment setup for pervaporation experiments requires maintenance and careful control of pressure since this is the driving force for mass transport across the membrane.

ii. Pervaporation experiments proved that permeate pressure, feed temperature and the quality of the ethanol concentration in a feed directly impact the degree of separation achieved by a dehydrating PVA-based membrane. In addition, the membrane support (the material used in composite layers), and internal structure of a membrane (crosslinking) determines the strength of the membrane and subsequently, this governs the operating conditions a membrane can withstand before significant swelling occurs. Swelling results in increased flux due to loss in selectivity. Although the experimental results were not conclusive and some trends did not compare well with literature, the PERVAP^{TM} 4100 membrane employed did manage to break the ethanol/water azeotrope.

iii. With some exceptions, the broad trends match literatureIn the experiments investigating the effect of feed composition on pervaporation, it was found that ethanol permeance was almost four times that of water. This indicated plasticization, and membrane swelling, was due to the high ethanol content of the feed. Since the ethanol-water azeotrope is present at 95.62 wt.% ethanol and all experiments were conducted at high feed ethanol concentrations, swelling of the membrane was inevitable. In addition, the stirring bead may have compromised the structure and selectivity of the membrane. Therefore, the flux range was higher than the reported literature.

iv. Modelling of pervaporation, with the use of Aspen Custom Modeler®, was successfully carried out via parameter estimation from existing literature data. The methodology and robustness of the model was verified by modelling two separate data sets (Luyben and I-Lung, 2010; Wesslein et al., 1990) for the ethanol-water system, which comprised different feed and operating conditions. In addition, it was found that the unique models developed for the dehydration of various alcohol mixtures (ethanol-water, propan-1-ol–water, propan-

2-ol–water) correlated strongly with the experimental data of literature (Luyben and I-Lung, 2010; Wesslein et al., 1990; Will and Lichtenthaler, 1992). Models were successfully weighted to provide a best fit for the area near the azeotrope since this is the critical region in the alcohol-water mixtures studied. Deviations between model and experimental data did not exceed 5%.

v. Industrial pervaporation for the dehydration of propan-2-ol (IPA) with a PVA-based membrane was successfully simulated using Aspen Plus® and the user model developed in this work for a propan-2-ol–water system. The 3^2 factorial design resulted in 9 configuration variations, with feed temperature and maximum number of cells per module varied on 3 levels, to be simulated and optimized. The most feasible design configuration for this process consisted of 3 modules (3 cells per module and 8 cells in total out of a maximum of 9) and 2 heat exchangers for interstage heating of 373.15 K. This arrangement resulted in a total cost of 174.27 $/t propan-2-ol product which translated to a 34% saving using pervaporation, assuming a pre-concentrator cost of 1/3 of the total process costs from the literature studies thereby suggesting that pervaporation is a competitive alternative with promising application for pharmaceutical industries.

CHAPTER 9

Recommendations

- The experimental setup, which currently consists of a polysulfone cell can withstand temperatures of up to 358.15 K. This can be improved by replacement with a stainless-steel cell and pipelines. This would prevent pressure leakages downstream of the process especially on the membrane plate. A stainless-steel construction would also allow the cell to withstand greater temperatures and therefore, minimize the temperature difference observed between the feed and the control system.
- A motorized stirrer can replace the stirring bead and plate. This would reduce contact on the membrane which may have hindered permeation.
- The diffusion equations for the models are currently developed for a chosen feed composition range consisting of the azeotrope since the work in this study focused on azeotropic separation. It is difficult to model the separation for a full feed composition range of 0 – 100 wt.% alcohol due to the polynomial trend of the permeate concentration as reported in experiments of literature. It is advised that the model is created for the feed range of interest to maintain accuracy of the model results.
- Alternatively, the feed composition can be divided into segments with diffusivity equations developed for each segment. The diffusion equations can then be implemented into the code script with multiple if-statements depending on the feed composition input. Therefore, the model would describe pervaporation for a full composition range with great accuracy. The method described may be time consuming since the data must be weighted for the best fit in each composition segment. In addition, multiple if-statements will be required in the code script which must be compiled without errors.
- Aspen Custom Modeler® is easy to use and is capable of developing unit operations using modelling language. However, the optimization tools such as sensitivity analysis and design specification are not available on the program. In addition, the phase of each stream is not reported in the results table of ACM. It is recommended that models be exported to Aspen Plus® for rigorous analysis as done in this work. This would allow operating conditions such as feed temperature and pressure to be optimized to ensure a liquid phase feed and retentate is obtained.

REFERENCES

Abdel-rahman, Z.A., Mahmood, A.M., Ali, A.J., 2014. Ethanol-Water Separation by Pressure Swing Adsorption (PSA). Iraqi J. Chem. Pet. Eng. 15, 1–7.

Ahmed, H., Rask, N., Baldwin, E.D., 1989. Ethanol Fuel as an Octane Enhancer in the US Fuel. Biomass 19, 215–232.

Alzate, J.F., 2006. Design and performance of two-phase flow pervaporation and hybrid distillation processes. Diss. Abstr. Int. Technische Universiteit Eindhoven.

Amcor plc, 2021. Three Home Care Trends to Watch in 2021 [WWW Document]. URL https://www.amcor.com/insights/blogs/2021-homecare-packaging-trends (accessed 5.31.21).

Aminabhavi, T.M., Kulkarni, P. V, Kurkuri, M., 2006. Pervaporation membranes and methods of use. US 7,045,062 B1.

An, W., Lin, Z., Chen, J., Zhu, J., 2014. Simulation and analysis of a reactive distillation column for removal of water from ethanol-water mixtures. Ind. Eng. Chem. Res. 53, 6056–6064.

Arce, A., Rodil, E., Soto, A., 2006. Volumetric and Viscosity Study for the Mixtures of 2-Ethoxy-2-methylpropane, Ethanol, and 1-Ethyl-3-methylimidazolium Ethyl Sulfate Ionic Liquid. J. Chem. Eng. Data 51, 1453–1457.

Baker, R.W., Wijmans, J.G., Huang, Y., 2010. Permeability, permeance and selectivity: A preferred way of reporting pervaporation performance data. J. Memb. Sci. 348, 346–352.

Binning, R.C., Lee, R.J., Jennings, J.F., Martin, E.C., 1961. Separation of Liquid Mixtures. Ind. Eng. Chem. 53, 45–50.

Black, C., Ditsler, D.E., 1974. Dehydration of Aqueous Ethanol Mixtures by Extractive Distillation. In: Tassios, D.P. (Ed.), Extractive and Azeotropic Distillation. American Chemical Society, pp. 1–15.

Burshe, M.C., Sawant, S.B., Joshi, J.B., Pangarkar, V.G., 1997. Sorption and permeation of binary water-alcohol systems through PVA membranes crosslinked with multifunctional crosslinking agents. Sep. Purif. Technol. 12, 145–156.

Business Wire, I., 2021. China Household Care (Fabric Care, Home Care & Personal Hygiene) Market Insights & Forecast 2021-2025 with Impact of COVID-19 [WWW Document]. URL https://www.businesswire.com/news/home/20210416005329/en/China-Household-Care-Fabric-Care-Home-Care-Personal-Hygiene-Market-Insights-Forecast-2021-2025-with-Impact-of-COVID-19---ResearchAndMarkets.com (accessed 5.31.21).

Chan, W.-H., Ng, C.-F., Suei-Yee, L.-L., He, X., Cheung, O.-C., 1997. Water – Alcohol Separation by Pervaporation Through Poly(amide-sulfonamide)s (PASAs) Membranes. J. Appl. Polym. Sci. 65, 1113–1119.

Chemstations Inc., 2020. Heterogeneous Azeotropic Distillation [WWW Document]. URL https://www.chemstations.com/content/documents/Technical_Articles/DISTILLATION.PDF (accessed 5.22.21).

Chen, H.-H., Chen, M.-K., Chien, I.-L., 2017. Using [EMIM][OAC] as entrainer for isopropyl alcohol dehydration via extractive distillation. In: 2017 6th International Symposium on Advanced Control of Industrial Processes (AdCONIP). IEEE, pp. 257–262.

Chianese, A., Zinnamosca, F., 1990. Ethanol dehydration by azeotropic distillation with a mixed-solvent entrainer. Chem. Eng. J. 43, 59–65.

Chou, K.J., Hellmuth, K.M., 1994. Membrane separation process. US5281337.

Chua, W.J., Rangaiah, G.P., Hidajat, K., 2017. Design and optimization of isopropanol process based on two alternatives for reactive distillation. Chem. Eng. Process. Process Intensif. 118, 108–116.

Cook, R.A., Furter, W.F., 1968. Extractive Distillation Employing a Dissolved Salt as Separating Agent. Can. J. Chem. Eng. 46, 119–123.

De, D., Sai, M.S.N., Aniya, V., Jyothi, K.N., Satyavathi, B., 2019. Economic and environmental impact assessment of extractive distillation with renewable entrainers for reprocessing aqueous 2-Propanol. Chem. Eng. Process. Process Intensif. 143, 107616.

Dirk-Faitakis, C.B., Chuang, K.T., 2004. Simulation studies of the removal of water from ethanol by a catalytic distillation process. Ind. Eng. Chem. Res. 43, 762–768.

Doherty, M.F., Malone, M.F., Foucher, E.R., 1991. Automatic Screening of Entrainers for Homogeneous Azeotropic Distillation. Ind. Eng. Chem. Res. 30, 760–772.

Egorov, G.I., Makarov, D.M., Kolker, A.M., 2013. Liquid phase PVTx properties of (water+tert-butanol) binary mixtures at temperatures from 278.15 to 323.15K and pressures from 0.1 to 100MPa. J. Chem. Thermodyn. 61, 161–168.

Farobie, O., Leow, Z.Y.M., Samanmulya, T., Matsumura, Y., 2016. New insights in biodiesel production using supercritical 1-propanol. Energy Convers. Manag. 124, 212–218.

Feimer, J.L., Schucker, R.C., Darnell, C.P., 1990. Multi-stage Pervaporation Process Run At Progressively Higher Vacuum, Higher Temperature Or Both At Each Successive Retentate Stage. US4,962,270.

Feng, X., Huang, R.Y.M., 1996. Estimation of activation energy for permeation in pervaporation processes. J. Memb. Sci. 118, 127–131.

Font, A., Asensi, J.C., Ruiz, F., Gomis, V., 2004. Isobaric vapor-liquid and vapor-liquid-liquid equilibria data for the system water + isopropanol + isooctane. J. Chem. Eng. Data 49, 765–767.

Fu, Y.-J., Lai, C.-L., Chen, J.-T., Liu, C.-T., Huang, S.-H., Hung, W.-S., Hu, C.-C., Lee, K.-R., 2014. Hydrophobic composite membranes for separating of water–alcohol mixture by pervaporation at high temperature. Chem. Eng. Sci. 111, 203–210.

Galiano, F., Falbo, F., Figoli, A., 2016. Polymeric Pervaporation Membranes: Organic-Organic Separation. Nanostructured Polym. Membr. 2, 287–310.

García-Abuín, A., Gómez-Díaz, D., La Rubia, M.D., Navaza, J.M., Pacheco, R., 2009. Density, Speed of Sound, and Isentropic Compressibility of Triethanolamine (or N - Methyldiethanolamine) + Water + Ethanol Solutions from t = (15 to 50) °C. J. Chem. Eng. Data 54, 3114–3117.

Gil, I.D., Uyazán, A.M., Aguilar, J.L., Rodríguez, G., Caicedo, L.A., 2008. Separation of ethanol and water by extractive distillation with salt and solvent as entrainer: Process Simulation. Brazilian J. Chem. Eng. 25, 207–215.

Gomis, V., Pedraza, R., Francés, O., Font, A., Asensi, J.C., 2007. Dehydration of ethanol using azeotropic distillation with isooctane. Ind. Eng. Chem. Res. 46, 4572–4576.

Haaz, E., Toth, A.J., 2018. Methanol dehydration with pervaporation: Experiments and modelling. Sep. Purif. Technol. 205, 121–129.

Han, J., Jin, J., Eimer, D.A., Melaaen, M.C., 2012. Density of Water (1) + Monoethanolamine (2) + CO 2 (3) from (298.15 to 413.15) K and Surface Tension of Water (1) + Monoethanolamine (2) from (303.15 to 333.15) K. J. Chem. Eng. Data 57, 1095–1103.

Hartanto, D., Handayani, P.A., Sutrisno, A., Anugrahani, V.W., Mustain, A., Khoiroh, I., 2019. Isopropyl Alcohol Purification through Extractive Distillation using Glycerol as an Entrainer: Technical Performances Simulation and Design. J. Bahan Alam Terbarukan 8, 133–143.

Harvianto, G.R., Ahmad, F., Nhien, L.C., Lee, M., 2015. Vapor permeation-distillation Hybrid processes for cost-effective isopropanol dehydration : Modelling , simulation and optimization Vapor permeation – distillation hybrid processes for cost-effective isopropanol dehydration : modeling , simulation and opt. J. Memb. Sci. 497, 108–119.

Hassankhan, B., Raisi, A., 2020. Separation of isobutanol/water mixtures by hybrid distillation-pervaporation process: Modeling, simulation and economic comparison. Chem. Eng. Process. - Process Intensif. 155, 108071.

Haynes, W.M., 2014. CRC Handbook of Chemistry and Physics, 95th ed. CRC Press, Boca Raton, Florida.

Huang, Y., Ly, J., Nguyen, D., Baker, R.W., 2010. Ethanol Dehydration Using Hydrophobic and Hydrophilic Polymer Membranes. Ind. Eng. Chem. Res. 49, 12067–12073.

Iqbal, A., Ahmad, S.A., 2016. Pressure swing distillation of azeotropic mixture – A simulation study. Perspect. Sci. 8, 4–6.

Janakey Devi, V.K.P., Sai, P.S.T., Balakrishnan, A.R., 2017a. Heterogeneous azeotropic distillation for the separation of n-propanol + water mixture using n-propyl acetate as entrainer. Fluid Phase Equilib. 447, 1–11.

Janakey Devi, V.K.P., Sai, P.S.T., Balakrishnan, A.R., 2017b. Experimental studies and

thermodynamic analysis of isobaric vapor-liquid-liquid equilibria of 2-propanol + water system using n-propyl acetate and isopropyl acetate as entrainers. Fluid Phase Equilib. 454, 22–34.

Jia, H., Wang, H., Ma, K., Yu, M., Zhu, Z., Wang, Y., 2018. Effect of thermodynamic parameters on prediction of phase behavior and process design of extractive distillation. Chinese J. Chem. Eng. 26, 993–1002.

Kamesh, R., Chenna, S., Rani, K.Y., 2018. Thermodynamic Models for Prediction of Sorption Behavior in Pervaporation. Membr. Process. 169–209.

Karmakar, B., Samanta, S., Halder, G., 2020. Delonix regia heterogeneous catalyzed two-step biodiesel production from Pongamia pinnata oil using methanol and 2-propanol. J. Clean. Prod. 255, 120313.

Kiss, A.A., Suszwalak, D.J.-P.C., 2012. Efficient bioethanol dehydration in azeotropic and extractive dividing-wall columns. Procedia Eng. 42, 620 – 626.

Kober, P.A., 1917. Pervaporation, perstillation and percrystallization. J. Am. Chem. Soc. 39, 944–948.

Kruczek, B., 2015. Encyclopedia of Membranes. In: Drioli, E., Giorno, L. (Eds.), Encyclopedia of Membranes. Springer-Verlag Berlin Heidelberg, Ottawa, pp. 1–5.

Kujawski, W., Krajewska, S., Kujawski, M., Gazagnes, L., Larbot, A., Persin, M., 2007. Pervaporation properties of fluoroalkylsilane (FAS) grafted ceramic membranes. Desalination 205, 75–86.

Kujawski, W., Nguyen, T.Q., Neel, J., 1991. Dehydration of Water-Pyridine Mixtures by Pervaporation. Sep. Sci. Technol. 26, 1109–1121.

Laroche, Lionel, Andersen, H.W., Morari, M., Bekiaris, N., 1991. Homogeneous azeotropic distillation: comparing entrainers. Can. J. Chem. Eng. 69, 1302–1319.

Laroche, L, Bekiaris, N., Andersen, H.W., Morari, M., 1991. Homogenous Azeotropic Distillation: Comparing Entrainers. Can. J. Chem. Engineeering 69, 1302–1319.

Lee, L., Shen, H., 2003. Azeotropic Behavior of a Water + n-Propanol + Cyclohexane Mixture

Using Cyclohexane as an Entrainer for Separating the Water + n-Proponal Mixture at 760 mmHg. Ind. Eng. Chem. Res. 42, 5905–5914.

Leppäjärvi, T., Malinen, I., Korelskiy, D., Kangas, J., Hedlund, J., Tanskanen, J., 2015. Pervaporation of ethanol/water mixtures through a high-silica MFI membrane: Comparison of different semi-empirical mass transfer models. Period. Polytech. Chem. Eng. 59, 111–123.

Li, G., Bai, P., 2012. New Operation Strategy for Separation of Ethanol-Water by Extractive Distillation. Ind. Eng. Chem. Res. 51, 2723–2729.

Liang, K., Li, W., Luo, H., Xia, M., Xu, C., 2014. Energy-Efficient Extractive Distillation Process by Combining Preconcentration Column and Entrainer Recovery Column. Ind. Eng. Chem. Res. 53, 7121–7131.

Ligero, E.L., Ravagnani, T.M.K., 2003. Dehydration of ethanol with salt extractive distillation-a comparative analysis between processes with salt recovery. Chem. Eng. Process. Process Intensif. 42, 543–552.

Lipnizki, F., Field, R.W., Ten, P.-K., 1999. Pervaporation-based hybrid process: a review of process design, applications and economics. J. Mrmbrane Sci. 153, 183–210.

Lipnizki, F., Trägårdh, G., 2001. Modelling of pervaporation: Models to analyze and predict the mass transport in pervaporation. Sep. Purif. Rev. 30, 49–125.

Lladosa, E., Montón, J.B., Burguet, M.C., 2011. Separation of di-n-propyl ether and n-propyl alcohol by extractive distillation and pressure-swing distillation: Computer simulation and economic optimization. Chem. Eng. Process. Process Intensif. 50, 1266–1274.

Llano-Restrepo, M., Aguilar-Arias, J., 2003. Modeling and simulation of saline extractive distillation columns for the production of absolute ethanol. Comput. Chem. Eng. 27, 527–549.

Lokhandwala, K.A., Pinnau, I., He, Z., Amo, K.D., DaCosta, A.R., Wijmans, J.G., Baker, R.W., 2010. Membrane separation of nitrogen from natural gas: A case study from membrane synthesis to commercial deployment. J. Memb. Sci. 346, 270–279.

Luo, H.-P., Xiao, W.-D., 2001. A reactive distillation process for a cascade and azeotropic reaction

system: Carbonylation of ethanol with dimethyl carbonate. Chem. Eng. Sci. 56, 403–410.

Luo, H., Liang, K., Li, W., Li, Y., Xia, M., Xu, C., 2014. Comparison of pressure-swing distillation and extractive distillation methods for isopropyl alcohol/diisopropyl ether separation. Ind. Eng. Chem. Res. 53, 15167–15182.

Luyben, W.L., 2008. Comparison of extractive distillation and pressure-swing distillation for acetone-methanol separation. Ind. Eng. Chem. Res. 47, 2696–2707.

Luyben, W.L., 2013. Comparison of extractive distillation and pressure-swing distillation for acetone/chloroform separation. Comput. Chem. Eng. 50, 1–7.

Luyben, W.L., I-Lung, C., 2010. Design and control of distillation systems for separating azeotropes. John Wiley & Sons, Inc., Hoboken, New Jersey.

Lv, J.H., Xiao, G.M., 2011. Dehydration of water/pyridine mixtures by pervaporation using cellulose acetate/polyacrylonitrile. Water Sci. Technol. 63, 1695–1700.

Lynn, S., Hanson, D.N., 1986. Multieffect Extractive Distillation for Separating Aqueous Azeotropes. Ind. Eng. Chem. Process Des. Dev. 25, 936–941.

Makarov, D.M., Egorov, G.I., Kolker, A.M., 2015. Density and Volumetric Properties of Aqueous Solutions of Trimethylamine N -Oxide in the Temperature Range from (278.15 to 323.15) K and at Pressures up to 100 MPa. J. Chem. Eng. Data 60, 1291–1299.

Merry, A.J., 1996. Membrane equipment and plant design. In: Scott, K., Hughes, R. (Eds.), Industrial Membrane Separation Technology. Springer Netherlands, Dordrecht, pp. 32–66.

Minnesota Rural Water Association, 2001. Chapter19: Membrane Filtration. In: Minnesota Water Works Operations Manual. pp. 1–12.

Mixa, A., Staudt, C., 2008. Membrane-Based Separation of Phenol/Water Mixtures Using Ionically and Covalently Cross-Linked Ethylene-Methacrylic Acid Copolymers. Int. J. Chem. Eng. 2008, 1–12.

Mueanmas, C., Prasertsit, K., Tongurai, C., 2010. Feasibility Study of Reactive Distillation Column for Transesterification of Palm Oils. Int. J. Chem. Eng. Appl. 1, 77–83.

Mulder, M., 1994. Energy Requirements in Membrane Separation Processes. In: Crespo, J.G.,

Böddeker, K.W. (Eds.), Membrane Processes in Separation and Purification. Kluwer Academic Publishers, Enschede, pp. 445–475.

Mulder, M.H. V., Franken, T., Smolders, C.A., 1985. Preferential sorption versus preferential permeability in pervaporation. J. Memb. Sci. 22, 155–173.

Mulia-Soto, J.F., Flores-Tlacuahuac, A., 2011. Modeling, simulation and control of an internally heat integrated pressure-swing distillation process for bioethanol separation. Comput. Chem. Eng. 35, 1532–1546.

Muñoz, R., Montón, J.B., Burguet, M.C., de la Torre, J., 2006. Separation of isobutyl alcohol and isobutyl acetate by extractive distillation and pressure-swing distillation: Simulation and optimization. Sep. Purif. Technol. 50, 175–183.

Naidu, B.V.K., Aminabhavi, T.M., 2005. Pervaporation separation of water/2-propanol mixtures by use of the blend membranes of sodium alginate and (hydroxyethyl) cellulose: Roles of permeate-membrane interactions, zeolite filling, and membrane swelling. Ind. Eng. Chem. Res. 44, 7481–7489.

Naylor, T. deV, 1996. Polymer Membranes: Materials, Structures and Separation Performance. iSmithers Rapra Publishing, Shropshire.

Neel, J., Nguyen, Q.T., Clement, R., Lin, D.J., 1986. Influence of Downstream Pressure on the pervaporation of Water-Tetrahydrofuran Mixture through a Regenerated Cellulose Membrane (Cuprophan). J. Memb. Sci. 27, 217–232.

Nieuwenhuis, J., Tan, Y.Y., van Ekenstein, G.O.R.A., 1987. Pervaporation of water-n-propanol mixtures through membranes composed of poly(N-vinylpyrrolidone)-poly(methacrylic acid) complexes. Die Angew. Makromol. Chemie 147, 83–97.

Okada, T., Matsuura, T., 1991. A new transport model for pervaporation. J. Memb. Sci. 59, 133–149.

Pham, H.N., Doherty, M.F., 1990. Design and synthesis of heterogeneous azeotropic distillations-III. Column sequences. Chem. Eng. Sci. 45, 1845–1854.

Pienaar, C., Schwarz, C.E., Knoetze, J.H., Burger, A.J., 2013. Vapor-liquid-liquid equilibria

measurements for the dehydration of ethanol, isopropanol, and n-propanol via azeotropic distillation using DIPE and isooctane as entrainers. J. Chem. Eng. Data 58, 537–550.

Pla-Franco, J., Lladosa, E., Loras, S., Montón, J.B., 2014. Isobaric vapor-liquid-liquid equilibria for the ternary systems ethanol + water + propyl acetate and 1-propanol + water + propyl acetate. J. Chem. Eng. Data 59, 2054–2064.

Pla-Franco, J., Lladosa, E., Loras, S., Montón, J.B., 2015. Approach to the 1-propanol dehydration using an extractive distillation process with ethylene glycol. Chem. Eng. Process. Process Intensif. 91, 121–129.

Pla-Franco, J., Lladosa, E., Montón, J.B., Loras, S., 2013. Evaluation of the 2-methoxyethanol as entrainer in ethanol-water and 1-propanol-water mixtures. J. Chem. Eng. Data 58, 3504–3512.

Process Engineering, 2000. Sulzer gets into membranes with GFT buy [WWW Document]. URL http://processengineering.co.uk/article/1272794/sulzer-gets-into-membranes-with-gft-buy (accessed 1.30.18).

Raal, J.D., Mühlbauer, A.L., 1998. Phase Equilibria: Measurement and Computation. Taylor & Francis, Bristol.

Reuters, 2021. 3M profit beats on higher demand for personal safety, home care products [WWW Document]. URL https://www.reuters.com/article/us-3m-results-idUSKBN29V18M (accessed 5.31.21).

Roizard, D., Favre, E., 2012. Trends in design and preparation of polymeric membranes for pervaporation. Adv. Mater. Membr. Prep. 42, 163–204.

Rojas, J.V., Stinguel, L., Wolf-Maciel, M.R., Guirardello, R., 2016. Modeling and simulating complete extractive distillation process of ethanol-water mixture using equilibrium-stage distillation model and efficiency correlations (Barros & Wolf) on EMSO platform. Chem. Eng. Trans. 50, 331–336.

Rozicka, A., Niemistö, J., Keiski, R.L., Kujawski, W., 2014. Apparent and intrinsic properties of commercial PDMS based membranes in pervaporative removal of acetone, butanol and ethanol from binary aqueous mixtures. J. Memb. Sci. 453, 108–118.

Sakhre, V., 2019. Reactive Distillation - Modeling, Simulation, and Optimization. In: Steffen, V. (Ed.), Distillation - Modelling, Simulation and Optimization. IntechOpen, Dubai.

Sander, U., Soukup, P., 1988. Design and operation of a pervaporation plant for ethanol dehydration. J. Memb. Sci. 36, 463–475.

Scharzec, B., Waltermann, T., Skiborowski, M., 2017. A Systematic Approach towards Synthesis and Design of Pervaporation-Assisted Separation Processes. Chemie-Ingenieur-Technik 89, 1534–1549.

Schiffmann, P.M., 2014. Three step modelling approach for the simulation of industrial scale pervaporation modules. Technische Universität Bergakademie Freiberg.

Schmitt, D., Vogelpohl, A., 1983. Distillation of Ethanol-Water Solutions in the Presence of Potassium Acetate. Sep. Sci. Technol. 18, 547–554.

Seader, J.D., Henley, E.J., Roper, D.K., 2011. Separation Process Principles. John Wiley & Sons, New Jersey.

Singha, N.R., Das, P., Ray, S.K., 2013. Recovery of pyridine from water by pervaporation using filled and crosslinked EPDM membranes. J. Ind. Eng. Chem. 19, 2034–2045.

Sinnott, R., Towler, G., 2009. Chemical Engineering Design. Elsevier, Oxford.

Smith, J.M., Van Ness, H.C., Abbott, M.M., 2005. Introduction to Chemical Engineering Thermodynamics, 7th ed. McGraw-Hill, New York.

Teleman, D., Kreis, P., Lauterbach, S., Teodosiu, C., Balasanian, I., 2006. Determination of optimum operational conditions for pervaporation of binary mixture water / 1-propanol and ternary mixture water / 1- propanol / propionic acid. Roum. Biotechnol. Lett. 11, 2819–2832.

Teng, M.-Y., Lee, K.-R., Fan, S.-C., Liaw, D.-J., Huang, J., Lai, J.-Y., 2000. Development of aromatic polyamide membranes for. J. Memb. Sci. 164, 241–249.

The European Business Review, 2021. 5 Impacts Of COVID-19 On Household Cleaning Services.

Unilever, 2021. Strong full-year results demonstrate Unilever’s resilience and agility [WWW Document]. URL https://www.unilever.com/news/press-releases/2021/strong-full-year-results-demonstrate-unilevers-resilience-and-agility.html (accessed 5.31.21).

Urtiaga, A.M., Gorri, E.D., Ortiz, I., 2006. Pervaporative recovery of isopropanol from industrial effluents. Sep. Purif. Technol. 49, 245–252.

Van Hoof, V., Van den Abeele, L., Buekenhoudt, A., Dotremont, C., Leysen, R., 2004. Economic comparison between azeotropic distillation and different hybrid systems combining distillation with pervaporation for the dehydration of isopropanol. Sep. Purif. Technol. 37, 33–49.

Vane, L.M., 2020. Review of pervaporation and vapor permeation process factors affecting the removal of water from industrial solvents. J. Chem. Technol. Biotechnol. 95, 495–512.

Walas, S.M., 1985. Phase Equilibria in Chemical Engineering, Phase Equilibria in Chemical Engineering. Butterworth Publishers, Kansas.

Wang, S.-J., Wong, D.S.H., 2006. Control of reactive distillation production of high-purity isopropanol. J. Process Control 16, 385–394.

Wee, S.-L., Tye, C.-T., Bhatia, S., 2008. Membrane separation process-Pervaporation through zeolite membrane. Sep. Purif. Technol. 63, 500–516.

Weiss, S., Herfurth, H., Meirelles, A., 1992. Ethanol Dehydration by Extractive Distillation. J. Chem. Technol. Biotechnol. 53, 181–188.

Wesslein, M., Heintz, A., Lichtenthaler, R.N., 1990. Pervaporation of liquid mixtures through poly(vinyl alcohol) (PVA) membranes. I. Study of water containing binary systems with complete and partial miscibility. J. Memb. Sci. 51, 169–179.

Wijmans, J.G., Baker, R.W., 1993. A simple predictive treatment of the permeation process in pervaporation. J. Memb. Sci. 79, 101–113.

Wijmans, J.G., Baker, R.W., 1995. The solution-diffusion model: a review. J. Memb. Sci. 107, 1–21.

Will, B., Lichtenthaler, R.N., 1992. Comparison of the separation of mixtures by vapor permeation and by pervaporation using PVA composite membranes. II. The binary systems ammonia-water, methylamine-water, 1-propanol-methanol and the ternary system 1-propanol-methanol-water. J. Memb. Sci. 68, 119–125.

Win, N.N., Friedl, A., 2012. Separation of Ethanol-Water Mixture By Pervaporation With Organic Composite Membrane : Modelling of Separation Performance Using Model Parameters Derived From Experimental Data. ASEAN Eng. J. Part B 2, 28–37.

Yeom, C.K., Huang, R.Y.M., 1991. Pervaporation separation of aqueous mixtures using crosslinked poly(viny1 alcohol), I. Die Angew. Makromol. Chemie 184, 27–40.

Yu, C., Liu, Y., Chen, G., Gu, X., Xing, W., 2011. Pretreatment of isopropanol solution from pharmaceutical industry and pervaporation dehydration by NaA zeolite membranes. Chinese J. Chem. Eng. 19, 904–910.

Zafarani-Moattar, M.T., Majdan-Cegincara, R., 2008. Density, Speed of Sound, and Viscosity of Binary Mixtures of Poly(propylene glycol) 400 + Ethanol and + 2-Propanol at Different Temperatures. J. Chem. Eng. Data 53, 2211–2216.

Zhang, S., Driol, E., 1995. Pervaporation Membranes. Sep. Sci. Technol. 30, 1–31.

APPENDIX A

Expanded Literature

A.1 Salt distillation

Salt distillation requires a selective salt to “salt out” the undesired component. This would result in an activity increase in the non-saline region which in turn produces a highly concentrated equilibrium vapour. In the case of an ethanol-water separation, viable salts include potassium acetate or mercuric chloride (Cook and Furter, 1968). The salts differ in solubility. Potassium acetate is more soluble in water; mercuric chloride is more soluble in ethanol. Cook and Furter (1968) described a technique to overcome the common problem of foaming caused by malfunction of salt metering. A separate salt feed apparatus with a dissolving chamber was constructed to dissolve the salt into the reflux stream. In addition to the metering mechanism developed, antifoam agents are employed into the reflux stream to suppress the froth level to that which would be produced without the use of a salt in the system. Dow Corning Antifoam AF Emulsion was reported as being the most suitable salt for an ethanol-water system (Cook and Furter, 1968).

Another study conducted by Schmitt and Vogelpohl (1983) utilized an evaporator and melting pot in the salt recycle to avoid agglomeration and metering difficulties. Catalytic decomposition was prevented by using stainless-steel as a material of construction for any equipment processing the salt. The number of trays was strongly dependent on the reflux ratio and the salt concentration. Salt addition had to be regulated such that the reflux stream had a potassium acetate concentration greater than 6% to obtain anhydrous ethanol (Schmitt and Vogelpohl, 1983). It was noted that only one column was required for this method of separation. However, the overall Murphree plate efficiency decreased in salt distillation as compared to a salt-free separation due to the fluctuating hydrodynamic behaviour of froth. A few more uses of salt distillation can be seen in Table A.1.

Table A.1. Salt distillation of binary alcohol-water systems.

System	Salt	Total theoretical plates	R	Salt concentration (mol%)	Product alcohol (mol%)	Reference
Ethanol-water	Liquid potassium acetate	12	2	12.5	98.6	(Cook and Furter, 1968)
Ethanol-water	Potassium acetate	16	2	8.4	99.4	(Schmitt and Vogelpohl, 1983)
Ethanol-water	Potassium acetate	22	1.1	6.9	98.9	(Ligero and Ravagnani, 2003)
Ethanol-water	Calcium chloride	22	6.42	7.7	99.998	(Llano-Restrepo and Aguilar-Arias, 2003)

A.2 Pressure-swing distillation

Pressure-swing distillation is said to be the simplest and most economical method of the enhanced distillation methods (Iqbal and Ahmad, 2016). This technique was investigated since the azeotropic composition for an ethanol-water system changes significantly with changes in pressure. Iqbal and Ahmad (2016) reported that the first column operated at a low pressure and the bottoms produced was a highly pure water stream. As expected, the bottoms of the high-pressure column contained ethanol with a high purity. High reflux ratios were applied to both columns to obtain almost pure water and ethanol streams in the low- and high-pressure columns respectively. This may have indicated increased energy consumption. However, pressure-swing methods often include heat integration to greatly reduce energy costs. A heat exchanger can be used as both a condenser and a reboiler when the column heat duties are perfectly matched. Alternatively, auxiliary condensers or reboilers are implemented (Luyben, 2013). Additional pressure-swing examples are summarized in Table A.2.

Table A.2. Pressure swing distillation of binary alcohol systems at 1013.25 kPa (compiled in this study).

System	Feed stage location	Low pressure column					High pressure column				Reference
		Pressure (kPa)	Total theoretical plates	D/F	R	Product	Total theoretical plates	D/F	R	Product	
Ethanol-water	23	101.325	30	0.55	3.71	99.5 mol% water	30	0.80	4.29	99.7 mol% ethanol	(Iqbal and Ahmad, 2016)
Isopropanol-diisopropyl ether	6	101.325	38	0.57	1.05	99.15 mol% DIPE	18	0.76	2.00	99.70 mol% IPA	(Luo et al., 2014)
Isobutanol-isobutyl acetate	8	20	16	077	1.33	98.5 mol% IBA	30	0.67	1.86	99.5 mol% IBAc	(Muñoz et al., 2006)
Acetone-Methanol	17	101.325	52	0.63	2.84	99.5 mol% methanol	62	0.41	3.11	99.4 mol% acetone	(Luyben, 2008)
Di-n-propyl ether and n-propanol	7	30	12	0.22	0.72	99 mol% PA	12	1.07	0.71	99 mol% DPE	(Lladosa et al., 2011)

A.3 Thermodynamic approach of Flory-Huggins model

The Flory-Huggins theory predicts the liquid sorption in a polymer using Gibbs free energy of mixing as a basis (Kamesh et al., 2018). In the model, a ternary system is defined as a binary mixture and a non-crosslinked high molecular weight polymer membrane (Lipnizki and Trägårdh, 2001).

$$\frac{\Delta G_{mix}}{RT} = x_i \ln \Phi_i + x_j \ln \Phi_j + x_{mem} \ln \Phi_{mem} + \chi_{i,j} x_i \Phi_j + \chi_{i,mem} x_i \Phi_{mem} + \chi_{j,mem} x_j \Phi_{mem} \quad \text{(A.1)}$$

where Φ is volume fraction

$\chi_{i,j}$ is the interaction parameter for the binary solvent-solvent mixture

$\chi_{i,mem}$ is the binary interaction parameter of solvent i in the membrane

Chemical potential is defined in terms of activity as follows:

$$\ln a_i = \frac{\partial \left({}^{\Delta G_{mix}}/_{RT} \right)}{\partial x_i} = \ln \Phi_i + \left(1 - \frac{v_i}{v_{mem}}\right) \Phi_{mem} + \chi_{i,mem} {\Phi_{mem}}^2 \quad \text{(A.2)}$$

where v is the molar volume

The binary solvent-membrane interaction parameters are approximated using single solvent sorption data ($a_i = 1 \Rightarrow \ln a_i = 0$). Two experiments can be performed for this data; swelling experiments of the pure solvent in the presence of the membrane or using inverse gas chromatography (Lipnizki and Trägårdh, 2001). The former is preferred.

$$\chi_{i,mem} = -\frac{[\ln(1 - \Phi_{mem}) + \Phi_{mem}]}{{\Phi_{mem}}^2} \quad \text{(A.3)}$$

The binary interaction parameter describing the interactions between the two liquid solvents is strongly dependent on concentration (Kamesh et al., 2018).

$$\chi_{i,j} = \frac{1}{m_i u_i} \left[m_i \ln \left(\frac{m_i}{u_i} \right) + m_j \ln \left(\frac{m_j}{u_j} \right) + \frac{\Delta G^E}{RT} \right] \quad \text{(A.4)}$$

where m_i is the reduced mole fraction of solvent i

$$m_i = \frac{x_i}{x_i + x_j} \tag{A.5}$$

u_i is the reduced volume fraction of solvent i

$$u_i = \frac{\Phi_i}{\Phi_i + \Phi_j} \tag{A.6}$$

The excess Gibbs free energy is calculated from activity coefficient models based on vapour-liquid equilibria.

The activity of both components in the membrane is calculated by differentiating Equation A.1 with respect to x_i and x_j resulting in the following:

$$\ln a_i = \ln \Phi_i + (1 - \Phi_i) - \frac{V_i}{V_j}\Phi_j - \frac{V_i}{V_{mem}}\Phi_{mem} + \left(\chi_{i,j}\Phi_j + \chi_{i,mem}\Phi_{mem}\right)\left(\Phi_j + \Phi_{mem}\right) - \chi_{j,mem}\frac{V_i}{V_j}\Phi_j\Phi_{mem} \tag{A.7}$$

$$\ln a_j = \ln \Phi_j + \left(1 - \Phi_j\right) - \frac{V_j}{V_i}\Phi_i - \frac{V_j}{V_{mem}}\Phi_{mem} + \left(\chi_{i,j}\frac{V_j}{V_i}\Phi_i + \chi_{j,mem}\Phi_{mem}\right)(\Phi_i + \Phi_{mem}) - \chi_{i,mem}\frac{V_j}{V_i}\Phi_i\Phi_{mem} \tag{A.8}$$

where

$$\Phi_i + \Phi_j + \Phi_{mem} = 1 \tag{A.9}$$

The solvent volume fractions are solved for by substituting parameters into equations A.7 to A.9. This creates a set of non-linear algebraic equations which can be solved using optimization techniques or Matlab software package.

Finally, the sorption uptake levels (g/g dry membrane) are calculated from

$$w_i = \frac{\Phi_i \rho_i}{\Phi_{mem} \rho_{mem}} \tag{A.10}$$

The sorption levels predicted by the model must be validated by comparing against experimental data.

APPENDIX B

Additional Data for Experimental Study

B.1 Measured and calculated data of pervaporation experiments

Table B.1. Data for experiments of varying permeate pressures (2 – 5 kPa).

Run	T_f (K)	p_l (kPa)	$X_{io}{}^{L}$ (mol%)		x_i (wt.%)		Y_{il} (mol%)		y_i (wt.%)		$m_{i,j}$ (g)	$p_{i_{sat}}$ (kPa)		J_i (g.m^{-2}h^{-1})			j_i (cm^3(STP).cm^{-2}s^{-1})		$\frac{P_i{}^{G}}{L}$ (gpu)		α_{ij}	β_{ij}
			ethanol	water	ethanol	water	ethanol	water	ethanol	water	permeate mixture	ethanol	water	ethanol	water	total	ethanol	water	ethanol	water		
1	339.10	2.11	86.89	13.11	94.43	5.57	77.77	22.23	89.94	10.06	6.09	61.05	26.18	1311.28	146.59	1457.87	0.01771	0.005063	453.35	932.01	1.90	2.06
2	336.15	2.19	88.01	11.99	94.94	5.06	75.35	24.65	88.66	11.34	7.86	53.70	22.95	1667.54	213.37	1880.91	0.02252	0.007369	651.01	1718.60	2.40	2.64
3	336.60	2.08	88.01	11.99	94.94	5.06	79.55	20.45	90.87	9.13	7.03	54.77	23.42	1529.14	153.71	1682.85	0.02065	0.005309	584.93	1187.49	1.89	2.03
1	338.75	3.13	86.89	13.11	94.43	5.57	75.52	24.48	88.75	11.25	4.68	60.14	25.78	994.08	126.01	1120.10	0.01343	0.004352	354.09	850.09	2.15	2.40
2	335.85	3.10	88.01	11.99	94.94	5.06	75.24	24.76	88.60	11.40	5.77	53.00	22.64	1222.00	157.26	1379.26	0.01650	0.005431	491.01	1339.89	2.42	2.73
3	337.05	2.99	88.01	11.99	94.94	5.06	82.32	17.68	92.25	7.75	7.72	55.86	23.90	1703.17	143.05	1846.22	0.02300	0.004941	649.29	1100.12	1.58	1.69
1	336.10	3.88	88.01	11.99	94.94	5.06	68.02	31.98	84.47	15.53	3.69	53.58	22.89	745.39	137.06	882.44	0.01007	0.004734	298.07	1261.80	3.45	4.23
2	338.30	3.88	86.89	13.11	94.43	5.57	78.75	21.25	90.46	9.54	6.45	58.98	25.27	1395.23	147.19	1542.42	0.01884	0.005084	514.37	1024.16	1.79	1.99
3	336.55	4.10	88.01	11.99	94.94	5.06	80.60	19.40	91.40	8.60	6.34	54.65	23.36	1386.89	130.58	1517.46	0.01873	0.004510	551.05	1078.27	1.77	1.96
1	334.90	4.79	88.01	11.99	94.94	5.06	70.64	29.36	86.02	13.98	4.26	50.82	21.68	877.51	142.61	1020.12	0.01185	0.004926	377.78	1457.79	3.05	3.86
2	337.10	5.05	88.01	11.99	94.94	5.06	72.70	27.30	87.20	12.80	4.79	55.98	23.95	999.17	146.69	1145.86	0.01349	0.005067	389.99	1310.95	2.76	3.36
3	338.15	5.20	88.01	11.99	94.94	5.06	73.16	26.84	87.46	12.54	2.54	58.60	25.10	531.26	76.20	607.46	0.007175	0.002632	197.96	643.99	2.69	3.25

Table B.2. Data for experiments of varying feed temperatures (328 – 338 K).

Run	T_f (K)	p_l (kPa)	$X_{io}{}^{L}$ (mol%)		x_i (wt.%)		Y_{il} (mol%)		y_i (wt.%)		$m_{i,j}$ (g)	$p_{i_{sat}}$ (kPa)		J_i (g.m^{-2}h^{-1})			j_i (cm^3(STP).cm^{-2}s^{-1})		$\frac{P_i{}^{G}}{L}$ (gpu)		α_{ij}	β_{ij}
			ethanol	water	ethanol	water	ethanol	water	ethanol	water	permeate mixture	ethanol	water	ethanol	water	total	ethanol	water	ethanol	water		
1	329.45	2.15	87.86	12.14	94.87	5.13	62.34	37.66	80.89	19.11	2.15	39.74	16.83	238.54	56.34	294.88	0.003222	0.001946	126.49	677.40	4.37	5.36
2	330.10	2.07	87.86	12.14	94.87	5.13	71.08	28.92	86.27	13.73	2.07	40.94	17.35	423.00	67.31	490.31	0.005713	0.002325	218.27	740.41	2.94	3.39
3	330.50	2.11	87.86	12.14	94.87	5.13	75.48	24.52	88.73	11.27	2.11	41.69	17.68	526.03	66.84	592.87	0.007105	0.002308	267.23	706.20	2.35	2.64
1	333.25	2.19	87.86	12.14	94.87	5.13	73.82	26.18	87.82	12.18	2.19	47.22	20.10	988.80	137.13	1125.93	0.01335	0.004736	441.52	1271.17	2.57	2.88
2	334.10	2.05	87.86	12.14	94.87	5.13	75.83	24.17	88.92	11.08	2.05	49.05	20.90	1688.80	210.48	1899.28	0.02281	0.007270	723.78	1840.09	2.31	2.54
3	332.10	2.03	87.86	12.14	94.87	5.13	75.68	24.32	88.84	11.16	2.03	44.84	19.06	1828.94	229.86	2058.80	0.02470	0.007939	859.98	2223.25	2.33	2.59
1	339.10	2.11	86.89	13.11	94.43	5.57	77.77	22.23	89.95	10.05	2.11	61.05	26.18	1311.28	146.59	1457.87	0.01771	0.005063	453.35	932.01	1.90	2.06
2	336.15	2.19	87.86	12.14	94.87	5.13	75.35	24.65	88.66	11.34	2.19	53.70	22.95	1667.54	213.37	1880.91	0.02252	0.007369	652.01	1698.15	2.37	2.60
3	336.60	2.08	87.86	12.14	94.87	5.13	79.55	20.45	90.87	9.13	2.08	54.77	23.42	1529.14	153.71	1682.85	0.02065	0.005309	585.83	1173.66	1.86	2.00

Table B.3. Data for experiments of varying feed compositions (95 – 98 wt.% ethanol).

Run	T_f (K)	p_l (kPa)	$X_{io}{}^{L}$ (mol%)		x_i (wt.%)		Y_{il} (mol%)		y_i (wt.%)		$m_{i,j}$ (g)	$p_{i_{sat}}$ (kPa)		J_i (g.m^{-2}h^{-1})			j_i (cm^3(STP).cm^{-2}s^{-1})		$\frac{P_i{}^{G}}{L}$ (gpu)		α_{ij}	β_{ij}
			ethanol	water	ethanol	water	ethanol	water	ethanol	water	ethanol	ethanol	water	ethanol	water	total	ethanol	water	ethanol	water		
1	337.80	2.20	95.67	4.33	98.26	1.74	91.10	8.9	96.32	3.68	2.20	57.72	24.71	685.05	26.17	711.22	0.009252	0.0009040	231.07	493.65	2.16	2.14
2	337.40	2.20	95.67	4.33	98.26	1.74	91.36	8.64	96.43	3.57	2.20	56.72	24.27	1303.51	48.24	1351.75	0.01761	0.001666	447.75	925.42	2.09	2.07
3	340.35	2.11	96.06	3.94	98.42	1.58	89.66	10.34	95.68	4.32	2.10	64.42	27.67	561.55	25.34	586.89	0.007584	0.0008751	168.00	469.55	2.81	2.79
1	338.15	1.94	92.93	7.07	97.11	2.89	84.07	15.93	93.10	6.90	1.94	58.60	25.10	606.42	44.94	651.36	0.008190	0.001552	205.59	524.03	2.49	2.55
2	337.80	2.11	92.93	7.07	97.11	2.89	88.22	11.78	95.04	4.96	2.11	57.72	24.71	1170.71	61.16	1231.87	0.015812	0.002112	404.97	714.23	1.75	1.76
3	339.20	2.10	93.85	6.15	97.50	2.50	80.76	19.24	91.48	8.52	2.10	61.32	26.30	180.77	16.84	197.61	0.002441	0.0005815	58.01	220.72	3.63	3.80
1	338.75	2.07	90.24	9.76	95.94	4.06	74.44	25.56	88.16	11.84	2.07	60.14	25.78	349.21	46.89	396.10	0.004716	0.001619	118.30	404.63	3.17	3.42
2	337.55	1.99	90.24	9.76	95.94	4.06	76.71	23.29	89.39	10.61	1.99	57.09	24.44	629.22	74.70	703.92	0.008498	0.002580	224.80	674.97	2.81	3.00
3	339.00	2.17	91.51	8.49	96.50	3.50	79.84	20.16	91.01	8.99	2.17	60.79	26.07	483.32	47.73	531.05	0.006528	0.001649	160.40	458.82	2.72	2.86
1	340.05	2.22	88.68	11.32	95.24	4.76	71.01	28.99	86.23	13.77	2.22	63.60	27.31	117.51	18.76	136.27	0.001587	0.0006479	38.21	134.14	3.20	3.51
2	338.00	2.04	88.68	11.32	95.24	4.76	72.83	27.17	87.27	12.73	2.04	58.22	24.93	672.84	98.17	771.00	0.009087	0.003391	239.18	764.31	2.92	3.20
3	340.20	2.07	89.06	10.94	95.42	4.58	70.96	29.04	86.21	13.79	2.07	64.01	27.49	534.81	85.57	620.38	0.007223	0.002955	171.75	623.87	3.33	3.63

Table B.4. Data for Arrhenius plot of system energies for varying feed temperatures.

$\frac{1}{T_{ref}} - \frac{1}{T_f}$ (1000 K^{-1})	$\ln \frac{P_i^G}{L}$ ($g.m^{-2}.h^{-1}.kPa^{-1}$)	
	ethanol	water
0.06	1.95	2.69
0.07	2.50	2.78
0.07	2.70	2.73
0.09	3.20	3.32
0.10	3.70	3.69
0.08	3.87	3.88
0.15	3.23	3.01
0.12	3.59	3.61

B.2 Supporting information for the calculation of permeance

Table B.5. Constants for the Antoine Equation[a] for saturation pressures of pure species (Smith et al., 2005).

Component	A_i	B_i	C_i
Ethanol	16.8958	3795.17	230.918
Water	16.3872	3885.70	230.170

[a]Vapour pressure, $p_{i_{sat}}$, is calculated by the standard Antoine equation (Smith et al., 2005)

$$ln(p_{i_{sat}}) = A_i - \frac{B_i}{T + C_i}$$

where $p_{i_{sat}}$ is in kPa and T is in °C.

B.3 Permeate compositions plotted for the experimental study

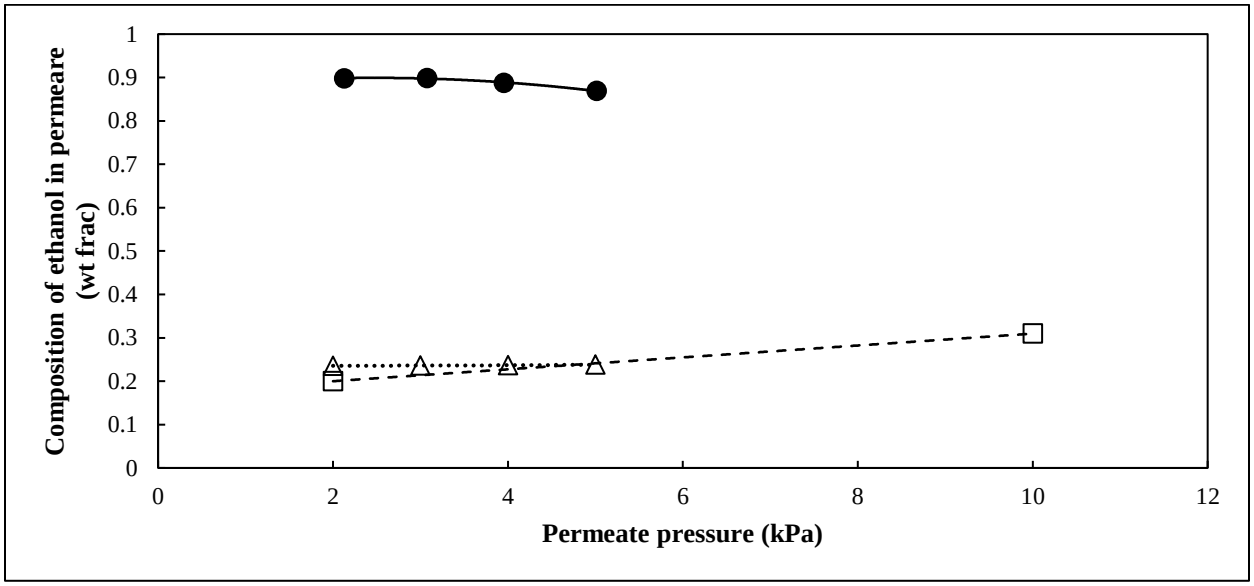

Figure B.1. The effect of permeate pressure on permeate quality for the ethanol (1) + water (2) system based on 5 wt.% feed water and a feed temperature of 338 K. ●, Exp, This work; ∆, Win et al. (2012); □, Wesslein et al. (1990). Lines represent a smooth polynomial fit.

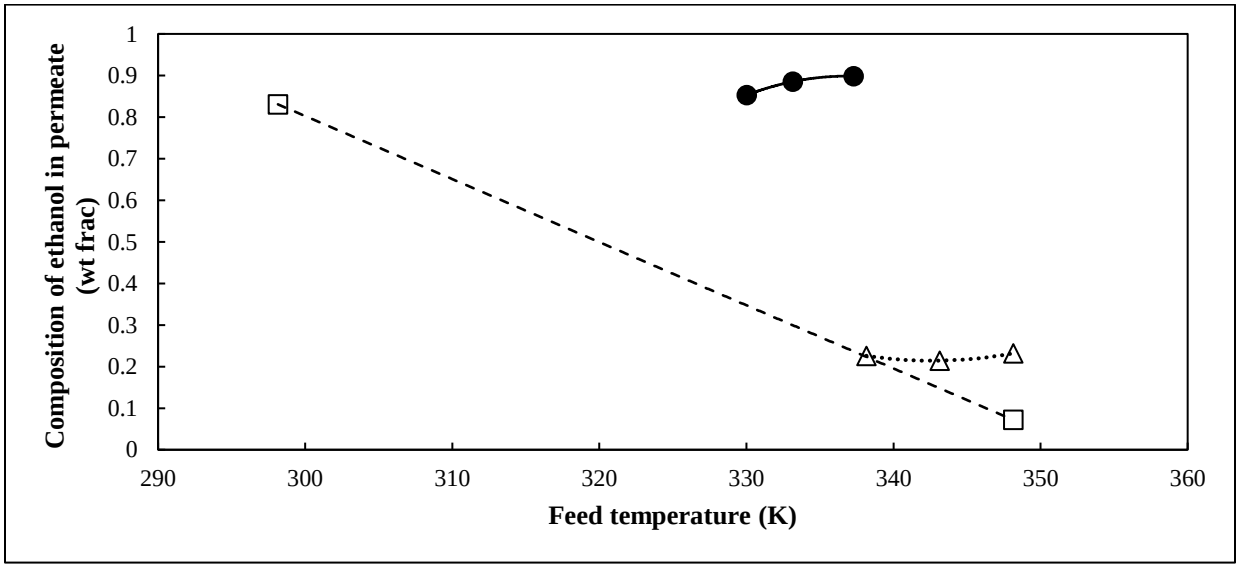

Figure B.2. The effect of feed temperature on permeate quality for the ethanol (1) + water (2) system based on 5 wt.% feed water and a permeate pressure of 2 kPa. ●, Exp, This work; ∆, Win et al. (2012); □, Wesslein et al. (1990). Lines represent a smooth polynomial fit.

B.4 Separation factors plotted for the experimental study

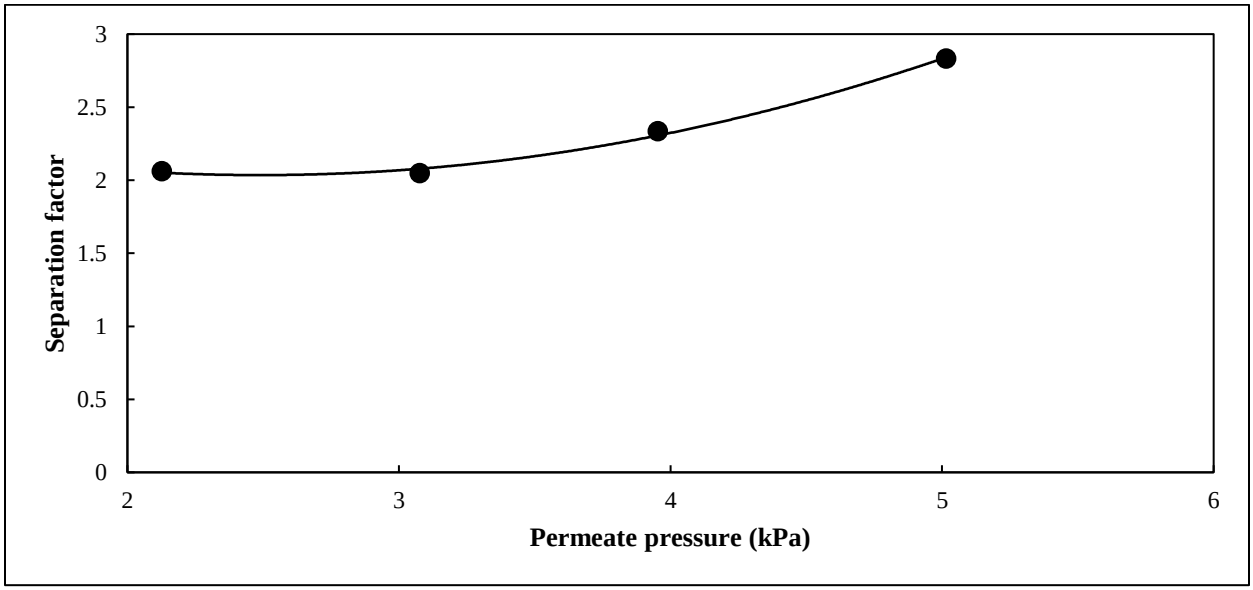

Figure B.3. Separation factor versus permeate pressure for the ethanol (1) + water (2) system based on 5 wt.% feed water and a feed temperature of 338 K. ●, Exp, This work. Lines represent a smooth polynomial fit.

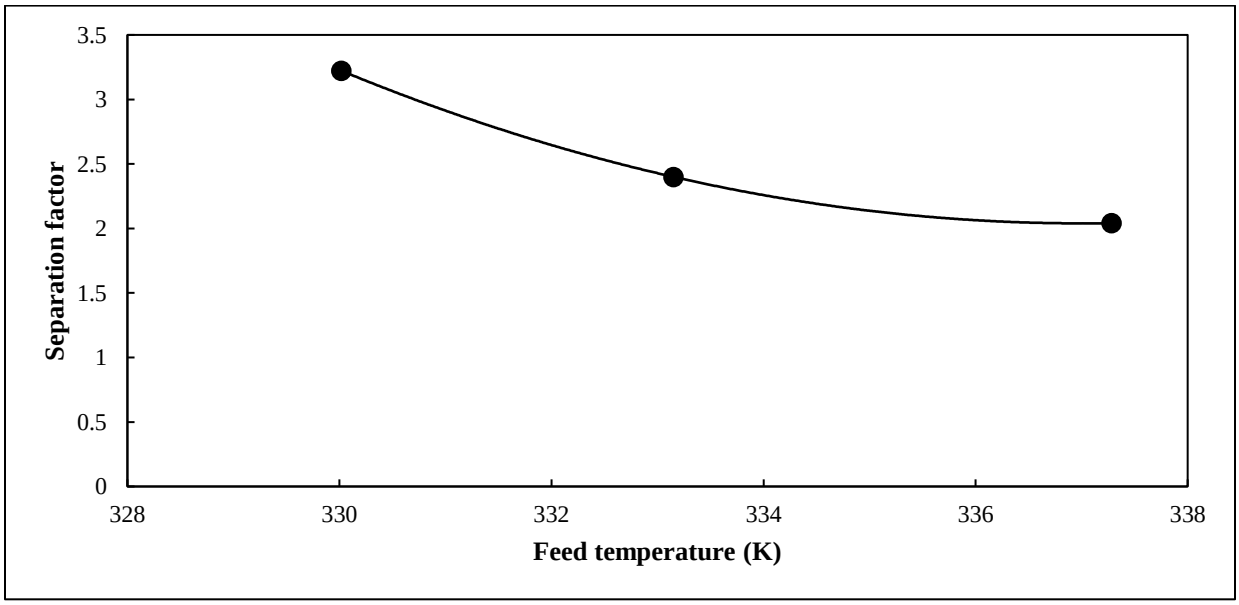

Figure B.4. Separation factor versus feed temperature for the ethanol (1) + water (2) system based on 5 wt.% feed water and a permeate pressure of 2 kPa. ●, Exp, This work. Lines represent a smooth polynomial fit.

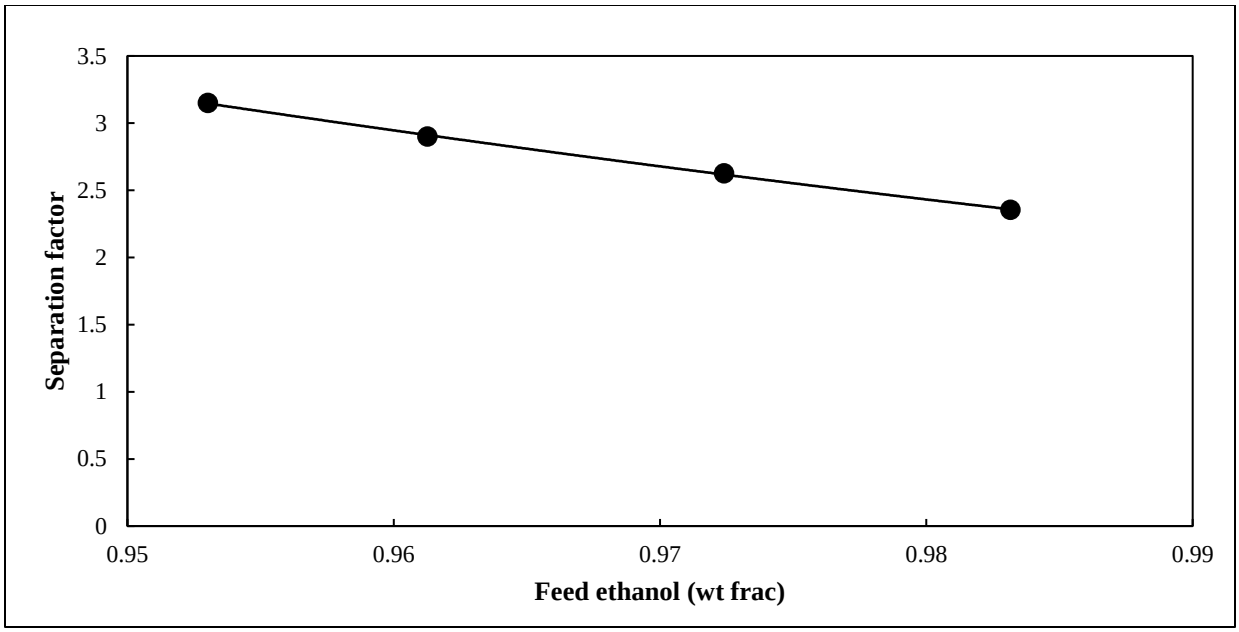

Figure B.5. Separation factor versus feed composition for the ethanol (1) + water (2) system based on a feed temperature of 338 K and permeate pressure of 2 kPa. ●, Exp, This work. Lines represent a smooth polynomial fit.

B.5 Sample calculations for experimental study

Part 1 of this report focused on experiments performed for the ethanol (1) + water (2) system. The measured data, such as permeate weight and composition, was used to calculate pervaporation parameters namely; mass flux, molar flux, permeance, separation factor, and selectivity. Both measured and calculated data for all experiments are presented in Table C.1 to Table C.3. An example of the calculations performed for a sample set is detailed as follows:

Row 1 of Table B.1 corresponds to a feed of 13.11 mol% water. The resulting permeate sample of weight 6.09 g contained 22.23 mol% water. The specie mole fractions for the feed and permeate were found using the calibration curves (Figure 5.5 and Figure 5.7). The mass fractions were calculated using molecular weight.

It must be noted that calculations were performed using Microsoft Excel without rounding intermediate results to avoid compromising the accuracy. The values presented in this report were rounded off to 2 decimal places except in cases where a greater number of significant figures were required. Therefore, slight discrepancies may be noticed.

The feed compositions were calculated as:

$$x_i = \frac{{X_{io}}^L \times M_i}{\sum_{i=1}^{n}\left({X_{io}}^L \times M_i\right)} \tag{B.1}$$

$$x_2 = \frac{0.1311 \times 18.02}{\left[(0.1311 \times 18.02) + \left((1 - 0.1311) \times 46.07\right)\right]} \times 100 = 5.57\ wt.\% \tag{B.2}$$

$$\therefore x_1 = 100 - 5.57 = 94.43\ wt.\% \tag{B.3}$$

Similarly, the permeate compositions were calculated.

$$y_i = \frac{Y_{il} \times M_i}{\sum_{i=1}^{n}(Y_{il} \times M_i)} \tag{B.4}$$

$$y_2 = \frac{0.2223 \times 18.02}{\left[(0.2223 \times 18.02) + \left((1 - 0.2223) \times 46.07\right)\right]} \times 100 = 10.06\ wt.\% \tag{B.5}$$

$$\therefore y_1 = 100 - 10.06 = 89.94\ wt.\% \tag{B.6}$$

The mass flux for both species were calculated using Equation (3.37) as follows:

$$J_1 = \frac{m_1}{At} = \frac{6.09 \times 0.8994}{0.00418 \times 1} = 1311.28\ g.m^{-2}.h^{-1} \tag{B.7}$$

$$J_2 = \frac{m_2}{At} = \frac{6.09 \times 0.1006}{0.00418 \times 1} = 146.59\ g.m^{-2}.h^{-1} \tag{B.8}$$

$$J_T = J_1 + J_2 = 1311.28 + 146.59 = 1457.87\ g.m^{-2}.h^{-1} \tag{B.9}$$

The molar flux, and consequently permeance, for both species were calculated using Equations (3.39) and (3.40), respectively. The activity coefficients were obtained from Aspen Plus® for the specified feed composition. As expected, saturated vapour pressures were calculated using Antoine's Equation together with the component-specific constants presented in Table B.5. All necessary unit conversions were taken into consideration.

$$j_1 = \frac{J_1 {v_1}^G}{M_1} = \frac{1311.28 \times 22.4 \times 100}{46.07 \times 1000 \times 3600} = 0.01771\ cm^3(STP).cm^{-2}.s^{-1} \tag{B.10}$$

$$j_2 = \frac{J_2 {v_2}^G}{M_2} = \frac{146.59 \times 22.4 \times 100}{18.02 \times 1000 \times 3600} = 0.005063\ cm^3(STP).cm^{-2}.s^{-1} \tag{B.11}$$

$$p_{1_{sat}} = exp\left(A_1 - \frac{B_1}{T + C_1}\right) = exp\left(16.8958 - \frac{3795.17}{65.95 + 230.918}\right) \quad \text{(B.12)}$$
$$= 61.05\ kPa$$

$$p_{2_{sat}} = exp\left(A_2 - \frac{B_2}{T + C_2}\right) = exp\left(16.3872 - \frac{3885.70}{65.95 + 230.170}\right) \quad \text{(B.13)}$$
$$= 26.18\ kPa$$

$$\frac{{P_1}^G}{L} = \frac{j_1}{{\gamma_{1o}}^L {X_{1o}}^L p_{1_{sat}} - Y_{1l} p_l} = \frac{0.01771 \times 10^6}{(1.01019 \times 0.8689 \times 45.91) - (0.7777 \times 1.58)} \quad \text{(B.14)}$$
$$= 453.35\ gpu$$

$$\frac{{P_2}^G}{L} = \frac{j_2}{{\gamma_{2o}}^L {X_{2o}}^L p_{2_{sat}} - Y_{2l} p_l} = \frac{0.005063 \times 10^6}{(2.24184 \times 0.1311 \times 19.69) - (0.2223 \times 1.58)} \quad \text{(B.15)}$$
$$= 932.01\ gpu$$

Finally, the computation of dimensionless parameters, namely; separation factor and selectivity, was executed as follows:

$$\alpha_{21} = \frac{{y_2}/{y_1}}{{x_2}/{x_1}} = \frac{{10.06}/{89.94}}{{5.57}/{94.43}} = 1.90 \quad \text{(B.16)}$$

$$\beta_{21} = \frac{{{P_2}^G}/{L}}{{{P_1}^G}/{L}} = \frac{932.01}{453.35} = 2.06 \quad \text{(B.17)}$$

Since a PVA-based membrane is generally employed for dehydration purposes, the separation factor and selectivity were calculated with respect to water.

APPENDIX C

Model Development

C.1 Calculated diffusivities for the alcohol-water systems studied

Table C.1. Diffusivities for ethanol (1) + water (2) system based on data from Luyben and I-Lung (2010).

x_i (wt.%)		y_i (wt.%)		J_T (kg.m^{-2}.h^{-1})	J_i (kg.m^{-2}.h^{-1})	j_i (kmol.m^{-2}.h^{-1})		$c_{io(m)}$ (kmol.m^{-3})		$c_{il(m)}$ (kmol.m^{-3})		D_i (m.h^{-1})	
ethanol	water	ethanol	water	mixture	water	ethanol	water	ethanol	water	ethanol	water	ethanol	water
92.00	8.00	2.25	97.75	0.8951	0.8750	0.00044	0.04861	14.58829	3.24889	0.000004	0.000486	0.000030	0.014965
93.00	7.00	2.50	97.50	0.7897	0.7700	0.00043	0.04278	14.74685	2.84278	0.000005	0.000485	0.000029	0.015050
94.00	6.00	3.00	97.00	0.6753	0.6550	0.00044	0.03639	14.90542	2.43667	0.000006	0.000484	0.000029	0.014937
95.00	5.00	3.25	96.75	0.5685	0.5500	0.00040	0.03056	15.06399	2.03056	0.000006	0.000484	0.000027	0.015051
96.00	4.00	3.50	96.50	0.4560	0.4400	0.00035	0.02444	15.22256	1.62444	0.000007	0.000483	0.000023	0.015052
97.00	3.00	4.00	96.00	0.3438	0.3300	0.00030	0.01833	15.38113	1.21833	0.000008	0.000482	0.000019	0.015054
98.00	2.00	6.25	93.75	0.2400	0.2250	0.00033	0.01250	15.53970	0.81222	0.000012	0.000478	0.000021	0.015399
99.00	1.00	12.00	88.00	0.1193	0.1050	0.00031	0.00583	15.69826	0.40611	0.000025	0.000465	0.000020	0.014380
100.00	0.00	78.00	22.00	0.0000	0.0000	0.00000	0.00000	15.85683	0.00000	0.000285	0.000206	0.000000	0.000000

Table C.2. Diffusivities for propan-1-ol (1) + water (2) system based on data from Will and Lichtenthaler (1992).

x_i (wt.%)		y_i (wt.%)		J_T (kg.m^{-2}.h^{-1})	J_i (kg.m^{-2}.h^{-1})	j_i (kmol.m^{-2}.h^{-1})		$c_{io(m)}$ (kmol.m^{-3})		$c_{il(m)}$ (kmol.m^{-3})		D_i (m.h^{-1})	
propan-1-ol	**water**	**propan-1-ol**	**water**	**mixture**	**water**	**propan-1-ol**	**water**	**propan-1-ol**	**water**	**propan-1-ol**	**water**	**propan-1-ol**	**water**
0.00	100.00	0.00	100.00	8.5000	8.5000	0.00000	0.47182	0.00000	41.00741	0.000000	0.001037	#DIV/0!	0.011506
8.75	91.25	8.57	91.43	8.3375	7.6229	0.01189	0.42313	1.07565	37.41926	0.000028	0.001008	0.011056	0.011308
19.05	80.95	11.84	88.16	7.8523	6.9224	0.01547	0.38425	2.34155	33.19648	0.000040	0.000997	0.006608	0.011575
29.78	70.22	12.11	87.89	7.0568	6.2026	0.01421	0.34430	3.66063	28.79632	0.000041	0.000996	0.003883	0.011957
38.98	61.02	11.84	88.16	6.4048	5.6463	0.01262	0.31342	4.79154	25.02384	0.000040	0.000997	0.002634	0.012525
49.05	50.95	10.92	89.08	5.3370	4.7541	0.00970	0.26389	6.02950	20.89425	0.000037	0.001000	0.001609	0.012631
60.81	39.19	8.10	91.90	4.1667	3.8294	0.00561	0.21256	7.47596	16.06918	0.000027	0.001010	0.000751	0.013229
72.05	27.95	6.28	93.72	2.2955	2.1513	0.00240	0.11942	8.85666	11.46344	0.000020	0.001016	0.000271	0.010418
80.91	19.09	4.55	95.45	0.8636	0.8244	0.00065	0.04576	9.94629	7.82869	0.000015	0.001022	0.000066	0.005846
89.89	10.11	12.89	87.11	0.3409	0.2969	0.00073	0.01648	11.04988	4.14734	0.000044	0.000993	0.000066	0.003975
93.70	6.30	21.84	78.16	0.2386	0.1865	0.00087	0.01035	11.51816	2.58525	0.000080	0.000957	0.000075	0.004006
96.74	3.26	78.05	21.95	0.1364	0.0299	0.00177	0.00166	11.89292	1.33513	0.000535	0.000502	0.000149	0.001245
100.00	0.00	100.00	0.00	0.0000	0.0000	0.00000	0.00000	12.29316	0.00000	0.001037	0.000000	0.000000	#DIV/0!

Table C.3. Diffusivities for propan-2-ol (1) + water (2) system based on data from Will and Lichtenthaler (1992).

x_i (wt.%)		y_i (wt.%)		J_T (kg.m^{-2}.h^{-1})	J_i (kg.m^{-2}.h^{-1})	j_i (kmol.m^{-2}.h^{-1})		$c_{io(m)}$ (kmol.m^{-3})		$c_{il(m)}$ (kmol.m^{-3})		D_i (m.h^{-1})	
propan-2-ol	water	propan-2-ol	water	mixture	water	propan-2-ol	water	propan-2-ol	water	propan-2-ol	water	propan-2-ol	water
0.00	100.00	0.00	100.00	3.8333	3.8333	0.00000	0.21278	0.00000	40.13926	0.000000	0.001084	#DIV/0!	0.005301
8.95	91.05	8.13	91.88	3.6944	3.3943	0.00499	0.18841	1.07663	36.54785	0.000028	0.001056	0.004640	0.005155
20.00	80.00	11.09	88.91	3.4474	3.0649	0.00636	0.17013	2.40658	32.11141	0.000039	0.001044	0.002644	0.005298
33.89	66.11	12.03	87.97	2.7868	2.4516	0.00558	0.13608	4.07782	26.53651	0.000043	0.001041	0.001368	0.005128
48.06	51.94	11.25	88.75	1.9474	1.7283	0.00365	0.09593	5.78248	20.85012	0.000040	0.001044	0.000630	0.004601
60.00	40.00	8.13	91.88	1.3750	1.2633	0.00186	0.07012	7.21974	16.05570	0.000028	0.001056	0.000257	0.004368
74.17	25.83	6.09	93.91	0.6553	0.6153	0.00066	0.03416	8.92441	10.36931	0.000021	0.001063	0.000074	0.003294
87.36	12.64	6.09	93.91	0.2895	0.2718	0.00029	0.01509	10.51208	5.07316	0.000021	0.001063	0.000028	0.002975
93.95	6.05	27.03	72.97	0.8636	0.6302	0.00388	0.03498	11.30460	2.42948	0.000108	0.000975	0.000344	0.014404
100.00	0.00	100.00	0.00	0.0000	0.0000	0.00000	0.00000	12.03291	0.00000	0.001084	0.000000	0.000000	#DIV/0!

C.2 Sample calculations for diffusivities

The process of developing temperature-dependent diffusion equations for the model script was described in Chapter 6. An example of the calculations performed for a sample set is detailed as follows:

Row 1 of Table C.1 corresponds to the ethanol (1) + water (2) system with a feed of 8 wt.% water, a permeate with 97.75 wt.% water and a water flux of 0.875 kg.m^{-2}h^{-1}. The total flux, specie molar flux, concentration of the retentate and permeate as well as the diffusion coefficients were calculated using Microsoft Excel. Intermediate results were not rounded to prevent inaccuracies. The values reported in this section were rounded to 4 significant figures. Therefore, slight discrepancies may be observed.

$$J_T = \frac{J_2}{y_2} = \frac{0.875}{0.9775} = 0.8951\ kg.m^{-2}.h^{-1} \tag{C.1}$$

$$Y_i = \frac{{}^{m_i}/_{M_i}}{\sum_{i=1}^{n}\left({}^{m_i}/_{M_i}\right)} \tag{C.2}$$

$$Y_1 = \frac{{}^{0.0225}/_{46.07}}{\left[\left({}^{0.0225}/_{46.07}\right)+\left({}^{0.9775}/_{18.02}\right)\right]} \times 100 = 0.8907\ mol\% \tag{C.3}$$

$$\therefore Y_2 = 100 - 0.8907 = 99.11\ mol\% \tag{C.4}$$

The specie molar flux was calculated as follows:

$$j_2 = \frac{J_2}{M_2} = \frac{0.875}{18.02} = 0.04861\ kmol.m^{-2}.h^{-1} \tag{C.5}$$

$$j_1 = j_2 \times \frac{Y_1}{Y_2} = 0.04861 \times \frac{0.008907}{0.9911} = 0.0004369\ kmol.m^{-2}.h^{-1} \tag{C.6}$$

The concentration of the retentate was calculated using Equation (3.48.

$$c_{1o(m)} = \frac{\rho_l\, x_1}{M_1} = \frac{731 \times 0.9200}{46.07} = 14.59\ kmol.m^{-3} \tag{C.7}$$

$$c_{2o(m)} = \frac{\rho_l\, x_2}{M_2} = \frac{731 \times 0.0800}{18.02} = 3.249\ kmol.m^{-3} \tag{C.8}$$

The concentration of the permeate was calculated using Equation (3.49.

$$c_{1l(m)} = \frac{p_{1l}\, Y_1}{RT_p} = \frac{0.008907 \times 0.015}{0.08206 \times 373} = 4.365 \times 10^{-6}\ kmol.m^{-3} \quad \text{(C.9)}$$

$$c_{2l(m)} = \frac{p_{2l}\, Y_2}{RT_p} = \frac{0.9911 \times 0.015}{0.08206 \times 373} = 4.857 \times 10^{-4}\ kmol.m^{-3} \quad \text{(C.10)}$$

Finally, specie diffusivities were calculated using a rearranged form of Equation (3.21 as follows:

$$D_1 = \frac{j_1}{\left(c_{1o(m)} - c_{1l(m)}\right)} = \frac{0.0004369}{(14.59 - 4.365 \times 10^{-6})} = 2.995 \times 10^{-5}\ m.h^{-1} \quad \text{(C.11)}$$

$$D_2 = \frac{j_2}{\left(c_{2o(m)} - c_{2l(m)}\right)} = \frac{0.04861}{\left(3.249 - 4.857 \times 10^{-4}\right)} = 1.497 \times 10^{-2}\ m.h^{-1} \quad \text{(C.12)}$$

C.3 Method of weighting the area near the azeotrope

Diffusivities were calculated for the feed composition range reported in the literature sources used to model the various systems. This was performed using the equations outlined in Chapter 3. Specie diffusivities were analysed for the range which displayed minor deviations. Since the models were developed for the dehydration of alcohol-water systems, a fairly constant water diffusivity was of particular importance. Tabulated diffusivities are presented in Section C.1 with highlighted values indicating the composition range selected to calculate average diffusivities for both the alcohol (ethanol, propan-1-ol and propan-2-ol) and water.

Two factors governed the chosen feed range for average diffusivities considered:

i. The azeotrope composition must be included.
ii. Systems exhibiting a non-linear trend in literature for permeate composition versus feed composition (as observed with the C3 alcohol systems) must be described with a narrow range to avoid large deviations from experimental data points when running the model on Aspen Custom Modeler®.

Literature sources state the feed temperature utilized for pervaporation experiments performed. Therefore, the average values calculated for the specie diffusivities described the systems at these reported temperatures. According to Sander and Soukup (1988), flux doubles with a 10 K increase in temperature. Since flux is directly proportional to diffusivity (Equation (3.21)), the following temperature-dependent diffusivities were obtained:

Table C.4. Temperature-dependent diffusivities for ethanol (1) + water (2) system at 373 K using data of Luyben and I-Lung (2010).

T (K)	$\frac{1}{T}$ (K^{-1})	D_i ($m.h^{-1}$)	
		ethanol	water
373	0.00268	0.000021992	0.013320985
368	0.00272	0.000016497	0.009992405
363	0.00275	0.000011002	0.006663825

Table C.5. Temperature-dependent diffusivities for propan-1-ol (1) + water (2) system at 348 K using data of Will and Lichtenthaler (1992).

T (K)	$\frac{1}{T}$ (K^{-1})	D_i ($m.h^{-1}$)	
		propan-1-ol	water
348	0.00287	0.000510793	0.011823425
353	0.00283	0.000765933	0.017729226
358	0.00279	0.001021074	0.023635027

Table C.6. Temperature-dependent diffusivities for propan-2-ol (1) + water (2) system at 333 K using data of Will and Lichtenthaler (1992).

T (K)	$\frac{1}{T}$ (K^{-1})	D_i ($m.h^{-1}$)	
		propan-2-ol	water
333	0.00300	0.000034904	0.002365
338	0.00296	0.000052338	0.003547
343	0.00292	0.000069773	0.004728

Row 1 of Table C.4 to Table C.6 represents the average of the highlighted values for each of the three systems studied. Row 3 represents a 10 K rise in temperature from initial feed temperatures, and a doubling in the alcohol and water diffusivities. Row 2 is an additional intermediate value, resembling a midpoint, to create a pronounced exponential trend.

A plot of specie diffusivity versus the temperature inverse generated a trendline. The trendline equations represented the alcohol and water diffusivities (D_1 and D_2) reported as Equation (7.1) to (7.8). Diffusivity equations were implemented into the model script of ACM. The permeate composition for varying feed alcohol content was plotted as seen in Figure 7.1, Figure 7.7 and Figure 7.13. The plotted data indicated if the model described the literature data well and if diffusion equations required further improvement.

C.4 Validation of model calculations against manual calculations

The calculation procedure of the model in Aspen Custom Modeler® was validated by comparing the result to manual calculations performed on Microsoft Excel. The purpose of this exercise was to ensure all variables were linked, and the mathematical relations of Chapter 3 were set up correctly within ACM. At this early stage of the user model development, the input values were not of particular importance as much as the ability of the model to perform rigorous calculation correctly. Therefore, arbitrary values were initially assigned for the input variables. The model was later correctly specified, according to the available literature, to accurately depict the separation performance.

An initial guess was required for the permeate composition (Y_i). Thereafter, the concentration of the permeate ($c_{il(m)}$) as well as the specie and total molar flux (j_i, j_T) were calculated. These parameters were calculated similar to Equations (C.9 to (C.12 of Section C.2, with the use of the specie diffusivities obtained from the temperature-dependent diffusion expressions. The quotient of the specie and total molar flux was then compared to the initial guess and the procedure repeated until convergence was reached. Although the iterations cannot be viewed on ACM, Table C.7 illustrates the manner in which the iterations were executed using the manual calculations. The highlighted values indicate convergence.

The computation procedure was validated for an ethanol (1) + water (2) system using the developed diffusion equations of Chapter 7. An arbitrary feed flowrate of 10 kmol.hr^{-1} consisting of 10 mol% feed water was assumed. A feed temperature of 373 K and a permeate pressure of 1.5 kPa was used. In addition, an effective membrane area of 0.004 m^2 was specified. An initial guess for the permeate composition was set at 95 mol% water. The calculated permeate composition was used as the estimate for the next iteration.

Table C.7. Iteration for the permeate composition using manual calculations.

Trial	Y_i (Initial guess)		$c_{il(m)}$ (kmol.m^{-3})		j_i[a] (kmol.h^{-1})		j_T[b] (kmol.h^{-1})	$Y_i = \frac{j_i}{j_T} \times 100$ (Calculated)	
	ethanol	water	ethanol	water	ethanol	water	total	ethanol	water
1	5	95	2.45031E-05	4.65559E-04	1.45773E-06	9.24606E-05	9.39184E-05	1.5521271	98.4478729
2	1.5521271	98.4478729	7.60638E-06	4.82455E-04	1.45773E-06	9.24597E-05	9.39174E-05	1.5521441	98.4478559
3	1.5521441	98.4478559	7.60647E-06	4.82455E-04	1.45773E-06	9.24597E-05	9.39174E-05	1.5521441	98.4478559

[a, b]Flux is multiplied by area to provide component and total flowrates in the permeate stream.

C.5 Modelled data for the various alcohol-water systems

Table C.8. Modelled data for the ethanol (1) + water (2) system for varying feed compositions based on (Luyben and I-Lung, 2010).

x_i (wt.%)		y_i (wt.%)		J_i ($g.m^{-2}h^{-1}$)		
ethanol	**water**	**ethanol**	**water**	**ethanol**	**water**	**total**
95.84	4.16	3.88	96.12	16.62	412.13	428.74
96.28	3.72	4.33	95.67	16.69	368.51	385.21
96.71	3.29	4.90	95.10	16.77	325.46	342.23
97.14	2.86	5.62	94.38	16.84	282.96	299.80
97.56	2.44	6.56	93.44	16.92	240.99	257.90
97.98	2.02	7.85	92.15	16.99	199.54	216.53
98.40	1.60	9.71	90.29	17.06	158.62	175.68
98.81	1.20	12.66	87.34	17.13	118.20	135.33
99.21	0.79	18.02	81.98	17.20	78.28	95.48
99.61	0.39	30.77	69.23	17.27	38.85	56.12
1.00	0	1.00	1.13E-15	17.34	1.96E-14	17.34

Table C.9. Modelled data for the ethanol (1) + water (2) system for varying feed temperatures based on (Luyben and I-Lung, 2010).

T_f (K)	y_i (wt.%)		J_i ($g.m^{-2}h^{-1}$)		
	ethanol	**water**	**ethanol**	**water**	**total**
323	3.875670	96.124330	0.336999	8.358246	8.695245
328	3.875659	96.124341	0.525018	13.021519	13.546537
333	3.875647	96.124353	0.807094	20.017657	20.824751
338	3.875638	96.124362	1.225028	30.383385	31.608413
343	3.875633	96.124367	1.836881	45.558758	47.395640
348	3.875635	96.124365	2.722433	67.522401	70.244835
353	3.875645	96.124355	3.990149	98.964303	102.954452
358	3.875666	96.124334	5.786010	143.504722	149.290732
363	3.875703	96.124297	8.304602	205.968859	214.273461

368	3.875760	96.124240	11.802901	292.728382	304.531283
373	3.875844	96.124156	16.617277	412.122288	428.739565

Table C.10. Modelled data for the ethanol (1) + water (2) system for varying permeate pressures based on (Luyben and I-Lung, 2010).

p_l (kPa)	y_i (wt.%)		J_i (g.m^{-2}h^{-1})		
	ethanol	water	ethanol	water	total
0.100	3.874851	96.125149	16.617394	412.235079	428.852473
1.109	3.875566	96.124434	16.617389	412.155823	428.773213
2.118	3.876281	96.123719	16.617384	412.076569	428.693953
3.127	3.876997	96.123003	16.617379	411.997314	428.614693
4.136	3.877713	96.122287	16.617374	411.918059	428.535433
5.145	3.878429	96.121571	16.617369	411.838806	428.456175
6.155	3.879145	96.120855	16.617363	411.759554	428.376918
7.164	3.879862	96.120138	16.617358	411.680302	428.297660
8.173	3.880579	96.119421	16.617353	411.601049	428.218403
9.182	3.881296	96.118704	16.617348	411.521799	428.139148
10.191	3.882014	96.117986	16.617343	411.442547	428.059890

Table C.11. Modelled data for the propan-1-ol (1) + water (2) system for varying feed compositions based on (Will and Lichtenthaler, 1992).

x_i (wt.%)		y_i (wt.%)		J_i (g.m^{-2}h^{-1})		
propan-1-ol	water	propan-1-ol	water	propan-1-ol	water	total
61.00	39.00	1.40	98.60	127.21	3415.85	3543.06
64.24	35.76	1.61	98.39	123.39	3132.73	3256.13
68.98	31.02	1.98	98.02	118.09	2722.79	2840.87
73.19	26.81	2.42	97.58	113.26	2356.34	2469.60
76.94	23.06	2.94	97.06	108.94	2028.59	2137.53
80.30	19.70	3.57	96.43	105.05	1733.75	1838.80

83.34	16.66	4.35	95.65	101.52	1467.14	1568.66
86.10	13.90	5.33	94.67	98.32	1224.90	1323.22
88.62	11.38	6.60	93.40	95.39	1003.86	1099.25
90.92	09.08	8.33	91.67	92.71	801.37	894.08
93.03	6.97	10.81	89.19	90.26	615.26	705.52
94.98	05.02	14.66	85.34	87.98	443.51	531.49
96.78	03.22	21.43	78.57	85.87	284.60	370.47
98.45	01.55	36.55	63.45	83.91	137.14	221.05
1.00	0.00	1.00	0.00	82.082	0.00	82.08

Table C.12. Modelled data for the propan-1-ol (1) + water (2) system for varying feed temperatures based on (Will and Lichtenthaler, 1992).

T_f (K)	y_i (wt.%)		J_i (g.m^{-2}h^{-1})		
	propan-1-ol	**water**	**propan-1-ol**	**water**	**total**
304	2.419136	97.580864	4.128206	85.89717	68.18907
307	2.419145	97.580855	5.420863	112.7937	90.02538
310	2.419156	97.580844	7.081042	147.3372	118.2146
313	2.419170	97.580830	9.202595	191.4801	154.4182
316	2.419188	97.580812	11.90057	247.6161	200.6827
319	2.419212	97.580788	15.31536	318.6656	259.5167
322	2.419243	97.580757	19.61746	408.1757	333.981
325	2.419281	97.580719	25.01306	520.435	427.7932
328	2.419329	97.580671	31.75036	660.6059	545.4481
331	2.419390	97.580610	40.12686	834.8752	692.3563
334	2.419465	97.580535	50.49758	1050.625	875.0021
337	2.419559	97.580441	63.2844	1316.627	1101.123
340	2.419674	97.580326	78.98645	1643.255	1379.912
343	2.419816	97.580184	98.19177	2042.729	1722.242
346	2.419989	97.580011	113.2797	2356.486	2140.92
348	2.420224	97.579776	121.5901	2529.375	2469.766

349	2.420201	97.579799	149.9869	3119.919	2650.965
352	2.420458	97.579542	184.3186	3833.796	3269.906
355	2.420769	97.579231	225.6691	4693.487	4018.115
358	2.421143	97.578857	275.287	5724.871	4919.157
361	2.421593	97.578407	334.604	6957.591	6000.158
364	2.422131	97.577869	405.2533	8425.433	7292.195
367	2.422772	97.577228	489.0891	10166.7	8830.686
370	2.423532	97.576468	588.205	12224.56	10655.79
373	2.424432	97.575568	4.128206	85.89717	12812.77

Table C.13. Modelled data for the propan-1-ol (1) + water (2) system for varying permeate pressures based on (Will and Lichtenthaler, 1992).

p_l (kPa)	y_i (wt.%)		J_i (g.m^{-2}h^{-1})		
	propan-1-ol	**water**	**propan-1-ol**	**water**	**total**
0.500	2.420071	97.579929	113.278887	2356.549789	2469.828675
1.505	2.420093	97.579907	113.2783662	2356.527481	2469.805847
2.510	2.420115	97.579885	113.2778454	2356.505173	2469.783018
3.000	2.420123	97.579877	113.2775442	2356.494326	2469.77187
3.515	2.420136	97.579864	113.2773245	2356.482865	2469.76019
4.520	2.420158	97.579842	113.2768037	2356.460558	2469.737361
5.525	2.420180	97.579820	113.2762831	2356.43825	2469.714533
6.530	2.420202	97.579798	113.2757625	2356.415948	2469.69171
7.535	2.420224	97.579776	113.2752416	2356.39364	2469.668882
8.540	2.420245	97.579755	113.274721	2356.371332	2469.646053
9.545	2.420267	97.579733	113.2742001	2356.349024	2469.623225
10.551	2.420289	97.579711	113.2736792	2356.326717	2469.600396

Table C.14. Modelled data for the propan-2-ol (1) + water (2) system for varying feed compositions based on (Will and Lichtenthaler, 1992).

x_i (wt.%)		y_i (wt.%)		J_i ($g.m^{-2}h^{-1}$)		
propan-2-ol	**water**	**propan-2-ol**	**water**	**propan-2-ol**	**water**	**total**
74.00	26.00	1.24	98.76	85.20	959.47	1044.68
86.10	13.90	3.67	97.33	53.73	513.00	566.74
86.62	13.38	3.88	97.22	52.38	493.79	546.17
87.13	12.87	4.00	97.09	51.05	474.90	525.95
87.64	12.36	4.64	96.96	49.74	456.36	506.10
88.13	11.87	5.18	96.82	48.46	438.15	486.60
88.62	11.38	5.93	96.67	47.19	420.26	467.45
89.09	10.91	6.68	96.52	45.95	402.68	448.64
89.56	10.44	7.55	96.35	44.74	385.41	430.15
90.02	9.98	8.73	96.17	43.54	368.44	411.98
90.47	9.53	9.83	95.97	42.36	351.76	394.12
90.92	9.08	11.14	95.76	41.21	335.36	376.57
91.35	8.65	12.46	95.54	40.07	319.24	359.31
91.78	8.22	13.71	95.29	38.95	303.38	342.33
92.20	7.80	15.27	95.03	37.85	287.79	325.64
92.62	7.38	16.96	94.74	36.77	272.46	309.22
93.03	6.97	18.77	94.43	35.70	257.37	293.07
93.43	6.57	20.92	94.08	34.66	242.53	277.18
93.83	6.17	23.30	93.70	33.63	227.92	261.55
94.22	5.78	26.02	93.28	32.61	213.55	246.16
94.60	5.40	28.79	92.81	31.62	199.40	231.01
94.98	5.02	31.71	92.29	30.63	185.47	216.11
95.35	4.65	34.71	91.69	29.67	171.76	201.43
95.71	4.29	37.98	91.02	28.71	158.26	186.98
96.07	3.93	41.26	90.24	27.78	144.97	172.75
96.43	3.57	44.96	89.34	26.85	131.88	158.73
96.78	3.22	48.94	88.28	25.94	118.99	144.93

97.12	2.88	53.53	87.02	25.05	106.29	131.33
97.46	2.54	58.80	85.50	24.17	93.77	117.94
97.79	2.21	65.39	83.61	23.30	81.44	104.74
98.12	1.88	71.77	81.23	22.44	69.29	91.73
98.45	1.55	78.40	78.10	21.59	57.32	78.92
98.77	1.23	84.35	73.85	20.76	45.52	66.28
99.08	0.92	89.70	67.70	19.94	33.89	53.83
99.39	0.61	93.97	58.03	19.13	22.43	41.56
99.70	0.30	97.39	40.61	18.34	11.13	29.46

Table C.15. Modelled data for the propan-2-ol (1) + water (2) system for varying feed temperatures based on (Will and Lichtenthaler, 1992).

T_f (K)	y_i (wt.%)		J_i (g.m^{-2}h^{-1})		
	propan-2-ol	**water**	**propan-2-ol**	**water**	**total**
308	3.326690	96.673310	6.840806928	60.91824318	67.75905011
313	3.326697	96.673303	10.31806339	91.88357907	102.2016425
318	3.326709	96.673291	15.36276302	136.8070533	152.1698163
323	3.326729	96.673271	22.59334003	201.195713	223.789053
328	3.326758	96.673242	32.83786891	292.4232775	325.2611464
333	3.326801	96.673199	47.19339862	420.2583283	467.4517269
338	3.326862	96.673138	67.09861864	597.5110686	664.6096873
343	3.326946	96.673054	94.42196915	840.8173501	935.2393192
348	3.327063	96.672937	131.5674517	1171.579874	1303.147326
353	3.327220	96.672780	181.6004924	1617.087215	1798.687707
358	3.327432	96.672568	248.3962552	2211.831549	2460.227804
363	3.327713	96.672287	336.8127813	2999.045515	3335.858297
368	3.328083	96.671917	452.8912105	4032.477168	4485.368379
373	3.328566	96.671434	604.085116	5378.419452	5982.504568

Table C.16. Modelled data for the propan-2-ol (1) + water (2) system for varying permeate pressures based on (Will and Lichtenthaler, 1992).

p_l (kPa)	y_i (wt.%)		J_i (g.m^{-2}h^{-1})		
	propan-2-ol	water	propan-2-ol	water	total
0.100	3.326582	96.673418	47.19568	420.288	467.4837
1.090	3.326657	96.673343	47.19493	420.2782	467.4731
2.080	3.326731	96.673269	47.19418	420.2683	467.4625
3.000	3.326801	96.673199	47.19348	420.2591	467.4526
3.070	3.326806	96.673194	47.19343	420.2584	467.4518
4.060	3.326880	96.673120	47.19268	420.2485	467.4412
5.050	3.326955	96.673045	47.19193	420.2386	467.4306
6.040	3.327030	96.672970	47.19118	420.2287	467.4199
7.030	3.327104	96.672896	47.19043	420.2189	467.4093

APPENDIX D

Supplementary Model Investigations

D.1 Influence of Membrane Area on Model 1-A FLux

Table D.1. The influence of cell membrane area on water flux for varying feed compositions using Model 1-A based on the data obtained from Luyben and I-Lung (2010).

$x_{ethanol}$ (wt. frac)	J_{water} (g.m^{-2}.h^{-1})	
	$A = 0.004\ m^2$	$A = 0.002\ m^2$
0.9007	964.59	974.00
0.9109	866.06	873.81
0.9209	769.94	776.28
0.9307	676.15	681.18
0.9402	584.59	588.53
0.9494	495.18	498.17
0.9584	407.79	410.02
0.9671	322.52	324.01
0.9756	239.12	240.07
0.9840	157.59	158.11
0.9921	77.87	78.08
1.0000	0.00	0.00

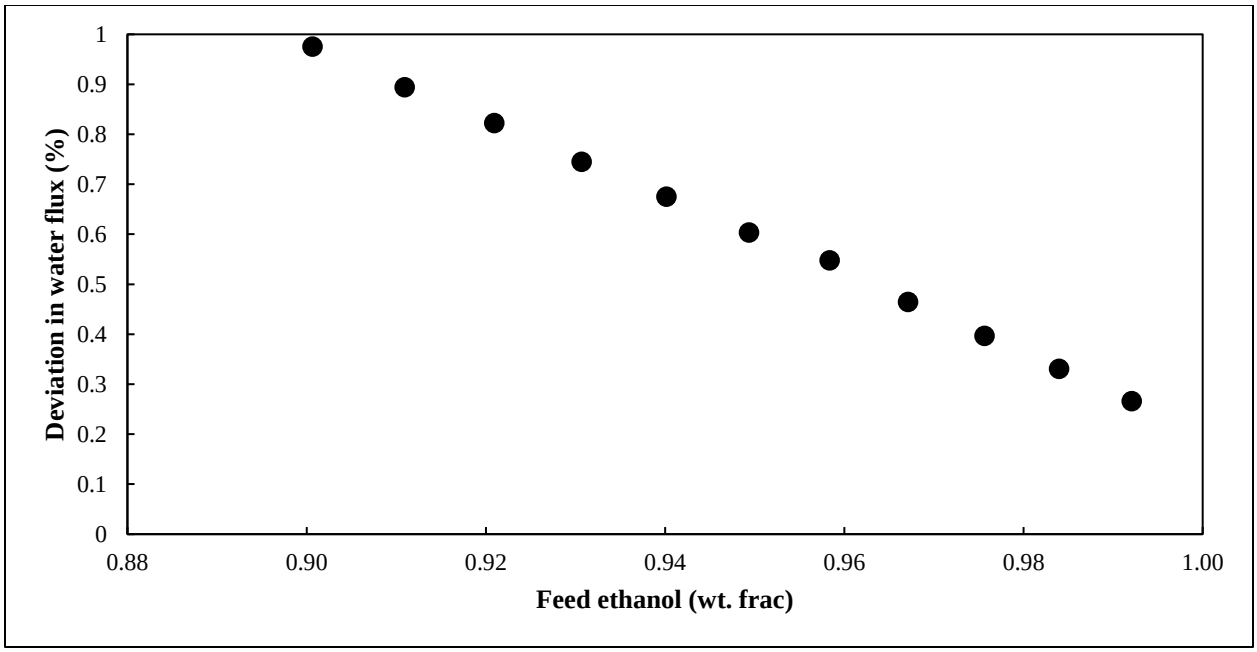

Figure D.1. Deviation in water flux from a membrane area of 0.004 m^2 to 0.002 m^2 for the ethanol (1) + water (2) system based on Luyben and I-Lung (2010).

D.2 Basic calculation of an upscaled propan-2-ol (1) + water (2) system

A basic manual calculation was attempted for the dehydration of an industrial propan-2-ol stream. Case 1 of Figure 7.21 (a) with an interstage heat of 363.15 K and a maximum of 3 cells per module was used as a basis. All calculations were performed using Microsoft Excel. Intermediate results were not rounded to prevent inaccuracies. The values reported in this section were rounded to 4 significant figures. Therefore, slight discrepancies may be observed. A comparison of calculated and simulated data is presented in Table D.3.

The following calculation represents the separation of cell 1 in module 1. A feed of 85 wt.% propan-2-ol with a flowrate of 306.77 kg/h was used along with a constant permeate pressure of 2 kPa as specified in section 7.1. A permeate composition of 3.45 wt.% propan-2-ol was estimated using the composition curve of Figure 7.13.

$$X_{1,P_1} = \frac{{x_{1,P_1}}/{M_1}}{{x_{1,P_1}}/{M_1} + {x_{2,P_1}}/{M_2}} = \frac{{0.03445}/{60.09}}{\left[\left({0.03445}/{60.09}\right) + \left({0.9775}/{18.02}\right)\right]} \times 100 \quad \text{(D.1)}$$

$$= 1.058\ mol\%$$

$$\therefore X_{2,P_1} = 100 - 1.058 = 98.94\ mol\% \tag{D.2}$$

The concentration of the permeate was calculated using Equation (3.49).

$$c_{1l(m)} = \frac{p_l\, X_{1,P_1}}{RT_p} = \frac{0.01974 \times 0.01058}{0.08206 \times 363} = 7.010 \times 10^{-6}\ kmol.m^{-3} \tag{D.3}$$

$$c_{2l(m)} = \frac{p_l\, X_{2,P_1}}{RT_p} = \frac{0.01974 \times 0.9842}{0.08206 \times 363} = 6.554 \times 10^{-4}\ kmol.m^{-3} \tag{D.4}$$

The specie diffusivities for propan-2-ol and water were calculated from the derived Equations (7.7) and (7.8) respectively.

$$D_1 = 7.522\ \times\ 10^5\ e^{\left(-\frac{7917}{T_f}\right)} = 7.522\ \times\ 10^5\ e^{\left(-\frac{7917}{363}\right)} = 2.561\ \times 10^{-4}\ m.h^{-1} \tag{D.5}$$

$$D_2 = 5.097\ \times\ 10^7\ e^{\left(-\frac{7917}{T_f}\right)} = 5.097\ \times\ 10^7\ e^{\left(-\frac{7917}{363}\right)} = 1.735\ \times 10^{-2}\ m.h^{-1} \tag{D.6}$$

It was assumed that the initial retentate composition is equivalent to the feed. The concentration of the retentate was calculated using Equation 3.48.

$$c_{1o(m)} = \frac{\rho_l\, x_{1,R_1}}{M_1} = \frac{723 \times 0.8500}{60.09} = 10.23\ kmol.m^{-3} \tag{D.7}$$

$$c_{2o(m)} = \frac{\rho_l\, x_{2,R_1}}{M_2} = \frac{723 \times 0.1500}{18.02} = 6.021\ kmol.m^{-3} \tag{D.8}$$

Specie molar flux was calculated using an adjusted version of Equation (3.21) as follows:

$$j_1 = D_1\left(c_{1o(m)} - c_{1l(m)}\right) = 2.561\ \times 10^{-4}(10.23 - 7.010 \times 10^{-6}) = 0.002619\ kmol.m^{-2}.h^{-1} \tag{D.9}$$

$$j_2 = D_2\left(c_{2o(m)} - c_{2l(m)}\right) = 1.735\ \times 10^{-2}(6.021 - 6.554 \times 10^{-4}) = 0.1045\ kmol.m^{-2}.h^{-1} \tag{D.10}$$

Specie mass flux was calculated using molecular weight.

$$J_1 = j_1 \times M_1 = 0.002619 \times 60.09 = 0.1574\ kg.m^{-2}.h^{-1} \tag{D.11}$$

$$J_2 = j_2 \times M_2 = 0.1045 \times 18.02 = 1.882\ kg.m^{-2}.h^{-1} \tag{D.12}$$

The permeate flowrate from cell 1 was calculated using a summation of specie mass flux and the membrane area of 5 m^2.

$$P_1 = (J_1 + J_2) \times A = (0.1574 + 1.882) \times 5 = 10.20\ kg.h^{-1} \quad \text{(D.13)}$$

The flowrate of the retentate was calculated using a simple mass balance over cell 1.

$$R_1 = F - P_1 = 306.77 - 10.20 = 296.58\ kg.h^{-1} \quad \text{(D.14)}$$

The composition of the retentate was calculated from a specie mass balance over cell 1.

$$x_{1,R_1} = \frac{x_{1,F}F - x_{1,P}P_1}{R_1} = \frac{(0.85 \times 306.77) - (0.03445 \times 10.20)}{296.58} \times 100 \quad \text{(D.15)}$$

$$= 87.80\ wt.\%$$

$$x_{2,R_1} = 1 - x_{2,R_1} = 1 - 0.8780 = 0.1220\ wt.\% \quad \text{(D.16)}$$

It was assumed that each cell would experience a 10 K loss in temperature during operation. This was estimated using the simulation data which revealed an average temperature drop of 10.88 K. Therefore, the feed temperatures of cell 2 and cell 3 were estimated to be 353.15 K and 343.15 K respectively.

It is important to note that the retentate of a cell becomes the charge fed to the next cell. The manner in which streams are passed from one cell to the next, and between modules is represented in Figure D.2. Since the feed flowrate, composition and temperature for cell 2 is known, the above set of calculations were repeated until cell 11 was reached. A summary of the calculated results is presented in Table D.2. In Case 1, three cells are housed in a module. The feed before each module was reheated to 363.15 K to avoid a significant drop in temperature during separation.

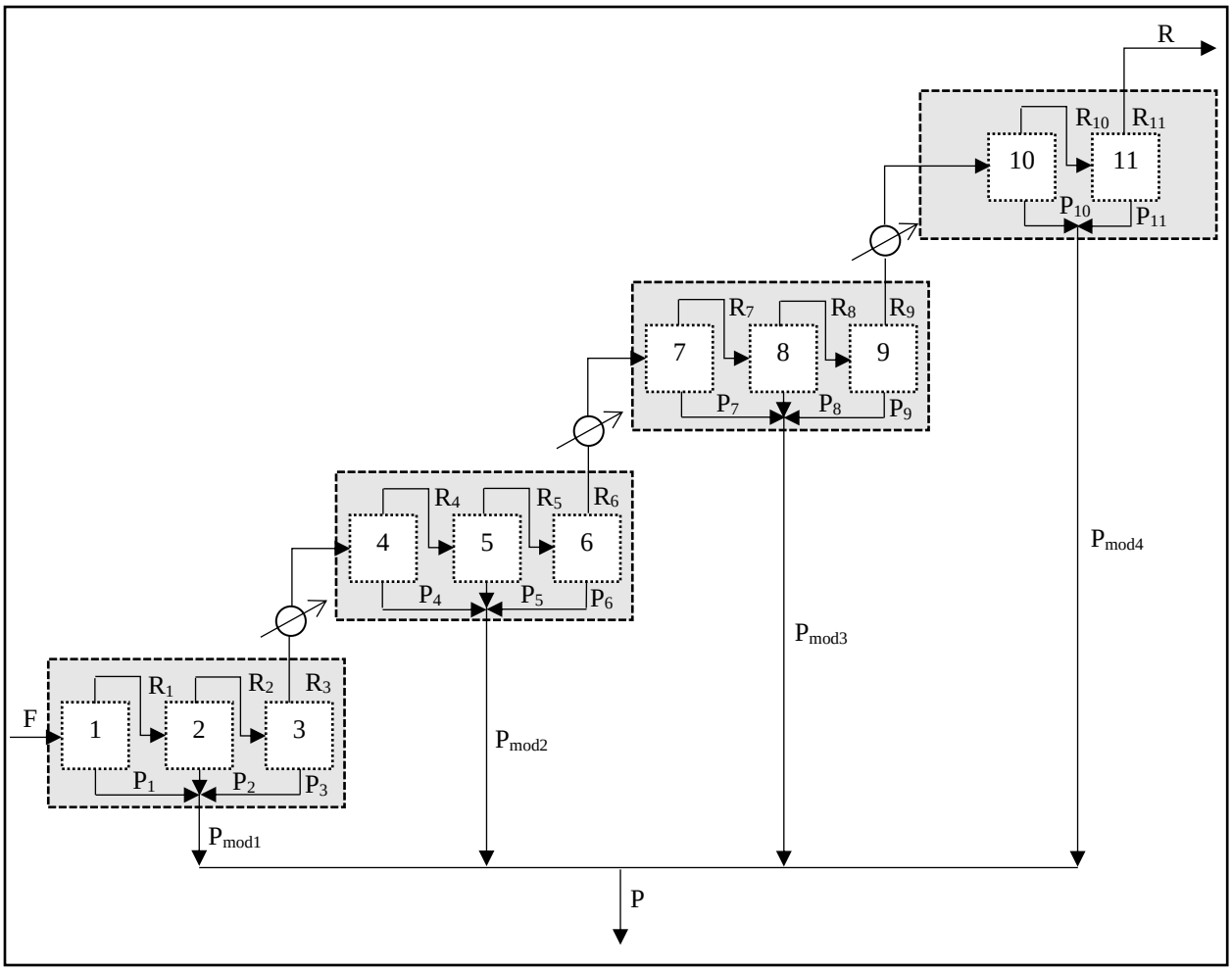

Figure D.2. Detailed schematic of cell and module configuration for Case 1.

The permeate flowrate of each module was calculated as a summation of the permeate streams leaving each cell.

$$P_{mod1} = P_1 + P_2 + P_3 = 10.20 + 4.565 + 2.150 = 16.91\ kg.h^{-1} \tag{D.17}$$

The composition of the permeate stream for each module was calculated using a specie mass summation.

$$\begin{aligned} x_{1,P_{mod1}} &= \frac{x_{1,P_1}P_1 + x_{1,P_2}P_2 + x_{1,P_3}P_3}{P_{mod1}} \times 100 \\ &= \frac{(0.03445 \times 10.20) + (0.04821 \times 4.565) + (0.06700 \times 2.150)}{16.91} \times 100 \\ &= 4.230\ wt.\% \end{aligned} \tag{D.18}$$

Similarly, the final permeate stream was calculated using a summation over the total number of modules.

$$P = P_{mod1} + P_{mod2} + P_{mod3} + P_{mod4} = 16.91 + 12.03 + 8.600 + 5.552 = 43.09\ kg.h^{-1} \quad \text{(D.19)}$$

$$x_{1,P} = \frac{x_{1,P_{mod1}} P_{mod1} + x_{1,P_{mod2}} P_{mod2} + x_{1,P_{mod3}} P_{mod3}}{P} \times 100$$

$$= \frac{(0.04230 \times 16.91) + (0.1072 \times 12.03) + (0.2348 \times 8.600) + (0.3460 \times 5.552)}{43.09} \quad \text{(D.20)}$$

$$\times 100 = 13.80\ wt.\%$$

A summary of the module flowrates and stream compositions is presented in Table D.3. The stream specifications of the final permeate and retentate for the overall process is also included.

Table D.2. Stream flowrates and compositions from manual calculation for Case 1 (Maximum of 3 cells per module; 4 modules).

Cell k	T_f (K)	x_{i,F_k} (wt.%)		x_{i,P_k} (wt.%)		D_i (m.h^{-1})		$c_{il(m)}$ (kmol.m^{-3})		$c_{io(m)}$ (kmol.m^{-3})		j_i (kmol.m^{-2}.h^{-1})		J_i (kg.m^{-2}.h^{-1})		P_k (kg.h^{-1})	R_k (kg.h^{-1})	x_{i,R_k} (wt.%)	
		propan-2-ol	water	propan-2-ol	water	propan-2-ol	water	propan-2-ol	water	propan-2-ol	water	propan-2-ol	water	propan-2-ol	water			propan-2-ol	water
1	363.15	85.00	15.00	3.45	96.56	2.56E-04	1.74E-02	7.01E-06	6.55E-04	10.23	6.02	0.00262	0.10445	0.1574	1.8817	10.20	296.57	87.80	12.20
2	353.15	87.80	12.20	4.82	95.18	1.38E-04	9.36E-03	1.02E-05	6.71E-04	10.57	4.90	0.00146	0.04581	0.0877	0.8252	4.56	292.01	89.10	10.90
3	343.15	89.10	10.90	6.70	93.30	7.19E-05	4.87E-03	1.48E-05	6.86E-04	10.72	4.37	0.00077	0.02130	0.0463	0.3837	2.15	289.86	89.71	10.29
4	363.15	89.71	10.29	7.95	92.05	2.56E-04	1.74E-02	1.67E-05	6.46E-04	10.80	4.13	0.00276	0.07164	0.1661	1.2905	7.28	282.58	91.82	8.18
5	353.15	91.82	8.18	13.85	86.15	1.38E-04	9.36E-03	3.13E-05	6.50E-04	11.05	3.28	0.00153	0.03072	0.0917	0.5535	3.23	279.35	92.72	7.28
6	343.15	92.72	7.28	17.40	82.60	7.19E-05	4.87E-03	4.16E-05	6.59E-04	11.16	2.92	0.00080	0.01423	0.0482	0.2563	1.52	277.83	93.13	6.87
7	363.15	93.13	6.87	19.33	80.67	2.56E-04	1.74E-02	4.44E-05	6.18E-04	11.21	2.76	0.00287	0.04781	0.1724	0.8614	5.17	272.66	94.53	5.47
8	353.15	94.53	5.47	28.31	71.69	1.38E-04	9.36E-03	7.21E-05	6.09E-04	11.38	2.19	0.00157	0.02053	0.0944	0.3699	2.32	270.34	95.10	4.90
9	343.15	95.10	4.90	32.72	67.28	7.19E-05	4.87E-03	8.92E-05	6.12E-04	11.44	1.97	0.00082	0.00957	0.0494	0.1725	1.11	269.23	95.36	4.64
10	363.15	95.36	4.64	34.80	65.20	2.56E-04	1.74E-02	9.14E-05	5.71E-04	11.48	1.86	0.00294	0.03232	0.1766	0.5823	3.79	265.43	96.22	3.78
11	353.15	96.22	3.78	42.83	57.17	1.38E-04	9.36E-03	1.25E-04	5.56E-04	11.58	1.52	0.00160	0.01418	0.0961	0.2555	1.76	263.68	96.58	3.42

D.3 Comparison of calculated and simulated data for industrial separation

Table D.3. Summary of feed and product streams of the overall process with accompanying module breakdown.

Section m	Calculated						Simulated					
	F_m (kg.h^{-1})	x_{i^a,F_m} (wt.%)	P_m (kg.h^{-1})	x_{i,P_m} (wt.%)	R_m (kg.h^{-1})	x_{i,R_m} (wt.%)	F_m (kg.h^{-1})	x_{i,F_m} (wt.%)	P_m (kg.h^{-1})	x_{i,P_m} (wt.%)	R_m (kg.h^{-1})	x_{i,R_m} (wt.%)
Module 1	306.77	85.00	16.91	4.23	289.86	89.71	306.77	85.00	15.81	3.19	290.96	89.45
Module 2	289.86	89.71	12.03	10.72	277.83	93.13	290.96	89.45	13.16	5.04	277.80	93.44
Module 3	277.83	93.13	8.60	23.48	269.23	95.36	277.80	93.44	10.24	9.11	267.56	96.67
Module 4	269.23	95.36	5.55	34.60	263.68	96.58	267.56	96.67	5.66	18.00	261.89	98.37
Overall process	*306.77*	*85.00*	*43.09*	*13.80*	*263.68*	*96.58*	*306.77*	*85.00*	*44.88*	*6.95*	*261.89*	*98.37*

[a]Component *i* corresponds to propan-2-ol.

APPENDIX E

Breakdown of Economic Evaluation

The total cost of each process configuration was calculated using the method employed by Van Hoof *et al.* (2004). The total cost (C_T) of Equation (E.1 was based on three components: operating cost (C_O), investment cost (C_I) and maintenance cost (C_M).

$$C_T = C_O + C_I + C_M \tag{E.1}$$

E.1 Operating cost calculation

The operating cost, also known as utilities, included cooling water (C_{cw}) for the condensation of the permeate, steam (C_s) to reheat the retentate streams before being fed to the next membrane module and, electricity (C_{elec}) to operate the condensers, feed heaters and vacuum pump.

$$C_O = C_{cw} + C_s + C_{elec} \tag{E.2}$$

Each term of Equation (E.2 was calculated using fluid flowrates, annual operation time and the price of individual utilities as follows:

$$C_{cw} = \dot{V} \cdot t_a \cdot P_{X,cw} \tag{E.3}$$

$$C_s = \dot{m} \cdot t_a \cdot P_{X,s} \tag{E.4}$$

$$C_{elec} = t_a \cdot P_{X,elec} \left(W_{VP} + W_{COND} + \sum_{k=1}^{NS} W_{HE} \right) \tag{E.5}$$

where $\dot{V}$ is the flowrate of water in the condenser [kL.h^{-1}]

t_a is the annual operating hours for the pervaporation plant, 7200 [h]

$P_{X,cw}$ is the price rate of cooling water, 0.40 [$/kL]

$\dot{m}$ is the flowrate of steam in the heater [kg.h^{-1}]

$P_{X,s}$ is the price rate of steam, 0.06 [$/kg]

W is the power requirement for the vacuum pump, condenser and interstage heaters [kW]

NS is the number of interstage heaters

$P_{X,elec}$ is the price rate of electricity, 0.13 [$/kWh]

An annual operation time of 24 hours a day for 300 days was considered. The flowrate of the coolant and steam, obtained using Aspen Plus®, were implemented in the cost calculation of Equations (E.3 and (E.4. The electricity cost of Equation (E.5 comprised of the power consumption for the vacuum pump (VP), condenser (COND) and the total number of heaters (HE) to preheat feed.

E.2 Investment cost calculation

The investment cost of Equation (E.6 included the cost of the pervaporation unit (C_{PV}) and the annual depreciation (C_{dep}) of the membrane modules for a period of 10 years. Furthermore, the cost of the pervaporation unit (Equation (E.7) is made up of two components viz. the cost of the membrane modules, which is dependent on the membrane area as per the supplier DeltaMem AG, and the installation and auxiliary unit cost. Depreciation (Equation (E.8) was 5% of the pervaporation unit cost.

$$C_I = C_{PV} + C_{dep} \tag{E.6}$$

$$C_{PV} = A \cdot C_{module} + C_{ix} \tag{E.7}$$

$$C_{dep} = C_{PV} \cdot 5\% \tag{E.8}$$

where C_{module} is the price of membrane modules as per DeltaMem AG, 1192.68 [$/m^2]

C_{ix} is the cost of installation and auxiliary units

According to Van Hoof *et al.* (2004), the cost for a pervaporation unit, C_{PV}, (390000€ for 2 modules with a total membrane area of 70 m^2) included the membrane modules, membrane, piping, cooling installation, pumps etc. DeltaMem AG provided a membrane module cost of $1192.68/m^2 for 2021. Using an inflation rate of 28.55% between 2004 and 2021, the cost of the membrane module would have been $927.79/m^2. The resulting cost of the membrane modules for 70 m^2 equated to $64945.62, or 48466.88€ using the conversion rate of 1.00€ = $1.34 for the year 2004. Therefore, the cost of installation and the auxiliary units, C_{ix}, (341533.12€), was calculated as the difference between the total cost of a pervaporation unit and the total membrane module cost (rearranging Equation (E.7).

An index representing the cost contribution of C_{ix} to C_{PV} was calculated using Equation (E.9.

$$\% \, C_{ix} = \frac{C_{ix}}{C_{PV}} \times 100 \tag{E.9}$$

It was evident that C_{ix} was directly proportional to the number of modules fitted in the pervaporation unit. Hence, the Equation (E.9 was applied to the 2- and 4-module arrangement of Van Hoof *et al.* (2004) to provide Equations (E.10 and (E.11 as follows:

$$\% \, C_{ix,2\ modules} = \frac{341533.12}{390000} \times 100 = 87.57\% \tag{E.10}$$

$$\% \, C_{ix,4\ modules} = \frac{383066.72}{480000} \times 100 = 79.81\% \tag{E.11}$$

Linear interpolation was applied for a 3-module arrangement. The index served to approximate the C_{ix} for various module arrangements. This was imperative since the various design cases presented in Chapter 7 ranged from 2 – 4 modules. Table E.1 displays a summary of the module arrangement and corresponding index.

Table E.1. Cost index (C_{ix}) for varying number of module arrangements.

Number of modules	% C_{ix}
2	87.57
3	83.69
4	79.81

E.3 Maintenance cost calculation

The maintenance cost of Equation (E.12 included the cost of replacing the membrane twice throughout a 10-year period (C_{mem}) as well as the maintenance on the pervaporation unit (C_{mpv}) which was calculated to be 2.5% of the total pervaporation module cost.

$$C_M = C_{mem} + C_{mpv} \tag{E.12}$$

$$C_{mem} = A \cdot P_{X,mem} \cdot \frac{2}{10} \tag{E.13}$$

$$C_{mpv} = C_{PV} \cdot 2.5\% \tag{E.14}$$

where $P_{X,mem}$ is the price of the membrane as per DeltaMem AG, 608.34 [\$/m^2]